Beyond the Surface

Deciphering Atopic Dermatitis Mechanisms through Innovative Epidermal Models

Luca Dulce Meesters

RADBOUD UNIVERSITY PRESS

Radboud Dissertation Series

Beyond the Surface

Deciphering Atopic Dermatitis Mechanisms through Innovative Epidermal Models

Luca Dulce Meesters

Beyond the Surface: Deciphering Atopic Dermatitis Mechanisms through Innovative Epidermal Models
Luca Dulce Meesters

Radboud Dissertation Series
ISSN: 2950-2772 (Online); 2950-2780 (Print)

Published by RADBOUD UNIVERSITY PRESS
Postbus 9100, 6500 HA Nijmegen, The Netherlands
www.radbouduniversitypress.nl

Design: Proefschrift AIO | Guus Gijben
Cover: Proefschrift AIO | Guntra Laivacuma
Printing: DPN Rikken/Pumbo

ISBN: 9789465150741
DOI: 10.54195/9789465150741
Free download at: https://doi.org/10.54195/9789465150741

RADBOUD
UNIVERSITY
PRESS

Beyond the Surface

Deciphering Atopic Dermatitis Mechanisms through Innovative Epidermal Models

Proefschrift ter verkrijging van de graad van doctor
aan de Radboud Universiteit Nijmegen
op gezag van de rector magnificus prof. dr. J.M. Sanders,
volgens besluit van het college voor promoties
in het openbaar te verdedigen op
woensdag 3 september 2025
om 14.30 uur precies

door

Luca Dulce Meesters
geboren op 21 januari 1997
te 's-Hertogenbosch

Promotoren:
Prof. dr. Ellen van den Bogaard
Dr. Jo Huiqing Zhou

Copromotor:
Dr. Hanna Niehues

Manuscriptcommissie:
Prof. dr. Alessandra Cambi
Prof. dr. Nael Nadif Kasri
Dr. Marieke Bolling (UMC Groningen)

Table of contents

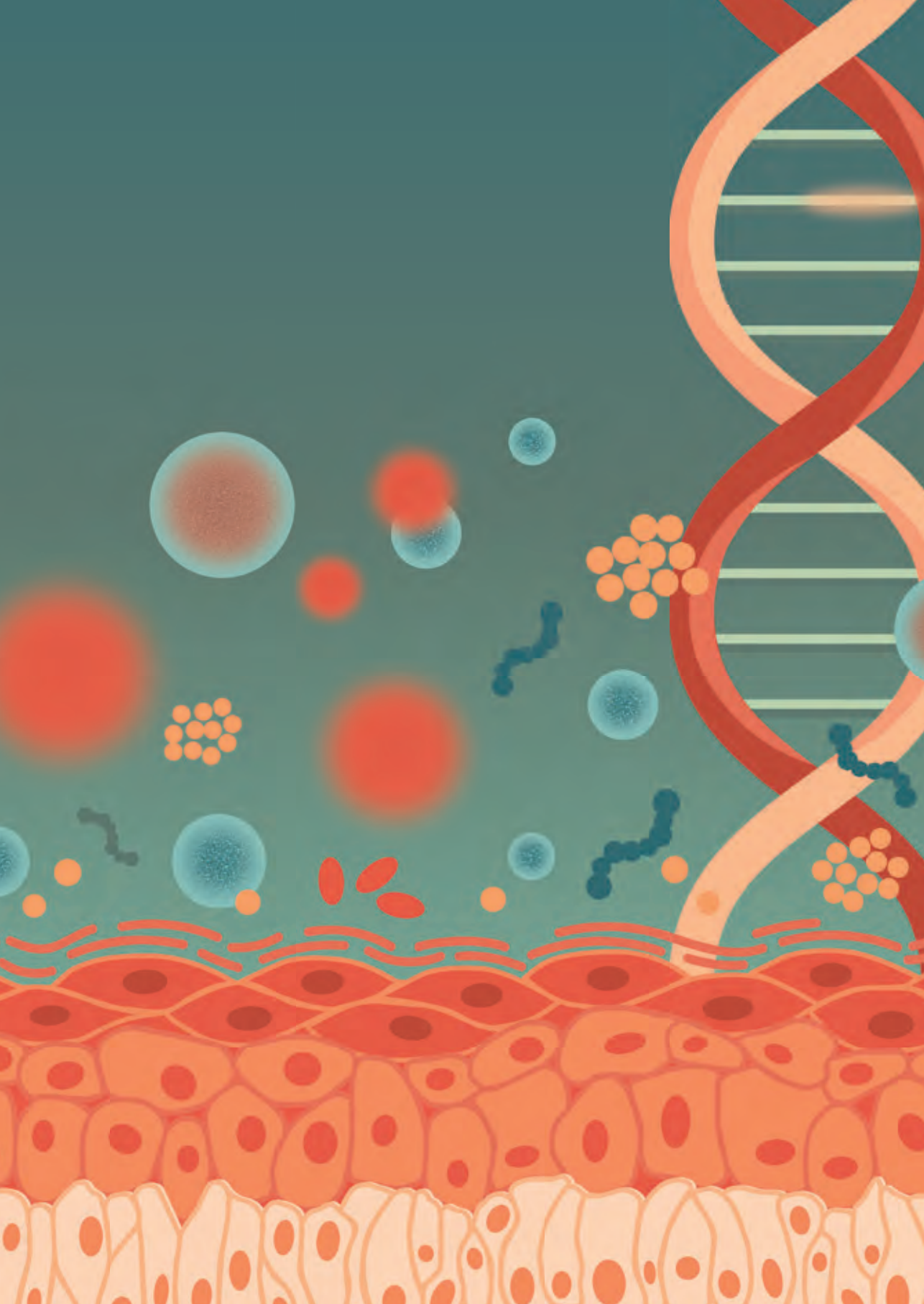

Chapter 1.

General introduction and thesis outline

Part of this chapter is published in:

Targeting the Complexity of In Vitro Skin Models: A Review of Cutting-Edge Developments

Cristina Quílez[1], Luís B. Bebiano[2], Eleri Jones[3], Uroš Maver[4], Luca D. Meesters[5], Piotr Parzymies[3], Emma Petiot[6], Gijs Rikken[5], Ignacio Risueño[1], Hamza Zaidi[6], Tanja Zidarič[7], Sander Bekeschus[8], Ellen H. van den Bogaard[5], Matthew Caley[3], Helen Colley[9], Nuria Gago López[10], Sophia Letsiou[11], Christophe Marquette[6], Tina Maver[4], Rúben F. Pereira[12], Desmond J. Tobin[13], Diego Velasco[14]

Affiliations

[1] Bioengineering Department, Universidad Carlos III de Madrid, Leganés, Spain; Fundación Instituto de Investigación Sanitaria de la Fundación Jiménez Díaz, Madrid, Spain.

[2] i3S - Instituto de Investigação e Inovação em Saúde, Universidade do Porto, Porto, Portugal; Instituto de Engenharia Biomédica (INEB), Universidade do Porto, Porto, Portugal.

[3] Centre for Cell Biology and Cutaneous Research, Blizard Institute, Faculty of Medicine and Dentistry, Queen Mary University of London, London, United Kingdom.

[4] Institute of Biomedical Sciences, Faculty of Medicine, University of Maribor, Maribor, Slovenia; Department of Pharmacology, Faculty of Medicine, University of Maribor, Maribor, Slovenia.

[5] Department of Dermatology, Radboud University Medical Center, Nijmegen, The Netherlands.

[6] 3d.FAB, CNRS, INSA, Univ Lyon, CPE-Lyon, UMR5246, ICBMS, Université Lyon 1, Villeurbanne Cedex, France.

[7] Institute of Biomedical Sciences, Faculty of Medicine, University of Maribor, Maribor, Slovenia.

[8] Clinic and Policlinic for Dermatology and Venerology, Rostock University Medical Center, Rostock, Germany; ZIK plasmatis, Leibniz Institute for Plasma Science and Technology (INP Greifswald), Greifswald, Germany.

[9] School of Clinical Dentistry, University of Sheffield, Sheffield, United Kingdom.

[10] Melanoma group, Molecular Oncology Programme, Spanish National Cancer Research Center (CNIO), Madrid, Spain.

[11] Department of Biomedical Sciences, University of West Attica, Athens, Greece; Department of Food Science and Technology, University of West Attica, Athens, Greece.

[12] i3S - Instituto de Investigação e Inovação em Saúde, Universidade do Porto, Porto, Portugal; Instituto de Engenharia Biomédica (INEB), Universidade do Porto, Porto, Portugal; ICBAS - Instituto de Ciências Biomédicas Abel Salazar, Universidade do Porto, Porto, Portugal.

[13] Charles Institute of Dermatology, University College Dublin, Dublin, Ireland; Conway Institute of Biomolecular and Biomedical Research, University College Dublin, Dublin, Ireland.

[14] Bioengineering Department, Universidad Carlos III de Madrid, Leganés, Spain; Fundación Instituto de Investigación Sanitaria de la Fundación Jiménez Díaz, Madrid, Spain. Electronic address: divelasc@ing.uc3m.es.

Published in

J Invest Dermatol. 2024 Dec;144(12):2650-2670. doi: 10.1016/j.jid.2024.04.032.

Atopic dermatitis

The skin is a versatile organ of approximately 2 m^2 in adults, which accounts for up to 10 to 15 percent of the total body weight. Being on the outside of our body, the skin interacts with both internal and external stimuli. These challenges can result in various inflammatory skin diseases, of which atopic dermatitis (AD), also known as atopic eczema, is one of the most common. Almost 3% of the worldwide population is estimated to be affected by AD [1]. Due to the complex disease pathophysiology, AD can present clinically heterogeneous, but patients often suffer from red, scaly, dry and itching skin (Figure 1) [2]. Treatment options include emollients (moisturizers), topical corticosteroids, ultraviolet phototherapy and systemic therapies including immune-modulating biologics, Janus Kinase (JAK) inhibitors and conventional immunosuppressants, like cyclosporin. However, poor adherence to topical therapy and the varying pathophysiology between patients contribute to disease recurrence or even lack of response at all to systemic therapies [3, 4]. The need to switch treatments is accompanied by a high physical, psychological and economic burden for both the patient and society [5, 6]. Understanding of AD disease mechanisms is essential for improving current therapeutic strategies and discovery of new drug targets.

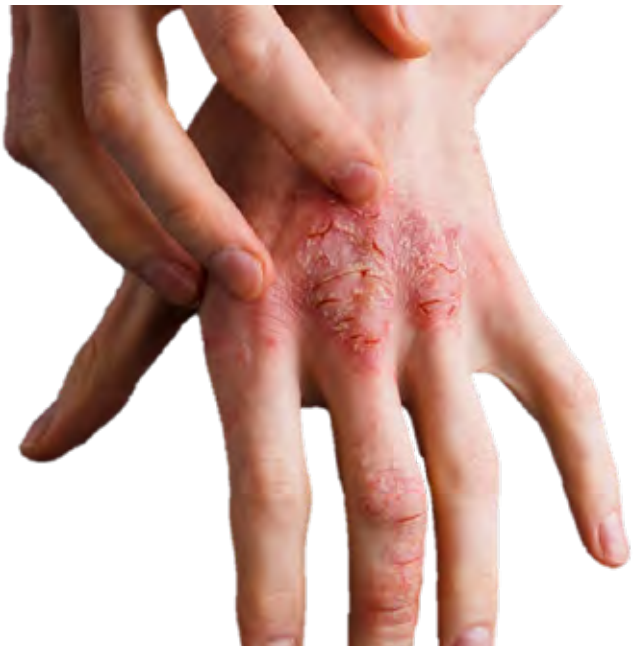

Figure 1. Clinical presentation of AD: red, scaly, dry and itching skin. Adapted from National Eczema Association.

Epidermal structure

The skin is a multilayered organ. The most inner layer is a subcutaneous adipose layer. This is followed by the dermis with fibroblasts and collagen fibers where sweat glands, hair follicles, neurons and blood vessels reside. The outer layer is the keratinocyte, melanocyte and Langerhans cell populated epidermis [7]. As this outer layer of the skin, the epidermis plays an important role in skin homeostasis and its barrier function [8]. The epidermis mainly consists of keratinocytes that proliferate in the basal layer to regenerate the epidermis, after which they terminally differentiate upwards to form the spinous, granular and cornified layer (Figure 2) [9]. While keratinocytes differentiate, they change from keratin (KRT)5/14 positive to KRT1/10 and involucrin (IVL) positive, and eventually express proteins like loricrin (LOR) and filaggrin (FLG) [10, 11]. FLG is also the main component of the keratohyalin granules that are visible in the granular layer (Figure 2). Within the epidermis, a calcium (Ca^{2+}) gradient is present that regulates epidermal barrier formation, with low levels in the basal layer and the highest levels in the granular layers [12, 13]. Another important regulator of epidermal development, besides its role in epidermal commitment, is the transcription factor protein 63 (P63) [14]. P63 is involved in multiple epidermal processes, including cell adhesion, proliferation and differentiation [15, 16]. It directly drives expression of basal (e.g., KRT14) as well as stratified (KRT1, KRT10, IVL) keratinocyte proteins, but also acts through proteins like zinc finger protein (ZNF)750, Interferon regulatory factor (IRF)6 or Transcription Factor AP (TFAP)2A [17]. To maintain an optimal number of epidermal layers, the regenerative process involves a tight coordination between keratinocyte proliferation, terminal differentiation and desquamation of corneocytes from the cornified layer.

In AD, this epidermal homeostasis is disturbed by a disbalance between proliferation, differentiation, cornification and involvement of apoptosis. AD lesions are often characterized by epidermal thickening, also called acanthosis, as a result of hyperproliferative basal keratinocytes [18]. Critical mitogens that are associated with keratinocyte hyperproliferation have been identified, including cytokines, growth factors and hormones, as demonstrated by research from our group [19]. Another epidermal hallmark of AD is increased keratinocyte apoptosis in suprabasal layers [20]. Type 1 T-cell derived molecules including interferon (IFN)-γ and tumor necrosis factor (TNF)-α, and type 2 T-cell derived interleukin (IL)-4 and IL-13, that are abundant in different stages and endotypes of AD [21-23], increase the expression of Fas receptor (FasR) on keratinocytes [20, 24]. This makes keratinocytes more susceptible to apoptosis triggers such as Fas ligand (FasL) produced by T cells [20, 25]. Moreover, keratinocyte apoptosis leads to loss

of intercellular cohesion and space for fluid influx from the dermis [26]. Type 1 and 2 cytokines also decrease cell-cell adhesion molecule E-cadherin, and augment intercellular hyaluronan accumulation, that has osmotic properties [27]. Altogether, this contributes to the onset of edema, that is visible as white gaps in the epidermis of AD patients and is also called spongiosis. In the upper epidermal layers, keratinocyte differentiation defects result in a discontinuous granular layer, ranging from patches with a normal granular layer to a reduced number of granular keratinocytes, termed hypogranulosis (Figure 2) [28]. These features can be a result of genetic predisposition, as well as the cutaneous inflammatory milieu, and lead to an impaired epidermal barrier.

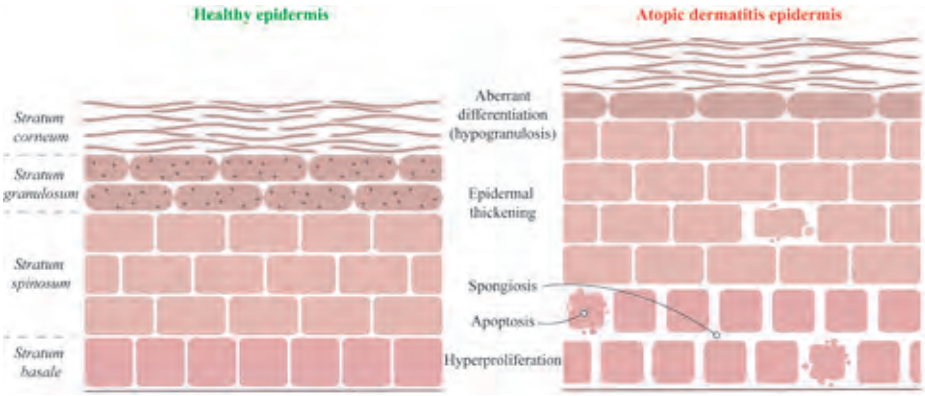

Figure 2. The epidermal morphology in health and AD. Healthy epidermis contains a basal layer (*stratum basale*), spinous layers (*stratum spinosum*), granular layers (*stratum granulosum*) and cornified layers (*stratum corneum*). In (acute) AD lesions, hyperproliferation leads to increased basal layers and overall epidermal thickening; apoptosis and spongiosis are present; and differentiation defects result in an irregular granular layer.

Epidermal barrier formation and function

Healthy skin functions as a barrier to retain water inside and keep harmful stimuli like pathogenic bacteria outside the body. The epidermis is the main skin component contributing to the physical skin barrier. Keratinocytes in the granular layer are physically connected by tight junctions [29]. In the cornified layer, corneocytes are embedded in networks of cross-linked structural proteins like IVL, LOR and FLG, and lipids including ceramides [30, 31]. To do so, structural proteins aggregate with keratin intermediate filaments through the action of transglutaminases, thereby forming the cornified envelope [32-34]. FLG, that is derived from profilaggrin, is also processed through proteolysis giving rise to natural moisturizing factors

(NMFs) that are responsible for water retention [35]. The breakdown of FLG amino acids leads to formation of trans-urocanic acid (UCA) and pyrrolidone-5-carboxylic acid (PCA), which are important for maintaining the skin's natural pH and thereby its metabolism [36]. Therefore, a loss of functional FLG in AD, of which causes will be discussed later, can greatly impact epidermal homeostasis. Next to the physical epidermal barrier of tight junctions and the cornified envelope, keratinocytes produce chemical factors that contribute to the cutaneous immune defense, exemplified by antimicrobial peptides and cytokines [37-39]. Some epidermal differentiation proteins like late cornified envelope (LCE)3A and cysteine rich tail 1 (CYSRT1) have antimicrobial effects as well [40, 41].

In contrast, AD lesions are characterized by skin barrier defects, leading to increased transepidermal water loss (TEWL) and decreased electrical impedance spectroscopy (EIS) values, and therefore dehydration [42-46]. FLG deficiency has been linked to these barrier defects in multiple ways. Since FLG both associates with the cornified envelope, as well as keratin filaments, its loss was suggested to compromise both of these structures that are important for the epidermal integrity [47]. In addition, AD patients have lower levels of NMFs, and the NMF value has been associated to disease severity [48, 49]. Loss of NMFs and their water retention effects contributes to the development of dry skin [50], a characteristic of AD lesions. In addition, dysfunctional tight junctions, and more specifically reduced tight junction protein claudin (CLDN)1, have been found in AD lesions [51-53]. This was suggested to contribute to the epidermal barrier defects not only directly through weakening of cell-cell contacts, but also by altering *stratum corneum* lipids and filaggrin processing [54]. The lipid profile of AD patients differs from healthy controls, illustrated by a reduced average chain length of ceramides [55-57] and free fatty acids [58, 59], and increased cholesterol [60, 61]. However, alterations might depend on underlying causes of AD, including *FLG* genotype [62] or *Staphylococcus aureus* (*S. aureus*) colonization status [60]. The increased risk of microbial skin colonization and infections in AD, predominantly by *S. aureus* [63-66], is also a sign of barrier impairment. This could be explained by physical barrier defects in combination with insufficient antimicrobial defense mechanisms [67, 68] or lower levels of receptors that recognize pathogen associated molecular patterns (PAMP) [69-71].

While the occurrence of epidermal barrier defects in AD are evident, with clear hypotheses on the contributing mechanisms, it is difficult to unravel the initiating or core factors driving the disease in individual patients. The complex pathophysiology and simultaneous occurrence of disease modifying events compromise cause-effect studies *in vivo*. However, knowledge on driving factors

would be valuable to improve or create personalized therapeutic approaches. Generally speaking, defects in the epidermal barrier in AD have been linked to I) genetic predisposition, II) an inflammatory milieu and III) microbiome dysbiosis, which will be further specified below and are illustrated in Figure 3.

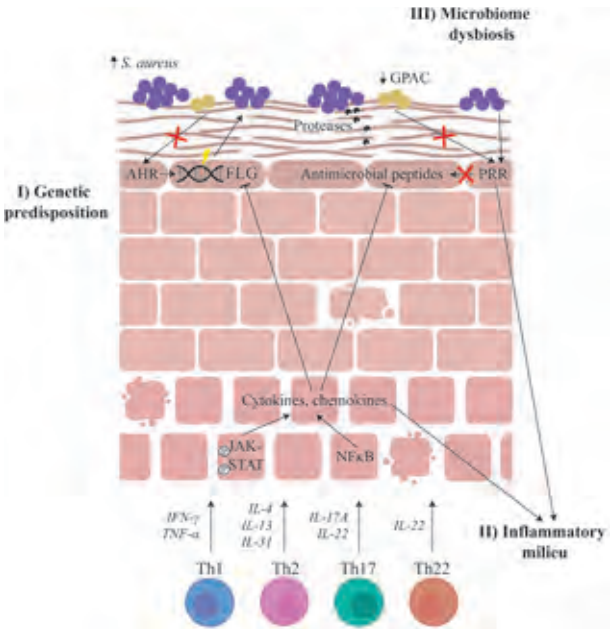

Figure 3. Multifactorial cause of a defective epidermal barrier in AD. The genetic predisposition of *FLG* variants are linked to barrier defects and *S. aureus* overgrowth. The inflammatory milieu causes JAK-STAT phosphorylation and NFκB activation that further exacerbate the inflammation, decrease expression of epidermal differentiation proteins like FLG and repress production of antimicrobial peptides. This in turn stimulates *S. aureus* overgrowth, which produce proteases that weaken the epidermal barrier and stimulate immune cells. *S. aureus* overgrowth is part of the microbiome dysbiosis together with lower abundance of GPAC. Less GPAC also means reduced production of antimicrobial peptides and FLG.

Genetic predisposition

Mutations in many epidermal barrier-related genes that are normally expressed by keratinocytes have been linked to AD, including *FLG*, *hornerin* (*HRNR*), *serine protease inhibitor Kazal-type 5* (*SPINK5*), *small proline-rich protein 3* (*SPRR3*) and *CLDN1* [72-74]. Loss-of-function variants in the *FLG* gene form the strongest predisposition for the development of AD [75]. The odds of developing AD were estimated to be three times higher for individuals with *FLG* variants as for individuals without [76]. Due to the prominent role of epidermal barrier proteins like FLG in epidermal homeostasis, a loss of (functional) FLG expression, as is often the case genetically or acquired due to proinflammatory cytokines in AD, causes disturbances in epidermal integrity

and barrier functioning. However, many people with *FLG* variants do not present with AD [77], showing the multifactorial nature of the disease. This raises questions on which gene-environment interactions initiate the development of AD, requiring experimental models to study.

Inflammatory milieu

The main responsible drivers for the acquired defects in epidermal structure and barrier proteins are inflammatory cells and cytokines, as reviewed previously [78]. Various immune cells, ranging from innate dendritic, lymphoid and Langerhans cells to adaptive B and T cells are thought to play a role in the AD pathophysiology. Focusing on the T cells, that excrete cytokines which are known to be high in AD, the disease is typically characterized by T helper (Th)1, Th2, Th17 and Th22 polarization as compared to healthy controls [79, 80]. The contribution of each Th cell and its cytokines depends on the disease severity, phase (acute or chronic) and endotype [81, 82]. In general, the acute phase is dominated by Th2 and Th22 cells and cytokines, whereas a Th1 and Th17 response becomes more driving in the chronic phase, with each cytokine having a distinct effect on the epidermis. The association of individual or combinations of cytokines with epidermal AD hallmarks is, however, not easily investigated *in vivo*. For this purpose, *in vitro* skin models, which are easier to control and manipulate, could be better suitable.

Th1-derived cytokines TNF-α and IFN-γ are pro-inflammatory mediators promoting keratinocytes to produce more cytokines [83-85]. This is mainly regulated by nuclear factor-kappa-B (NFκB) and JAK-signal transducer and activator of transcription (STAT) signaling in keratinocytes, which are phosphorylated to mediate their effects. For instance, TNF-α binding to its receptor activates and translocates NFκB to the nucleus [86, 87], leading to transcription of genes like IL-6 and IL-8 [87, 88]. TNF-α is also known for its apoptosis inducing effects in keratinocytes [88-90], which is one of the epidermal hallmarks of AD. However, TNF-α inhibitor effectiveness in the treatment of AD has been conflicting [91], and it may even elicit AD [92, 93], implying a non-driving role in disease pathology. IFN-γ induces JAK2-STAT1 signaling in keratinocytes [94-96], which is followed by expression of target genes like C-X-C motif chemokine ligand (CXCL)9 and 10 [97]. Next to that, IFN-γ has been suggested to downregulate tight junction function through reduction of CLDN1 [98]. Yet, similar to TNF-α inhibition, modulating IFN-γ levels as AD treatment is controversial [99] and has not reached the clinic.

Th2 cells produce cytokines like IL-4, IL-5, IL-13 and IL-31, of which the effect of IL-4 and IL-13 on keratinocytes and the epidermis is mostly studied. IL-4 signaling starts

at the IL-4 receptor, whereas IL-13 can bind to both the IL-4 and IL-13 receptor. This induces phosphorylation of JAK1/2-STAT6 [100] and downstream target expression of among many IL-20 and C-C motif chemokine ligand (CCL)26 [100, 101]. IL-4 and IL-13 have also been shown to reduce the expression of epidermal differentiation complex proteins including FLG, IVL and LOR [102, 103]. Th2 immune axis targeting therapeutics such as biologics (e.g., dupilumab) or small molecule drugs (JAK inhibitors like tofacitinib) are the first effective targeted therapies that have emerged for AD over the last decade. This indicates that the Th2 axis is a key driver in the pathophysiology. However, many patients do not respond sufficiently [104, 105], implying that other immune cells and mediators are also important and that AD presents heterogeneously between patients. Recent characterizations demonstrated differences between AD endotypes, including immune polarization to Th17 and Th22 [23].

Th17 cells are mainly producing IL-17A and IL-22, of which the latter is also excreted by Th22 cells. IL-17A and IL-22, acting through JAK-STAT1/3 [106-108], have been described as inhibitors of epidermal differentiation [108-112]. In addition, these cytokines are known for their induction of antimicrobial peptide (AMP) production by epidermal keratinocytes, however the relatively low levels of IL-17A and high levels of Th2 cytokines in AD, as compared to psoriasis, represses the AMP response in AD, as reviewed elsewhere [113].

Microbiome dysbiosis

The skin microbiome composition has been extensively characterized at multiple body sites and varies between moist and dry environments [114]. It consists of bacteria (e.g., *Corynebacterium*, *Cutibacterium* and *Staphylococcus*), fungi (e.g., *Malassezia*), viruses (less well studied) and other microbiota that educate the immune system and prevent colonization of pathogens. AD skin generally exhibits a decreased bacterial diversity and altered numbers of microbiota, also known as skin microbiome dysbiosis. Specifically, AD lesions are often colonized, and later infected, by *S. aureus*, and FLG-deficient skin shows a lower abundance of commensal Gram-positive anaerobe cocci (GPAC) [115-117]. These GPAC appear important in the epidermal host-defense response through upregulation of antimicrobial peptides and terminal differentiation [118]. In this way, they could contribute to alarming keratinocytes to prepare for encounter with pathogens, and their lower abundance in AD may contribute to the impaired barrier.

Cellular receptors for microbial metabolites or structural components are crucial in host-microbe interactions and are needed to recognize pathogens and initiate a

host defense response. Keratinocytes express various pattern recognition receptors (PRR), that can detect PAMPs like microbial lipopolysaccharides (LPS), RNA and DNA, including toll like receptors (TLRs), NOD-like receptors (NLRs), RIG-like helicases (RLRs) and C-type lectins (CLRs) [119, 120]. While their role in recognizing skin microbes and subsequential upregulation of proinflammatory molecules is well acknowledged [119, 121], their contribution to AD is under debate, with some studies showing altered expression in AD as compared to healthy skin and others not [122]. Another receptor that can be activated by microbial molecules is the environmental sensor and transcription factor aryl hydrocarbon receptor (AHR) [123-125]. Upon ligand binding, AHR translocates to the nucleus and forms a heterodimer with AHR nuclear translocator (ARNT) [126, 127]. This complex binds to DNA to initiate transcription of target genes like *CYP1A1*, but also epidermal differentiation genes including *IVL*, *LOR* and *FLG* [126, 128, 129]. Moreover, AHR activation in keratinocytes was suggested to reduce their IL-4 and IL-13-driven STAT6 phosphorylation and production of inflammatory proteins like CCL26 [126]. An example of an AHR ligand that can be produced by microbiota is Indole-3-aldehyde, which was found to be significantly lower on AD skin as compared to healthy volunteers [125]. Moreover, topical and oral Indole-3-aldehyde alleviated skin inflammation in an AHR-dependent manner in mice with AD-like dermatitis [125]. This implies that AHR activation may finetune epidermal homeostasis and regulate inflammatory processes, which is corroborated by the fact that AHR targeting therapies, including coal tar and tapinarof [126, 130], are effective topical therapies in the treatment of AD [131, 132].

It is under debate whether skin microbiome dysbiosis can cause or aggravate AD, or whether AD causes dysbiosis. Interestingly, reversing microbiome dysbiosis with antibiotics prevented development of eczematous lesions in a mouse model [133]. In line, the proteolytic activity of *S. aureus* enhanced its penetration through the epidermis inflicting inflammation [134]. In addition, *S. aureus* is an important inducer of itch and thereby scratch-induced skin damage [135, 136]. On the other hand, genetically driven barrier defects like by FLG loss-of-function increase the penetration of *S. aureus* [134]. This indicates that *S. aureus* can both exploit the weakened epidermal barrier for its overgrowth and infection, as well as to cause a more defective barrier. Either way, the interplay between the host and microbe appears dysregulated in AD which favors disease symptoms and could be a target for intervention. This requires sufficient evidence generated from relevant disease models that indicate the molecular targets, or causal effects on skin function and health.

Pre-clinical experimental dermatology

While there is ample evidence on the potential contributors to the development and exacerbation of AD by analyzing serum or skin, it is difficult to pinpoint direct correlations in patient samples due to the complexity of the disease and presence of many cell types and molecular signatures derived thereof. Pre-clinical experimental models pose a solution to this problem, since they are easier to manipulate and the cell types and disease factors of interest can be added based on the research question. In particular, *in vitro* epidermal models made from human cells closely mimic the human *in vivo* epidermal barrier, and come with less ethical problems as compared to *in vivo* animal models. The development of *in vitro* epidermal models that closely resemble *in vivo* healthy and diseased epidermis fuels disease mechanism and drug (target) screening studies, and starts with the generation or acquirement of suitable keratinocyte cell sources (Figure 4).

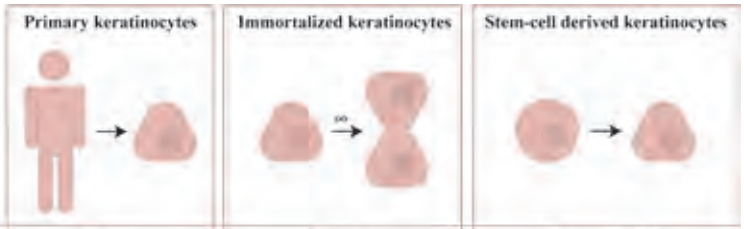

	Primary keratinocytes	Immortalized keratinocytes	Stem-cell derived keratinocytes
In vitro lifespan	Short	Long	Intermediate*
Donor variability	Yes	No	Yes
Resemblance to *in vivo*	Yes	Yes, except cell cycle mechanisms	Depends on differentiation success
Availability	Depends on donor skin	Often only in academics	Depends on donor tissue
Other			Developmental research possible
AD specific use	Patient cells	CRISPR-Cas9 editing	Patient cells & CRISPR-Cas9 editing

Figure 4. Overview of keratinocyte sources and their (dis)advantages for dermatological research.
* Stem cells have an extended lifespan, but keratinocytes derived thereof do not.

Keratinocyte cell sources for generating *in vitro* models

Normal human epidermal keratinocytes (NHEK), or primary keratinocytes, are the most commonly used cells to generate *in vitro* epidermal models since they most closely resemble *in vivo* keratinocytes, and results are more generalizable when keratinocytes from various donors are used. The benefit of using primary keratinocytes in AD research is that they can also be directly obtained from AD patients, thereby containing the specific genetic code that might contribute to the disease pathophysiology, as well as the disease-specific sensitivity to AD-related

stimuli. The first can be exemplified by the presence of *FLG* mutations [137], whereas the latter could present as an exaggerated cytokine response of keratinocytes from AD patients to T-cell-derived cytokines as compared to healthy controls [84]. This is hypothesized to be caused by alterations in regulatory elements of cytokine genes. The drawback of using NHEK is that they have a short *in vitro* lifespan and that they are not widely available as their retrieval depends on healthy volunteers or patients. Moreover, while donor-specific responses could be of benefit in the context of personalized medicine, the heterogeneity between keratinocytes from different donors could hamper the interpretation of results.

When long-term cultures are required, for instance for genetic modification by CRISPR/Cas9 (clustered regularly interspaced short palindromic repeats and CRISPR-associated protein 9), immortal keratinocytes can be the preferred cell source. HaCaT cells were the first widely used immortal keratinocytes, obtained by spontaneous transformation [138]. While they were initially proven capable of some keratinization with expression of IVL and FLG, they are aneuploid and do not stratify well into all epidermal layers [139, 140]. Two decades ago, new immortalized keratinocytes were generated by retroviral upregulation of human telomerase (hTERT) and spontaneous loss of the $P16^{INK4a}$-dependent cell cycle mechanism, called N/TERT-1 and N/TERT-2G [141]. Ever since, they have been characterized and compared to NHEK, showing they are capable of forming all epidermal strata with a functional barrier, respond similarly to inflammatory cytokines as primary keratinocytes and can be used for drug-screening [142-144]. To study AD, CRISPR/Cas9-based editing of the *FLG* gene in immortal keratinocytes to knock-out FLG or specifically insert a patient-derived *FLG* variant could provide more information on direct and indirect effects of this genetic predisposition on other epidermal proteins or barrier function. This could overcome the diversity in genetic backgrounds from primary patient-derived and (FLG) genotype-defined models [137].

Recently, great progress is made in the pluripotent stem cell field including the generation of stem cell-derived keratinocytes. Pluripotent stem cells are suitable for gene editing technologies due to their long *in vitro* lifespan, and they can be used in developmental biology studies by analyzing their differentiation towards keratinocytes. Moreover, pluripotent stem cells can in theory be differentiated into any (skin) cell type e.g. fibroblasts, neuronal cells and keratinocytes with the same genetic background favoring studies with multicellular models. Embryonic stem cells (ESC) could be a source for stem-cell derived keratinocytes. These are present inside an embryo from day 4 until 7 after fertilization [145], so their collection comes with ethical issues. Also they are less useful for personalized modeling, because at

the stage of retrieval it is unknown whether the embryo would have developed diseases later in life, and therefore what the role of their genetic code would be. Overcoming these issues, the discovery that induced pluripotent stem cells (iPSC) can be generated by introduction of the Yamanaka factors Oct3/4, Sox2, c-Myc, and Klf4 to a somatic cell has revolutionized stem cell biology and regenerative medicine [146]. iPSC provide the opportunity to correct a patient-related genetic variant by genetic modification to show the effect of this variant in the disease development. This has been demonstrated for the rare inherited blistering skin disorder epidermolysis bullosa [147, 148]. However, iPSC have not extensively been used in the field of skin inflammation, or specifically AD. Generation of iPSC from AD patient cells with a FLG variant and subsequent differentiation into keratinocytes has only been reported once [149]. However, to our knowledge, comparison of their epidermal development to iPSC without FLG variants has not yet been performed. Moreover, the suitability of iPSC-derived or induced keratinocytes (iKC) to study the inflammatory and microbiome dysbiosis components of AD has not yet been investigated. This could advance the development of personalized human skin equivalents to study disease mechanisms and screen therapeutics. To do so, the iPSC to keratinocyte differentiation needs to yield iKC that are functionally similar to primary keratinocytes (pKC) before they can be optimally used in experimental studies. For example, so far, the generation of human epidermal and skin equivalents from iKC did often lead to poor epidermal integrities [150-152], with the exception of a not yet reproduced study [153]. Therefore, optimization of current iPSC to keratinocyte differentiation and subsequent epidermal differentiation protocols is required.

Depending on the experimental question, a specific cell type can be chosen to generate *in vitro* epidermal models. This decision could be based on the availability of cells, similarity to the *in vivo* situation with respect to the topic of interest (e.g., hyperproliferation vs differentiation defects), the research phase (e.g., initial compound screening vs testing of few selected drugs), readout parameters, time and costs (Figure 4). To this end, knowledge on how each cell type responds to AD-specific stimuli, like cytokines and microbiota, would facilitate the decision making process and improve the relevance of study outcomes.

In vitro epidermal models

Monolayer keratinocyte cultures are high throughput *in vitro* models to study the response of keratinocytes to skin-related stimuli and on keratinocyte-keratinocyte interactions. For example, the inflammatory or antimicrobial keratinocyte response to inflammatory cytokines or live and heat-killed bacteria can be relatively easily investigated [120, 154]. To study defects in early keratinocyte differentiation in 2D, monolayers can be stimulated with Ca^{2+} or serum [155, 156]. However, to study the epidermal barrier function or long-term host-microbe interactions, fully stratified epithelium and therefore organotypic epidermal models are needed. The morphology and barrier function of *in vitro* organotypic epidermal models resembles *in vivo* epidermis, as summarized and shown in [157, 158]. *In vitro* epidermal models, also called human epidermal equivalents (HEE), are generated by exposing the epidermal keratinocytes to air to induce their stratification [158]. Barrier function assays often include dye permeation, with lucifer yellow being used for the outside-in barrier and biotin for the inside-out barrier [158]. This qualitative measure requires harvesting of the model before analysis is possible. Quantitative non-intrusive assays, like TEWL and transepithelial resistance measurements are more accurate but also extremely labor intense for longitudinal analysis during the tissue culture period. While both techniques allow for longitudinal barrier assessment, current methods provide variable outcomes depending on the type and positioning of the probe/electrode and are influenced by environmental factors like temperature. The development of sensitive standardized high throughput technologies for non-intrusive quantitative analysis of epidermal barrier function *in vitro* is therefore in high demand.

HEEs are often cultured in a transwell system, which allows for application of stimuli from the bottom (like cytokines that normally come from immune cells in the dermis) and the top (like microbiota that naturally reside on the skin). Multiple studies have utilized this system to show contributions of cytokine combinations to the AD pathophysiology, as summarized in Table 1, although these studies used varying cytokine concentrations, cell types and read-out parameters. In addition, due to the high risk at basolateral culture infections the long-term host-microbe interaction and dysbiosis studies are scarce.

Table 1. *In vitro* epidermal models with cytokines. Adapted from [159]. CA2: carbonic anhydrase 2, NELL2: neural EGFL like 2, HAS3: hyaluronan synthase 3, MβCD: methyl-β-cyclodextrin, TSLP: thymic stromal lymphopoietin, Poly(I:C): polyinosinic:polycytidylic acid, Ki67: kiel 67, ABCA: ATP binding cassette subfamily A, EdU: 5-ethynyl-2′-deoxyuridine, ITGA: integrin subunit alpha, PLAUR: plasminogen activator urokinase receptor, TGM: transglutaminase, KLK: kallikrein-related peptidase, AQP: aquaporin, TNC: tenascin c

Cytokines	Morphological hallmarks	Disease markers	Additional comments	Ref.
IL-4, IL-13, IL-25	Spongiosis, hypogranulosis, epidermal barrier weakening	↓ FLG, LOR ↑ CA2, NELL2, HAS3	Other disease initiation factors: +MβCD (cholesterol depletion and TSLP production)	[160]
IL-4, IL-13	Hypogranulosis	↓ FLG ↑ TSLP,CLDN1	Other inflammatory factors: +Poly(I:C), Pam3CKS4 (TLR ligands)	[161]
IL-4, IL-13, IL-31, TNF-α	Spongiosis	↓ FLG, LOR, cholesterol ↑TSLP, Ki67, ceramides Altered lipid organisation	–	[162]
IL-4, IL-13, IL-25	Spongiosis	↓ FLG, LOR, *E-cadherin, ABCA1, ABCA12* ↑ CA2*, NELL2, HAS3*	–	[163]
IL-4 or IL-13	Acanthosis, hyperplasia	↑ Ki67, EdU incorporation	Part of a larger panel of inflammation molecules	[19]
IL-4, IL-13, IL-22, TNF-α	Loss of tissue cohesion, orthokeratosis	↓ FLG ↑ S100A7	No information on number of donors, significance of results	[164]
IL-4, IL-13, TNF-α	Spongiosis	↓ FLG, LOR, IVL, *KRT1, KRT10, ITGA2* ↑ TSLP, IL-8, *CXCL8, CA2, NELL2, TLR2, STAT2, SPINK5, PLAUR, IL1A, TGM1, S100A8, S100A9, KLK7, AQP3 and TNC*	Other inflammatory factors: +Poly(I:C)	[165]

Thesis aims and outline

Organotypic epidermal models have been proven useful to study the AD pathophysiology, exemplified in Table 1, for drug target discovery and therapeutic screening. However, challenges remain in AD modeling that preclude investigations on causal or contributing disease mechanisms that compromise effective therapeutic targeting in patients.

Therefore, the overarching aims of my thesis are:

- AIM 1. To develop 3D human epidermal atopic dermatitis models and readouts to study disease pathophysiology (**Chapter 4-7**);
- AIM 2. To investigate which keratinocyte cell sources are valuable to unravel the different underlying genetic, inflammatory and microbiome mechanisms of AD (**Chapter 6-8**);
- AIM 3. To dissect how genetic predisposition, inflammatory cytokines and microbiome dysbiosis drive epidermal defects and how these can be restored upon treatment (**Chapter 4-7)**.

First, we provide an overview of how various components of the AD pathophysiology, ranging from genetic variants to inflammation and microbiome dysbiosis, can be modeled in organotypic skin models (**Chapter 2**). For genetic engineering of cells, CRISPR/Cas9 is a commonly used technique nowadays, yet not in epidermal keratinocytes. Key factors for failure and success of CRISRP/Cas9 genome editing in keratinocytes are presented in **Chapter 3**. Identified success factors have been implemented in our strategy for creating a FLG knockout keratinocyte line with CRISPR/Cas9 to mimic the loss-of-function of FLG in many AD patients and investigate its effects on epidermis development (**Chapter 4**). In **Chapter 5** we validated a novel technique, called electrical impedance spectroscopy (EIS), to quantitatively assess the epidermal barrier function in organotypic human epidermal models. To model inflammation-driven alterations in the epidermis in **Chapter 6,** we investigated an optimized AD-specific cytokine cocktail for development of AD-like HEEs, and reveal which epidermal AD hallmarks are driven by specific (combinations of) inflammatory cytokines, and can be inhibited by various therapeutic compounds. To study host-microbe interactions and the functional consequences of microbiome dysbiosis in AD, a novel methodology for bacterial inoculation of HEEs, and specifically by *S. aureus*, was developed in **Chapter 7**. Finally, we optimized iPSC to keratinocyte differentiation protocols and demonstrate the potential of these induced keratinocytes (iKC) in dermatological research (**Chapter 8**).

References

1. Tian, J., et al., Global epidemiology of atopic dermatitis: a comprehensive systematic analysis and modelling study. Br J Dermatol, 2023. **190**(1): p. 55-61.
2. Eichenfield, L.F., et al., Guidelines of care for the management of atopic dermatitis: section 1. Diagnosis and assessment of atopic dermatitis. J Am Acad Dermatol, 2014. **70**(2): p. 338-51.
3. Eichenfield, L.F., et al., Guidelines of care for the management of atopic dermatitis: section 2. Management and treatment of atopic dermatitis with topical therapies. J Am Acad Dermatol, 2014. **71**(1): p. 116-32.
4. Davis, D.M.R., et al., Guidelines of care for the management of atopic dermatitis in adults with phototherapy and systemic therapies. J Am Acad Dermatol, 2024. **90**(2): p. e43-e56.
5. Eyerich, K., et al., Real-world clinical, psychosocial and economic burden of atopic dermatitis: Results from a multicountry study. J Eur Acad Dermatol Venereol, 2024. **38**(2): p. 340-353.
6. Adamson, A.S., The Economic Impact of Atopic Dermatitis. Adv Exp Med Biol, 2024. **1447**: p. 91-104.
7. Agarwal, S. and K. Krishnamurthy, Histology, Skin, in StatPearls. 2024, StatPearls Publishing. Copyright © 2024, StatPearls Publishing LLC.: Treasure Island (FL).
8. Lefèvre-Utile, A., et al., Five Functional Aspects of the Epidermal Barrier. Int J Mol Sci, 2021. **22**(21).
9. Yin, H., M. Hu, and D. Li, Regulation of epidermal stratification and development by basal keratinocytes. J Cell Physiol, 2023. **238**(4): p. 742-748.
10. Cohen, E., et al., Revisiting the significance of keratin expression in complex epithelia. J Cell Sci, 2022. **135**(20).
11. Bickenbach, J.R., et al., Loricrin expression is coordinated with other epidermal proteins and the appearance of lipid lamellar granules in development. J Invest Dermatol, 1995. **104**(3): p. 405-10.
12. Menon, G.K., S. Grayson, and P.M. Elias, Ionic calcium reservoirs in mammalian epidermis: ultrastructural localization by ion-capture cytochemistry. J Invest Dermatol, 1985. **84**(6): p. 508-12.
13. Lee, S.H., et al., Calcium and potassium are important regulators of barrier homeostasis in murine epidermis. J Clin Invest, 1992. **89**(2): p. 530-8.
14. Soares, E. and H. Zhou, Master regulatory role of p63 in epidermal development and disease. Cell Mol Life Sci, 2018. **75**(7): p. 1179-1190.
15. Truong, A.B., et al., p63 regulates proliferation and differentiation of developmentally mature keratinocytes. Genes Dev, 2006. **20**(22): p. 3185-97.
16. Carroll, D.K., et al., p63 regulates an adhesion programme and cell survival in epithelial cells. Nat Cell Biol, 2006. **8**(6): p. 551-61.
17. Kouwenhoven, E.N., H. van Bokhoven, and H. Zhou, Gene regulatory mechanisms orchestrated by p63 in epithelial development and related disorders. Biochim Biophys Acta, 2015. **1849**(6): p. 590-600.
18. Sapuntsova, S.G., et al., Proliferative processes in the epidermis of patients with atopic dermatitis treated with thymodepressin. Bull Exp Biol Med, 2002. **133**(5): p. 488-90.
19. Niehues, H., et al., Identification of Keratinocyte Mitogens: Implications for Hyperproliferation in Psoriasis and Atopic Dermatitis. JID Innov, 2022. **2**(1): p. 100066.
20. Trautmann, A., et al., T cell-mediated Fas-induced keratinocyte apoptosis plays a key pathogenetic role in eczematous dermatitis. J Clin Invest, 2000. **106**(1): p. 25-35.
21. Grewe, M., et al., Lesional expression of interferon-gamma in atopic eczema. Lancet, 1994. **343**(8888): p. 25-6.

22. Facheris, P., et al., Age of onset defines two distinct profiles of atopic dermatitis in adults. Allergy, 2023. **78**(8): p. 2202-2214.
23. Czarnowicki, T., et al., Atopic dermatitis endotypes and implications for targeted therapeutics. J Allergy Clin Immunol, 2019. **143**(1): p. 1-11.
24. Kamsteeg, M., et al., Type 2 helper T-cell cytokines induce morphologic and molecular characteristics of atopic dermatitis in human skin equivalent. Am J Pathol, 2011. **178**(5): p. 2091-9.
25. Matsue, H., et al., Keratinocytes constitutively express the Fas antigen that mediates apoptosis in IFN gamma-treated cultured keratinocytes. Arch Dermatol Res, 1995. **287**(3-4): p. 315-20.
26. Tanei, R. and Y. Hasegawa, Immunological Pathomechanisms of Spongiotic Dermatitis in Skin Lesions of Atopic Dermatitis. Int J Mol Sci, 2022. **23**(12).
27. Ohtani, T., et al., Increased hyaluronan production and decreased E-cadherin expression by cytokine-stimulated keratinocytes lead to spongiosis formation. J Invest Dermatol, 2009. **129**(6): p. 1412-20.
28. Guttman-Yassky, E., K.E. Nograles, and J.G. Krueger, Contrasting pathogenesis of atopic dermatitis and psoriasis--part I: clinical and pathologic concepts. J Allergy Clin Immunol, 2011. **127**(5): p. 1110-8.
29. Kirschner, N., et al., Tight junctions form a barrier in human epidermis. Eur J Cell Biol, 2010. **89**(11): p. 839-42.
30. López, O., et al., New arrangement of proteins and lipids in the stratum corneum cornified envelope. Biochim Biophys Acta, 2007. **1768**(3): p. 521-9.
31. van Smeden, J. and J.A. Bouwstra, Stratum Corneum Lipids: Their Role for the Skin Barrier Function in Healthy Subjects and Atopic Dermatitis Patients. Curr Probl Dermatol, 2016. **49**: p. 8-26.
32. Steinert, P.M., et al., Characterization of a class of cationic proteins that specifically interact with intermediate filaments. Proc Natl Acad Sci U S A, 1981. **78**(7): p. 4097-101.
33. Steinert, P.M. and L.N. Marekov, The proteins elafin, filaggrin, keratin intermediate filaments, loricrin, and small proline-rich proteins 1 and 2 are isodipeptide cross-linked components of the human epidermal cornified cell envelope. J Biol Chem, 1995. **270**(30): p. 17702-11.
34. Matsuki, M., et al., Defective stratum corneum and early neonatal death in mice lacking the gene for transglutaminase 1 (keratinocyte transglutaminase). Proc Natl Acad Sci U S A, 1998. **95**(3): p. 1044-9.
35. Kezic, S., et al., Loss-of-function mutations in the filaggrin gene lead to reduced level of natural moisturizing factor in the stratum corneum. J Invest Dermatol, 2008. **128**(8): p. 2117-9.
36. Jungersted, J.M., et al., Stratum corneum lipids, skin barrier function and filaggrin mutations in patients with atopic eczema. Allergy, 2010. **65**(7): p. 911-8.
37. Simanski, M., et al., The Inflammasome and the Epidermal Growth Factor Receptor (EGFR) Are Involved in the Staphylococcus aureus-Mediated Induction of IL-1alpha and IL-1beta in Human Keratinocytes. PLoS One, 2016. **11**(1): p. e0147118.
38. Lai, Y., et al., Activation of TLR2 by a small molecule produced by Staphylococcus epidermidis increases antimicrobial defense against bacterial skin infections. J Invest Dermatol, 2010. **130**(9): p. 2211-21.
39. Sørensen, O.E., et al., Differential regulation of beta-defensin expression in human skin by microbial stimuli. J Immunol, 2005. **174**(8): p. 4870-9.
40. Niehues, H., et al., CYSRT1: An Antimicrobial Epidermal Protein that Can Interact with Late Cornified Envelope Proteins. J Invest Dermatol, 2023. **143**(8): p. 1498-1508.e7.
41. Niehues, H., et al., Psoriasis-Associated Late Cornified Envelope (LCE) Proteins Have Antibacterial Activity. J Invest Dermatol, 2017. **137**(11): p. 2380-2388.

42. Montero-Vilchez, T., et al., Skin Barrier Function in Psoriasis and Atopic Dermatitis: Transepidermal Water Loss and Temperature as Useful Tools to Assess Disease Severity. J Clin Med, 2021. **10**(2).
43. Wang, S., et al., Either transepidermal water loss rates or stratum corneum hydration levels can predict quality of life in children with atopic dermatitis. Pediatr Investig, 2021. **5**(4): p. 277-280.
44. Polańska, A., et al., Nonlesional skin in atopic dermatitis is seemingly healthy skin - observations using noninvasive methods. Wideochir Inne Tech Maloinwazyjne, 2013. **8**(3): p. 192-9.
45. Rinaldi, A.O., et al., Electrical impedance spectroscopy for the characterization of skin barrier in atopic dermatitis. Allergy, 2021. **76**(10): p. 3066-3079.
46. Sasaki, M., et al., Electrical impedance spectroscopy detects skin barrier dysfunction in childhood atopic dermatitis. Allergy, 2024. **79**(1): p. 142-152.
47. Gruber, R., et al., Filaggrin genotype in ichthyosis vulgaris predicts abnormalities in epidermal structure and function. Am J Pathol, 2011. **178**(5): p. 2252-63.
48. Nouwen, A.E.M., et al., Natural moisturizing factor as a clinical marker in atopic dermatitis. Allergy, 2020. **75**(1): p. 188-190.
49. Basu, M.N., et al., Natural moisturizing factors in children with and without eczema: Associations with lifestyle and genetic factors. J Eur Acad Dermatol Venereol, 2022. **36**(2): p. 255-262.
50. Proksch, E., et al., Dry skin management: practical approach in light of latest research on skin structure and function. J Dermatolog Treat, 2020. **31**(7): p. 716-722.
51. Bergmann, S., et al., Claudin-1 decrease impacts epidermal barrier function in atopic dermatitis lesions dose-dependently. Sci Rep, 2020. **10**(1): p. 2024.
52. Batista, D.I., et al., Profile of skin barrier proteins (filaggrin, claudins 1 and 4) and Th1/Th2/Th17 cytokines in adults with atopic dermatitis. J Eur Acad Dermatol Venereol, 2015. **29**(6): p. 1091-5.
53. Gruber, R., et al., Diverse regulation of claudin-1 and claudin-4 in atopic dermatitis. Am J Pathol, 2015. **185**(10): p. 2777-89.
54. Yuki, T., et al., Impaired tight junctions obstruct stratum corneum formation by altering polar lipid and profilaggrin processing. J Dermatol Sci, 2013. **69**(2): p. 148-58.
55. Berdyshev, E., et al., Lipid abnormalities in atopic skin are driven by type 2 cytokines. JCI Insight, 2018. **3**(4).
56. Ishikawa, J., et al., Changes in the ceramide profile of atopic dermatitis patients. J Invest Dermatol, 2010. **130**(10): p. 2511-4.
57. Janssens, M., et al., Increase in short-chain ceramides correlates with an altered lipid organization and decreased barrier function in atopic eczema patients. J Lipid Res, 2012. **53**(12): p. 2755-66.
58. Macheleidt, O., H.W. Kaiser, and K. Sandhoff, Deficiency of epidermal protein-bound omega-hydroxyceramides in atopic dermatitis. J Invest Dermatol, 2002. **119**(1): p. 166-73.
59. van Smeden, J., et al., The importance of free fatty acid chain length for the skin barrier function in atopic eczema patients. Exp Dermatol, 2014. **23**(1): p. 45-52.
60. Li, S., et al., Altered composition of epidermal lipids correlates with Staphylococcus aureus colonization status in atopic dermatitis. Br J Dermatol, 2017. **177**(4): p. e125-e127.
61. Di Nardo, A., et al., Ceramide and cholesterol composition of the skin of patients with atopic dermatitis. Acta Derm Venereol, 1998. **78**(1): p. 27-30.
62. Angelova-Fischer, I., et al., Distinct barrier integrity phenotypes in filaggrin-related atopic eczema following sequential tape stripping and lipid profiling. Exp Dermatol, 2011. **20**(4): p. 351-6.
63. Langan, S.M., et al., Increased Risk of Cutaneous and Systemic Infections in Atopic Dermatitis-A Cohort Study. J Invest Dermatol, 2017. **137**(6): p. 1375-1377.

64. Sator, P.G., J.B. Schmidt, and H. Hönigsmann, Comparison of epidermal hydration and skin surface lipids in healthy individuals and in patients with atopic dermatitis. J Am Acad Dermatol, 2003. **48**(3): p. 352-8.
65. Hon, K.L., et al., Comparison of skin hydration evaluation sites and correlations among skin hydration, transepidermal water loss, SCORAD index, Nottingham Eczema Severity Score, and quality of life in patients with atopic dermatitis. Am J Clin Dermatol, 2008. **9**(1): p. 45-50.
66. Brook, I., E.H. Frazier, and J.K. Yeager, Microbiology of infected atopic dermatitis. Int J Dermatol, 1996. **35**(11): p. 791-3.
67. Ong, P.Y., et al., Endogenous antimicrobial peptides and skin infections in atopic dermatitis. N Engl J Med, 2002. **347**(15): p. 1151-60.
68. Nomura, I., et al., Cytokine milieu of atopic dermatitis, as compared to psoriasis, skin prevents induction of innate immune response genes. J Immunol, 2003. **171**(6): p. 3262-9.
69. Ahmad-Nejad, P., et al., The toll-like receptor 2 R753Q polymorphism defines a subgroup of patients with atopic dermatitis having severe phenotype. J Allergy Clin Immunol, 2004. **113**(3): p. 565-7.
70. Zdolsek, H.A. and M.C. Jenmalm, Reduced levels of soluble CD14 in atopic children. Clin Exp Allergy, 2004. **34**(4): p. 532-9.
71. Weidinger, S., et al., Association of NOD1 polymorphisms with atopic eczema and related phenotypes. J Allergy Clin Immunol, 2005. **116**(1): p. 177-84.
72. Liang, Y., C. Chang, and Q. Lu, The Genetics and Epigenetics of Atopic Dermatitis-Filaggrin and Other Polymorphisms. Clin Rev Allergy Immunol, 2016. **51**(3): p. 315-328.
73. Dębińska, A., H. Danielewicz, and B. Sozańska, Genetic Variants in Epidermal Differentiation Complex Genes as Predictive Biomarkers for Atopic Eczema, Allergic Sensitization, and Eczema-Associated Asthma in a 6-Year Follow-Up Case-Control Study in Children. J Clin Med, 2022. **11**(16).
74. Greisenegger, E.K., et al., Association of the chromosome 11q13.5 variant with atopic dermatitis in Austrian patients. Eur J Dermatol, 2013. **23**(2): p. 142-5.
75. Palmer, C.N., et al., Common loss-of-function variants of the epidermal barrier protein filaggrin are a major predisposing factor for atopic dermatitis. Nat Genet, 2006. **38**(4): p. 441-6.
76. Rodríguez, E., et al., Meta-analysis of filaggrin polymorphisms in eczema and asthma: robust risk factors in atopic disease. J Allergy Clin Immunol, 2009. **123**(6): p. 1361-70.e7.
77. Baurecht, H., et al., Toward a major risk factor for atopic eczema: meta-analysis of filaggrin polymorphism data. J Allergy Clin Immunol, 2007. **120**(6): p. 1406-12.
78. Beck, L.A., et al., Type 2 Inflammation Contributes to Skin Barrier Dysfunction in Atopic Dermatitis. JID Innov, 2022. **2**(5): p. 100131.
79. He, H., et al., Tape strips detect distinct immune and barrier profiles in atopic dermatitis and psoriasis. J Allergy Clin Immunol, 2021. **147**(1): p. 199-212.
80. Gittler, J.K., et al., Progressive activation of T(H)2/T(H)22 cytokines and selective epidermal proteins characterizes acute and chronic atopic dermatitis. J Allergy Clin Immunol, 2012. **130**(6): p. 1344-54.
81. Renert-Yuval, Y., et al., The molecular features of normal and atopic dermatitis skin in infants, children, adolescents, and adults. J Allergy Clin Immunol, 2021. **148**(1): p. 148-163.
82. Facheris, P., et al., The translational revolution in atopic dermatitis: the paradigm shift from pathogenesis to treatment. Cell Mol Immunol, 2023. **20**(5): p. 448-474.
83. Oh, J.H., et al., Purpurin suppresses atopic dermatitis via TNF-α/IFN-γ-induced inflammation in HaCaT cells. Int J Immunopathol Pharmacol, 2022. **36**: p. 3946320221111135.

84. Pastore, S., et al., Interferon-gamma promotes exaggerated cytokine production in keratinocytes cultured from patients with atopic dermatitis. J Allergy Clin Immunol, 1998. **101**(4 Pt 1): p. 538-44.
85. Mizuno, K., et al., Dexamethasone but not tacrolimus suppresses TNF-α-induced thymic stromal lymphopoietin expression in lesional keratinocytes of atopic dermatitis model. J Dermatol Sci, 2015. **80**(1): p. 45-53.
86. Bahar-Shany, K., A. Ravid, and R. Koren, Upregulation of MMP-9 production by TNFalpha in keratinocytes and its attenuation by vitamin D. J Cell Physiol, 2010. **222**(3): p. 729-37.
87. Young, C.N., et al., Reactive oxygen species in tumor necrosis factor-alpha-activated primary human keratinocytes: implications for psoriasis and inflammatory skin disease. J Invest Dermatol, 2008. **128**(11): p. 2606-2614.
88. Banno, T., A. Gazel, and M. Blumenberg, Effects of tumor necrosis factor-alpha (TNF alpha) in epidermal keratinocytes revealed using global transcriptional profiling. J Biol Chem, 2004. **279**(31): p. 32633-42.
89. Reinartz, J., M.J. Bechtel, and M.D. Kramer, Tumor necrosis factor-alpha-induced apoptosis in a human keratinocyte cell line (HaCaT) is counteracted by transforming growth factor-alpha. Exp Cell Res, 1996. **228**(2): p. 334-40.
90. Zimmermann, M., et al., TNF-like weak inducer of apoptosis (TWEAK) and TNF-α cooperate in the induction of keratinocyte apoptosis. J Allergy Clin Immunol, 2011. **127**(1): p. 200-7, 207.e1-10.
91. Montes-Torres, A., et al., Biological Treatments in Atopic Dermatitis. J Clin Med, 2015. **4**(4): p. 593-613.
92. Esmailzadeh, A., et al., Predictive factors of eczema-like eruptions among patients without cutaneous psoriasis receiving infliximab: a cohort study of 92 patients. Dermatology, 2009. **219**(3): p. 263-7.
93. Pagan, A.D., et al., Atopic dermatitis induced during anti-TNF-α therapy for inflammatory bowel disease: Potential for Th2 inhibition with dupilumab. J Allergy Clin Immunol Pract, 2023. **11**(7): p. 2235-2238.e1.
94. Hongqin, T., et al., Triptolide inhibits IFN-γ signaling via the Jak/STAT pathway in HaCaT keratinocytes. Phytother Res, 2011. **25**(11): p. 1678-85.
95. Sung, Y.Y. and H.K. Kim, Illicium verum extract suppresses IFN-γ-induced ICAM-1 expression via blockade of JAK/STAT pathway in HaCaT human keratinocytes. J Ethnopharmacol, 2013. **149**(3): p. 626-32.
96. Federici, M., et al., Impaired IFN-gamma-dependent inflammatory responses in human keratinocytes overexpressing the suppressor of cytokine signaling 1. J Immunol, 2002. **169**(1): p. 434-42.
97. Kanda, N., et al., IL-18 enhances IFN-gamma-induced production of CXCL9, CXCL10, and CXCL11 in human keratinocytes. Eur J Immunol, 2007. **37**(2): p. 338-50.
98. Mizutani, Y., et al., Interferon-γ downregulates tight junction function, which is rescued by interleukin-17A. Exp Dermatol, 2021. **30**(12): p. 1754-1763.
99. Brar, K. and D.Y. Leung, Recent considerations in the use of recombinant interferon gamma for biological therapy of atopic dermatitis. Expert Opin Biol Ther, 2016. **16**(4): p. 507-14.
100. Bao, L., V.Y. Shi, and L.S. Chan, IL-4 regulates chemokine CCL26 in keratinocytes through the Jak1, 2/Stat6 signal transduction pathway: Implication for atopic dermatitis. Mol Immunol, 2012. **50**(1-2): p. 91-7.

101. Bao, L., V.Y. Shi, and L.S. Chan, IL-4 up-regulates epidermal chemotactic, angiogenic, and pro-inflammatory genes and down-regulates antimicrobial genes in vivo and in vitro: relevant in the pathogenesis of atopic dermatitis. Cytokine, 2013. **61**(2): p. 419-25.
102. Kim, B.E., et al., Loricrin and involucrin expression is down-regulated by Th2 cytokines through STAT-6. Clin Immunol, 2008. **126**(3): p. 332-7.
103. Amano, W., et al., The Janus kinase inhibitor JTE-052 improves skin barrier function through suppressing signal transducer and activator of transcription 3 signaling. J Allergy Clin Immunol, 2015. **136**(3): p. 667-677.e7.
104. Boesjes, C.M., et al., Long-Term Effectiveness and Reasons for Discontinuation of Dupilumab in Patients With Atopic Dermatitis. JAMA Dermatol, 2024. **160**(10): p. 1044-1055.
105. Beck, L.A., et al., Dupilumab in Adults With Moderate to Severe Atopic Dermatitis: A 5-Year Open-Label Extension Study. JAMA Dermatol, 2024. **160**(8): p. 805-812.
106. Subramaniam, S.V., R.S. Cooper, and S.E. Adunyah, Evidence for the involvement of JAK/STAT pathway in the signaling mechanism of interleukin-17. Biochem Biophys Res Commun, 1999. **262**(1): p. 14-9.
107. Shi, X., et al., IL-17A upregulates keratin 17 expression in keratinocytes through STAT1- and STAT3-dependent mechanisms. J Invest Dermatol, 2011. **131**(12): p. 2401-8.
108. Boniface, K., et al., IL-22 inhibits epidermal differentiation and induces proinflammatory gene expression and migration of human keratinocytes. J Immunol, 2005. **174**(6): p. 3695-702.
109. Wolk, K., et al., IL-22 regulates the expression of genes responsible for antimicrobial defense, cellular differentiation, and mobility in keratinocytes: a potential role in psoriasis. Eur J Immunol, 2006. **36**(5): p. 1309-23.
110. Wolk, K., et al., IL-22 and IL-20 are key mediators of the epidermal alterations in psoriasis while IL-17 and IFN-gamma are not. J Mol Med (Berl), 2009. **87**(5): p. 523-36.
111. Ha, H.L., et al., IL-17 drives psoriatic inflammation via distinct, target cell-specific mechanisms. Proc Natl Acad Sci U S A, 2014. **111**(33): p. e3422-31.
112. Sato, E., et al., Interleukin-17A suppresses granular layer formation in a 3-D human epidermis model through regulation of terminal differentiation genes. J Dermatol, 2020. **47**(4): p. 390-396.
113. Hata, T.R. and R.L. Gallo, Antimicrobial peptides, skin infections, and atopic dermatitis. Semin Cutan Med Surg, 2008. **27**(2): p. 144-50.
114. Byrd, A.L., Y. Belkaid, and J.A. Segre, The human skin microbiome. Nat Rev Microbiol, 2018. **16**(3): p. 143-155.
115. Zeeuwen, P.L., et al., Gram-positive anaerobe cocci are underrepresented in the microbiome of filaggrin-deficient human skin. J Allergy Clin Immunol, 2017. **139**(4): p. 1368-1371.
116. Bjerre, R.D., et al., Skin dysbiosis in the microbiome in atopic dermatitis is site-specific and involves bacteria, fungus and virus. BMC Microbiol, 2021. **21**(1): p. 256.
117. Leyden, J.J., R.R. Marples, and A.M. Kligman, Staphylococcus aureus in the lesions of atopic dermatitis. Br J Dermatol, 1974. **90**(5): p. 525-30.
118. van der Krieken, D.A., et al., Gram-positive anaerobic cocci guard skin homeostasis by regulating host-defense mechanisms. iScience, 2023. **26**(4): p. 106483.
119. de Koning, H.D., et al., Pattern recognition receptors in infectious skin diseases. Microbes Infect, 2012. **14**(11): p. 881-93.
120. Jiang, Y., et al., Cytokinocytes: the diverse contribution of keratinocytes to immune responses in skin. JCI Insight, 2020. **5**(20): p. e142067.

121. Coates, M., S. Blanchard, and A.S. MacLeod, Innate antimicrobial immunity in the skin: A protective barrier against bacteria, viruses, and fungi. PLoS Pathog, 2018. **14**(12): p. e1007353.

122. de Koning, H.D., et al., Pattern recognition receptors in immune disorders affecting the skin. J Innate Immun, 2012. **4**(3): p. 225-40.

123. Magiatis, P., et al., Malassezia yeasts produce a collection of exceptionally potent activators of the Ah (dioxin) receptor detected in diseased human skin. J Invest Dermatol, 2013. **133**(8): p. 2023-30.

124. Rademacher, F., et al., Staphylococcus epidermidis Activates Aryl Hydrocarbon Receptor Signaling in Human Keratinocytes: Implications for Cutaneous Defense. J Innate Immun, 2019. **11**(2): p. 125-135.

125. Yu, J., et al., A tryptophan metabolite of the skin microbiota attenuates inflammation in patients with atopic dermatitis through the aryl hydrocarbon receptor. J Allergy Clin Immunol, 2019. **143**(6): p. 2108-2119.e12.

126. van den Bogaard, E.H., et al., Coal tar induces AHR-dependent skin barrier repair in atopic dermatitis. J Clin Invest, 2013. **123**(2): p. 917-27.

127. Reyes, H., S. Reisz-Porszasz, and O. Hankinson, Identification of the Ah receptor nuclear translocator protein (Arnt) as a component of the DNA binding form of the Ah receptor. Science, 1992. **256**(5060): p. 1193-5.

128. van den Bogaard, E.H., et al., Genetic and pharmacological analysis identifies a physiological role for the AHR in epidermal differentiation. J Invest Dermatol, 2015. **135**(5): p. 1320-1328.

129. Sutter, C.H., et al., 2,3,7,8-Tetrachlorodibenzo-p-dioxin increases the expression of genes in the human epidermal differentiation complex and accelerates epidermal barrier formation. Toxicol Sci, 2011. **124**(1): p. 128-37.

130. Smith, S.H., et al., Tapinarof Is a Natural AhR Agonist that Resolves Skin Inflammation in Mice and Humans. J Invest Dermatol, 2017. **137**(10): p. 2110-2119.

131. Slutsky, J.B., et al., An evidence-based review of the efficacy of coal tar preparations in the treatment of psoriasis and atopic dermatitis. J Drugs Dermatol, 2010. **9**(10): p. 1258-64.

132. Silverberg, J.I., et al., Tapinarof cream 1% once daily: Significant efficacy in the treatment of moderate to severe atopic dermatitis in adults and children down to 2 years of age in the pivotal phase 3 ADORING trials. J Am Acad Dermatol, 2024. **91**(3): p. 457-465.

133. Kobayashi, T., et al., Dysbiosis and Staphylococcus aureus Colonization Drives Inflammation in Atopic Dermatitis. Immunity, 2015. **42**(4): p. 756-66.

134. Nakatsuji, T., et al., Staphylococcus aureus Exploits Epidermal Barrier Defects in Atopic Dermatitis to Trigger Cytokine Expression. J Invest Dermatol, 2016. **136**(11): p. 2192-2200.

135. Deng, L., et al., S. aureus drives itch and scratch-induced skin damage through a V8 protease-PAR1 axis. Cell, 2023. **186**(24): p. 5375-5393.e25.

136. Gallo, R.L. and A.R. Horswill, Staphylococcus aureus: The Bug Behind the Itch in Atopic Dermatitis. J Invest Dermatol, 2024. **144**(5): p. 950-953.

137. Niehues, H., et al., Epidermal equivalents of filaggrin null keratinocytes do not show impaired skin barrier function. J Allergy Clin Immunol, 2017. **139**(6): p. 1979-1981.e13.

138. Boukamp, P., et al., Normal keratinization in a spontaneously immortalized aneuploid human keratinocyte cell line. J Cell Biol, 1988. **106**(3): p. 761-71.

139. Mini, C.A., et al., Immortalized equivalent human epidermis as a platform to evaluation hair dyes toxicity: Efficiency comparison between 3D and monolayer culture. Chem Biol Interact, 2020. **330**: p. 109227.

140. Boelsma, E., M.C. Verhoeven, and M. Ponec, Reconstruction of a human skin equivalent using a spontaneously transformed keratinocyte cell line (HaCaT). J Invest Dermatol, 1999. **112**(4): p. 489-98.
141. Dickson, M.A., et al., Human keratinocytes that express hTERT and also bypass a p16(INK4a)-enforced mechanism that limits life span become immortal yet retain normal growth and differentiation characteristics. Mol Cell Biol, 2000. **20**(4): p. 1436-47.
142. Smits, J.P.H., et al., Immortalized N/TERT keratinocytes as an alternative cell source in 3D human epidermal models. Sci Rep, 2017. **7**(1): p. 11838.
143. van Drongelen, V., et al., Barrier properties of an N/TERT-based human skin equivalent. Tissue Eng Part A, 2014. **20**(21-22): p. 3041-9.
144. Moran, M.C., et al., Characterization of Human Keratinocyte Cell Lines for Barrier Studies. JID Innov, 2021. **1**(2): p. 100018.
145. Research, N.R.C.U.a.I.o.M.U.C.o.t.B.a.B.A.o.S.C., CHAPTER THREE Embryonic Stem Cells, in Stem Cells and the Future of Regenerative Medicine, N.A.P. (US), Editor. 2002: https://www.ncbi.nlm.nih.gov/books/NBK223690/.
146. Takahashi, K. and S. Yamanaka, Induction of pluripotent stem cells from mouse embryonic and adult fibroblast cultures by defined factors. Cell, 2006. **126**(4): p. 663-76.
147. Jacków, J., et al., CRISPR/Cas9-based targeted genome editing for correction of recessive dystrophic epidermolysis bullosa using iPS cells. Proc Natl Acad Sci U S A, 2019. **116**(52): p. 26846-26852.
148. Itoh, M., et al., Footprint-free gene mutation correction in induced pluripotent stem cell (iPSC) derived from recessive dystrophic epidermolysis bullosa (RDEB) using the CRISPR/Cas9 and piggyBac transposon system. J Dermatol Sci, 2020. **98**(3): p. 163-172.
149. Devito, L., et al., Induced pluripotent stem cell line from an atopic dermatitis patient heterozygous for c.2282del4 mutation in filaggrin: KCLi001-A. Stem Cell Res, 2018. **31**: p. 122-126.
150. Itoh, M., et al., Generation of keratinocytes from normal and recessive dystrophic epidermolysis bullosa-induced pluripotent stem cells. Proc Natl Acad Sci U S A, 2011. **108**(21): p. 8797-802.
151. Ruiz-Torres, S., et al., Directed differentiation of human pluripotent stem cells into epidermal stem and progenitor cells. Mol Biol Rep, 2021. **48**(8): p. 6213-6222.
152. Kajiwara, K., et al., Fetal Therapy Model of Myelomeningocele with Three-Dimensional Skin Using Amniotic Fluid Cell-Derived Induced Pluripotent Stem Cells. Stem Cell Reports, 2017. **8**(6): p. 1701-1713.
153. Petrova, A., et al., 3D In vitro model of a functional epidermal permeability barrier from human embryonic stem cells and induced pluripotent stem cells. Stem Cell Reports, 2014. **2**(5): p. 675-89.
154. Wanke, I., et al., Skin commensals amplify the innate immune response to pathogens by activation of distinct signaling pathways. J Invest Dermatol, 2011. **131**(2): p. 382-90.
155. Bikle, D.D., Z. Xie, and C.L. Tu, Calcium regulation of keratinocyte differentiation. Expert Rev Endocrinol Metab, 2012. **7**(4): p. 461-472.
156. Borowiec, A.S., et al., Optimal differentiation of in vitro keratinocytes requires multifactorial external control. PLoS One, 2013. **8**(10): p. e77507.
157. Niehues, H., et al., 3D skin models for 3R research: The potential of 3D reconstructed skin models to study skin barrier function. Exp Dermatol, 2018. **27**(5): p. 501-511.
158. Rikken, G., H. Niehues, and E.H. van den Bogaard, Organotypic 3D Skin Models: Human Epidermal Equivalent Cultures from Primary Keratinocytes and Immortalized Keratinocyte Cell Lines. Methods Mol Biol, 2020. **2154**: p. 45-61.

159. Quílez, C., et al., Targeting the Complexity of In Vitro Skin Models: A Review of Cutting-Edge Developments. J Invest Dermatol, 2024. **144**(12): p. 2650-2670.

160. De Vuyst, É., et al., Methyl-β-cyclodextrin concurs with interleukin (IL)-4, IL-13 and IL-25 to induce alterations reminiscent of atopic dermatitis in reconstructed human epidermis. Exp Dermatol, 2018. **27**(4): p. 435-437.

161. Castex-Rizzi, N., et al., In vitro approaches to pharmacological screening in the field of atopic dermatitis. Br J Dermatol, 2014. **170 Suppl 1**: p. 12-8.

162. Danso, M.O., et al., TNF-α and Th2 cytokines induce atopic dermatitis-like features on epidermal differentiation proteins and stratum corneum lipids in human skin equivalents. J Invest Dermatol, 2014. **134**(7): p. 1941-1950.

163. Hubaux, R., C. Bastin, and M. Salmon, On the relevance of an in vitro reconstructed human epidermis model for drug screening in atopic dermatitis. Exp Dermatol, 2018. **27**(12): p. 1403-1407.

164. Bernard, F.X., et al., Keratinocytes under Fire of Proinflammatory Cytokines: Bona Fide Innate Immune Cells Involved in the Physiopathology of Chronic Atopic Dermatitis and Psoriasis. J Allergy (Cairo), 2012. **2012**: p. 718725.

165. Rouaud-Tinguely, P., et al., From the morphological to the transcriptomic characterization of a compromised three-dimensional in vitro model mimicking atopic dermatitis. Br J Dermatol, 2015. **173**(4): p. 1006-14.

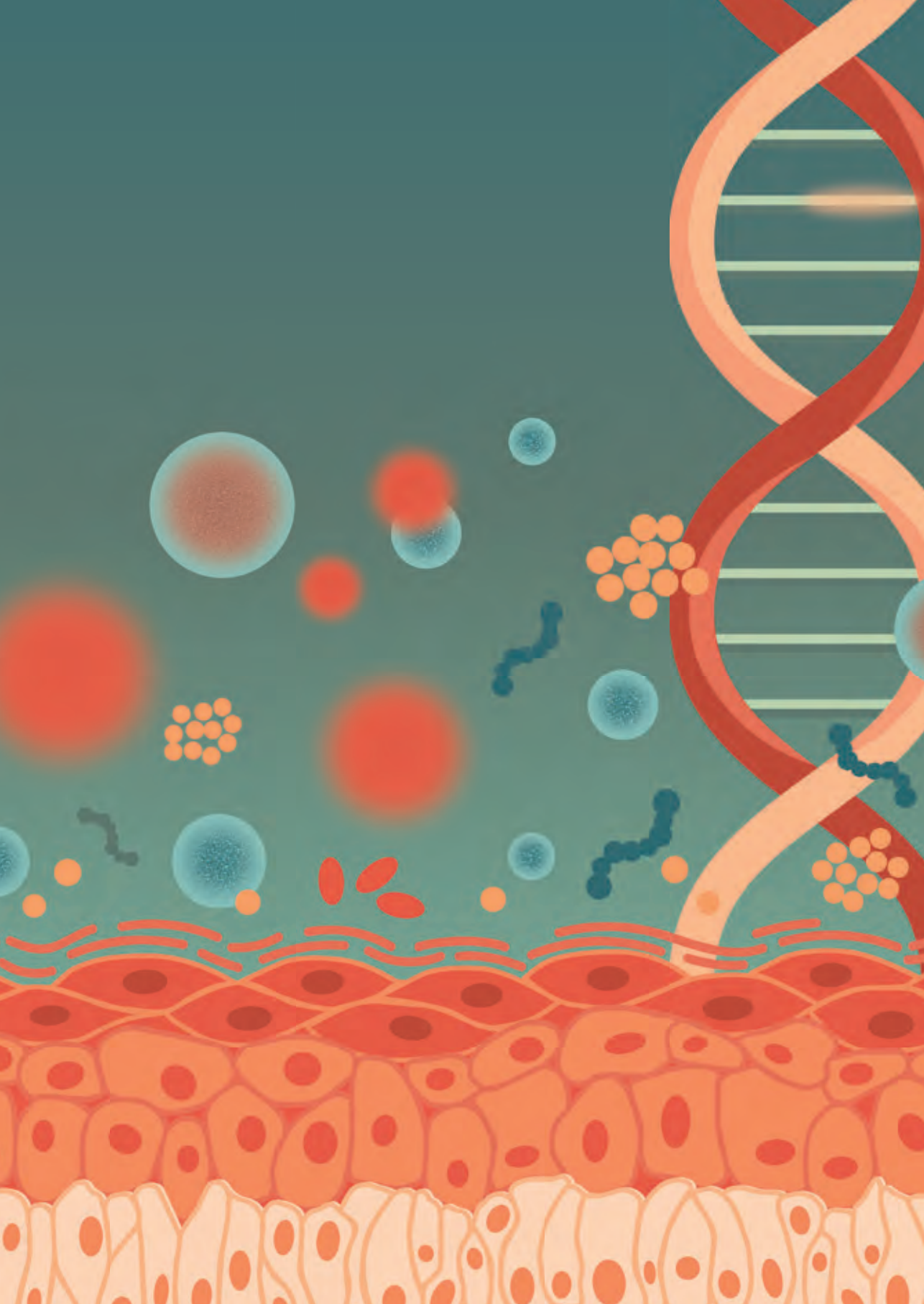

Chapter 2.

Keratinocyte signaling in atopic dermatitis: Investigations in organotypic skin models toward clinical application

Luca D. Meesters[1], Hanna Niehues[1], Luke Johnston[2], Jos P.H. Smits[1], Patrick L.J.M. Zeeuwen[1], Sara J. Brown[2], and Ellen H. van den Bogaard[1]

Affiliations

[1] Department of Dermatology, Radboud University Medical Center (Radboudumc), Nijmegen, The Netherlands

[2] Centre for Genomic and Experimental Medicine, University of Edinburgh, Edinburgh, Scotland, UK

Published in

J Allergy Clin Immunol. 2023 May;151(5):1231-1235. doi: 10.1016/j.jaci.2023.02.012.

The epidermal barrier in atopic dermatitis

Atopic dermatitis (AD) is a common complex chronic inflammatory skin disease. Notwithstanding the key contribution of immune-mediated disease factors, ever since the identification of *filaggrin* (*FLG*) loss-of-function mutations as a major predisposing factor for AD, epidermal barrier defects have been one important initiating factor of the disease based on the inside-out and outside-in barrier hypothesis. Most therapeutic agents target immune cells, cytokines, or related signaling pathways. The importance of more direct skin barrier-supporting therapies has recently been tested in multiple studies aimed at reducing the risk or delaying the onset of AD by using emollient application in early infancy. Although pilot work and some subsequent studies have suggested that emollients may protect against AD, Kelleher *et al*. (2021) performed a meta-analysis of larger cohorts and did not detect a preventive effect. Instead, emollients appear to increase skin infections and may also increase allergic sensitization to food. For future studies, an evidence-based consensus opinion regarding the type of emollient to be used (*e.g.,* petrolatum-based, or defined ceramide-based) and the appropriate timing of the start of intervention are required. Investigative studies toward better understanding of epidermal signaling events that contribute to atopic inflammation may fill the current knowledge gap regarding keratinocyte-specific druggable targets per disease endotype.

Epidermal keratinocytes contribute to the physical skin barrier function by controlling skin permeation and water evaporation via networks of structural proteins, including cross-linked FLG and tight junctions of claudins and occludins and the biosynthesis of a myriad of lipids required for proper *stratum corneum* (SC) formation. Multi-omics (single-cell) analysis of skin biopsy samples or SC tapes have elucidated genotype (*FLG*)-specific transcriptome changes in lesional and nonlesional skin. Olah *et al*. (2022) found more deregulated immune-related genes in patients with wild-type *FLG*, and less transcriptomic deregulation and skin barrier-related differential gene expression in patients with *FLG* mutations. *FLG* mutations could therefore lower the skin's threshold for developing AD. Analyzing the first keratinocyte-specific transcriptome by laser dissection allowed for pinpointing deregulated transcription in AD keratinocytes. A complex immune signature of not only Th2 cell-driven but also strong Th17 and Th22 cell-driven marker genes and a clear deregulation of specific tight junction genes has been found in the epidermis [1]. Building on the first single-cell transcriptomic analysis of AD lesional skin [2], emerging bioinformatic tools and disease maps help future scrutinization of AD-related keratinocyte signaling and the key factors involved.

Keratinocytes function as crucial innate immune cells in the first line of defense and regulate adaptive immune responses. Through cytokine and chemokine production, keratinocytes draw effector and regulatory immune cells into the skin and influence immune cell plasticity and polarization. In addition, keratinocytes drive the chemical and microbial barrier function with key roles for FLG: i) FLG peptides and their breakdown products regulate skin pH, ii) FLG (and its paralogs) may possess antimicrobial activity, and iii) FLG deficiency is associated with lower abundance of commensal gram-positive anaerobic cocci (GPAC), which are postulated to depend on FLG-derived amino acids for their growth [3]. Furthermore, the characteristic alteration in keratinocyte terminal differentiation by the AD inflammatory milieu not only affects SC formation but also putatively influences skin host defense mechanisms, as these major epidermal proteins (*e.g.,* late cornified envelope proteins, FLG, hornerin) were recently coined as cationic intrinsically disordered antimicrobial peptides (CIDAMPs) [4].

To dissect cell- and disease-specific signaling events and pinpoint targets for drug development and screening, preclinical human skin models that recapitulate AD disease mechanisms are of utmost importance. Although *in vivo* animal models may recapitulate the skin's complexity and encompass sequential immunologic responses, organotypic *in vitro* epidermal or full-thickness skin models enable focused studies into disease-related keratinocyte signaling, including those on AD-specific genetics, immunologic responses, skin microbiota, and environmental cues, which will be further discussed later in this article and are illustrated in Figure 1 and 2.

Organotypic skin models for drug target discovery and therapeutic screening

Signaling influenced by genetic factors

At the genomic level, *FLG* loss-of-function mutations pose the strongest risk for development of AD, but many other risk loci have been discovered by genome-wide association studies, as reviewed by Liang (2015) and Brown *et al*. (2021). At the epigenetic level, AD-keratinocytes display changes in DNA methylation status, microRNA expression and histone acetylation (reviewed in Schmidt *et al*. (2021)). To model genetic risk factors in human epidermal equivalents (HEE), human skin equivalents (HSE) or skin organoids, various keratinocyte sources can be utilized including i) primary keratinocytes from patients with known *FLG* null mutations, ii) transient or stable gene knockdown by small interfering (si)RNA or short hairpin (sh)RNA, respectively, iii) CRISPR/Cas9 genome editing in primary or immortalized

(e.g., N/TERT) keratinocyte cell lines, or iv) patient-derived induced pluripotent stem cells (iPSC). Studies on the consequences of FLG deficiency have yielded mostly conflicting results, likely owing to the lack in protocol standardization between research groups and the use of cells with different genetic backgrounds. To identify cause-effect relationships on how (epi)genetic risk factors lead to abnormal keratinocyte signaling and dysfunction, multi-omics technologies are advocated with a focus on the integration of transcription regulation with proteomic and/or lipidomic analyses for functional end-products. Proteomic analysis of *FLG* knockdown organotypic models [5] revealed quantitative changes in networks that are consistent with transcriptome analysis of skin biopsy samples stratified by *FLG* genotype. Similar comparative analyses between publicly available omics data from patient cohorts and experimental organotypic models will help in improvement of model systems and functional validation of identified biomarkers.

Immunologic signaling events

To study keratinocyte-expressed receptor activation, signaling transduction pathways and downstream effects, HEE or HSE can be manipulated by the addition of relevant inflammatory molecules to the culture medium. Traditionally, Th2 cytokines IL-4 and IL-13 have been used to model AD and supplemented with IL-25, IL-31, IL-31 + TNF-α, or IL-22 + TNF-α (reviewed by Das *et al*. (2022)). In principle, the epidermal response to any disease-related cytokine can be dissected *in vitro,* and many signal transduction pathways have thereby been identified (*e.g.,* Janus kinase/signal transducer and activator of transcription (JAK/STAT), MAPK, PI3K/Akt, as recently reviewed by Humeau *et al*. (2022)). With use of this approach, epidermal AD hallmarks including hyperproliferation, spongiosis, impaired differentiation, and SC lipid changes have been successfully modeled. These are targeted by therapeutics that are indicated for AD (*e.g.,* dupilumab, tofacitinib, coal tar, tapinarof). More complex immunocompetent, vascular or even innervated organotypic skin models have attempted to more closely mimic the intercellular cross talk in AD in a 3-dimensional microenvironment. However, this increasing complexity brings additional challenges for reproducibility, and cell viability and function, and it precludes high-throughput screening.

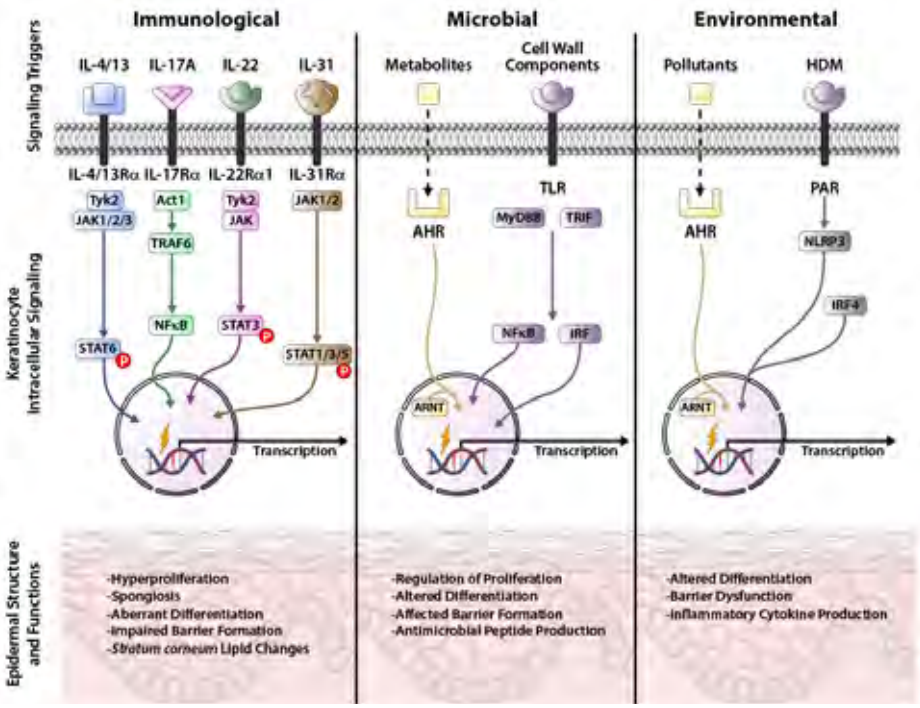

Figure 1. AD-related intracellular epidermal keratinocyte signaling cascades. Keratinocytes contribute to AD pathophysiology via a plethora of intracellular signaling cascades based on genetic, immunologic, microbial, or environmental cues. Here we illustrate a few important genes, ligands and receptors, but we also appreciate that these can represent only the tip of the iceberg. Interactions between disease-related cytokines and keratinocyte-expressed receptors and the resulting immunologic signal transduction pathways that regulate gene transcription have been extensively studied, successfully targeted by therapeutics, and reviewed in detail. Microbes and their secreted metabolites or cell wall components can trigger epidermal signaling through activation of environmental ligand-activated transcription factors (*e.g.,* AHR) or PPRs (*e.g.,* TLRs). Environmental pollutants can also activate AHR signaling (hence the current debate on beneficial or detrimental effects of AHR activation on skin health), and allergens like HDM activate intracellular PRRs, as exemplified here by NLRP3. These intracellular and extracellular cues may also interact with a person's genetic profile (illustrated by the nuclear lightning strike) and lead to the onset or conservation of pathologic processes, e.g., dysregulation of proliferation and differentiation, induced inflammatory cytokine production, aberrant barrier formation, altered antimicrobial activity, and changes in SC lipid deposition. *Abbreviations: AhR, aryl hydrocarbon receptor; ARNT, Aryl hydrocarbon receptor nuclear translocator; HDM, house dust mite; IL, interleukin; IRF, interferon regulatory factor; JAK, Janus kinase; MyD88, myeloid differentiation primary response 88; NFkB, nuclear factor κ-light-chain enhancer of activated B cells; NLRP3, NLR family pyrin domain containing 3; PAR, protease activated receptor; PRR, pattern recognition receptor; Rα, receptor subunit alpha; STAT, signal transducer and activator of transcription; TLR, toll-like receptor; TRAF, TNF receptor associated factor; TRIF, TIR-domain-containing adapter-inducing interferon-β; Tyk, tyrosine kinase.*

Microbiome-mediated signaling

Although the extent to which microbiome dysbiosis is a cause or consequence of AD remains unclear, the involvement of the skin microbiome in AD pathophysiology is generally accepted. Microbiome-mediated receptor signaling in keratinocytes has been studied mostly in the context of pattern recognition receptors (PPR). More recently, commensal skin microbiota have been found to hijack a different signaling route, namely the aryl hydrocarbon receptor (AHR) pathway. The AHR is a ligand-activated transcription factor that is known mostly for interacting with microbiome and diet-derived metabolites in the gut. Intriguingly, gut microbiome dysbiosis may steer disease in peripheral organs and also in the skin (better known as the gut-skin axis). We recently postulated that keratinocyte proliferation, differentiation, antimicrobial peptide expression and skin barrier function may be under the control of the skin microbiota through AHR-driven cellular signaling events [6], however this concept may further extend to the gut microbiome as well. Regarding AD, we found that commensal GPAC also target the AHR (van der Krieken *et al*. (2023)) and are underrepresented on FLG-deficient skin [3]. Barrier dysfunction in AD may thus arise because of aberrant gene (*FLG*)-microbe (GPAC) interactions. The adverse host-microbe interactions in AD could be targeted by future microbiome therapies based on prebiotics, probiotics or postbiotics, or species-specific targeting of pathogenic subpopulations within the microbiome via phages, plasmids, or transposable elements.

For host-microbe interaction studies, organotypic skin models offer a biologically relevant growth substrate (the SC) that mimics natural skin factors (*e.g.,* physical and chemical barrier) defining communication between microbial metabolites and keratinocyte receptors *in vivo*. The choice of specific bacterial strains (*e.g.,* disease-related, pathogenic or healthy commensal) for cocultures will fundamentally affect the experimental outcome, and no single strain can represent the diversity within a bacterial species. Furthermore, a mixed community of microbiota influences skin processes more than a single species alone [7] and specific culture conditions (*e.g.,* temperature, humidity, oxygen levels, pH, log growth *versus* stationary phase) will influence bacterial growth and metabolite production through quorum sensing mechanisms [8]. Also, for the analysis of microbial communities *in vitro,* several hurdles in distinguishing viable bacteria and estimating actual bacterial number (by culture-based methods versus by the capturing the complete microbiota composition by 16S rRNA gene or shotgun sequencing) arise, and to date they have precluded the wide implementation of organotypic models for skin microbiome research.

Environmental cues driving keratinocyte signaling

Specific genetic defects within keratinocytes cause disorders of cornification with local and systemic atopic features, illustrating that epithelial cells in skin and other barrier organs can contribute to the outcome of an allergen-encounter. However, the specific mechanisms of gene-environment interaction remain to be defined. Of relevance to AD, there is an increased prevalence of atopic disease in individuals with *FLG* null mutations who are exposed to allergens and irritants such as pet dander and surfactants. Exposure to cats in childhood does not affect AD prevalence except in those with *FLG* null mutations, conversely early exposure to dog allergens may actually provide protection against AD [9]. Although allergens may be inhaled, the interaction with FLG expression raises the possibility of a direct effect of pet allergens on keratinocyte function, which can be modeled *in vitro* (unpublished data).

Sodium lauryl sulphate (SLS) is a surfactant present in soap and skin care products ranging in concentrations from 0.01% to 50%. SLS is known to drive skin irritation through i) the removal of natural moisturizing factor (NMF), ii) changes in the microbiota composition, iii) altered keratinocyte differentiation including downregulation of profilaggrin, and iv) an increase in keratinocyte-derived inflammatory cytokine expression. Greater barrier dysfunction occurs after SLS exposure in individuals with *FLG* null mutations [10].

Environmental temperature and humidity affect SC hydration, having a well-recognized impact on AD prevalence and severity. The molecular mechanisms underpinning this effect are likely mediated via transcriptional regulation of FLG and other key barrier proteins within the epidermis, again highlighting the potential for gene-environment interactions in AD, that may be dissected with the organotypic epidermal models described in this article.

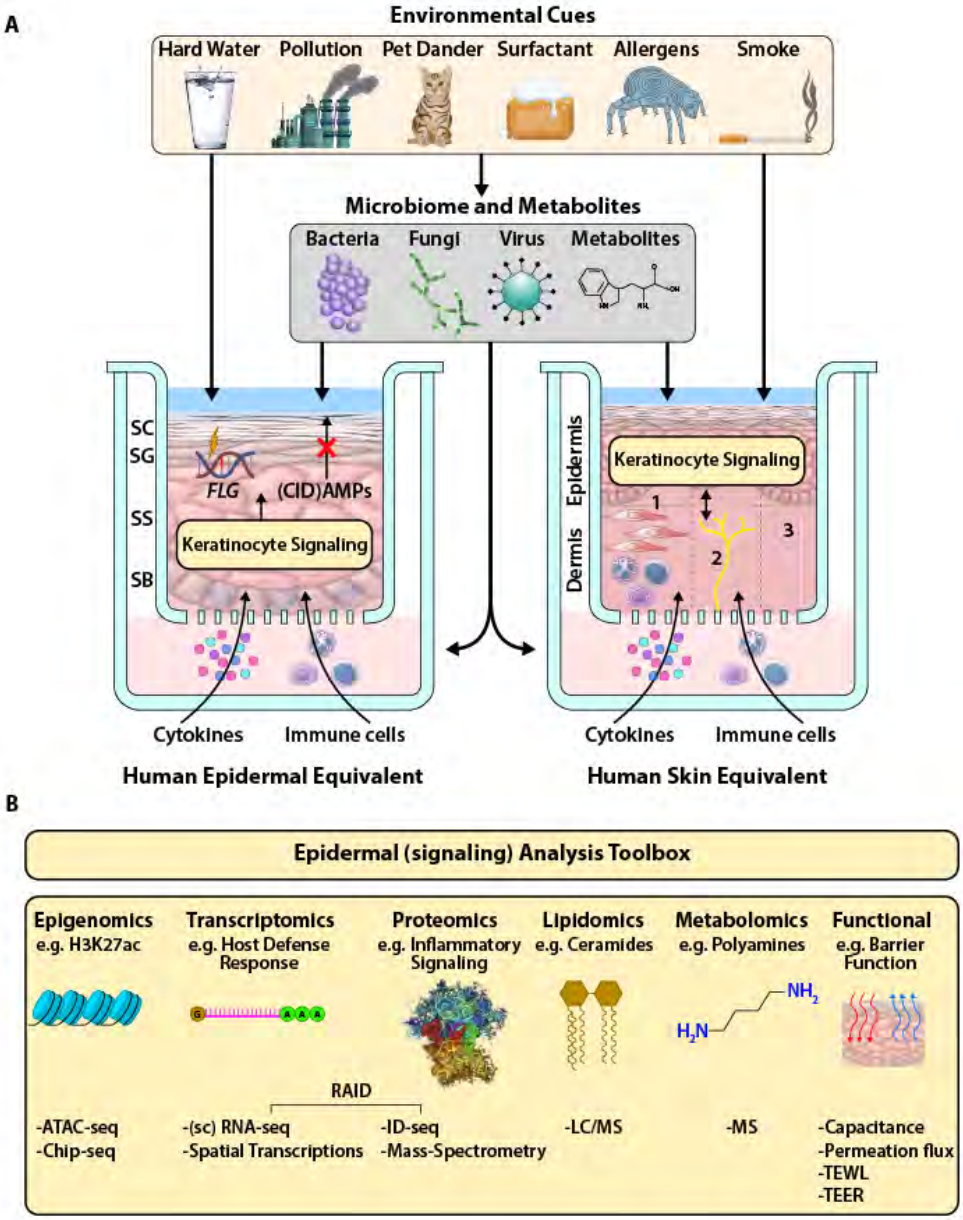
A
Environmental Cues
Hard Water
Pollution
Pet Dander
Surfactant
Allergens
Smoke
Microbiome and Metabolites
Bacteria
Fungi
Virus
Metabolites
SC
SG
SS
SB
FLG
(CID)AMPs
Keratinocyte Signaling
Cytokines
Immune cells
Human Epidermal Equivalent
Epidermis
Dermis
Keratinocyte Signaling
1
2
3
Cytokines
Immune cells
Human Skin Equivalent
B
Epidermal (signaling) Analysis Toolbox
Epigenomics
e.g. H3K27ac
Transcriptomics
e.g. Host Defense Response
Proteomics
e.g. Inflammatory Signaling
Lipidomics
e.g. Ceramides
Metabolomics
e.g. Polyamines
Functional
e.g. Barrier Function
RAID
-ATAC-seq
-Chip-seq
-(sc) RNA-seq
-Spatial Transcriptions
-ID-seq
-Mass-Spectrometry
-LC/MS
-MS
-Capacitance
-Permeation flux
-TEWL
-TEER

< Figure 2. *In vitro* modeling of AD disease factors and in-depth molecular analysis of cause-effect relationships. (**A**) In organotypic skin models, either epidermal equivalents or full thickness skin models, a wide range of environmental cues and microbiome-derived inflammatory factors can be applied to study keratinocyte responses, including intracellular signal transduction. With use of keratinocytes with disease-associated genetic profiles (*e.g., FLG* mutations) and addition of proinflammatory cytokines or immune cells, specific AD endotypes can be mimicked. Interaction of this inflammatory milieu with vascular endothelial cells can further fine-tune the molecular disease phenotype. Cutaneous neuroimmune interactions that are important in AD have been modeled by reinnervation of organotypic models or *ex vivo* skin using rat dorsal root ganglions or induced pluripotent stem cell-derived peripheral neurons. However, incorporation of all these disease-related cellular components in one complex tissue-engineered model has not yet been successful, as indicated by the separation via dotted lines. (**B**) A comprehensive omics-driven signaling analysis toolbox has been generated over the past decade, with the included tools ranging from pretranscriptional epigenomic regulation to measurements of keratinocyte-derived metabolites and end-point functional analytics. As these sophisticated technologies are becoming more affordable by the day, data-driven model optimization by molecular comparison with patient skin can enable researchers to leverage the full potential of organotypic skin models as true alternatives to patients and minimize the need for animal experimentation in experimental and translational dermatology research. The meanings of the numerals are as follows: *1 = nerve innervation, 2 = fibroblast, 3 = vasculature. Abbreviations: ATAC, Assay for transposase-accessible chromatin, ChIP, chromatin immunoprecipitation; (CID)AMP, (cationic intrinsically disordered) antimicrobial peptide; FLG, filaggrin; H3K27ac, acetylation of the lysine residue at N-terminal position 27 of histone protein H3; ID-seq, immunodetection by sequencing (van Buggenum et el. Nat Comm 2018, DOI: 10.1038/s41467-018-04761-0); LC/MS, liquid chromatography–mass spectrometry; RAID, RNA and immunodetection; SB, stratum basale; SC, stratum corneum; sc, single cell; seq, sequencing; SG, stratum granulosum; SS, stratum spinosum; TEER, transepithelial electric resistance; TEWL, transepidermal water loss.*

Discussion and conclusion

To date, neither the complexity of native skin nor the magnitude of intercellular interactions in AD can be captured in organotypic skin models. Studies are focusing instead on single epidermal and/or dermal signaling cues, circumventing the challenges in creating a favorable culture condition for many different cell types and the lack of perfusion in the overall static organotypic models. In addition, the skin tissue architecture and its plasticity are difficult to recreate in 3-dimensional models. Lack of rete-ridges and hair follicles deprive these models from bearing various anatomic tissue niches important for keratinocyte biology. Current advances in bioprinting and biomaterial engineering may provide solutions for creating tailor-made and disease-specific skin tissue microenvironments. At the same time, improvements in genetic and tissue engineering methodologies, and rapid innovations in omics technologies provide ample opportunities for precise modeling of disease parameters and investigation of cause-effect relationships in the controlled laboratory environment. Epidermal keratinocytes should be considered as *bona fide* cellular targets for primary or secondary prevention of

atopic disease and for breaching the vicious cycle of chronic inflammation and alleviating major AD symptoms. We envision that in the near future, the collective efforts regarding integrative dermatology will pay off by combining longitudinal clinical trial data with high-tech organotypic human skin models, yielding important human skin screening platforms for the discovery and development of drugs to modulate keratinocyte signaling.

Acknowledgements

This work was supported by a grant from Health-Holland (PAST4FUTURE LSHM20043-HSGF to EB). EB and SB received funding from the Innovative Medicines Initiative 2 Joint Undertaking (JU) under grant agreement No 821511. The JU receives support from the European Union's Horizon 2020 research and innovation programme and EFPIA. SJB and LJ are supported by a Wellcome Trust senior research fellowship awarded to SJB (220875/Z/20/Z). All authors declare no conflict of interest. This publication reflects only the author's view and the Joint Undertaking is not responsible for any use that may be made of the information it contains.

References

1. Esaki, H., et al., Identification of novel immune and barrier genes in atopic dermatitis by means of laser capture microdissection. J Allergy Clin Immunol, 2015. **135**(1): p. 153-63.
2. Reynolds, G., et al., Developmental cell programs are co-opted in inflammatory skin disease. Science, 2021. **371**(6527).
3. Zeeuwen, P.L., et al., Gram-positive anaerobe cocci are underrepresented in the microbiome of filaggrin-deficient human skin. J Allergy Clin Immunol, 2017. **139**(4): p. 1368-1371.
4. Latendorf, T., et al., Cationic Intrinsically Disordered Antimicrobial Peptides (CIDAMPs) Represent a New Paradigm of Innate Defense with a Potential for Novel Anti-Infectives. Sci Rep, 2019. **9**(1): p. 3331.
5. Elias, M.S., et al., Functional and proteomic analysis of a full thickness filaggrin-deficient skin organoid model. Wellcome Open Res, 2019. **4**: p. 134.
6. van den Bogaard, E.H., C. Esser, and G.H. Perdew, The aryl hydrocarbon receptor at the forefront of host-microbe interactions in the skin: A perspective on current knowledge gaps and directions for future research and therapeutic applications. Exp Dermatol, 2021. **30**(10): p. 1477-1483.
7. Loomis, K.H., et al., A mixed community of skin microbiome representatives influences cutaneous processes more than individual members. Microbiome, 2021. **9**(1): p. 22.
8. Williams, M.R., et al., Quorum sensing between bacterial species on the skin protects against epidermal injury in atopic dermatitis. Sci Transl Med, 2019. **11**(490).
9. Pelucchi, C., et al., Pet exposure and risk of atopic dermatitis at the pediatric age: a meta-analysis of birth cohort studies. J Allergy Clin Immunol, 2013. **132**(3): p. 616-622.e7.
10. Danby, S.G., et al., The Effect of Water Hardness on Surfactant Deposition after Washing and Subsequent Skin Irritation in Atopic Dermatitis Patients and Healthy Control Subjects. J Invest Dermatol, 2018. **138**(1): p. 68-77.

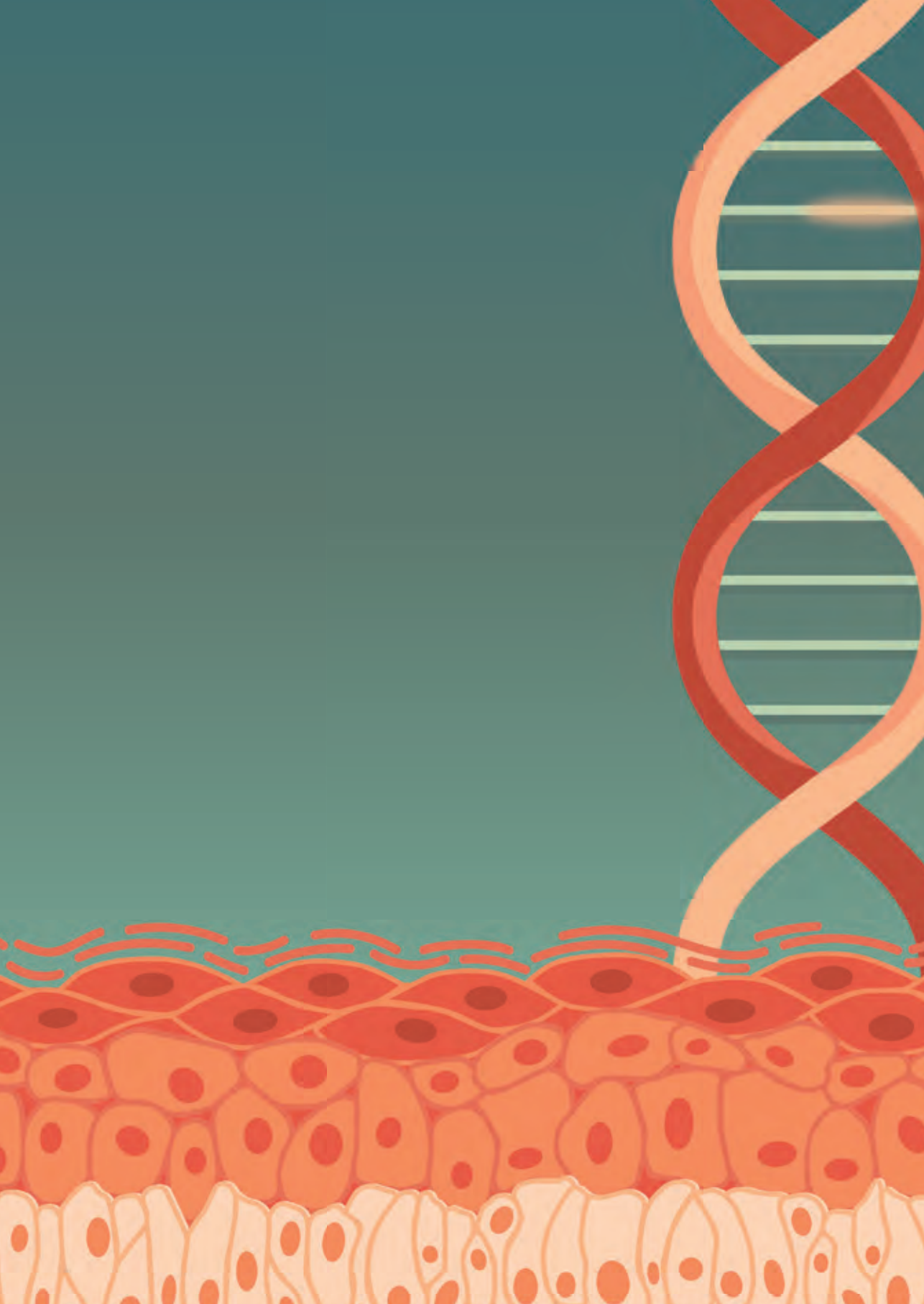

Chapter 3.

CRISPR/Cas9-based genomic engineering in keratinocytes: from technology to application

Jos P.H. Smits[1], Luca D. Meesters[1], Berber G.W. Maste[1], Huiqing Zhou[2,3], Patrick L.J.M. Zeeuwen[1], Ellen H. van den Bogaard[1]

Affiliations

[1] Department of Dermatology, Radboud University Medical Center (Radboudumc), Nijmegen, The Netherlands

[2] Department of Molecular Developmental Biology, Faculty of Science, Radboud University, Nijmegen, The Netherlands

[3] Department of Human Genetics, Radboudumc, Nijmegen, The Netherlands

Published in

JID Innov. 2021 Dec 1;2(2):100082. doi: 10.1016/j.xjidi.2021.100082.

Abstract

CRISPR/Cas9 is the most straightforward genome editing tool to date. However, its implementation across disciplines is hampered by variable genome editing efficiencies, reduced cell viability, and low success rates in obtaining clonal cell lines. This review aims to recognize all CRISPR/Cas9 related work within the experimental dermatology field to identify key factors for successful strategies in the different keratinocyte cell sources available. Based on these findings we conclude that most groups use immortalized keratinocytes for generating knockout keratinocytes. Our critical considerations for future studies using CRISPR/Cas9, both for fundamental and clinical applications, may guide implementation strategies of CRISPR/Cas9 technologies in the (experimental) dermatology field.

Introduction to CRISPR/Cas9 as a genomic editing tool

Clustered Regularly Interspaced Short Palindromic Repeats (CRISPRs) were known in the bacterial genome as hypervariable loci typically consisting of direct repeats, separated by sections of variable sequences called spacers, in proximity of *CRISPR-associated* (*Cas*) genes. The mechanism of the CRISPR/Cas system to specifically target DNA for genome editing was utilized successfully for the first time in mammalian cells almost a decade ago [1-3], and functions as described extensively [4] and schematically visualized in Figure 1A. Many bacterial species have variants of CRISPR and *Cas* loci with the most extensively investigated variant as genome editing tool being the CRISPR/Cas9 system [5]. CRISPR/Cas9-mediated genome editing requires a Cas9-guide RNA (gRNA) complex containing Cas9, crRNA, and tracrRNA (see Box 1. CRISPR terminology). The complex can be introduced to target cells by various methods, as reviewed before [6, 7]. By guidance of crRNA, the complex binds to complement DNA accompanied by a flanking protospacer adjacent motif (PAM) – 5'-NGG-3' for *Streptococcus pyogenes* Cas9 [8]. The Cas9-gRNA complex induces a double stranded break at the target site [9, 10] which can be repaired by the target cell via either non-homologous end joining (NHEJ) [11] or homology directed repair (HDR) [12]. In NHEJ, the broken DNA strands are re-ligated, either directly or after random nucleotide insertions or deletions [13]. Often this leads to frameshift mutations and premature stop codons and therefore this mechanism is readily used to knockout protein expression of interest. In HDR, the double stranded breaks are repaired with the use of a sister chromatid as homologous template strand. By multiple crossovers, DNA synthesis and ligation, the damaged strand can be precisely repaired [13]. Instead of a sister chromatid as template strand, an exogenous DNA template harboring a desired mutation or gene cassette can be introduced as single-strand or double-strand DNA, with homologous arms on the outsides [14-16].

Box 1. CRISPR terminology	
CRISPR	Clustered Regularly Interspaced Short Palindromic Repeats
Cas9	CRISPR-associated protein 9
Cas9n	Cas9 nickase
dCas9	Deactivated Cas9
PAM	Protospacer adjacent motif
crRNA	CRISPR RNA
tracrRNA	Trans-activating CRISPR RNA
(s)gRNA	(Single) guide RNA
RNP	Ribonucleoprotein
HDR	Homology-directed repair
NHEJ	Non-homologous end joining

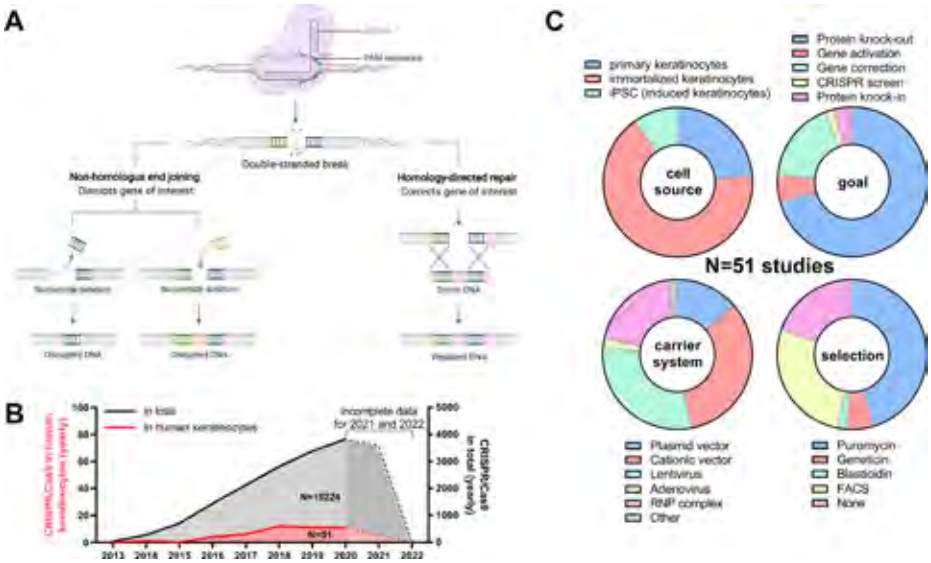

Figure 1. CRISPR/Cas9-initiated genomic repair in human keratinocytes. (**A**) Schematic overview of CRISPR/Cas9 mechanism (Created with BioRender.com). (**B-C**) Graphical representation of publications using CRISPR/Cas9 in human keratinocytes, split by cell source, experimental goal, carrier system applied, and selection (marker) deployed.

Over the years, an increasing number of studies in the field of experimental dermatology harnessed the CRISPR/Cas9 toolbox, although current numbers are limited but increasing over the past five years (Figure 1B-C, Table 1). This review aims to recognize all CRISPR/Cas9 work performed in human epidermal keratinocytes, to identify best practices and key determinants for successful strategies in different human keratinocyte cell sources available, accompanied by critical considerations for future studies using CRISPR/Cas9, both for a fundamental and clinical application.

Delivery of the CRISPR/Cas9 machinery into keratinocytes

Cationic vectors, lentiviral vectors, or adenoviral vectors are mostly utilized for transducing the expression of Cas9 and a specific gRNA. Lentiviral vectors especially designed for this purpose, like lentiCRISPR v2 deposited by Feng Zhang's lab [17], are readily available via Addgene (ID52961) and easily amendable to encode the gRNA sequence(s) of interest. Lentiviral infection is often very efficient and leads to random incorporation of the encoded DNA into the infected cell's genome, causing a permanent transfer – and often also permanent induction – of Cas9 and the encoded gRNA sequence. Consequently, the constitutive expression of Cas9 and gRNA increases the risk of off-target cleavage of DNA, potentially leading to unforeseen genomic changes. In addition, lentiviral delivery can result in unwanted gene rearrangements and transgene silencing [6]. The use of adenovirus over lentiviruses is preferred, as adenoviruses do not integrate easily into the genome [18]. Both lentivirus and adenovirus can induce strong immunogenic responses [19, 20], complicating their suitability for *in vivo* therapeutic use. Therefore, adeno-associated virus (AAV) particles, which show limited immunogenicity compared to adenovirus vectors [21], might be more suitable. Nevertheless, the drawback of AAV is that these particles have a smaller loading capacity than adenoviruses and lentiviruses, which can limit their use with relatively large plasmids encoding like gRNAs and Cas9.

Electroporation or transfection of Cas9 and gRNAs, either as plasmids, mRNA, or RNP complexes, is nowadays often used in immortalized keratinocytes (Table 1). These delivery methods are easy to use, can be highly efficient (especially electroporation of RNP complexes), and the transient expression of gRNAs and Cas9 limits the risk for off-target effects.

CRISPR/Cas9 in human primary keratinocytes

To study protein function, biological processes, or disease mechanisms, experimental cell or tissue culture models often include primary epidermal keratinocytes of healthy individuals, taken from excess skin that was removed during surgical procedures. Genetic predispositions are key in the pathogenesis of many skin diseases, from the obvious monogenetic to complex polygenic and multifactorial diseases. For example, ichthyosis vulgaris (IV) and epidermolysis bullosa (EB) are the results of homozygous (or compound heterozygous) mutations in *FLG* (for IV), and type VII collagen gene *COL7A1* and *LAMB3* (both for EB) [22-25]. Through genomic engineering, models for these monogenetic skin diseases can be created, allowing to study the contribution of the genetic risk factors in an *in vitro* setting against nonengineered keratinocytes with an identical genetic background. Potential gene therapy strategies can be developed and validated for use *in vitro* and eventually *in vivo*. So far, CRISPR/Cas9 has been used in primary keratinocytes, mainly to knockout or correct genes, as shown in Table 1.

In 2018, a protocol for the generation of knockout human primary keratinocytes was published [26]. To increase the life time of human primary cells, they were cocultured with 3T3-J2 fibroblasts as feeder cells, in the presence of proliferation enhancing Rho-associated protein kinase (ROCK) inhibitor Y-27632 [27], while the CRISPR/Cas9 machinery is delivered via lentiviral transduction of plasmid DNA including a puromycin resistance cassette. Selection of modified keratinocytes was performed on mitotically inactivated and puromycin resistant fibroblasts. The modified keratinocytes were still able to differentiate and were able to form three-dimensional skin equivalents [26, 28]. In the studies mentioned earlier, antibiotic resistance was often conferred allowing for selection of keratinocytes that were successfully infected. These keratinocytes did not undergo successful genomic editing per se. In other words, the generation of isogenic clonal cell lines that harbor precisely the intended mutations is preferred over using selection procedures that will result in a mixed cell population with unspecified genomic alterations. Indeed, clonal expansion of primary keratinocytes is a challenge given the limited lifespan. Nevertheless, EB-derived patient keratinocytes, grown on feeder fibroblast cells and in presence of Y-27632, were successfully targeted by CRISPR/Cas9 [29, 30]. Others circumvented the proliferative limitations by immortalizing the genetically altered primary keratinocytes using a retroviral vector carrying human papillomavirus type 16 (HPV16) genes E6 and E7 prior to grafting experiments and organotypic 3D cultures for studies on junctional epidermolysis bullosa (JEB) [31] or Netherton's syndrome [32].

Most research utilizing CRISPR/Cas9 in primary keratinocytes is focused on EB using patient-derived EB keratinocytes, as reviewed recently [33]. In EB, the connection between the dermis and the epidermis is fragile, leading to severe clinical features such as blistering and subsequent debilitating infections. Using CRISPR/Cas9 induced HDR, the type VII collagen gene *COL7A1* in recessive dystrophic epidermolysis bullosa (RDEB) patient-derived keratinocytes [30, 34-36] and RDEB patient-derived fibroblasts [36] can be restored, leading to re-expression of type VII collagen. The type VII collagen-corrected keratinocytes were able to develop into high quality skin equivalents when transplanted onto immunodeficient mice. Others showed that the use of dual single-guide RNA (sgRNA)-guided Cas9 nuclease can restore the *COL7A1* reading frame and reinstate the expression of type VII collagen in RDEB patient-derived keratinocytes, enabling long-term regeneration of high quality, properly adhesive skin after grafting onto immunodeficient mice [29]. For JEB a similar approach was successful: primary keratinocytes carrying the homozygous *LAMB3* mutation in exon 14 were immortalized and corrected by HDR via an adenoviral (AdV) vector carrying Cas9 and gRNA cassettes and a lentiviral vector carrying a wild-type *LAMB3* donor template flanked by homology arms [31]. These elegant studies illustrate that CRISPR/Cas9 can be utilized for restoration of protein expression in patient-derived keratinocytes via highly specific approaches, for example through incorporation of a donor oligonucleotide via HDR, or via the use of dual sgRNA to remove a specific DNA sequence to correct for frameshift mutations. In addition, these studies show that gene-corrected, patient-derived keratinocytes generated are usually of high quality in terms of skin equivalent generation and suitable for grafting onto immunodeficient mice. In principle, that would make them good candidates for ex vivo gene and cell therapy, like showcased by Hirsch *et al.* in the first ever total body transplantation with autologous cells that were corrected and expanded *ex vivo* [37].

Human immortalized keratinocytes as alternative cell source

Human primary keratinocytes in epidermal equivalent culture models represent the *in vivo* epidermis quite well. However, human donor skin is not always available, primary keratinocyte isolation is time-consuming, and primary keratinocytes have a short *in vitro* lifespan. This conflicts with the extensive culture protocols and serial passaging that are necessary for genome editing strategies. Therefore, many researchers make use of immortalized keratinocytes in studies that are usually aimed at: i) gene and protein function by full knock out [38], ii) the biological consequence of a knock out on cell function or during therapeutic conditions [38-46], iii) validation of therapeutic target [38, 47], or iv) to generate disease model cell lines [48, 49].

Immortalized keratinocytes, such as the spontaneously immortalized HaCaT keratinocytes, the N/TERT-1 and N/TERT-2G keratinocytes, or the less used HPV16 induced immortalized keratinocytes, do not have these limitations and thus provide an alternative unlimited cell source [50, 51]. Therefore, most studies using CRISPR/Cas9 in human keratinocytes have been performed in either of the immortalized keratinocyte cell lines (Figure 1C, Table 1). Although multiple cell sources are available, they are not equally comparable to primary keratinocytes and are not necessarily similarly suited for genomic engineering procedures. The HaCaT keratinocytes are frequently used as model for keratinocytes in vitro as both monolayer and human skin equivalents [52]. However, epidermal stratification is abnormal, aberrant epidermal differentiation protein expression is observed and a *stratum corneum* is often lacking. Another drawback is that HaCaT cells show aneuploidy. Taken together, this makes HaCaT keratinocytes less suitable for genome editing and studying epidermal differentiation. The N/TERT-1 and N/TERT-2G keratinocyte cell lines were immortalized by the introduction of the human telomerase reverse transcriptase (hTERT) gene and by spontaneous loss of the pRB/p16^{INK4A} cell cycle control mechanism [53]. The N/TERT keratinocyte cell lines are (largely) diploid (N/TERT-1: 47, XY+20, N/TERT-2G: 46, XY) and show similar differentiation characteristics to those of human primary keratinocytes [50], which renders them more suitable for genomic intervention tools such as CRISPR/Cas9. Immortalized keratinocytes are well suited for fundamental studies into protein function, possible therapeutic targets, or disease modeling studies, but are not applicable for *in vivo* treatment purposes. In contrast, keratinocytes derived from induced pluripotent stem cells (iPSCs) would be more suitable with regard to regenerative medicine.

Keratinocytes derived from CRISPR/Cas9 edited iPSCs

Human pluripotent stem cells (hPSCs) and induced pluripotent stem cells (iPSCs) offer great promise in regenerative medicine, both for disease modeling and for tissue regeneration, because they can proliferate indefinitely and can be differentiated to almost any cell type in the human body [54]. Owing to their unlimited proliferation capacity [55], hPSCs and iPSCs have an apparent advantage over other somatic cells or even adult stem cells in genomic editing studies using CRISPR/Cas9, especially when clonal selection is necessary. Numerous studies reported such strategies to obtain genome edited cells from tissues that are normally not easily retrievable [56, 57]. In dermatological research, most studies are on EB patient-derived iPSCs. For example, iPSCs were generated from fibroblasts derived from a patient with dominant dystrophic epidermolysis bullosa (DDEB) carrying a heterozygous *COL7A1* mutation. Subsequently, plasmids carrying Cas9

and mutation-site specific sgRNAs were transfected into these iPSCs, before positive selection by flow cytometry. The mutation-site specific sgRNAs ensured that the correction of the genetic sequence occurred only on the mutated allele, but not on the wildtype [58]. Others show correction of the *COL7A1* gene in RDEB iPSCs via adeno-associated genome editing [59], by the introduction of three plasmids encoding Cas9, gRNA, and donor repair template [60] or electroporation with sgRNA/Cas9 ribonucleoprotein (RNP) complexes [61]. Induced keratinocytes (iKC) derived from gene-corrected iPSCs were grafted onto immunodeficient mice, and two months post grafting a normal expression of COL7A1 is shown [61]. Although generation of genome edited iPSCs is relatively easy, differentiation from iPSC toward iKC, especially for resembling primary keratinocytes, is less straightforward [62-64]. In addition, iPSC-derived keratinocytes are often immature, as compared to primary keratinocytes derived from the skin, which is a common feature of many iPSC-derived cells [65, 66]. Although the traditional air-liquid interface cultures are challenging in iPSC-derived cells, other options are available. Groundbreaking work has shown a human iPSC-based organoid culture system in which skin appendages (e.g., hair follicles and sebaceous glands) are present [67]. Organoids as such would be suitable to study aspects that are impossible to study in traditional skin equivalents, such as (early) developmental processes. Empowered by CRISPR/Cas9 genomic engineering and analysis techniques at single cell resolution, these organoid cultures are highly promising options for future research into the skin.

Future perspective for the use of CRISPR/Cas9 in experimental dermatology

To date, no clinical experiments have been performed or are registered using CRISPR/Cas9 in primary keratinocytes to treat skin disorders, although CRISPR/Cas9-based *in vivo* experiments have been reported in murine models. For example, mouse tail skin was successfully electroporated with DNA plasmids (encoding gRNAs and Cas9) and RNP complexes of synthetic Cas9 and *in vitro* transcribed sgRNAs [68]. In 2017, Hirsch and colleagues experimentally treated a JEB patient with a homozygous mutation in the LAMB3 gene which, due to the blistering and infections, had lost over 80% of his epidermis [37]. Although this is a great example of gene therapy, it was not CRISPR/Cas9-based, but through *ex vivo* gene replacement by viral transduction of *LAMB3* cDNA.

Conclusion and future directions

Before *in vivo* CRISPR/Cas9 can be considered in clinical practice, many improvements on CRISPR/Cas9 machinery, i.e. component stability, *in vivo* delivery, editing accuracy, nonspecific and unintended off-target effects, and control of cellular repair mechanisms are necessary [69]. Additionally, Cas9 has been reported to elicit immune responses in mice [70, 71] and humans [72, 73], posing a challenge for CRISPR/Cas9 based genomic engineering [74]. Nevertheless, the impact of this immunological challenge needs to be studied in immune-competent (humanized) animal models to assess potential strategies to minimize the impact of anti-Cas9 antibodies and T-cells. Until then, realistic and important goals for CRISPR/Cas9 implementation are to further develop *in vitro* human disease models to benefit preclinical research, therapeutic target discovery and drug screening.

Monogenetic disorders of the epidermis can be modeled and the effects of therapies can be studied extensively without the need for primary keratinocytes, patient biopsies or animal models. Besides keratinocytes, other skin cell types – such as fibroblasts – are of interest too. Research on dystrophic EB pathogenesis indicated that both keratinocytes and fibroblasts are responsible for the expression of type VII collagen (*COL7A1*), where the contribution of fibroblasts overrules that of keratinocytes [75]. Fibroblasts are considered a more robust and easier to culture type of cells, compared to keratinocytes, which renders them suitable for prolonged culturing and genomic engineering [76], and a potential target cell type for gene and cell therapy in dystrophic epidermolysis bullosa [35, 36, 60, 77, 78]. As this field of research expands, lessons can be taken from experimental approaches that were successful in epidermal keratinocytes and applied to dermal fibroblasts, and vice versa.

Nonspecific endonuclease activity can result in off-target unintended genomic alterations. Ever since the first application of CRISPR/Cas9 in mammalian cells, progress has been made to mitigate the incidence of off-target DNA cleavage by nonspecific endonuclease activity resulting in off-target unintended genomic alterations, as reviewed recently [79]. These strategies range from – but are not limited to – modification of gRNA, modification of Cas9 (e.g., deactivated Cas9 (dCas9), Cas9 nickase (Cas9n), high fidelity Cas9), fine-tuning delivery methodology, application of base editors (dCas9 combined with deaminase and gRNA), and application of prime editing (Cas9n combined with reverse transcriptase). Therefore, besides selecting editing strategies based on maximizing editing efficiencies and cell viability, different options are now available to minimize off-target risks.

These should be taken into consideration depending on which safety measures are applicable for the purpose of genomic engineering.

Besides investing in methodological improvements using currently available (immortalized) keratinocytes (e.g., target DNA site selection, sgRNA design and delivery methods, off-target DNA cleavage, NHEJ and HDR incidence and efficiency, and Cas9 activity), efforts should also be directed to the generation of new skin cell sources to increase experimental diversity and account for population, sex and age differences. Having CRISPR/Cas9 technology at hand, more complex, multicellular, immunocompetent, and vascularized organotypic skin models with higher throughput can be developed. These innovations will further propel the implementation and acceptance of organotypic human skin models as excellent alternatives or superior experimental models to the traditional use of animals in biomedical research.

Acknowledgements

This work was supported by a LEO foundation grant (LF18068, to EB and PZ), and PAST4FUTURE grant LSHM20043-HSGF (to EB and HZ). The authors declare no conflicts of competing financial interests.

Abbreviations

CRISPR - clustered regularly interspaced short palindromic repeat, Cas9 - CRISPR-associated protein 9, EB - epidermolysis bullosa, HDR - homology directed repair, HEE - human epidermal equivalent, hPSCs - Human pluripotent stem cells, HPV16 - human papillomavirus type 16, iPSCs - induced pluripotent stem cells, JEB - junctional epidermolysis bullosa, NHEJ - non-homologous end joining, RDEB - recessive dystrophic epidermolysis bullosa, RNP - ribonucleoprotein, ROCK - Rho-associated protein kinase, TERT - telomerase reverse transcriptase

Table 1. Characteristics of studies that utilize CRISPR/Cas9 in human keratinocytes. Abbreviations: E6/E7: papillomavirus E6/E7 protein; FACS: fluorescence-activated cell sorting; HDR: homology-directed repair; IDLV: integrase-deficient lentiviral particles; JEB: junctional epidermolysis bullosa; NHEJ: non-homologous end joining; RDEB: recessive dystrophic epidermolysis bullosa; RNP: ribonucleoprotein complex.

	Publication	PMID	Cell types (all human)	Research goal
Primary keratinocytes	[80]	26828486	Adult primary keratinocytes	protein knockout
	[81]	28777946	Foreskin primary keratinocytes	gene activation
	[34]	28800953	RDEB primary keratinocytes	gene correction
	[82]	28888469	Adult primary keratinocytes	protein knockout
	[83]	29287762	Adult primary keratinocytes	protein knockout
	[26]	30096351	Adult primary keratinocytes	protein knockout
	[35]	30195791	RDEB primary keratinocytes	gene correction
	[84]	30225000	Adult primary keratinocytes	protein knockout
	[85]	30938974	Adult primary keratinocytes	CRISPR screen
	[86]	30594489	Adult primary keratinocytes	gene activation
	[87]	31409528	Adult primary keratinocytes	protein knockout
	[28]	31502220	Adult primary keratinocytes	protein knockout
Immortalized keratinocytes	[47]	26228041	HPV16-transformed foreskin primary keratinocytes	protein knockout
	[46]	28805349	HaCaT keratinocytes	protein knockout
	[88]	28588028	HaCaT keratinocytes	protein knockout
	[49]	30021804	N/TERT foreskin keratinocytes	protein knockout
	[42]	29434599	N/TERT foreskin keratinocytes	protein knockout
	[41]	30252954	HaCaT keratinocytes and adult primary keratinocytes	protein knockout
	[31]	30122422	Immortalized JEB adult primary keratinocytes	protein knockout
	[89]	29263274	HaCaT keratinocytes	protein knockout
	[90]	29330493	HaCaT keratinocytes	protein knockin/ knockout
	[91]	29807809	HaCaT keratinocytes	protein knockout
	[92]	30132045	HaCaT keratinocytes	protein knockin
	[93]	30410676	HaCaT keratinocytes	protein knockout
	[29]	30930113	Immortalized adult primary keratinocytes	protein knockout

Method of introduction	Carrier	Cas9 version	Repair	Selection
Electroporation	Plasmid vector	SpCas9	NHEJ	FACS
Electroporation	Plasmid vector	hCas9 D10A	HDR	puromycin
Xfect	Cationic vector	SpCas9	HDR	puromycin and blasticidin
Electroporation	Plasmid vector	SpCas9	NHEJ	blasticidin
lentiCRISPR v2	Lentivirus	SpCas9	NHEJ	puromycin
lentiCRISPR v2	Lentivirus	SpCas9	NHEJ	puromycin
IDLV	Lentivirus	SpCas9	HDR	none
FuGene HD	Cationic vector	SpCas9	NHEJ	puromycin
lentiCRISPR v2	Lentivirus	SpCas9	NHEJ	puromycin and blasticidin
Lipofectamine 2000	Cationic vector	dCas9	n/a	FACS
FuGene HD	Cationic vector	SpCas9	NHEJ	puromycin
lentiCRISPR v2	Lentivirus	SpCas9	NHEJ	puromycin
Lipofectamine 2000	Cationic vector	SpCas9	NHEJ	puromycin
Lipofectamine 3000	Cationic vector	SpCas9	NHEJ	FACS
pLKO.1-puro	Lentivirus and adenovirus	SpCas9	NHEJ	puromycin
TransfeX	Cationic vector	pSpCas9	NHEJ	geneticin
TransfeX	Cationic vector	pSpCas9	NHEJ	FACS
Ad5-CMV-Cas9 and Ad5-U6-sgRNA	Adenovirus	SpCas9	NHEJ	none
IDLV	Lentivirus	SpCas9	NHEJ	none
pSicoR-CRISPR-PuroR	Lentivirus	SpCas9	NHEJ	puromycin
Electroporation	Plasmid vector	SpCas9	NHEJ	puromycin
DNAJA4-gRNA-EGFP and Cas9-puro	Lentivirus	SpCas9	NHEJ	puromycin
GenJet	Cationic vector	SpCas9	HDR	geneticin
RNAi-Max	RNP complex	SpCas9	NHEJ	none
Electroporation	RNP complex	SpCas9	NHEJ	none

Table 1. Continued

	Publication	PMID	Cell types (all human)	Research goal
Immortalized keratinocytes	[43]	31391281	N/TERT foreskin keratinocytes	protein knockout
	[44]	32581101	Foreskin primary keratinocytes and N/TERT-1 foreskin keratinocytes	protein knockout
	[39]	31319135	HaCaT keratinocytes	protein knockout
	[94]	30972602	HaCaT keratinocytes	protein knockout
	[95]	31122679	HaCaT keratinocytes	protein knockout
	[96]	31178865	HaCaT keratinocytes	protein knockout
	[45]	32581101	Foreskin primary keratinocytes and N/TERT-1 foreskin keratinocytes	protein knockout
	[40]	31518892	HaCaT keratinocytes	protein knockout
	[32]	32637457	Immortalized primary adult keratinocytes	protein knockout
	[48]	32544098	N/TERT foreskin keratinocytes	protein knockout
	[97]	32142798	Immortalized adult primary keratinocytes and RDEB primary keratinocytes	gene activation and protein knockout
	[98]	32710848	N/TERT foreskin keratinocytes	protein knockout
	[99]	32917957	Immortalized epidermolytic ichthyosis keratinocytes	protein knockout
	[100]	32938703	N/TERT foreskin keratinocytes	protein knockout
	[101]	33297464	HaCaT keratinocytes	protein knockout
	[30]	33609734	Immortalized adult primary keratinocytes	protein knockout
	[38]	33321328	HPV16-transformed foreskin primary keratinocytes	protein knockout
	[102]	33354837	HaCaT keratinocytes	protein knockout
	[103]	34363036	Immortalized primary adult keratinocytes	protein knockout
	[104]	n/a	N/TERT foreskin keratinocytes	protein knockout
	[36]	34458008	Immortalized RDEB primary keratinocytes and fibroblasts	gene correction

Method of introduction	Carrier	Cas9 version	Repair	Selection
lentiCRISPR v2	Lentivirus	SpCas9	NHEJ	puromycin
lentiCRISPR v2 and pXPR_011	Lentivirus	SpCas9	NHEJ	puromycin and blasticidin
lentiCRISPR v2	Lentivirus	SpCas9	NHEJ	puromycin
lentiCRISPR v2	Lentivirus	SpCas9	NHEJ	puromycin
TransIT-LT1	Cationic vector	SpCas9	NHEJ	FACS
Lipofectamine 2000	Cationic vector	SpCas9	NHEJ	FACS
lentiCRISPR v2 and pXPR_011	Lentivirus	SpCas9	NHEJ	puromycin and blasticidin
lentiCRISPR v2	Lentivirus	SpCas9	NHEJ	puromycin
Electroporation	RNP complex	SpCas9	NHEJ	no
FuGene 6 and HiperFect	Cationic vector	SpCas9	NHEJ	FACS
Electroporation	RNP complex	SpCas9	NHEJ	none
lentiCRISPR v2	Lentivirus	SpCas9	NHEJ	puromycin and blasticidin
Xfect	Cationic vector	SpCas9	NHEJ	FACS
Calcium phosphate transfection	Plasmid vector	SpCas9	NHEJ	puromycin
Lipofectamine 3000	Cationic vector	SpCas9	NHEJ	FACS
Electroporation	RNP complex	SpCas9	NHEJ	none
Lipofectamine 3000	Cationic vector	SpCas9	NHEJ	FACS
Lipofectamine 2000	Cationic vector	SpCas9	NHEJ	FACS
Lipofectamine 3000	RNP complex	SpCas9	NHEJ	FACS
Electroporation	RNP complex	SpCas9	NHEJ	none
Electroporation	RNP complex	SpCas9 and Cas9n	HDR	none

Table 1. Continued

	Publication	PMID	Cell types (all human)	Research goal
iPSC	[59]	25429056	Induced pluripotent stem cell-derived keratinocytes	gene correction
	[60]	28250968	Induced pluripotent stem cells	gene correction
	[58]	27143720	Induced pluripotent stem cells	gene correction
	[61]	31818947	Induced pluripotent stem cells	gene correction
	[105]	32376152	Induced pluripotent stem cells	gene correction

Method of introduction	Carrier	Cas9 version	Repair	Selection
Electroporation	Plasmid vector	SpCas9	HDR	geneticin and ganciclovir
Electroporation	Plasmid vector	hCas9	HDR	puromycin
Electroporation	Plasmid vector	SpCas9	NHEJ	FACS
Electroporation	RNP complex	SpCas9	HDR	FACS
Electroporation	RNP complex	SpCas9	HDR	puromycin

References

1. Jinek, M., et al., A programmable dual-RNA–guided DNA endonuclease in adaptive bacterial immunity. science, 2012. **337**(6096): p. 816-821.
2. Cong, L., et al., Multiplex genome engineering using CRISPR/Cas systems. Science, 2013. **339**(6121): p. 819-823.
3. Mali, P., et al., RNA-guided human genome engineering via Cas9. Science, 2013. **339**(6121): p. 823-826.
4. Doudna, J.A. and E. Charpentier, The new frontier of genome engineering with CRISPR-Cas9. Science, 2014. **346**(6213): p. 1258096.
5. Makarova, K.S., et al., Evolution and classification of the CRISPR–Cas systems. Nature Reviews Microbiology, 2011. **9**(6): p. 467-477.
6. Lino, C.A., et al., Delivering CRISPR: a review of the challenges and approaches. Drug delivery, 2018. **25**(1): p. 1234-1257.
7. Shi, H., et al., Research Techniques Made Simple: Delivery of the CRISPR/Cas9 Components into Epidermal Cells. J Invest Dermatol, 2021. **141**(6): p. 1375-1381 e1.
8. Chylinski, K., A. Le Rhun, and E. Charpentier, The tracrRNA and Cas9 families of type II CRISPR-Cas immunity systems. RNA biology, 2013. **10**(5): p. 726-737.
9. Deltcheva, E., et al., CRISPR RNA maturation by trans-encoded small RNA and host factor RNase III. Nature, 2011. **471**(7340): p. 602-607.
10. Shah, S.A., et al., Protospacer recognition motifs: mixed identities and functional diversity. RNA biology, 2013. **10**(5): p. 891-899.
11. Hefferin, M.L. and A.E. Tomkinson, Mechanism of DNA double-strand break repair by non-homologous end joining. DNA repair, 2005. **4**(6): p. 639-648.
12. Liang, F., et al., Homology-directed repair is a major double-strand break repair pathway in mammalian cells. Proceedings of the National Academy of Sciences, 1998. **95**(9): p. 5172-5177.
13. Takata, M., et al., Homologous recombination and non-homologous end-joining pathways of DNA double-strand break repair have overlapping roles in the maintenance of chromosomal integrity in vertebrate cells. The EMBO journal, 1998. **17**(18): p. 5497-5508.
14. Chen, F., et al., High-frequency genome editing using ssDNA oligonucleotides with zinc-finger nucleases. Nature methods, 2011. **8**(9): p. 753.
15. Radecke, S., et al., Zinc-finger nuclease-induced gene repair with oligodeoxynucleotides: wanted and unwanted target locus modifications. Molecular Therapy, 2010. **18**(4): p. 743-753.
16. Rouet, P., F. Smih, and M. Jasin, Expression of a site-specific endonuclease stimulates homologous recombination in mammalian cells. Proceedings of the National Academy of Sciences, 1994. **91**(13): p. 6064-6068.
17. Sanjana, N.E., O. Shalem, and F. Zhang, Improved vectors and genome-wide libraries for CRISPR screening. Nat Methods, 2014. **11**(8): p. 783-784.
18. Stephen, S.L., et al., Chromosomal integration of adenoviral vector DNA in vivo. J Virol, 2010. **84**(19): p. 9987-94.
19. Nayak, S. and R.W. Herzog, Progress and prospects: immune responses to viral vectors. Gene Ther, 2010. **17**(3): p. 295-304.
20. Zaiss, A.K. and D.A. Muruve, Immunity to adeno-associated virus vectors in animals and humans: a continued challenge. Gene Ther, 2008. **15**(11): p. 808-16.

21. Zaiss, A.K., et al., Differential activation of innate immune responses by adenovirus and adeno-associated virus vectors. J Virol, 2002. **76**(9): p. 4580-90.
22. Floeth, M. and L. Bruckner-Tuderman, Digenic junctional epidermolysis bullosa: mutations in COL17A1 and LAMB3 genes. The American Journal of Human Genetics, 1999. **65**(6): p. 1530-1537.
23. Thyssen, J.P., E. Godoy-Gijon, and P.M. Elias, Ichthyosis vulgaris: the filaggrin mutation disease. Br J Dermatol, 2013. **168**(6): p. 1155-66.
24. Ryynänen, M., et al., Human type VII collagen: genetic linkage of the gene (COL7A1) on chromosome 3 to dominant dystrophic epidermolysis bullosa. American journal of human genetics, 1991. **49**(4): p. 797.
25. Smith, F.J., et al., Loss-of-function mutations in the gene encoding filaggrin cause ichthyosis vulgaris. Nat Genet, 2006. **38**(3): p. 337-42.
26. Fenini, G., et al., Genome editing of human primary keratinocytes by CRISPR/Cas9 reveals an essential role of the NLRP1 inflammasome in UVB sensing. Journal of Investigative Dermatology, 2018. **138**(12): p. 2644-2652.
27. Gandham, V.D., et al., Effects of Y27632 on keratinocyte procurement and wound healing. Clin Exp Dermatol, 2013. **38**(7): p. 782-6.
28. Grossi, S., et al., Generation of Knockout Human Primary Keratinocytes by CRISPR/Cas9. Methods Mol Biol, 2020. **2109**: p. 125-145.
29. Bonafont, J., et al., Clinically Relevant Correction of Recessive Dystrophic Epidermolysis Bullosa by Dual sgRNA CRISPR/Cas9-Mediated Gene Editing. Mol Ther, 2019. **27**(5): p. 986-998.
30. Bonafont, J., et al., Correction of Recessive Dystrophic Epidermolysis Bullosa by homology-directed repair-mediated genome editing. Mol Ther, 2021. **29**(6): p. 2008-2018.
31. Benati, D., et al., CRISPR/Cas9-mediated in situ correction of LAMB3 gene in keratinocytes derived from a junctional epidermolysis bullosa patient. Molecular Therapy, 2018. **26**(11): p. 2592-2603.
32. Galvez, V., et al., Efficient CRISPR-Cas9-Mediated Gene Ablation in Human Keratinocytes to Recapitulate Genodermatoses: Modeling of Netherton Syndrome. Mol Ther Methods Clin Dev, 2020. **18**: p. 280-290.
33. Kocher, T. and U. Koller, Advances in gene editing strategies for epidermolysis bullosa. Prog Mol Biol Transl Sci, 2021. **182**: p. 81-109.
34. Hainzl, S., et al., COL7A1 Editing via CRISPR/Cas9 in Recessive Dystrophic Epidermolysis Bullosa. Mol Ther, 2017. **25**(11): p. 2573-2584.
35. Izmiryan, A., et al., Ex Vivo COL7A1 Correction for Recessive Dystrophic Epidermolysis Bullosa Using CRISPR/Cas9 and Homology-Directed Repair. Mol Ther Nucleic Acids, 2018. **12**: p. 554-567.
36. Kocher, T., et al., A non-viral and selection-free COL7A1 HDR approach with improved safety profile for dystrophic epidermolysis bullosa. Mol Ther Nucleic Acids, 2021. **25**: p. 237-250.
37. Hirsch, T., et al., Regeneration of the entire human epidermis using transgenic stem cells. Nature, 2017. **551**(7680): p. 327-332.
38. Abboodi, F., et al., HPV-inactive cell populations arise from HPV16-transformed human keratinocytes after p53 knockout. Virology, 2021. **554**: p. 9-16.
39. Choi, M., et al., Establishment of Nrf2-deficient HaCaT and immortalized primary human foreskin keratinocytes and characterization of their responses to ROS-induced cytotoxicity. Toxicology in Vitro, 2019. **61**: p. 104602.

40. Casares, L., et al., Cannabidiol induces antioxidant pathways in keratinocytes by targeting BACH1. Redox Biol, 2020. **28**: p. 101321.
41. Trothe, J., et al., Hypotonic stress response of human keratinocytes involves LRRC8A as component of volume-regulated anion channels. Exp Dermatol, 2018. **27**(12): p. 1352-1360.
42. Swindell, W.R., et al., RNA-Seq Analysis of IL-1B and IL-36 Responses in Epidermal Keratinocytes Identifies a Shared MyD88-Dependent Gene Signature. Front Immunol, 2018. **9**: p. 80.
43. James, C.D., et al., SAMHD1 Regulates Human Papillomavirus 16-Induced Cell Proliferation and Viral Replication during Differentiation of Keratinocytes. mSphere, 2019. **4**(4): p. e00448-19.
44. Hatterschide, J., et al., PTPN14 degradation by high-risk human papillomavirus E7 limits keratinocyte differentiation and contributes to HPV-mediated oncogenesis. Proc Natl Acad Sci U S A, 2019. **116**(14): p. 7033-7042.
45. Hatterschide, J., et al., A Conserved Amino Acid in the C Terminus of Human Papillomavirus E7 Mediates Binding to PTPN14 and Repression of Epithelial Differentiation. J Virol, 2020. **94**(17).
46. Dahlhoff, M., et al., CRISPR-assisted receptor deletion reveals distinct roles for ERBB2 and ERBB3 in skin keratinocytes. FEBS J, 2017. **284**(19): p. 3339-3349.
47. Liu, Y.C., Z.M. Cai, and X.J. Zhang, Reprogrammed CRISPR-Cas9 targeting the conserved regions of HPV6/11 E7 genes inhibits proliferation and induces apoptosis in E7-transformed keratinocytes. Asian J Androl, 2016. **18**(3): p. 475-9.
48. Enjalbert, F., et al., 3D model of harlequin ichthyosis reveals inflammatory therapeutic targets. J Clin Invest, 2020. **130**(9): p. 4798-4810.
49. Sarkar, M.K., et al., Photosensitivity and type I IFN responses in cutaneous lupus are driven by epidermal-derived interferon kappa. Ann Rheum Dis, 2018. **77**(11): p. 1653-1664.
50. Smits, J.P., et al., Immortalized N/TERT keratinocytes as an alternative cell source in 3D human epidermal models. Scientific reports, 2017. **7**(1): p. 1-14.
51. Boelsma, E., M.C. Verhoeven, and M. Ponec, Reconstruction of a human skin equivalent using a spontaneously transformed keratinocyte cell line (HaCaT). Journal of investigative dermatology, 1999. **112**(4): p. 489-498.
52. Schoop, V.M., N.E. Fusenig, and N. Mirancea, Epidermal organization and differentiation of HaCaT keratinocytes in organotypic coculture with human dermal fibroblasts. Journal of investigative dermatology, 1999. **112**(3): p. 343-353.
53. Dickson, M.A., et al., Human keratinocytes that express hTERT and also bypass a p16INK4a-enforced mechanism that limits life span become immortal yet retain normal growth and differentiation characteristics. Molecular and cellular biology, 2000. **20**(4): p. 1436-1447.
54. Yamanaka, S. and H.M. Blau, Nuclear reprogramming to a pluripotent state by three approaches. Nature, 2010. **465**(7299): p. 704-12.
55. Takahashi, K. and S. Yamanaka, Induction of pluripotent stem cells from mouse embryonic and adult fibroblast cultures by defined factors. Cell, 2006. **126**(4): p. 663-76.
56. Hendriks, D., H. Clevers, and B. Artegiani, CRISPR-Cas Tools and Their Application in Genetic Engineering of Human Stem Cells and Organoids. Cell Stem Cell, 2020. **27**(5): p. 705-731.
57. Hockemeyer, D. and R. Jaenisch, Induced Pluripotent Stem Cells Meet Genome Editing. Cell Stem Cell, 2016. **18**(5): p. 573-86.
58. Shinkuma, S., Z. Guo, and A.M. Christiano, Site-specific genome editing for correction of induced pluripotent stem cells derived from dominant dystrophic epidermolysis bullosa. Proceedings of the National Academy of Sciences, 2016. **113**(20): p. 5676-5681.
59. Sebastiano, V., et al., Human COL7A1-corrected induced pluripotent stem cells for the treatment of recessive dystrophic epidermolysis bullosa. Sci Transl Med, 2014. **6**(264): p. 264ra163.

60. Webber, B.R., et al., CRISPR/Cas9-based genetic correction for recessive dystrophic epidermolysis bullosa. NPJ Regen Med, 2016. **1**.

61. Jackow, J., et al., CRISPR/Cas9-based targeted genome editing for correction of recessive dystrophic epidermolysis bullosa using iPS cells. Proc Natl Acad Sci U S A, 2019.

62. Kogut, I., D.R. Roop, and G. Bilousova, Differentiation of human induced pluripotent stem cells into a keratinocyte lineage. Methods Mol Biol, 2014. **1195**: p. 1-12.

63. Soares, E. and H. Zhou, Pluripotent Stem Cell Differentiation Toward Functional Basal Stratified Epithelial Cells. Methods Mol Biol, 2020.

64. Sah, S.K., et al., Generation of Keratinocytes from Human Induced Pluripotent Stem Cells Under Defined Culture Conditions. Cell Reprogram, 2021. **23**(1): p. 1-13.

65. Soares, E., et al., Single-cell RNA-seq identifies a reversible mesodermal activation in abnormally specified epithelia of p63 EEC syndrome. Proc Natl Acad Sci U S A, 2019. **116**(35): p. 17361-17370.

66. Friedman, C.E., et al., Single-Cell Transcriptomic Analysis of Cardiac Differentiation from Human PSCs Reveals HOPX-Dependent Cardiomyocyte Maturation. Cell Stem Cell, 2018. **23**(4): p. 586-598 e8.

67. Lee, J., et al., Hair-bearing human skin generated entirely from pluripotent stem cells. Nature, 2020. **582**(7812): p. 399-404.

68. Wu, W., et al., Efficient in vivo gene editing using ribonucleoproteins in skin stem cells of recessive dystrophic epidermolysis bullosa mouse model. Proc Natl Acad Sci U S A, 2017. **114**(7): p. 1660-1665.

69. Li, L., S. Hu, and X. Chen, Non-viral delivery systems for CRISPR/Cas9-based genome editing: Challenges and opportunities. Biomaterials, 2018. **171**: p. 207-218.

70. Chew, W.L., et al., A multifunctional AAV-CRISPR-Cas9 and its host response. Nat Methods, 2016. **13**(10): p. 868-74.

71. Wang, D., et al., Adenovirus-Mediated Somatic Genome Editing of Pten by CRISPR/Cas9 in Mouse Liver in Spite of Cas9-Specific Immune Responses. Hum Gene Ther, 2015. **26**(7): p. 432-42.

72. Wagner, D.L., et al., High prevalence of Streptococcus pyogenes Cas9-reactive T cells within the adult human population. Nat Med, 2019. **25**(2): p. 242-248.

73. Simhadri, V.L., et al., Prevalence of Pre-existing Antibodies to CRISPR-Associated Nuclease Cas9 in the USA Population. Mol Ther Methods Clin Dev, 2018. **10**: p. 105-112.

74. Crudele, J.M. and J.S. Chamberlain, Cas9 immunity creates challenges for CRISPR gene editing therapies. Nat Commun, 2018. **9**(1): p. 3497.

75. Goto, M., et al., Fibroblasts show more potential as target cells than keratinocytes in COL7A1 gene therapy of dystrophic epidermolysis bullosa. Journal of Investigative Dermatology, 2006. **126**(4): p. 766-772.

76. Chen, M. and D.T. Woodley, Fibroblasts as target cells for DEB gene therapy. Journal of Investigative Dermatology, 2006. **126**(4): p. 708-710.

77. Jackow, J., et al., Gene-Corrected Fibroblast Therapy for Recessive Dystrophic Epidermolysis Bullosa using a Self-Inactivating COL7A1 Retroviral Vector. J Invest Dermatol, 2016. **136**(7): p. 1346-1354.

78. Takashima, S., et al., Efficient Gene Reframing Therapy for Recessive Dystrophic Epidermolysis Bullosa with CRISPR/Cas9. J Invest Dermatol, 2019. **139**(8): p. 1711-1721 e4.

79. Naeem, M., et al., Latest Developed Strategies to Minimize the Off-Target Effects in CRISPR-Cas-Mediated Genome Editing. Cells, 2020. **9**(7).

80. Noske, K., et al., Mitotic Diversity in Homeostatic Human Interfollicular Epidermis. Int J Mol Sci, 2016. **17**(2).

81. Yue, J., et al., Engineered Epidermal Progenitor Cells Can Correct Diet-Induced Obesity and Diabetes. Cell Stem Cell, 2017. **21**(2): p. 256-263 e4.
82. Kocher, T., et al., Cut and Paste: Efficient Homology-Directed Repair of a Dominant Negative KRT14 Mutation via CRISPR/Cas9 Nickases. Mol Ther, 2017. **25**(11): p. 2585-2598.
83. Fenini, G., et al., The p38 Mitogen-Activated Protein Kinase Critically Regulates Human Keratinocyte Inflammasome Activation. J Invest Dermatol, 2018. **138**(6): p. 1380-1390.
84. Liu, X., et al., Loss of miR-143 and miR-145 in condyloma acuminatum promotes cellular proliferation and inhibits apoptosis by targeting NRAS. R Soc Open Sci, 2018. **5**(8): p. 172376.
85. Slivka, P.F., et al., Small Molecule and Pooled CRISPR Screens Investigating IL17 Signaling Identify BRD2 as a Novel Contributor to Keratinocyte Inflammatory Responses. ACS Chem Biol, 2019. **14**(5): p. 857-872.
86. Herter, E.K., et al., WAKMAR2, a Long Noncoding RNA Downregulated in Human Chronic Wounds, Modulates Keratinocyte Motility and Production of Inflammatory Chemokines. J Invest Dermatol, 2019. **139**(6): p. 1373-1384.
87. Jozic, I., et al., Pharmacological and Genetic Inhibition of Caveolin-1 Promotes Epithelialization and Wound Closure. Mol Ther, 2019. **27**(11): p. 1992-2004.
88. Gao, S., et al., The lysine methyltransferase SMYD2 methylates the kinase domain of type II receptor BMPR2 and stimulates bone morphogenetic protein signaling. J Biol Chem, 2017. **292**(30): p. 12702-12712.
89. Chiang, C., et al., The Human Papillomavirus E6 Oncoprotein Targets USP15 and TRIM25 To Suppress RIG-I-Mediated Innate Immune Signaling. J Virol, 2018. **92**(6).
90. Sawatsubashi, S., et al., Development of versatile non-homologous end joining-based knock-in module for genome editing. Sci Rep, 2018. **8**(1): p. 593.
91. Sun, Y.Z., et al., DNAJA4 deficiency enhances NF-kappa B-related growth arrest induced by hyperthermia in human keratinocytes. J Dermatol Sci, 2018. **91**(3): p. 256-267.
92. Zhong, G., et al., Advancing the predictivity of skin sensitization by applying a novel HMOX1 reporter system. Arch Toxicol, 2018. **92**(10): p. 3103-3115.
93. Baida, G., et al., Deletion of the glucocorticoid receptor chaperone FKBP51 prevents glucocorticoid-induced skin atrophy. Oncotarget, 2018. **9**(78): p. 34772-34783.
94. Stump, C.L., et al., Knocking down raptor in human keratinocytes affects ornithine decarboxylase in a post-transcriptional Manner following ultraviolet B exposure. Amino Acids, 2020. **52**(2): p. 141-149.
95. Muraguchi, T., et al., IGF-1R deficiency in human keratinocytes disrupts epidermal homeostasis and stem cell maintenance. J Dermatol Sci, 2019. **94**(2): p. 298-305.
96. Walter, E., et al., Role of Dsg1- and Dsg3-Mediated Signaling in Pemphigus Autoantibody-Induced Loss of Keratinocyte Cohesion. Front Immunol, 2019. **10**: p. 1128.
97. Kocher, T., et al., Predictable CRISPR/Cas9-Mediated COL7A1 Reframing for Dystrophic Epidermolysis Bullosa. J Invest Dermatol, 2020. **140**(10): p. 1985-1993 e5.
98. Dabelsteen, S., et al., Essential Functions of Glycans in Human Epithelia Dissected by a CRISPR-Cas9-Engineered Human Organotypic Skin Model. Dev Cell, 2020. **54**(5): p. 669-684 e7.
99. Imahorn, E., et al., Gene expression is stable in a complete CIB1 knockout keratinocyte model. Sci Rep, 2020. **10**(1): p. 14952.
100. James, C.D., et al., Werner Syndrome Protein (WRN) Regulates Cell Proliferation and the Human Papillomavirus 16 Life Cycle during Epithelial Differentiation. mSphere, 2020. **5**(5).

101. Sobiak, B. and W. Lesniak, Effect of SUV39H1 Histone Methyltransferase Knockout on Expression of Differentiation-Associated Genes in HaCaT Keratinocytes. Cells, 2020. **9**(12).

102. Wanuske, M.T., et al., Clustering of desmosomal cadherins by desmoplakin is essential for cell-cell adhesion. Acta Physiol (Oxf), 2021. **231**(4): p. e13609.

103. O'Keeffe Ahern, J., et al., Non-viral delivery of CRISPR-Cas9 complexes for targeted gene editing via a polymer delivery system. Gene Ther, 2021.

104. Evrard, C.F., E.; De Vuyst, E.; Svensek, O.; De Glas, V.; Bergerat, D.; Salmon, M.; De Backer, O.; Le-Buanec, H.; Lambert de Rouvroit, C.; Poumay, Y., Deletion of TNFAIP6 gene in human keratinocytes demonstrates a role for TSG-6 to retain hyaluronan inside epidermis. JID Innovations, 2021.

105. Itoh, M., et al., Footprint-free gene mutation correction in induced pluripotent stem cell (iPSC) derived from recessive dystrophic epidermolysis bullosa (RDEB) using the CRISPR/Cas9 and piggyBac transposon system. J Dermatol Sci, 2020. **98**(3): p. 163-172.

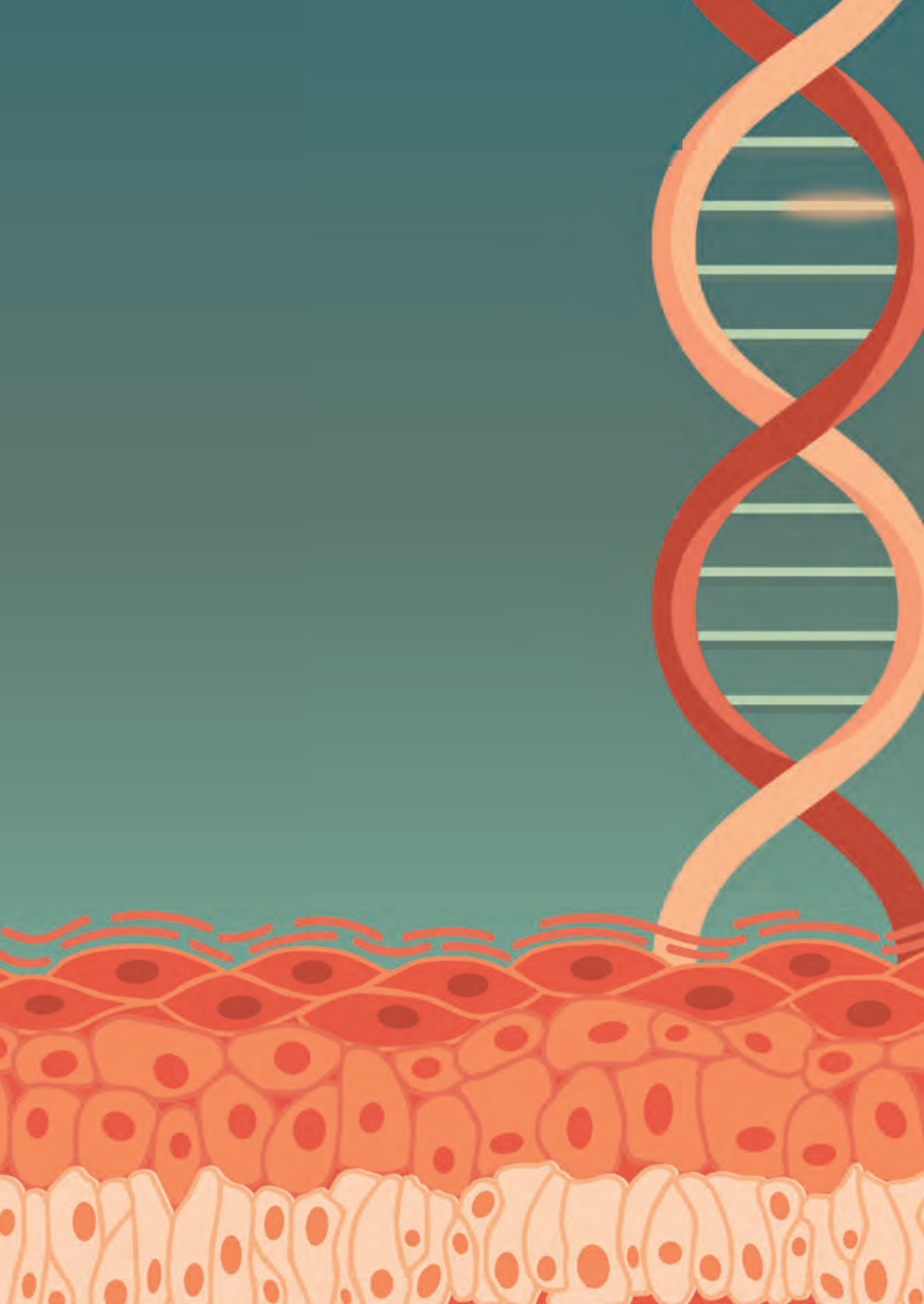

Chapter 4.

Investigations into the FLG null phenotype: showcasing the methodology for CRISPR/Cas9 editing of human keratinocytes

Jos P.H. Smits[1,2], Noa J.M. van den Brink[1], Luca D. Meesters[1,3], Hadia Hamdaoui[1], Hanna Niehues[1], Patrick A.M. Jansen[1], Ivonne M.J.J. van Vlijmen-Willems[1], Diana Rodijk-Olthuis[1], Céline Evrard[4], Yves Poumay[4], Michel van Geel[5,6,7], Wiljan J.A.J. Hendriks[8], Joost Schalkwijk[1], Patrick L.J.M. Zeeuwen[1], Ellen H. van den Bogaard[1]

Affiliations

[1] Department of Dermatology, Radboud University Medical Center (Radboudumc), Nijmegen, The Netherlands

[2] Department of Dermatology, University Hospital Düsseldorf, Medical Faculty, Heinrich Heine University, Düsseldorf, Germany

[3] Department of Molecular Developmental Biology, Faculty of Science, Radboud University, Nijmegen, The Netherlands

[4] Research Unit for Molecular Physiology, NARILIS, University of Namur, Namur, Belgium

[5] Department of Dermatology, Maastricht University Medical Center+, Maastricht, The Netherlands

[6] GROW School for Oncology and Developmental Biology, Maastricht University, Maastricht, The Netherlands

[7] Department of Clinical Genetics, Maastricht University Medical Center+, Maastricht, The Netherlands

[8] Department of Cell Biology, Radboudumc, Nijmegen, The Netherlands

Published in

J Invest Dermatol. 2023 Aug;143(8):1520-1528.e5. doi: 10.1016/j.jid.2023.02.021.

Abstract

Ever since the association between filaggrin (FLG) loss-of-function variants and ichthyosis vulgaris and atopic dermatitis disease onset was identified, filaggrin's function has been under investigation. Intraindividual genomic predisposition, immunological confounders, and environmental interactions complicate the comparison between *FLG* genotypes and related causal effects. Using CRISPR/Cas9, we generated human FLG knockout (ΔFLG) N/TERT-2G keratinocytes. Filaggrin deficiency was demonstrated by immunohistochemistry of human epidermal equivalent (HEE) cultures. Next to (partial) loss of structural proteins (IVL, HRNR, KRT2, and TGM1), the *stratum corneum* was more dense and lacked the typical basket weave appearance. In addition, electrical impedance spectroscopy and transepidermal water loss analyses highlighted a compromised epidermal barrier in ΔFLG-HEEs. Correction of *FLG* reinstated the presence of keratohyalin granules in the *stratum granulosum*, filaggrin protein expression, and expression of aforementioned proteins. The beneficial effects on *stratum corneum* formation were reflected by normalization of EIS and TEWL. This study demonstrates the causal phenotypical and functional consequences of filaggrin deficiency, indicating filaggrin is not only central in epidermal barrier function but also vital for epidermal differentiation by orchestrating the expression of other important epidermal proteins. These observations pave the way to fundamental investigations into the exact role of filaggrin in skin biology and disease.

Graphical abstract

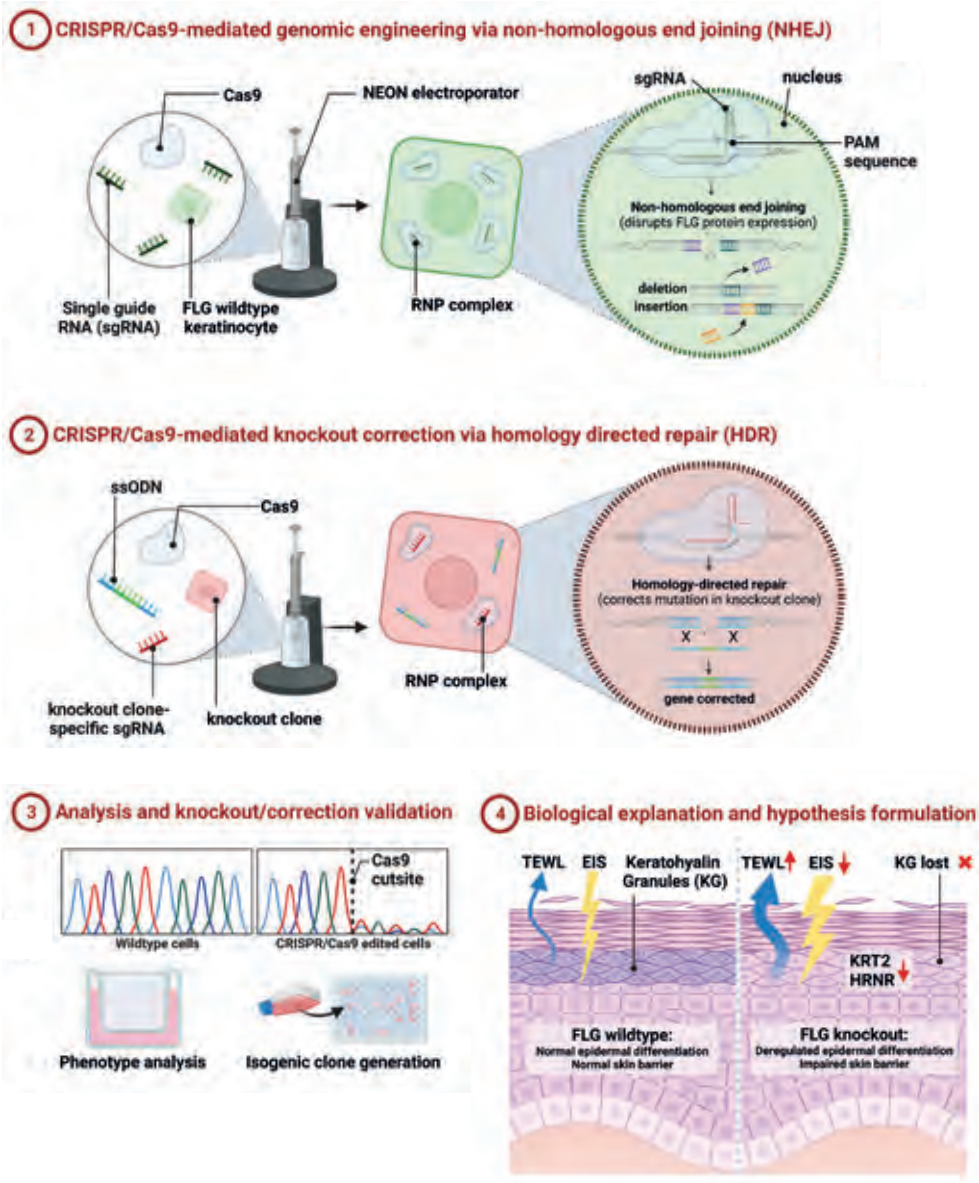

Introduction

Atopic dermatitis (AD) is a common chronic inflammatory skin condition which is characterized by itchy, dry, erythematous, plaques, and an impaired skin barrier function. The pathophysiologic basis of AD is multifactorial, including genetic polymorphisms, environmental stimuli, and deregulation of innate and adaptive immunity. The seminal work from the McLean group, identifying genetic risk factors such as loss-of-function variants in the filaggrin gene (*FLG*) in AD [1] and ichthyosis vulgaris (IV) [2], has caused a paradigm shift indicating that epidermal biology and the skin barrier proteins themselves are of importance in complex inflammatory skin diseases like AD. The *FLG* gene is located at chromosome 1q21 within the epidermal differentiation complex (EDC). This gene complex encodes proteins that are typically involved in the terminal differentiation and cornification of keratinocytes. Profilaggrin protein can be proteolytically degraded into filaggrin monomers and further converted into natural moisturizing factors (NMFs) [3]. Hygroscopic NMFs maintain epidermal hydration of the skin, and reduction of NMFs directly results in dry skin [4]. Loss-of-function variants in *FLG* lead to reduced levels of NMFs in the *stratum corneum* (SC) [5]. NMF levels directly correlate to filaggrin genotype and AD severity [6] and are found to correlate with corneocyte morphology in AD patients [6]. In mouse models, filaggrin deficiency results in barrier impairment and allergen sensitization [7]. When comparing AD patients with and without *FLG* variants, increased water loss and skin permeability were found in both groups [8-10], while others report that *FLG* variants do not influence transepidermal water loss (TEWL) [11]. In experimental *in vitro* studies, the lack of consistency between cell sources, organotypic models, and knockdown efficiencies have yielded contradictory evidence on the consequences of filaggrin deficiency [11]. Although the importance of filaggrin for healthy skin barrier development and maintenance is widely accepted, interpatient differences complicate genotype-phenotype studies, and the short life span of primary cells in culture limits the meticulous dissection of all functional properties of (pro)filaggrin.

To overcome these limitations, genomic engineering by the Clustered Regularly Interspaced Short Palindromic Repeats (CRISPR) and CRISPR associated protein 9 (Cas9) [12-15] could be a powerful technique. Yet, the introduction of the CRISPR/Cas9 machinery into the notoriously difficult-to-transfect keratinocytes has been proven troublesome, although many options are seemingly available [16]. Some CRISPR/Cas9 related work is performed in primary keratinocytes, although most of the published research utilizes immortalized keratinocytes [17]. The immortalized human N/TERT keratinocyte cell lines (N/TERT-1 and N/TERT-2G) have been available [18] and our recent studies on their excellence as alternatives to primary

keratinocytes sparked great interest in these cell lines [19]. N/TERT keratinocytes are more amenable to transfection with foreign DNA or ribonucleoprotein complexes (RNPs) followed by clonal expansion as they are less prone to terminal differentiation than primary keratinocytes. Additionally, the N/TERT cells are diploid [19] in contrast to other immortal lines, and thus very useful as an alternative to primary keratinocytes in genome editing experiments.

In this study, we illustrate the complementary potential of both the human N/TERT keratinocytes and a high efficiency CRISPR/Cas9 gene editing protocol for generating and functionally characterizing filaggrin knockout (ΔFLG) isogenic N/TERT-2G keratinocytes. The subsequent repair of the induced knockout in clonal cell lines of identical genomic background underlines the apparent genotype-phenotype relationship. These key and to our knowledge novel aspects of profilaggrin expression and downstream regulation of epidermal biology have clear implications for our understanding of skin diseases that are characterized by the loss of filaggrin.

Methods

Culturing and freezing of human N/TERT-2G keratinocytes

Human N/TERT keratinocyte cell line N/TERT-2G, purchased from J. Rheinwald laboratory (Harvard Medical School, Boston, USA), was cultured in Epilife medium (MEPI500CA, ThermoFisher Scientific, Waltham, MA, USA), complemented with human keratinocyte growth supplement (S0015, ThermoFisher Scientific) and 1% penicillin/streptomycin (P4333, Sigma-Aldrich, Saint-Louis, MO, USA). Upon generation of the different clonal N/TERT-2G keratinocyte cell lines, they were frozen in liquid nitrogen. In short, N/TERT-2G keratinocytes were detached from culture plastic using 0.25% trypsin/EDTA (25200-072, ThermoFisher Scientific). A similar amount of DMEM containing fetal calf serum (FCS) was used to stop trypsin/EDTA activity and the cells were washed twice with DPBS (BE17-512F, Lonza Bioscience, Basel, Switzerland) before resuspension in Epilife medium. After cell counting, the cell suspension was diluted one-on-one with DMEM containing 20% FCS and 20% DMSO and slowly frozen in MrFrosty freezing containers (ThermoFisher Scientific) before moving them to liquid nitrogen storage.

N/TERT-2G human epidermal equivalent (HEE) generation

Epidermal equivalents were generated as previously described [19], with minor adjustments. Briefly, inert Nunc cell culture inserts (141002, ThermoFisher Scientific)

were coated with rat tail collagen (100 µg/mL, BD Biosciences, Bedford, MA, USA) at 4°C for 1 hour. A total of 1.5 x 10^5 N/TERT-2G keratinocytes were seeded on the transwells in 150 µL Epilife medium (ThermoFisher Scientific) supplemented with 1% penicillin/streptomycin (Sigma-Aldrich) in a 24 wells format. After 48 hours, cultures were switched to a mixture of CnT-PR-3D medium (CELLnTEC, Bern, Switzerland) and DMEM medium (60:40 (v/v)) without penicillin/streptomycin for 24 hours and then cultured at the air-liquid interface for an additional ten days. Culture medium was refreshed every other day until harvesting on day 10 of the air-exposed phase.

Single guide RNA design, single strand donor oligonucleotide and synthetic Cas9

Synthetic sgRNAs to knockout *FLG* gene and purified Edit-R Cas9 nuclease protein (NLS, #CAS11200) were obtained from Synthego Corporation (Menlo Park, CA, USA) and IDT Technologies (Coralville, IA, USA), respectively. Custom synthetic Alt-R sgRNAs and single strand donor oligonucleotide (ssODN) to correct FLG expression were ordered from IDT Technologies. See Supplementary Table S4 for details on the sgRNAs and ssODN used.

Electroporation of ribonucleoprotein (RNP) complexes and analysis of editing efficiency

N/TERT-2G keratinocytes were electroporated using the NEON transfection system 10 µL kit (ThermoFisher Scientific) [20]. Per electroporation condition, synthetic sgRNA (300 ng) and Cas9 (1.5 µg) were incubated with 5 µL resuspension buffer R for 20 minutes before adding 1 x 10^5 N/TERT-2G keratinocytes. After mixing the cell suspension, the cells were electroporated using 1 pulse of 1700V for a duration of 20 ms before immediate seeding in a 6-well plate. DNA was isolated using the QIAamp DNA blood mini kit (51106, Qiagen, Hilden, Germany) according to manufacturer's protocol after reaching approximately 50% confluency and CRISPR/Cas9 induced editing efficiency was analyzed by PCR and separation of amplicon on 2% agarose gel containing 1:10,000 GelRed nucleic acid gel stain (41003, Biotium Inc., Fremont, CA, USA). Amplicons were purified by MinElute Gel extraction kit (28606, Qiagen) using the manufacturers protocol and Sanger sequenced to assess editing efficiency. Sanger sequencing reads were analyzed using the Inference of CRISPR edits (ICE) webtool (ice.synthego.com, v2, Synthego Corporation). See Supplementary Table S5 for details on the PCR primers used.

Generation of clonal ΔFLG N/TERT keratinocytes

Δ*FLG* N/TERT-2G keratinocyte cell pool and *FLG* gene-corrected N/TERT-2G keratinocyte cell pool were diluted to 1 cell per 100 µL Epilife medium and seeded into 6 x 96-well plates, 100 µL cell suspension per well, and allowed to grow for one week before refreshing the medium. After another week of culture, cells were passaged, as described earlier, into 24-well plates, 6-wells plates, T25 flasks, and T75 flasks subsequently before freezing them into liquid nitrogen. Cell clonality was assessed by Sanger sequencing and analyzing genomic DNA at the targeted *FLG* locus with help of the ICE webtool (ice.synthego.com, v2, Synthego Corporation).

Results

Generation of human Δ*FLG* N/TERT-2G keratinocytes via CRISPR/Cas9

A single guide RNA (sgRNA) was designed to target exon 3 of the *FLG* gene in order to disrupt filaggrin protein expression, as schematically visualized (Figure 1a). Immortalized human keratinocyte N/TERT-2G cells were electroporated with RNP complex containing the *FLG* targeting sgRNA and synthetic spCas9 protein [20]. Targeted Cas9 introduced a double strand break typically repaired through non-homologous end joining (NHEJ). This efficiently generated indels giving rise to human ΔFLG N/TERT-2G keratinocytes as analyzed by the Inference of CRISPR Edits webtool (ICE, http://ice.synthego.com, v2), showing 99% indels with 87% protein knockout prediction in the cell pool (Figure 1b). 3-dimensional human epidermal equivalents (HEEs) generated from N/TERT-2G control keratinocytes ('FLG wild type') and the ΔFLG N/TERT-2G keratinocyte cell pool ('ΔFLG pool') showed absence of keratohyalin granules in the ΔFLG pool culture. Specific filaggrin protein staining validated the partial loss of filaggrin expression (Figure 1c). We obtained clonal cell lines by seeding single cells from the ΔFLG pool into 96 well plates, one cell per well. The ΔFLG clonal line presented (Figure 1C) was further analyzed and used throughout the study.

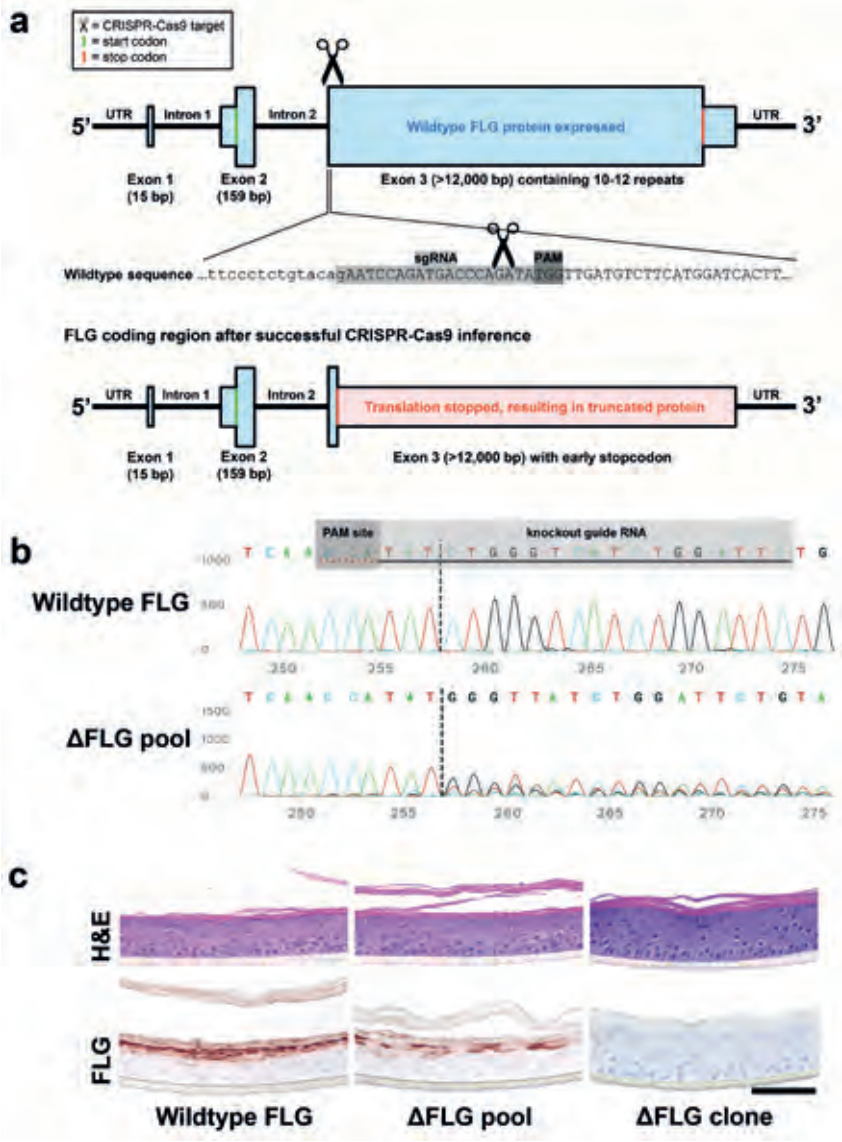

Figure 1. Generation of a Δ*FLG* N/TERT-2G clonal keratinocyte cell line. (**A**) Schematic representation of the *FLG* knockout experiment. N/TERT-2G keratinocytes were electroporated with RNP complex containing *FLG*-specific gRNA and synthetic SpCas9 protein, introducing NHEJ-induced insertions and deletions leading to a frameshift mutation. (**B**) *FLG* gene was analyzed after PCR amplification of the knockout locus (reverse complement sequence depicted). ΔFLG pool of keratinocytes show aberrant sequence reads starting 3 nucleotides 5′ of the PAM site. (**C**) Δ*FLG* pool was used to generate human epidermal equivalents (HEEs), showing partial loss of keratohyalin granules and filaggrin expression. After clonal expansion of ΔFLG pool, full ΔFLG clonal cells (c.152del5 encoding p.P51HfsX3) show complete absence of keratohyalin granules and filaggrin protein. Bar = 100 µm.

Characterization of FLG genotype-defined clonal N/TERT-2G keratinocyte cell lines

After generating a number of single cell clones from the ΔFLG pool, we proceeded to analyze these clones for *FLG* variants at the sgRNA targeted Cas9 cleavage site to identify which clones were likely 100% knockout for FLG protein expression. Out of 14 clones isolated, 6 had mutations on both alleles but were heterozygous knockout (data not shown) while 3 clones were predicted and validated to be fully knockout for filaggrin protein expression (Supplementary Table S1, Supplementary Figure S1). One particular ΔFLG clone demonstrated the deletion of 5 bases (c.152del5) on both alleles, leading to a predicted p.P51HfsX3 frameshift mutation and an early stop codon (Figure 2a and 2c). This cell line was used for further experiments ('ΔFLG clone').

Genomic engineering via CRISPR/Cas9 potentially introduces off-target effects. The CRISPOR tool [21] was used to find and rank potential sgRNA specific off-target sites based on cutting frequency determination (CFD) score (Supplementary Table S2). The top-5 potential off-target sites were amplified by PCR and the amplicons were Sanger sequenced. None of the predicted off-target mutations were found (data not shown). In addition, to prove specific genotype-phenotype correlations we engineered a N/TERT-2G keratinocyte cell line corrected for the 5 bases deletion ('FLG corrected'). Hereto, a ΔFLG clone-specific sgRNA and single strand donor oligonucleotide (ssODN) was designed. The ssODN encodes the wild type *FLG* sequence plus a silent variant (c.139-11C>T) 22 bases downstream of the protospacer adjacent motif (PAM) to allow identification of the rescued clone from unedited wild type cells. Through CRISPR/Cas9 induced homology directed repair (HDR), the previously induced homozygous *FLG* variant would be restored ultimately leading to reinstation of filaggrin protein expression, as schematically depicted (Figure 2b). HDR yielded a correction efficiency of 27% and the FLG corrected cell pool was expanded to generate FLG corrected clones. Off-target effects were screened again as described earlier (Supplementary Table S3), and none were detected (data not shown).

To validate the CRISPR/Cas9 mediated genomic engineering and clonality of our cell lines, *FLG* PCR amplicons were sequenced via Sanger sequencing (Figure 2c). These results indicate clonality of the ΔFLG clone and the FLG corrected clone and show the introduction of the silent intronic variant in the FLG corrected clone. The comparison of HEEs from wild type FLG keratinocytes (HEE^{WT}) and from the ΔFLG clone ($HEE^{\Delta FLG}$), demonstrated that knockout of FLG results in the absence of keratohyalin granules and abrogated filaggrin protein expression (Figure 2d). In the

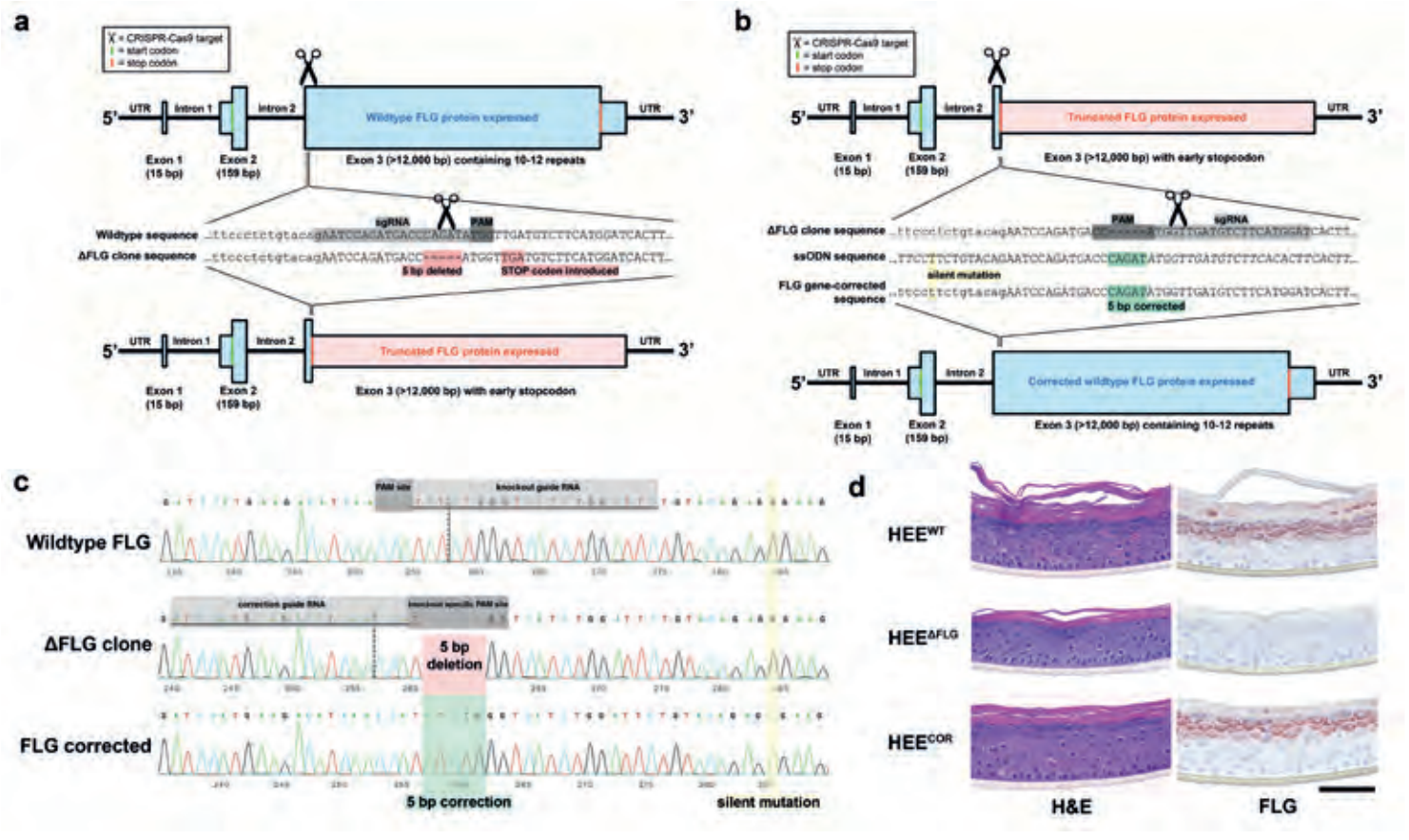

Figure 2. Validation of filaggrin expression in ΔFLG and FLG corrected cultures. (**A-B**) Schematic representation of the genomic changes in the ΔFLG clone and FLG corrected clone, respectively. (**C**) PCR amplified *FLG* sequence (reverse complement sequence depicted) indicates a 5 bp deletion (c.152del5) leading to a predicted p.P51HfsX3 frameshift mutation with an early stop codon in the ΔFLG clone and restoration of the 5bp deletion in the FLG corrected clone. (**D**) Filaggrin protein expression is lost in HEE$^{\Delta FLG}$, accompanied by a complete loss of keratohyalin granules, while filaggrin expression and keratohyalin granules are fully restored in HEE^{COR}. Bar = 100 µm.

FLG corrected clone (HEE^{COR}), the presence of keratohyalin granules was reinstated together with the complete recovery of filaggrin expression, as it was expected from the protein sequences (Supplementary Table S1).

Filaggrin regulates epidermal differentiation gene and protein expression

Next, the expression of key epidermal marker proteins was analyzed through immunohistochemistry (Figure 3a). Interestingly, specific alterations in protein expression profiles due to the presence or absence of FLG were observed. The expression of involucrin (IVL) and transglutaminase 1 (TGM1) was partially lost in $HEE^{\Delta FLG}$ but restored in HEE^{COR}, while expression of hornerin (HRNR) and keratin 2 (KRT2) was completely abrogated in $HEE^{\Delta FLG}$ and (partially) restored in HEE^{COR}. The knockout of filaggrin expression therefore seems pivotal for the deregulated expression of other differentiation proteins. Keratin 10 (KRT10), loricrin (LOR), and late cornified envelope (LCE)2, and LCE3 were similar between HEE^{WT}, $HEE^{\Delta FLG}$, and HEE^{COR}. To assess whether the differential expression originates from transcriptional or post-translational processes, we analyzed gene expression levels corresponding to the investigated differentially expressed proteins. These gene expression levels followed a similar pattern as for protein, with strong and significantly downregulated *HRNR* and *KRT2* levels in the ΔFLG clone. Gene expression of *KRT2* was rescued upon FLG correction, although *HRNR* expression remained downregulated (Figure 3b). These results indicate that loss of filaggrin can lead to (sustained) transcriptional changes in keratinocytes.

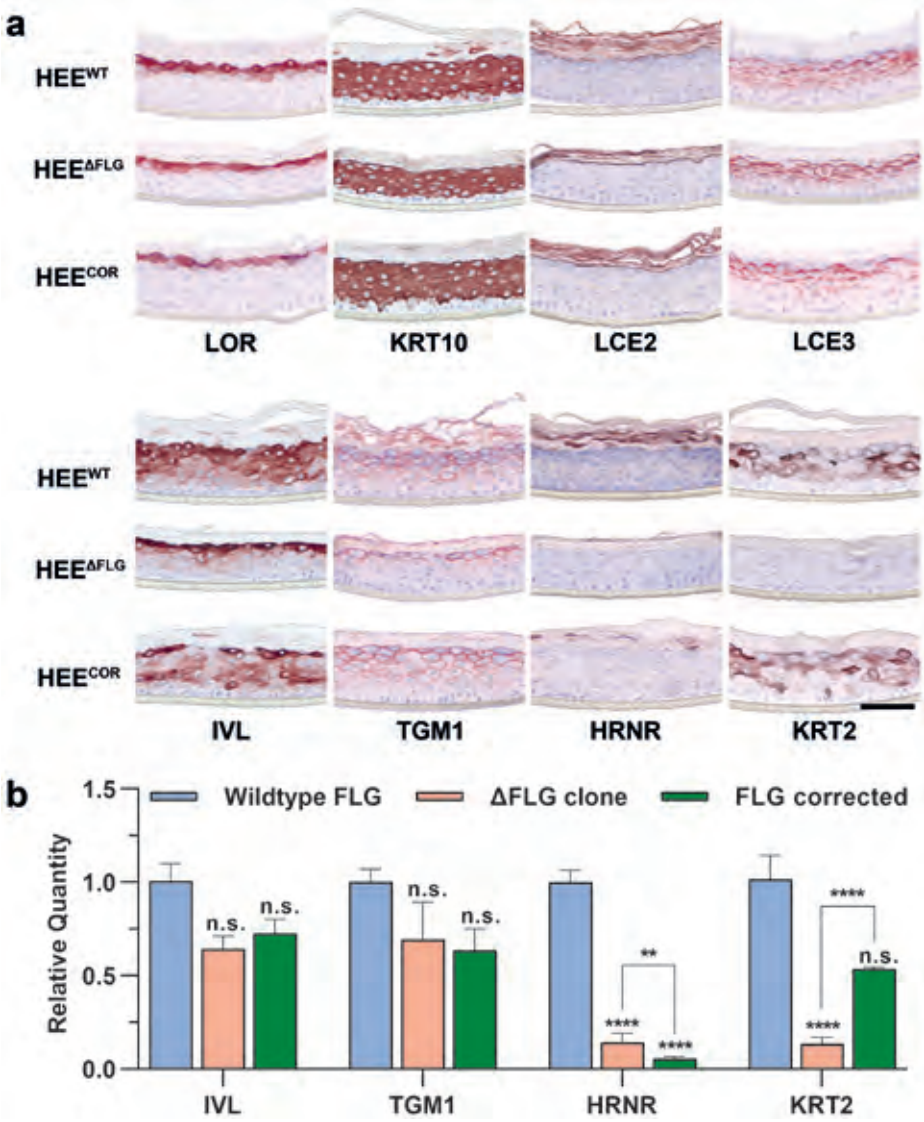

Figure 3. KRT2 and HRNR are completely abrogated as a result of FLG knockout. (**A**) Immunohistochemical staining for several differentiation proteins expressions shows similarities between FLG wild type (HEE^{WT}), ΔFLG clone ($HEE^{\Delta FLG}$) and FLG corrected clone (HEE^{COR}) (upper panel). Nevertheless, $HEE^{\Delta FLG}$ displays a downregulation of IVL and TGM1 while KRT2 and HRNR expressions were completely lost. Upon FLG correction (HEE^{COR}), the expression of IVL, TGM1, and KRT2 was completely restored, while HRNR expression is partly restored (lower panel). (**B**) Quantitative PCR to analyze gene expression of differentially expressed proteins shows minor downregulation of *IVL* and *TGM1* and major downregulation of *HRNR* and *KRT2* in ΔFLG clone. FLG correction shows no effect on *IVL*, *TGM1*, and *HRNR* expression, while *KRT2* expression is partially restored to control levels. N=3 HEE cultures, ** p-value <0.01, **** p-value <0.0001, n.s. non-significant. Bar = 100 µm.

Filaggrin expression is essential for epidermal barrier function

To study whether the differential gene and protein expression patterns in HEE$^{\Delta FLG}$ would have functional consequences, we first performed two qualitative microscopic analyses by small molecule permeation of lucifer yellow (for gross SC defects) and EZ-link sulfo-NHS-LC-biotin (for qualitative tight junction functioning [22, 23]). No apparent changes in permeation of the dyes were observed (Figure 4a). Similar to what is known from *in vivo* studies in patients with known FLG deficiency [9], the quantitative barrier analyses by electrical impedance spectroscopy (EIS, Figure 4b) and TEWL (Figure 4c) showed a significant impairment of barrier function (lower EIS and higher TEWL) upon FLG deficiency (HEE$^{\Delta FLG}$), while functional properties were regained upon *FLG* gene-correction (HEE^{COR}).

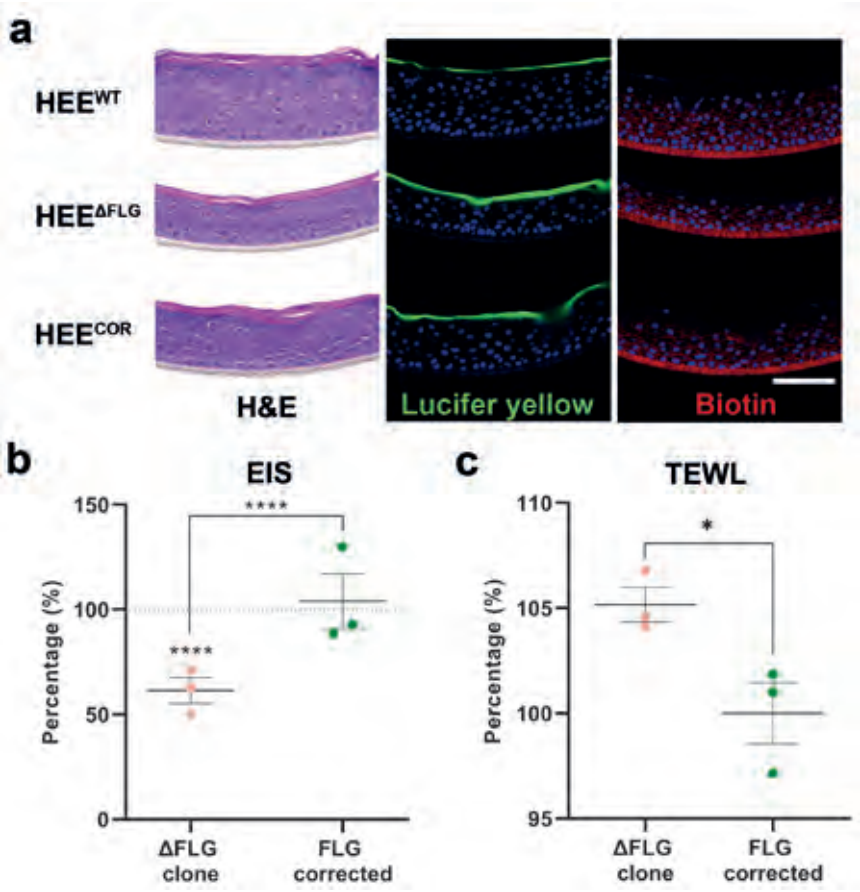

Figure 4. Knockout of *FLG* is accompanied by subtle changes in functional barrier properties that improve upon FLG reinstation. (**A**) Lucifer yellow and biotin permeation assays do not display aberrant functional barrier properties of the 3D epidermal equivalent cultures. Nevertheless, (**B**) electrical impedance spectroscopy (EIS) and (**C**) transepidermal water loss (TEWL) analysis show significant improvement of barrier properties in FLG corrected keratinocytes compared to the ΔFLG clone. N=3 HEE, * p-value <0.05, **** p-value <0.0001. Bar = 100 µm.

Discussion

In this study, we showcase straightforward RNP-based genomic editing in immortalized N/TERT keratinocytes without the use of plasmids or viral vectors that incorporate their genetic material. Because N/TERT-2G keratinocytes can be expanded in clonal (dilution) series, there is no need for antibiotic or fluorescence activated selection procedures, thereby CRISPR/Cas9 genome editing can be harnessed rather easily in many research programs and may revolutionize the investigative dermatology field. In reality, we observed that its implementation is rather slow, based on number of publications using (immortalized) keratinocytes compared to publications using any cell type [17]. Therefore, we deem it important to showcase how to disrupt (and to reinstate) the protein of interest in the immortalized N/TERT-2G keratinocyte cell line. Genome editing as we performed utilizes NHEJ, a repair mechanism that is completely stochastic and unpredictable, but suitable to generate random indels [24]. For subsequent specific corrective editing we successfully employed a HDR strategy by supplying a donor oligonucleotide carrying the desired gene-correcting DNA sequence. Given the highly intriguing, yet partly undefined, role of (pro)filaggrin in skin barrier function and the remaining knowledge gap on the therapeutic targeting of FLG deficiency, we focused on the *FLG* gene in this proof-of-principle study by targeting its N-terminal domain leading to a full protein knockout.

The identification of *FLG* loss-of-function variants and copy number variations as genetic risk factors for AD [1, 25-27] underscores the importance of the epidermal compartment in the pathogenesis of complex immune-mediated diseases. Fundamental research into the role of profilaggrin in AD pathophysiology has primarily addressed the palette of contributing profilaggrin-degrading factors [28, 29], *e.g.* skin-specific retroviral-like aspartic protease (SASPase) [30], kallikrein-related peptidase 5 (KLK5) [31], matriptase (MT-SP1) [32], and furin [33]. Further processing of filaggrin into NMFs can be attributed to proteases like caspase 14 (CASP14) [34] and bleomycin hydrolase (BLMH) [35]. While these studies on the breakdown and processing of profilaggrin into filaggrin monomers and amino-acids, and crosslinking to keratin intermediate filaments are abundant, studies on the N-terminal domains of profilaggrin and their functions are scarce.

Analysis of the structure and functional domains of profilaggrin showed that the N-terminal fragment of profilaggrin contains a nuclear localization signal enabling its translocation to the nucleus before onset of terminal differentiation [36-39]. It has been hypothesized that the translocated N-terminal fragment promotes

keratinocyte denucleation in apoptotic terminally differentiating keratinocytes [37]. In addition, the profilaggrin N-terminal fragment potentially regulates epidermal differentiation genes, as suggested before [40], and may halt keratinocyte proliferation upon overexpression of the profilaggrin N-terminus [39]. Similar to our experiments on ΔFLG clonal keratinocytes, siRNA-mediated knockdown studies also do not report on altered proliferation rates or epidermal thickness due to filaggrin loss [41].

The truncated profilaggrin that is expressed in AD and IV disease-associated genotypes (*e.g.*, p.R501X, c.2282del4, p.R2447X) still has an unaffected N-terminus that potentially can translocate to the nucleus. In fact, the most predominant variants in the *FLG* gene are situated downstream of the A and B domains, although truncating sequence variants have also been found in the A domain [42]. Whether these rare early variants are also associated with atopic disease is not clear. Early truncating variants, *e.g.*, the deletion of 17 nucleotides (c.411del17 [43]), are located downstream of the nuclear localization signal, suggesting a great importance of the A and (partial) B domain of profilaggrin. Moreover this would imply that expression of truncated profilaggrin and downstream proteolytic processing of the N-terminal part of profilaggrin – at least including the nuclear localization signal – might be intact in all of the known disease-associated *FLG* genotypes. The herein reported ΔFLG keratinocytes express an incomplete N-terminal fragment that harbors only part of the profilaggrin A domain (50 amino acids) and completely lacks the B domain. The B domain contains a putative nuclear localization signal. These ΔFLG keratinocytes could leverage a new cellular model to study the biological function of filaggrin in the epidermis when comparing these cells to similarly created cells harboring disease-associated *FLG* genotypes. This will be the subject of further research.

Our data indicate that the loss of profilaggrin expression results in altered differentiation gene expression, *e.g.*, HRNR and IVL are both downregulated, as was previously shown by FLG knockdown experiments [44]. Interestingly, these genes are commonly downregulated in AD [45] and their expression is reduced upon stimulation with T-helper (Th)2 cytokines IL-4 and IL-13 *in vitro* [46-48]. Furthermore, parallel downregulation of HRNR and FLG has been described [48], which is in line with the data presented in this paper. The concomitant downregulation in AD may thus not be due to merely the T helper 2-cytokine milieu, as previously suggested [48], but also result from loss-of-function variants in *FLG*. In addition, we identified other important proteins to be largely downregulated in ΔFLG keratinocytes. Of particular interest is KRT2, the disease-causing gene in superficial epidermolytic ichthyosis (or ichthyosis bullosa of Siemens) [49, 50], a congenital skin disease,

characterized by dry skin and barrier loss [51], and recently found to be differentially expressed in vesicular hand eczema patients [52]. We hypothesize that the profilaggrin N-terminal fragment can fulfill a regulatory function in the epidermis. This would explain the observed loss of specific epidermal proteins, such as KRT2, under knockout conditions, while its loss is not reported in any of the well-studied *FLG* loss-of-function variants that still express the N-terminal profilaggrin fragment. Besides having a potential regulatory function in the epidermis, it was reported that filaggrin might function as a structural anchoring protein in the terminally differentiating keratinocytes [53, 54]. The loss of filaggrin then implies that other differentiation proteins, *e.g.*, IVL, are less stabilized and consequently more prone to degradation by proteasomal machinery. Although this does not explain sustained downregulation even after correction of the ΔFLG genotype, like seen for HRNR.

Microscopic qualitative analysis of lucifer yellow and biotin permeation did not indicate gross functional barrier disturbance in HEEs from ΔFLG keratinocytes, which is in line with our previous findings on patient-derived *FLG* null keratinocytes [11]. Nevertheless, the quantitative and presumably more sensitive barrier measurements we now performed (EIS and TEWL), indicate that the loss of filaggrin does affect barrier properties of HEEs, which is reversed by reinstating filaggrin expression. Whether this is directly or indirectly linked to the proposed scaffolding properties of filaggrin [55] requires further investigation, likewise the comparison of the ΔFLG-associated barrier impairment to patient-derived HEEs. Furthermore, additional analyses could be focused at the regulation of tight junction associated genes and proteins [10], and at the organization of structural intercellular lipid lamellae which are considered important for functional barrier properties of the SC [6].

For the clinical translation of our findings, next steps are aimed at the reproduction of common *FLG* variants (*e.g.*, p.R501X, c.2282del4, and p.R2447X) in N/TERT-2G immortalized keratinocytes to allow for a better comparison of genotype-phenotype differences in organotypic skin models within an otherwise identical genetic background. The subsequent exposure to disease-associated inflammatory mediators or environmental factors enables the characterization of gene-environment interactions that drive multifactorial diseases, like AD. We here present the key technology and translational tools for generating unique human keratinocytes to create epidermal models with defined *FLG* variants, in which future integrative multiomics analysis can elucidate the modes of action by which profilaggrin controls terminal differentiation, and potentially finding new therapeutic options for atopic dermatitis and ichthyosis vulgaris to restore epidermal homeostasis.

Acknowledgements

This work was supported by a LEO foundation grant LF18068 (PZ and EB), PAST4FUTURE grant LSHM20043-HSGF (EB), and Innovative Medicines Initiative 2 Joint Undertaking (JU) grant under grant agreement no. 821511 (EB). The JU receives support from the European Union's Horizon 2020 research and innovation program and EFPIA. The Graphical abstract was created with Biorender.com. The authors declare no conflicts of interest. This publication reflects only the author's view and the JU is not responsible for any use that may be made of the information it contains.

Abbreviations

AD - atopic dermatitis, CRISPR - clustered regularly interspaced short palindromic repeat, Cas9 - CRISPR-associated protein 9, EIS - electrical impedance spectroscopy, HDR - homology directed repair, HEE - human epidermal equivalent, LY - Lucifer Yellow, NHEJ - non-homologous end joining, NMF - natural moisturizing factor, PAM - protospacer adjacent motif, SC - stratum corneum, SG - stratum granulosum, sgRNA - single guide RNA, ssODN - single strand donor oligonucleotide, TEER - transepithelial electrical resistance, TERT - telomerase reverse transcriptase, TEWL - transepidermal water loss

References

1. Palmer, C.N., et al., Common loss-of-function variants of the epidermal barrier protein filaggrin are a major predisposing factor for atopic dermatitis. Nat Genet, 2006. **38**(4): p. 441-6.
2. Smith, F.J., et al., Loss-of-function mutations in the gene encoding filaggrin cause ichthyosis vulgaris. Nat Genet, 2006. **38**(3): p. 337-42.
3. Scott, I.R. and C.R. Harding, Filaggrin breakdown to water binding compounds during development of the rat stratum corneum is controlled by the water activity of the environment. Dev Biol, 1986. **115**(1): p. 84-92.
4. Horii, I., et al., Stratum corneum hydration and amino acid content in xerotic skin. Br J Dermatol, 1989. **121**(5): p. 587-92.
5. Kezic, S., et al., Loss-of-function mutations in the filaggrin gene lead to reduced level of natural moisturizing factor in the stratum corneum. J Invest Dermatol, 2008. **128**(8): p. 2117-9.
6. Riethmuller, C., et al., Filaggrin breakdown products determine corneocyte conformation in patients with atopic dermatitis. J Allergy Clin Immunol, 2015. **136**(6): p. 1573-1580 e2.
7. Kawasaki, H., et al., Altered stratum corneum barrier and enhanced percutaneous immune responses in filaggrin-null mice. J Allergy Clin Immunol, 2012. **129**(6): p. 1538-46 e6.
8. Jakasa, I., et al., Skin barrier function in healthy subjects and patients with atopic dermatitis in relation to filaggrin loss-of-function mutations. J Invest Dermatol, 2011. **131**(2): p. 540-2.
9. Flohr, C., et al., Filaggrin loss-of-function mutations are associated with early-onset eczema, eczema severity and transepidermal water loss at 3 months of age. Br J Dermatol, 2010. **163**(6): p. 1333-6.
10. Winge, M.C., et al., Filaggrin genotype determines functional and molecular alterations in skin of patients with atopic dermatitis and ichthyosis vulgaris. PLoS One, 2011. **6**(12): p. e28254.
11. Niehues, H., et al., Epidermal equivalents of filaggrin null keratinocytes do not show impaired skin barrier function. J Allergy Clin Immunol, 2017. **139**(6): p. 1979-1981 e13.
12. Jinek, M., et al., A programmable dual-RNA-guided DNA endonuclease in adaptive bacterial immunity. Science, 2012. **337**(6096): p. 816-21.
13. Gasiunas, G., et al., Cas9-crRNA ribonucleoprotein complex mediates specific DNA cleavage for adaptive immunity in bacteria. Proc Natl Acad Sci U S A, 2012. **109**(39): p. E2579-86.
14. Cong, L., et al., Multiplex genome engineering using CRISPR/Cas systems. Science, 2013. **339**(6121): p. 819-23.
15. Mali, P., et al., RNA-guided human genome engineering via Cas9. Science, 2013. **339**(6121): p. 823-6.
16. Shi, H., et al., Research Techniques Made Simple: Delivery of the CRISPR/Cas9 Components into Epidermal Cells. J Invest Dermatol, 2021. **141**(6): p. 1375-1381 e1.
17. Smits, J.P.H., et al., CRISPR-Cas9Based Genomic Engineering in Keratinocytes: From Technology to Application. JID Innov, 2022. **2**(2): p. 100082.
18. Dickson, M.A., et al., Human keratinocytes that express hTERT and also bypass a p16(INK4a)-enforced mechanism that limits life span become immortal yet retain normal growth and differentiation characteristics. Mol Cell Biol, 2000. **20**(4): p. 1436-47.
19. Smits, J.P.H., et al., Immortalized N/TERT keratinocytes as an alternative cell source in 3D human epidermal models. Sci Rep, 2017. **7**(1): p. 11838.

20. Evrard, C., et al., Deletion of TNFAIP6 Gene in Human Keratinocytes Demonstrates a Role for TSG-6 to Retain Hyaluronan Inside Epidermis. JID Innov, 2021. **1**(4): p. 100054.
21. Concordet, J.P. and M. Haeussler, CRISPOR: intuitive guide selection for CRISPR/Cas9 genome editing experiments and screens. Nucleic Acids Res, 2018. **46**(W1): p. W242-W245.
22. Chen, Y., et al., COOH terminus of occludin is required for tight junction barrier function in early Xenopus embryos. J Cell Biol, 1997. **138**(4): p. 891-9.
23. Furuse, M., et al., Claudin-based tight junctions are crucial for the mammalian epidermal barrier: a lesson from claudin-1-deficient mice. J Cell Biol, 2002. **156**(6): p. 1099-111.
24. Gallagher, D.N. and J.E. Haber, Repair of a Site-Specific DNA Cleavage: Old-School Lessons for Cas9-Mediated Gene Editing. ACS Chem Biol, 2018. **13**(2): p. 397-405.
25. Barker, J.N., et al., Null mutations in the filaggrin gene (FLG) determine major susceptibility to early-onset atopic dermatitis that persists into adulthood. J Invest Dermatol, 2007. **127**(3): p. 564-7.
26. Brown, S.J., et al., Intragenic copy number variation within filaggrin contributes to the risk of atopic dermatitis with a dose-dependent effect. J Invest Dermatol, 2012. **132**(1): p. 98-104.
27. Sandilands, A., et al., Comprehensive analysis of the gene encoding filaggrin uncovers prevalent and rare mutations in ichthyosis vulgaris and atopic eczema. Nat Genet, 2007. **39**(5): p. 650-4.
28. de Veer, S.J., et al., Proteases: common culprits in human skin disorders. Trends Mol Med, 2014. **20**(3): p. 166-78.
29. Ovaere, P., et al., The emerging roles of serine protease cascades in the epidermis. Trends Biochem Sci, 2009. **34**(9): p. 453-63.
30. Matsui, T., et al., SASPase regulates stratum corneum hydration through profilaggrin-to-filaggrin processing. EMBO Mol Med, 2011. **3**(6): p. 320-33.
31. Sakabe, J., et al., Kallikrein-related peptidase 5 functions in proteolytic processing of profilaggrin in cultured human keratinocytes. J Biol Chem, 2013. **288**(24): p. 17179-89.
32. List, K., et al., Loss of proteolytically processed filaggrin caused by epidermal deletion of Matriptase/MT-SP1. J Cell Biol, 2003. **163**(4): p. 901-10.
33. Pearton, D.J., et al., Proprotein convertase expression and localization in epidermis: evidence for multiple roles and substrates. Exp Dermatol, 2001. **10**(3): p. 193-203.
34. Hoste, E., et al., Caspase-14 is required for filaggrin degradation to natural moisturizing factors in the skin. J Invest Dermatol, 2011. **131**(11): p. 2233-41.
35. Kamata, Y., et al., Neutral cysteine protease bleomycin hydrolase is essential for the breakdown of deiminated filaggrin into amino acids. J Biol Chem, 2009. **284**(19): p. 12829-36.
36. Presland, R.B., et al., Evidence for specific proteolytic cleavage of the N-terminal domain of human profilaggrin during epidermal differentiation. J Invest Dermatol, 1997. **108**(2): p. 170-8.
37. Ishida-Yamamoto, A., et al., Translocation of profilaggrin N-terminal domain into keratinocyte nuclei with fragmented DNA in normal human skin and loricrin keratoderma. Lab Invest, 1998. **78**(10): p. 1245-53.
38. Zhang, D., et al., Characterization of mouse profilaggrin: evidence for nuclear engulfment and translocation of the profilaggrin B-domain during epidermal differentiation. J Invest Dermatol, 2002. **119**(4): p. 905-12.
39. Aho, S., et al., Regulatory role for the profilaggrin N-terminal domain in epidermal homeostasis. J Invest Dermatol, 2012. **132**(10): p. 2376-2385.

40. Pearton, D.J., B.A. Dale, and R.B. Presland, Functional analysis of the profilaggrin N-terminal peptide: identification of domains that regulate nuclear and cytoplasmic distribution. J Invest Dermatol, 2002. **119**(3): p. 661-9.
41. Mildner, M., et al., Knockdown of filaggrin impairs diffusion barrier function and increases UV sensitivity in a human skin model. J Invest Dermatol, 2010. **130**(9): p. 2286-94.
42. van Leersum, F.S., et al., Improving the diagnostic yield for filaggrin: Concealed mutations in the Dutch population. J Allergy Clin Immunol, 2020. **145**(6): p. 1704-1706 e2.
43. Oji, V., et al., Ichthyosis vulgaris: novel FLG mutations in the German population and high presence of CD1a+ cells in the epidermis of the atopic subgroup. Br J Dermatol, 2009. **160**(4): p. 771-81.
44. Pendaries, V., et al., Knockdown of filaggrin in a three-dimensional reconstructed human epidermis impairs keratinocyte differentiation. J Invest Dermatol, 2014. **134**(12): p. 2938-2946.
45. Wu, Z., et al., Highly complex peptide aggregates of the S100 fused-type protein hornerin are present in human skin. J Invest Dermatol, 2009. **129**(6): p. 1446-58.
46. van den Bogaard, E.H., et al., Coal tar induces AHR-dependent skin barrier repair in atopic dermatitis. J Clin Invest, 2013. **123**(2): p. 917-27.
47. Kim, B.E., et al., Loricrin and involucrin expression is down-regulated by Th2 cytokines through STAT-6. Clin Immunol, 2008. **126**(3): p. 332-7.
48. Pellerin, L., et al., Defects of filaggrin-like proteins in both lesional and nonlesional atopic skin. J Allergy Clin Immunol, 2013. **131**(4): p. 1094-102.
49. Steijlen, P.M., et al., Genetic linkage of the keratin type II gene cluster with ichthyosis bullosa of Siemens and with autosomal dominant ichthyosis exfoliativa. J Invest Dermatol, 1994. **103**(3): p. 282-5.
50. Kremer, H., et al., Ichthyosis bullosa of Siemens is caused by mutations in the keratin 2e gene. J Invest Dermatol, 1994. **103**(3): p. 286-9.
51. Traupe, H., et al., Ichthyosis bullosa of Siemens: a unique type of epidermolytic hyperkeratosis. J Am Acad Dermatol, 1986. **14**(6): p. 1000-5.
52. Voorberg, A.N., et al., Vesicular hand eczema transcriptome analysis provides insights into its pathophysiology. Exp Dermatol, 2021. **30**(12): p. 1775-1786.
53. Eckhart, L., et al., Cell death by cornification. Biochim Biophys Acta, 2013. **1833**(12): p. 3471-3480.
54. Candi, E., R. Schmidt, and G. Melino, The cornified envelope: a model of cell death in the skin. Nat Rev Mol Cell Biol, 2005. **6**(4): p. 328-40.
55. Gutowska-Owsiak, D., et al., Orchestrated control of filaggrin-actin scaffolds underpins cornification. Cell Death Dis, 2018. **9**(4): p. 412.
56. Bergboer, J.G., et al., Psoriasis risk genes of the late cornified envelope-3 group are distinctly expressed compared with genes of other LCE groups. Am J Pathol, 2011. **178**(4): p. 1470-7.
57. van Duijnhoven, J.L., et al., MON-150, a versatile monoclonal antibody against involucrin: characterization and applications. Arch Dermatol Res, 1992. **284**(3): p. 167-72.
58. Doench, J.G., et al., Optimized sgRNA design to maximize activity and minimize off-target effects of CRISPR-Cas9. Nat Biotechnol, 2016. **34**(2): p. 184-191.
59. Rice, P., I. Longden, and A. Bleasby, EMBOSS: the European Molecular Biology Open Software Suite. Trends Genet, 2000. **16**(6): p. 276-7.
60. Livak, K.J. and T.D. Schmittgen, Analysis of relative gene expression data using real-time quantitative PCR and the 2(-Delta Delta C(T)) Method. Methods, 2001. **25**(4): p. 402-8.

Supplemental figures

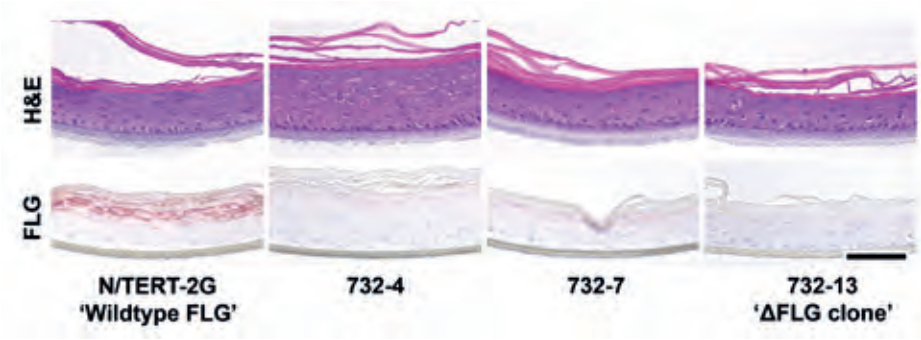

Supplementary Figure S1. Three ΔFLG N/TERT-2G clonal keratinocyte cell lines. After clonal expansion of the ΔFLG pool, ΔFLG clonal cells were isolated (732-4, 732-7, and 732-13). Clonal cells 732-13 were renamed to 'ΔFLG clone' and used throughout the manuscript. In HEE culture, all of the ΔFLG clonal cell lines show absence of keratohyalin granules and FLG expression, whilst epidermal thickness between clonal cell lines varies. Bar = 100 µm.

Supplemental tables

Supplementary Table S1: Genomic information on isolated clonal N/TERT-2G keratinocytes.

Name in manuscript	Cell line	Zygosity
"Wildtype FLG"	N/TERT-2G keratinocytes	Homozygous
"ΔFLG clone"; 732-13	ΔFLG N/TERT-2G keratinocytes	Homozygous
732-4	ΔFLG N/TERT-2G keratinocytes	Heterozygous
732-7	ΔFLG N/TERT-2G keratinocytes	Homozygous
"FLG corrected"	FLG corrected N/TERT-2G keratinocytes	Homozygous

Supplementary Table S2: Predicted off-target sites for guide RNA to generate FLG knockout N/TERT-2G keratinocytes
(Table available via online version: DOI: 10.1016/j.jid.2023.02.021)

Supplementary Table S3: Predicted off-target sites for guide RNA to generate FLG gene-corrected N/TERT-2G keratinocytes
(Table available via online version: DOI: 10.1016/j.jid.2023.02.021)

FLG expression	Allele 1	Allele 2	Predicted FLG protein
Yes	wildtype	wildtype	wildtype, 4061 amino acids
No	c.152_156del	c.152_156del	truncated, 52 amino acids
No	c.148_158del	c.151_160del	truncated, 50 amino acids and 60 amino acids
No	c.153_154del	c.153_154del	truncated, 53 amino acids
Yes	c.139-11C>T	c.139-11C>T	wildtype, 4061 amino acids

Supplementary Table S4: Sequences of the sgRNAs and ssODN.

Target	Name	sgRNA sequence (5′ – 3′)	PAM site	Strand
FLG	*FLG* wildtype	GAATCCAGATGACCCAGATA	TGG	-
Δ*FLG*	Δ*FLG* clone	ATCCATGAAGACATCAACCA	TGG	+
Target	**ssODN name**	**ssODN sequence**		
Δ*FLG*	Filaggrin correction ssODN	AATTGGCTGATAATGTGATTCTGTCTGATGCAGTCTCCCTCTGTGACTT CTCTCTGTACAGAATCCAGATGACCCAGATATGGTTGATGTCTTCATGG ATCACTTGGATATAGACCACAACAAGAAAATTGACTTCACTGAGTTTCTTCT		

Supplementary Table S5: PCR Primer sequences.

Gene	Target name	Forward primer (5′ – 3′)	Reverse primer (5′ – 3′)
FLG	*FLG* wildtype	TGGCTGATAATGTGATTCTGTC	CTGTTTCTCTTGGGCTCTTGG
Name	**Off-target site**	**Forward primer (5′ – 3′)**	**Reverse primer (5′ – 3′)**
KO_Off1	intergenic:PROM2-KCNIP3	TTGAGAAAGCTCAGGCACAC	CACTCAGGCTAGAAGCGATG
KO_Off2	intergenic:MIR873-LINC01242	CTCCAGCCAACATCAAGAAA	TTTCCAAAGGGAATTGATCC
KO_Off3	intron:ELAVL2	GGACAGACATCTGCATTCATTC	TTACCAGATTGCGTCCTGTG
KO_Off4	intergenic:GMNC-OSTN	AGAAGCAGGCTGACACCTTT	CCCAGTGATGAGGAATGGAT
KO_Off5	intergenic:Y_RNA-RP11-112L7.1	CTGTGGTTTGGTCCATTCAG	GGGAGGTCTTGTCCAGTGAT
Cor_Off1	intron:ZC3H13	CTTCTGACGCTTCATTTCCA	AACCCAACTTCCAAACAACC
Cor_Off2	intron:LINC00375	GCCAAGGTATTCAAAAGATGG	ACAACAAAGCCTCCCTGAAT
Cor_Off3	intergenic:AC090573.1-RP11-65D17.1	CGCTCCTGCAACTTCAGTAA	AGATGGCTTTGGGGAGTATG
Cor_Off4	intron:SLC16A9	TCCCACAAACATTCCATGAG	CATCTGTGAAGGCAGGCTAA
Cor_Off5	intergenic:RP11-574O16.1-AC010887.1	GAGCCACAGAGCCTTCTTCT	AGAGCTGGGATTTGAGCCTA

Supplementary Table S6: Antibodies used for immunohistochemistry.

Antibody; clone	Manufacturer	Dilution
FLG; 1957R	LifeSpan BioSciences, Inc., Seattle, WA, USA (catalog # LS-C751132)	1:200
LOR; polyclonal	Abcam, Cambridge, United Kingdom (catalog # ab85679)	1:3000
KRT10; DE-K10	Progen Biotechnik GmbH	1:100
LCE2; #74	Bergboer *et al* 2011 [56]	1:10000
LCE3; clone 7	Abmart, Berkeley Heights, NJ, USA	1:5000
IVL; Mon150	Van Duijnhoven *et al* 1992 [57]	1:20
TGM1; A-5	Santa Cruz Biotechnology Inc., Dallas, TX, USA (catalog # sc-365821)	1:100
HRNR; polyclonal	Sigma-Aldrich (catalog # HPA031469)	1:500
KRT2; Ks2.342.7.4	Progen Biotechnik GmbH, Heidelberg, Germany (catalog # 65191)	1:200

Supplementary Table S7: Quantitative PCR primer sequences.

Gene	Target name	Forward primer (5′ – 3′)	Reverse primer (5′ – 3′)
hARP	Human acidic ribosomal phosphoprotein P0	CACCATTGAAATCCTGAGTGATGT	TGACCAGCCCAAAGGAGAAG
IVL	Involucrin	ACTTATTTCGGGTCCGCTAGGT	GAGACATGTAGAGGGACAGAGTCAAG
TGM1	Transglutaminase 1	CCCCCGCAATGAGATCTACA	ATCCTCATGGTCCACGTACACA
HRNR	Hornerin	TACAAGGCGTCATCACTGTCATC	ATCTGGATCGTTTGGATTCTTCAG
KRT2	Keratin 2	CGCCACCTACCGCAAACT	GAAATGGTGCTGCTTGTCACA

Supplemental methods

In silico search for potential off-target effects

CRISPOR (version 4.98) [21] was used to search for potential off-target sites dependent on the *Streptococcus pyogenes* derived Cas9 (SpCas9) PAM site (5′-NGG-3′), target genome (homo sapiens GRCh38/hg38) and our specific sgRNA selection. The top-5 potential off-target sites, ranked on cutting frequency determination (CFD) score [58], were amplified by PCR and analyzed by Sanger sequencing to assure no off-target mutations occurred. See Supplementary Table S5 for details on the PCR primers used.

Protein sequence prediction

EMBOSS Transeq (https://www.ebi.ac.uk/Tools/st/emboss_transeq/), a webtool designed to predict the translation of mRNA sequence into protein amino acid sequence was used with standard settings to predict the result of the DNA mutations generated [59].

Morphological and immunohistochemical analysis

HEEs were fixed in 4% formalin solution for 4 hours and subsequently embedded in paraffin. 6 µm sections were stained with hematoxylin and eosin (H&E, Sigma-Aldrich) or processed for immunohistochemical analysis. Sections were blocked for 15 minutes with 5% serum in phosphate-buffered saline (PBS) and subsequently incubated with primary antibody against the protein of interest for 1 hour at room temperature. Next, a 30 minute incubation step with biotinylated secondary antibody (Vector Laboratories, Burlingame, CA, USA) was performed, followed by a 30 minute incubation with avidin-biotin complex (Vector laboratories). The peroxidase activity of 3-Amino-9-ethylcarbazole (AEC) was used to visualize the

protein expression and the sections were mounted using glycerol gelatin (Sigma-Aldrich). See Supplementary Table S6 for details on the primary antibodies used.

Transcriptional analysis

Total RNA was isolated using the Favorprep total tissue RNA kit (Favorgen Biotech, Taiwan), according to the manufacturer's protocol. cDNA was generated after DNase treatment and used for quantitative real-time PCR (RT-qPCR) by use of the MyiQ Single-Colour Real-Time Detection System (Bio-Rad laboratories, Hercules, CA, USA) for quantification with Sybr Green and melting curve analysis. Primers (Supplementary Table S7) were obtained from Biolegio (Nijmegen, The Netherlands) and Merck KGaA (Darmstadt, Germany). Target gene expression levels were normalized to the expression of *human acidic ribosomal phosphoprotein P0* (*RPLP0*). The relative expression levels of all genes of interest were measured using the 2-ΔΔCT method [60]. Two-way ANOVA with Tukey's multiple comparison tests were performed on the ΔCT values to assess statistical significance.

Lucifer yellow dye penetration assay

To study the outside-in SC barrier function, 20 µL Lucifer Yellow (1 mM, Sigma-Aldrich) was applied on top of the HEEs and was allowed to incubate for 60 minutes in the dark at room temperature. HEEs were fixed in buffered 4% formalin solution, embedded in paraffin and sectioned. 6 µm sections were deparaffinized and mounted with Fluoromount-G, containing DAPI (eBioscience Inc. San Diego, CA, USA).

Biotin penetration assay

To study the inside-out SC barrier function, the HEEs were turned upside down and 20 µL EZ-link sulfo-NHS-LC-biotin (3.3 mg/mL, Thermo Fisher Scientific, Waltham, MA, USA) was applied on the bottom of the filters and allowed to incubate for 60 minutes at room temperature. HEEs were fixated in buffered 4% formalin solution, embedded in paraffin and sectioned. 6 µm sections were deparaffinized and incubated for 30 minutes, in the dark, with 1:200 Alexa Fluor 594 streptavidin (Thermo Fisher Scientific) conjugate. The sections were mounted with Fluoromount-G containing DAPI.

Electrical impedance spectroscopy (EIS) and transepidermal water loss (TEWL)

Whereas transepithelial electrical resistance (TEER) measurements are suitable for detecting barrier properties related to tight junction presence and functionality, EIS is more suitable for epidermal equivalent cultures as it is a composed measure

of TEER and electrical capacity of the cell compartment. EIS was measured using the real-time impedance detector Locsense Artemis (Locsense, Enschede, The Netherlands) equipped with SmartSense lid for monitoring cells in conventional transwell plates containing inserts. After lowering of day 10 air-exposed HEE cultures to the middle position of the culture plate, 500 µL of PBS was added on top and 1100 µL PBS was added beneath the transwell filter. Following calibration, continuous impedance (Ω) was measured while sweeping frequency from 10Hz to 100.000Hz. Afterwards, measured impedance was corrected for blank impedance per electrode and corrected for culture insert size (0.47 cm^2), resulting in impedance per cm^2 values (Ω/cm^2). Subsequently, measured phase values along the same frequency reach were used to pinpoint the frequencies where contribution of cellular capacity was relatively limited. Mean impedance per cm^2 at these three frequencies was used to calculate relative differences between conditions. Two-way ANOVA with Tukey's multiple comparison test was performed to assess statistical significance. TEWL was measured, after equilibration of the HEE cultures to room temperature, using the Aquaflux AF200 (Biox, London, UK) on day 10 of the air-exposed phase of the HEE culture, as described before [11]. Unpaired parametric t test was used to assess statistical significance.

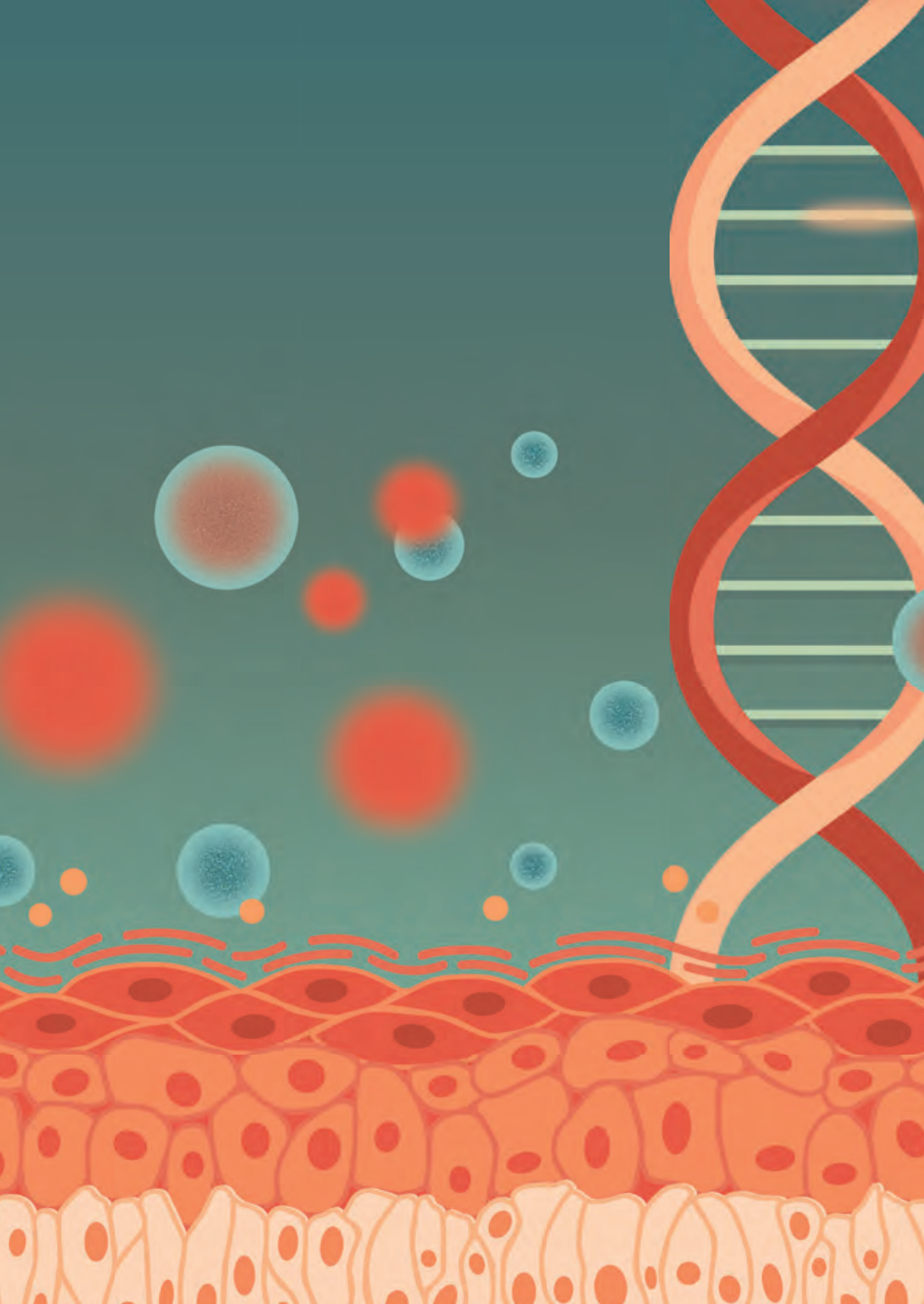

Chapter 5.

Electrical impedance spectroscopy quantifies skin barrier function in organotypic *in vitro* epidermis models

Noa J.M. van den Brink[1,†], Felicitas Pardow[1,2,†], Luca D. Meesters[1,2], Ivonne van Vlijmen-Willems[1], Diana Rodijk-Olthuis[1], Hanna Niehues[1], Patrick A.M. Jansen[1], Susan H. Roelofs[3], Matthew G. Brewer[4], Ellen H. van den Bogaard[1,#] and Jos P.H. Smits[1,5,#]

Affiliations

[1] Department of Dermatology, Radboudumc, Nijmegen, The Netherlands

[2] Department of Molecular Developmental Biology, Faculty of Science, Radboud University, Nijmegen, The Netherlands

[3] Locsense B.V., Enschede, The Netherlands

[4] Department of Dermatology, University of Rochester Medical Center, Rochester, New York, USA

[5] Department of Dermatology, Heinrich Heine University, University Hospital Düsseldorf, Düsseldorf, Germany

[†] contributed equally

[#] shared senior authorship

Published in

J Invest Dermatol. 2024 Nov;144(11):2488-2500.e4. doi: 10.1016/j.jid.2024.03.038.

Abstract

3-dimensional human epidermal equivalents (HEEs) are a state-of-the-art organotypic culture model in preclinical investigative dermatology and regulatory toxicology. Here, we investigated the utility of electrical impedance spectroscopy (EIS) for noninvasive measurement of HEE epidermal barrier function. Our setup comprised a custom–made lid fit with 12 electrode pairs aligned on the standard 24–transwell cell culture system. Serial EIS measurements for seven consecutive days did not impact epidermal morphology and readouts showed comparable trends to HEEs measured only once. We determined two frequency ranges in the resulting impedance spectra: a lower frequency range termed EIS^{diff} correlated with keratinocyte terminal differentiation independent of epidermal thickness, and a higher frequency range termed EIS^{SC} correlated with *stratum corneum* thickness. HEEs generated from CRISPR/Cas9 engineered keratinocytes that lack key differentiation genes *FLG*, *TFAP2A, AHR* or *CLDN1* confirmed that keratinocyte terminal differentiation is the major parameter defining EIS^{diff}. Exposure to proinflammatory psoriasis- or atopic dermatitis-associated cytokine cocktails lowered the expression of keratinocyte differentiation markers and reduced EIS^{diff}. This cytokine–associated decrease in EIS^{diff} was normalized after stimulation with therapeutic molecules. In conclusion, EIS provides a noninvasive system to consecutively and quantitatively assess HEE barrier function and to sensitively and objectively measure barrier development, defects and repair.

Graphical abstract

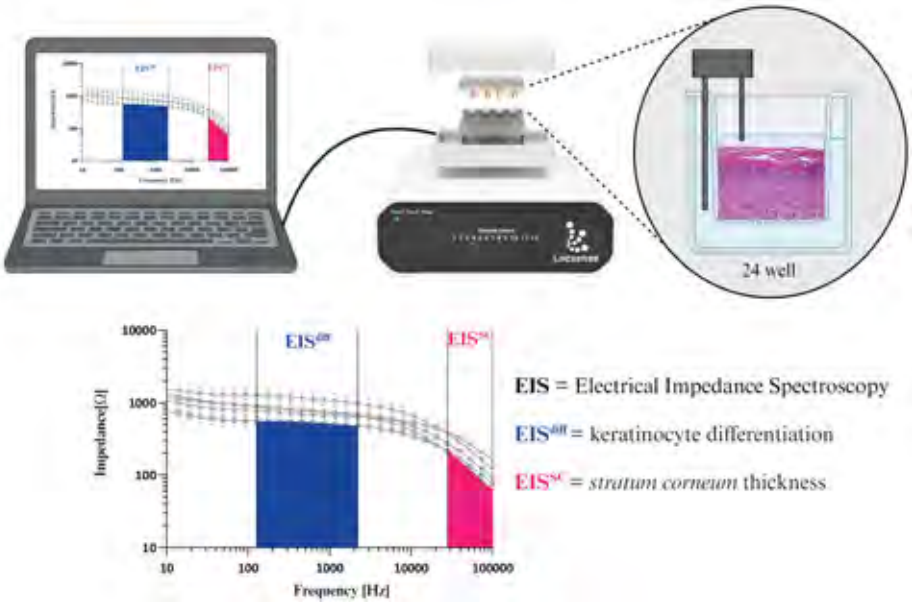

Introduction

Intact physical barriers are of highest importance for our body to define a biophysically enclosed environment. The skin, our largest barrier organ, serves a dual role: it forms an outside–in barrier, protecting the insides of our body from mechanical damage and environmental triggers, and it protects the epidermis and subjacent tissues from dehydration as an inside–out barrier. Barrier functionality is achieved most prominently by a highly organized physical barrier, constituted of tight junctions in the *stratum granulosum* and corneodesmosomes in the *stratum corneum* [1]. *Stratum corneum* corneocytes also are coated with a heavily crosslinked cornified envelope [2] and the intercellular space between is filled with lipids, generating a hydrophobic environment [3]. Next to this physical barrier, the additional chemical, microbial and immunological barriers complete the multifaceted barrier function of mammalian skin [4, 5].

The importance of the skin barrier is apparent from its malfunction in common skin diseases, like psoriasis and atopic dermatitis. The disease–associated pro–inflammatory milieu also negatively affects keratinocyte differentiation and impairs tight junction and corneodesmosome function [6-8]. Next to these multifactorial diseases, monogenic diseases caused by mutations in skin barrier–related genes illustrate the devastating effects of impaired skin barrier function on our health and wellbeing [9, 10]. Aside from these intrinsic factors, environmental factors including exhaust fumes or detergents influence the skin barrier function of healthy individuals and patients [11]. Determining the functional consequences of such genetic and environmental risk factors on the skin barrier will aid in our understanding of disease pathogenesis and may help in the possible future prevention of disease onset or exacerbation.

To investigate skin barrier function, *in vitro* organotypic skin and human epidermal equivalents (HEEs) have become a mainstay approach. By mimicking epidermal barrier morphology and function, HEEs offer advantages over *in vitro* monolayer cultures that lack epidermal stratification and *stratum corneum* formation. In addition, HEEs are considered relevant alternatives to *in vivo* animal models that prompt ethical questions and require depilation to measure biophysical barrier function. HEEs are used from fundamental research to preclinical drug testing to regulatory toxicology in a broad range of applications [5, 12].

To assess skin barrier function in HEEs, various technologies can be used ranging from mathematical penetration modelling [13, 14] and computational simulation of lipid

organization [15] to ultrastructural imaging [16] and measuring gene and/or protein expression. In a recent consensus paper, we and others have discussed the requirements and methodologies for barrier studies in organotypic skin models [17]. In summary, functional barrier assessment using Franz cell diffusion and permeation flux studies provide most accurate estimates of the outside–in barrier [18-20]. On the other hand, water evaporation (e.g. trans–epidermal water loss (TEWL)) is considered most relevant to describe inside–out barrier function [17, 21]. Unfortunately, these methods are often labor intensive and rely on highly specific expertise and equipment (Franz cell diffusion assay), are poorly standardized (transepithelial electrical resistance (TEER), TEWL) or require destructive endpoint measurements (permeation studies) (Table S1). Furthermore, the mechanistic correlation of such measurements to skin barrier function often remains unclear [8].

Electrical impedance spectroscopy (EIS) has been developed and implemented for the assessment of skin barrier function *in vivo* and appears to correlate well with disease severity of atopic dermatitis lesions [22]. For assessment of *in vitro* barrier function, EIS has been implemented for gut, airway and neuroepithelial *in vitro* cultures [23, 24] and *ex vivo* pig ear skin models [25]. Explorative studies have applied EIS in *in vitro* epidermis models [26, 27] and link EIS to viable epidermis and *stratum corneum* barrier properties [27]. Yet, a comprehensive study which extensively assesses EIS applicability and its relation to skin barrier properties in a broad range of experimental models and disease conditions is missing. Here, we demonstrate and validate the use of EIS as a reproducible, noninvasive and quantitative high–throughput system for HEE barrier assessment and assess its correlation to epidermal barrier physiology.

Methods

Cell culture

Human primary keratinocytes were isolated from surplus human skin obtained through plastic surgery according to the principles and guidelines of the principles of Helsinki. From the skin, biopsies were taken and keratinocytes were isolated as described previously [28]. N/TERT–2G keratinocytes were a kind gift of James Rheinwald, Brigham's Woman hospital [29] and were cultured as monolayers in CnT–prime (CELLnTEC, Bern, Switzerland, CnT–PR) until confluent before use in HEE cultures [30]. Knockout N/TERT–2G cell lines were generated through CRISPR/Cas9 and validated previously (FLG [31], CLDN1 [32], TFAP2A [33], AHR [33]).

Generation of HEEs

HEE cultures were performed as previously described [31]. In short, cell culture inserts in a 24-wells carrier plate (Nunc, Thermo Fisher Scientific, 141002) were coated using 100 µg/mL rat tail collagen (Sigma–Aldrich, C3867) for 1 hour at 4°C. After phosphate–buffered saline (PBS) washing the filters, 150,000 cells were seeded and submerged in CnT–prime medium (CELLnTEC, CnT–PR) at the lowest insert stand. After 48 hours, the medium was switched to differentiation medium (40% Dulbecco's modified Eagle's Medium (Sigma–Aldrich, D6546) and 60% 3D barrier medium (CELLnTEC, CnT–PR–3D)) and 24 hours afterwards the HEEs were lifted to the highest stand and air–exposed, and medium was refreshed every other day. For stimulation experiments, IL–4, IL–13, IL–17A or IL–22 (50 ng/mL per cytokine, Peprotech, Rocky Hill, NJ, USA, 200-04/200-13/200-17/200-22) supplemented with 0.05 % bovine serum albumin (Sigma–Aldrich, A2153) were added to the medium of HEEs of primary keratinocytes from day 5 of air exposure until day 8. AHR ligands (Table S2) were supplemented in the culture medium as previously described [34].

EIS measurements

For the EIS measurements the Locsense Artemis (Locsense, Enschede, the Netherlands) device was used and equipped with a custom–made incubator compatible smart lid. The Artemis consists of a detector element that is connected to the smart lid with electrodes aligning to the two middle rows of a 24–well plate. A laptop equipped with the Locsense Artemis monitoring software (version 2.0) displays the readouts. During the measurements each well contains two electrodes: one disc–shaped 4.2 mm diameter electrode situated in the center of the transwell insert and a rod–shaped 1.9 mm diameter electrode passing sideways of the transwell insert. Before measurements, HEEs were acclimated to room temperature and cultures were lowered to the middle position in the transwell plate while 1600 µL PBS at room temperature was added below and 500 µL PBS on top of the filter. Thereafter, the smart lid was placed on the wells ensuring both electrodes being submerged. Following device self–calibration, impedance was measured over a frequency range from 10 Hz to 100,000 Hz in 30 logarithmic intervals. Measurement output contains impedance as well as phase values. Phase values can be interpreted as raw values, while a PBS only blank measurement was subtracted from the corresponding electrode of the impedance output. For further specific considerations during measurements, see technical recommendations. For EIS^{diff} (127–2212 Hz) and EIS^{SC} (28,072–100,000 Hz) the area under the curve was calculated using the respective frequency ranges.

Immunohistochemistry

For histological processing, 4 mm biopsies were fixated in 4 % formalin solution for 4 hours and embedded in paraffin. Afterwards, 6 µm sections were deparaffinized and either stained with hematoxylin (Klinipath, 4085.9005) and eosin (Klinipath, 4082.9002) or by antibodies listed in Supplemental Table S3 followed by avidin–biotin complex (Vectastain, AK–5000). Epidermal thickness specifies the average of three measurements on H&E stained sample pictures while *stratum corneum* thickness was determined by subtracting epidermal from total construct thickness. Protein expression was quantified with ImageJ following sections C–E of [35] by freehand selecting the viable epidermis and measuring the "area" i.e. number of staining–positive square pixels.

Statistics

Datasets were analyzed using the GraphPad Prism 10 software version 10.1.1. All bar plots are shown as mean ± standard error of the mean and significance testing was performed using one–way analysis of variance (ANOVA) in combination with Dunnett correction for multiple testing and unpaired t–testing (exclusively in figure 2c, d, 5b and c). Differences under p value < 0.05 were considered statistically significant, p value > 0.05 was considered not significant, * p value < 0.05, ** p value < 0.01, *** p value < 0.001.

Correlation analysis of EIS to protein expression and HEE morphology

Correlation analysis was conducted using simple (epidermis thickness and *stratum corneum* thickness) and multiple linear regression modelling (protein expression) in Graphpad Prism and the R programming language (version 4.2.3) [36] with the psychometric package [37]. All correlation analysis were conducted with individual replicates, figures depict replicate averages for readability.

Results

Development of an EIS device for in vitro HEE application

For quantitative and reproducible *in vitro* skin barrier analysis we sought to develop and validate an EIS devise for use in HEEs. The system comprises a smart lid with fixed gold-plated electrodes that are customized to fit the individual wells of a Nunc carrier plate with cell culture inserts. The setup enables standardized and automated measurements with a run time of 2 minutes per well for a maximum of 12 wells (within a 24 well–plate format). To perform the measurements, the smart lid with fixed electrodes is placed onto the HEE-carrying culture plate and

the connected measurement device (Figure 1a). The electrodes apply a very low alternating voltage *V* in a frequency range from 10 Hz to 100 kHz through the culture while measuring the amplitude and phase shift of the resulting alternating current *I*. The EIS device returns the impedance, which reflects the opposition to an alternating current over time:

$$\text{Impedance } Z = \frac{V\ (t)}{I\ (t)}$$

Impedance and phase spectra are reported in the form of a Bode plot (Figure 1b, c).

For quantitative analysis of EIS spectra, an electrical equivalent circuit model of the examined culture system is required. In conventional 2-dimensional monolayer cultures, there are two main routes of the current: a paracellular, which is determined by the ionic conductance of cell junctions serving as a paracellular resistance (R_P), and a transcellular, which consists of the resistance and capacitance of apical and basolateral membrane (R_A, R_B and C_A, C_B) next to the resistance of the cytoplasm R_{Cyt} [38, 39] (Figure 1d). In a simplified model, both membranes can be reduced to R_{Cell} and C_{Cell} respectively. In 2-dimensional monolayers, the high cellular resistance R_{Cell} and the low cytoplasmatic resistance R_{Cyt} results in paracellular flux being determined by the cellular capacitance C_{Cell} [38]. In 3-dimensioanl HEEs, multiple individual cell layers result in a parallel series of n resistor–capacitor electrical circuits [26]. While we speculate R_P, R_{Cyt}, R_{Cell} and C_{Cell} to be changing depending on cell–cell contacts, differentiation status and the cell shape in the corresponding layer, we assume the dominance of C_{Cell} over R_{Cell} and R_{Cyt} to be persistent in 3-dimensional (Figure 1e). Lastly, the resistance of the culture medium R_{Medium} and the electrodes, acting as pure capacitors with a capacitance C_{El}, conclude the electrical circuit.

These electrical circuit elements also determine the generated impedance spectrum (Figure 1f) [38]. Both, R_{Medium} and C_{El} are fixed parameters whose characteristics are determined by the chosen setup and device. The variable parameters paracellular resistance R_P and cellular capacitance C_{Cell} are determined by the measured cells and the chosen culture system (monolayer vs 3-dimensional organoid). They influence the height and frequency span of a midrange plateau and the onset of its decline [40] (Figure 1g, h). To link EIS to epidermal barrier properties, we determined two frequency ranges in the HEE impedance spectrum approximately indicating R_P and C_{Cell} contribution, EIS^{diff} (127–2212 Hz) and EIS^{SC} (28072–100000 Hz) respectively, which we analyzed by calculating their area under the curve [38] (Figure 1i).

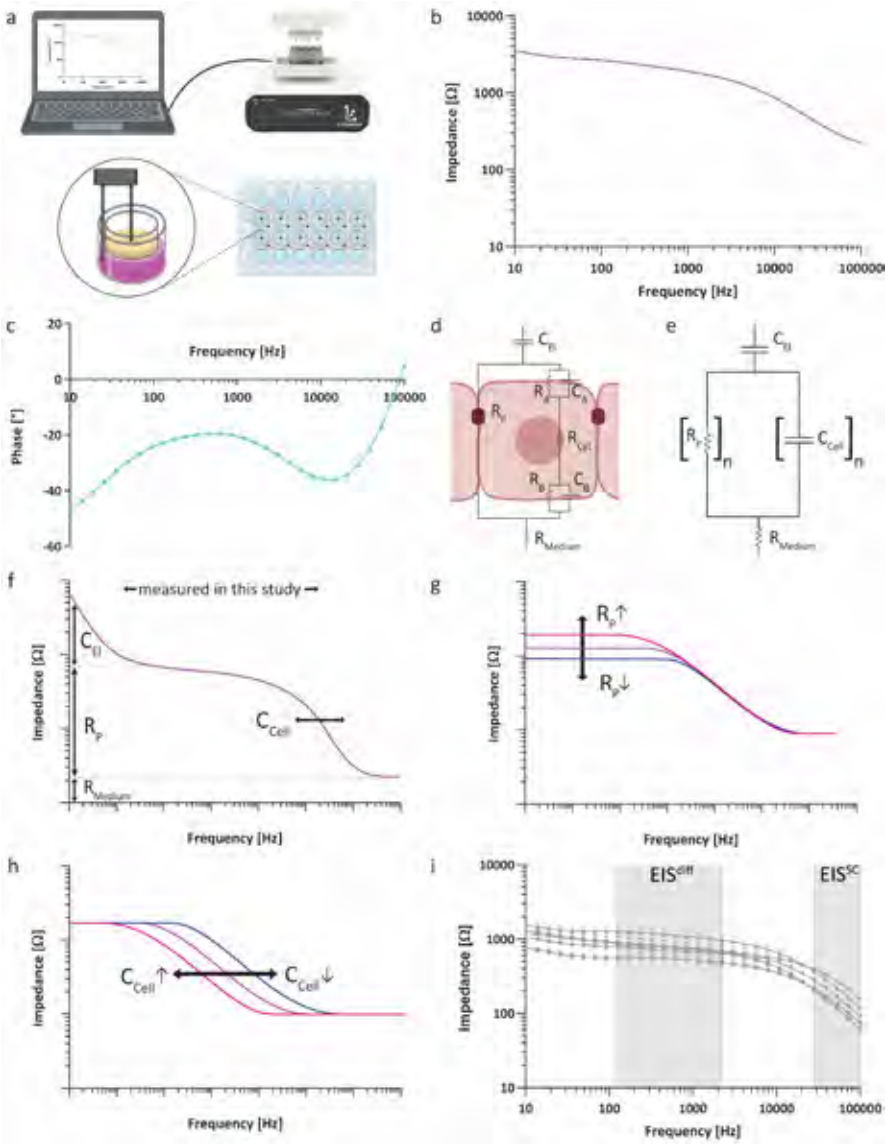

Figure 1: Design and function principle of a custom–made EIS device fitting the HEE culture system. (**A**) Schematic overview of the EIS setup on HEE cultures. (**B**) Impedance and (**C**) phase spectrum of a fully–developed NHEK HEE culture after 8 days of air exposure. (**D**) Extended electrical equivalent circuit of an epidermal monolayer culture made up of the capacitance of the electrodes C_{El}, paracellular resistance R_p, transcellular resistance of cytoplasm R_{Cyt}, apical and basolateral membrane R_A, R_B as well as their capacitance C_A, C_B and the resistance of the medium R_{Medium} (adapted from [40]). (**E**) Simplified electrical equivalent circuit of an HEE with the capacitance of both membranes taken together as C_{Cell} which together with R_p extends to a series of n parallel circuits in multilayered 3-dimensionalculture systems (adapted from [39] and [26]). (**F**) Schematic overview indicating the contribution of individual electrical circuit parameters to the impedance spectrum (adapted from [38]). (**G, H**) Simulated impedance spectra illustrating the influence of changes in (**G**) paracellular flux (R_p) and (**H**) transcellular flux (C_{Cell}) (adapted from [40]). (i) EIS impedance spectrum displaying EIS^{diff} (127–2212 Hz) and EIS^{SC} (28072–100000 Hz).

5

Serial measurements show increased electrical resistance without affecting HEE development

To determine whether EIS can be used to monitor the development of HEEs noninvasively, serial measurements were performed over consecutive days of immortalized N/TERT–2G keratinocyte air–liquid interface culture. When comparing serial with end point measurements performed directly before harvesting, EIS spectra showed similar trends (Figure 2a, b) and differences in EIS^{diff} and EIS^{SC} were not significant (Figure 2c, d). Morphological analysis by hematoxylin and eosin (H&E) staining did not indicate destructive effects of EIS in endpoint or in serial measurements (Figure 2e, top panel). In addition, neither keratinocytes proliferation capacity (Ki67 staining), expression of differentiation proteins (involucrin (IVL) and filaggrin (FLG)), nor the expression of stress–related markers (keratin 16 (KRT16) and skin–derived antileukoprotease (SKALP)) were changed by EIS measurements (Figure 2e). Of note, expression levels of SKALP and the proliferation marker KRT16 are known to be higher in neonatal–derived immortal N/TERT–2G than in primary adult keratinocytes [28, 30]. To further evaluate EIS' reliability, HEEs were subjected to EIS measurements six times within one hour (Figure 2f), clearly indicating a very high repeatability. When checking for potentially delayed cytotoxic effects, HEEs harvested 24 hours after repeated EIS measurements showed no morphological signs of cytotoxicity and continuing maturation, as seen by the formation of additional epidermal layers (Figure 2g).

Different electrical impedance spectra can be linked to keratinocyte differentiation and *stratum corneum* thickness

The EIS device measures impedance over a broad range of frequencies, which we sought to correlate with epidermal barrier properties. For this, we determined EIS^{diff} and EIS^{SC} of HEEs during barrier development (Figure 3a–c) and performed correlation analysis with principle epidermal barrier compartments (Figure 3d–g). We observed the thickness of viable epidermal layers to be increasing from day 1–10 before decreasing at day 12 and 14 (Figure S1a, b), which correlated with EIS^{diff} but not with EIS^{SC} (Figure 3d, e). At the same time *stratum corneum* thickness did not correlate with EIS^{diff} but strongly correlated with EIS^{SC} explaining 62 % of its variance (Figure 3f–g). Since keratinocyte terminal differentiation plays a major role in the formation of the skin barrier, we also investigated the protein expression of essential terminal differentiation proteins in relation to EIS^{diff} (Figure 3h–l). EIS^{diff} correlated with the quantified expression of keratinocyte differentiation markers FLG and IVL which increased in early days of HEE development before decreasing after maturation at day 14 (Figure 3h–j). Expression of the tight junction proteins, claudin 1 (CLDN1) and claudin 4 (CLDN4) could not be linked to EIS^{diff} (Figure 3h, k–l).

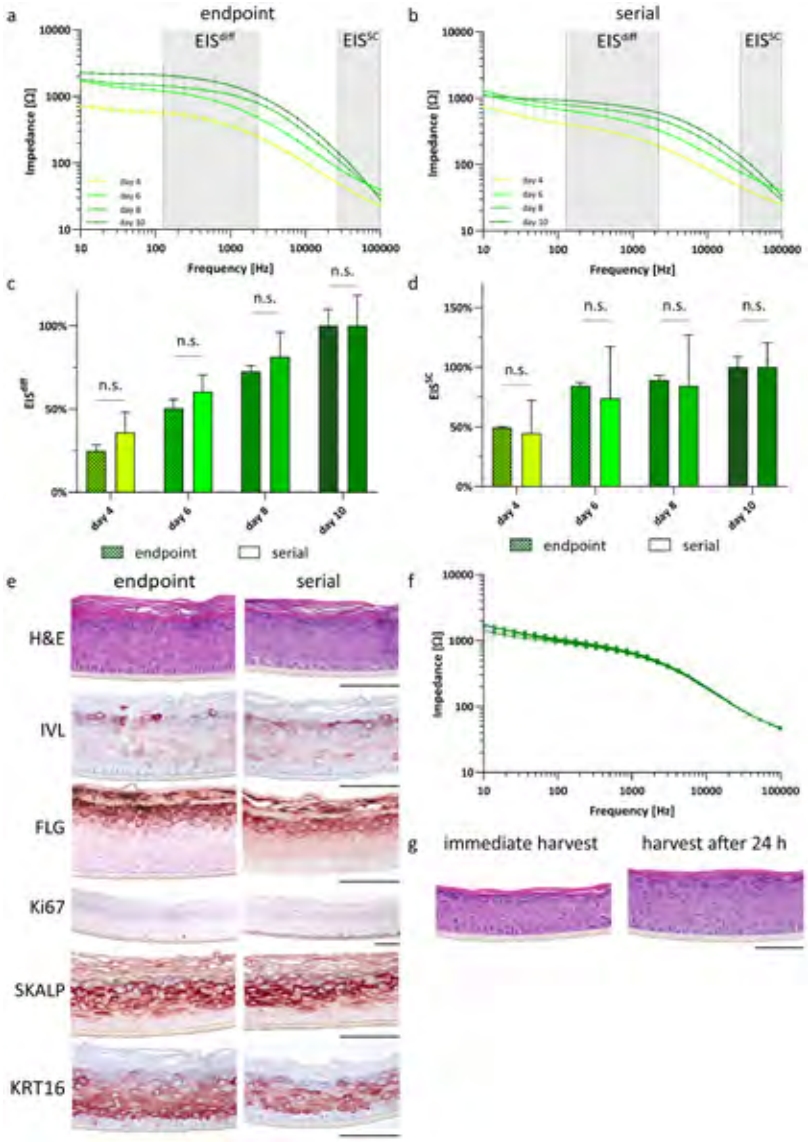

Figure 2: Relative EIS measurements are reproducible and do not impair HEE development. (**A, B**) EIS impedance spectra during HEE development with constructs being harvested (**A**) directly after measurements (endpoint measurements) and (**B**) at day 10 of air exposure (serial measurements). Each timepoint averages three biological replicates. (**C**) Comparison of EIS^{diff} and (**D**) EIS^{SC} between endpoint and serial measurements. (**E**) Histological comparison of HEEs undergoing endpoint or serial EIS measurements based on general morphology (H&E staining), differentiation status (FLG, IVL expression), proliferation (Ki67) and stress response (SKALP, KRT16). Pictures represent three biological replicates at day 10 of air exposure and taken at either 20x (Ki67) or 40x magnification. Size bars indicate 100 µm. (**F**) Impedance spectrum of HEEs (n = 3) measured 6 times within 1 hour at day 6 of air exposure. (**G**) Histological comparison of HEEs measured 6 times in 1 hour, either harvested directly or 24 hours after EIS measurements. Pictures represent three biological replicates and were taken at 40x magnification. Size bar indicates 100 µm.

When investigating the contributions of FLG, IVL, CLDN1 and CLDN4 altogether, CLDN1 and CLDN4 were not observed contributing to EIS^{diff} during HEE development and did not add additional explanatory value to the correlation model (Figure S1c, d). The expression of FLG, IVL and their collaborative interaction on the other hand together could explain 76 % of EIS^{diff} (Figure S1e, f).

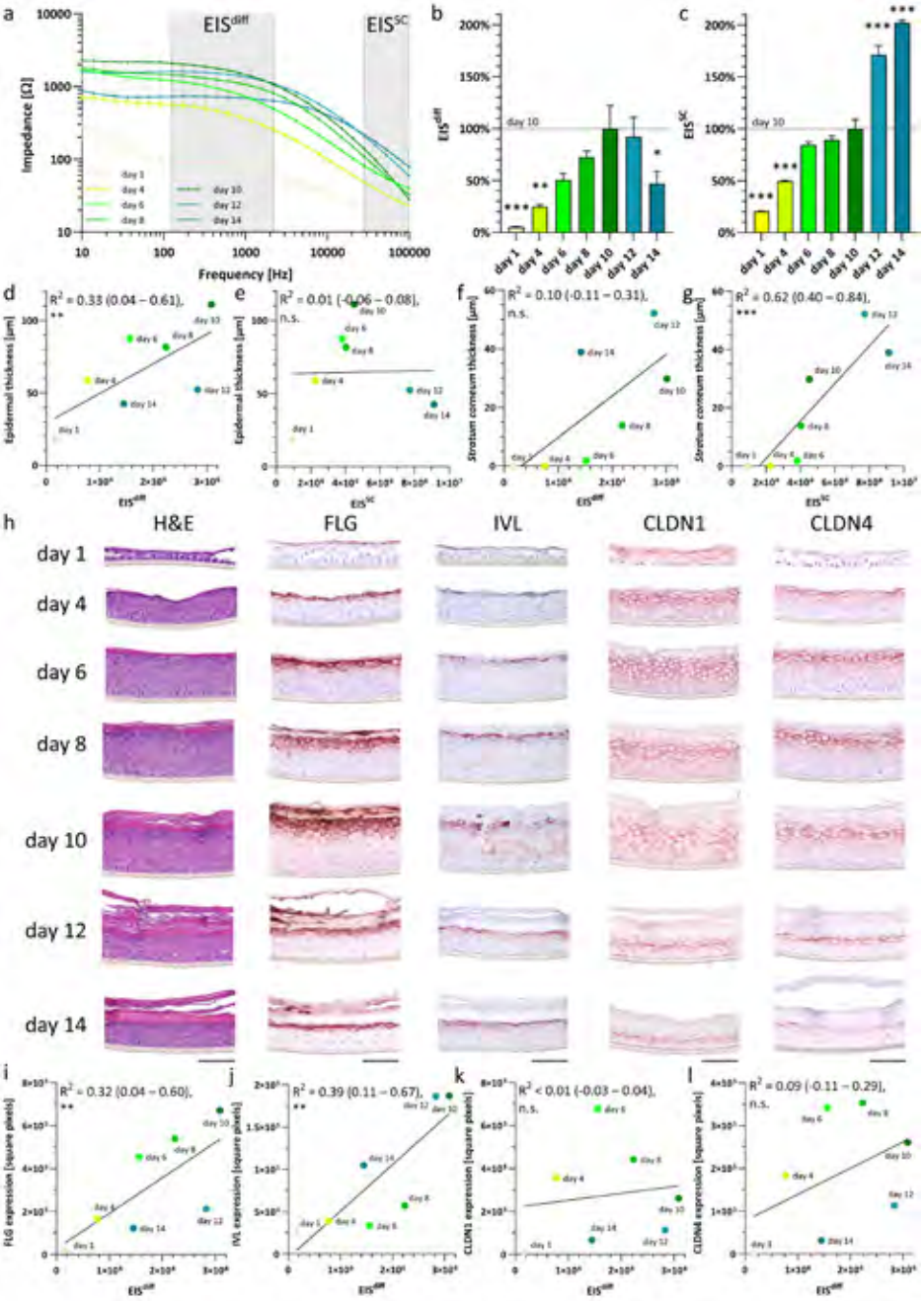

< Figure 3: During HEE development, EIS^{diff} correlates with keratinocyte differentiation and epidermal thickness while EIS^{SC} correlates with *stratum corneum* thickness. (**A**) Endpoint–measured impedance spectra, (**B**) EIS^{diff} and (**C**) EIS^{SC} during HEE development. Each timepoint represents three biological replicates and EIS^{diff} and EIS^{SC} were compared to 10 day air–exposed cultures. (**D – G**) Correlation of epidermal thickness with (**D**) EIS^{diff} and (e) EIS^{SC} and *stratum corneum* thickness with (**F**) EIS^{diff} and (**G**) EIS^{SC}. Each timepoint averages three biological replicates, R^2 values and significances indicate the correlation of individual replicates. (**H**) Staining of general morphology (H&E), keratinocyte differentiation (FLG, IVL) and cell–cell adhesions (CLDN1, CLDN4) during HEE development. Pictures represent three biological replicates and were taken at 40x magnification. Size bars indicate 100 µm. (**I – L**) Correlation of (**I**) FLG, (**J**) IVL, (**K**) CLDN1 and (**L**) CLDN4 protein expression with EIS^{diff}. Each timepoint averages three biological replicates, R^2 values and significances indicate the correlation of individual replicates.

Cytokine stimulation proves that EIS^{diff} is independent of epidermal thickness

After examining EIS in epidermal homeostasis we aimed to study the relevance of EIS in the context of disturbed homeostasis and to deepen our investigation into the correlation between EIS^{diff}, epidermal thickness and terminal differentiation. Therefore, HEEs from normal human epidermal keratinocytes (NHEKs) were stimulated with single cytokines (interleukin–(IL–)17A or IL–22) or cytokine mixes (IL–17A + IL–22 and IL–4 + IL–13) to mimic a proinflammatory milieu that is known to affect keratinocyte proliferation (IL–4, IL–13, IL–17A), the cell volume (IL–22), and terminal differentiation (all cytokines) (Figure 4a). We hypothesized that if EIS^{diff} would merely quantify epidermal thickness, cytokines known to increase epidermal thickness would increase EIS^{diff}. Nevertheless, while IL–4 + IL–13 stimulation of HEEs significantly increased epidermal thickness, a reduction of EIS^{diff} was observed (Figure 4b, d). Stimulation with IL–17A did not change epidermal thickness but resulted in increased EIS^{diff} and EIS^{SC} (Figure 4b–d). In contrast, IL–22 did not induce any changes in EIS^{diff}, while significantly increasing the epidermal thickness (Figure 4b–d). Correlation analysis furthermore showed no correlation between epidermal thickness and EIS^{diff} (Figure 4e). To reassess the relationship between EIS^{diff} and terminal differentiation, we analyzed the expression levels of key terminal differentiation proteins FLG and IVL which are known to be reduced in human skin related to barrier defects, and known to be affected upon stimulation with IL–4 + IL–13 cytokines *in vitro* [41].

Indeed, decreased expression levels of FLG and IVL as well as unchanged levels of CLDN4 in HEEs treated with IL–4 + IL–13 cytokines (Figure 4g) corresponded to reduced EIS^{diff} (Figure 4b). On the other hand, IL–17A treatment, which is known to strengthen tight junction function [42], significantly increased EIS^{diff}, while epidermal thickness and FLG and IVL expression appeared unchanged (Figure 4b, d, g). This again indicates EIS^{diff} to quantify the complex dynamics of terminal differentiation

and skin barrier formation rather than mirroring epidermal thickness. Quantifying FLG and IVL protein expression was not sufficient to model EIS^{diff} behavior (data not shown), indicating that the complex effect of cytokines on epidermal barrier function cannot be explained by the expression of FLG and IVL alone. EIS^{SC}, however, was also found here to significantly correlate with *stratum corneum* thickness (Figure 4f).

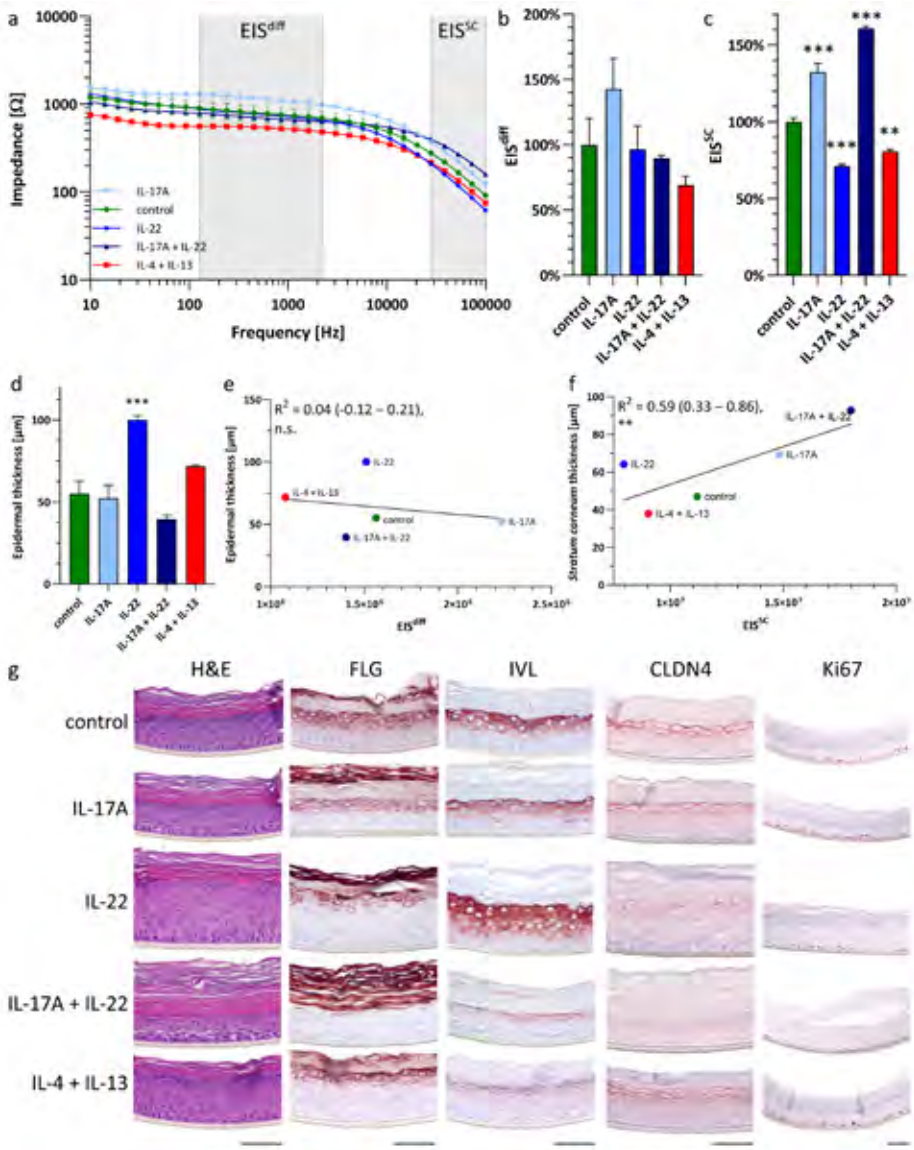

< Figure 4: Stimulation with cytokines proves EIS^{diff}–determined barrier function to be independent of epidermal thickness. (**A**) Endpoint–measured impedance spectra, (**B**) EIS^{diff} and (**C**) EIS^{SC} of cytokine–stimulated HEEs at day 8 of air exposure. Each condition represents three biological replicates and EIS^{diff} and EIS^{SC} were compared to control. (**D**) Epidermal thickness of cytokine–stimulated HEEs as compared to control. Correlation of (**E**) epidermal thickness to $EIS^{diff}$and (**F**) *stratum corneum* thickness to EIS^{SC}. Each condition averages three biological replicates, R^2 values and significances indicate the correlation of individual replicates. (**G**) HEEs stained for differentiation (FLG, IVL) and cell–cell adhesion (CLDN4) and proliferation (Ki67) proteins. Pictures represent three biological replicates and were taken at 20x (Ki67) or 40x magnification. Size bars indicate 100 µm.

Knockout out of epidermal differentiation and cell–cell adhesion genes links EIS^{diff} to HEE differentiation

To further test our hypothesis that keratinocyte terminal differentiation significantly defines EIS^{diff}, we knocked out key epidermal differentiation proteins by clustered regularly interspaced short palindromic repeats (CRISPR)/CRISPR–associated protein 9 (Cas9)–mediated genome editing through nonhomologous end–joining. We created keratinocyte cell lines lacking terminal differentiation protein FLG [31], tight junction protein CLDN1 [32] or transcription factors known to coordinate terminal differentiation namely aryl hydrocarbon receptor (AHR) [33] and transcription factor activating enhancer binding protein 2 alpha (TFAP2A) [33]. All knockout lines showed a reduction in EIS^{diff} and EIS^{SC} (Figure 5a–c). Notably, CLDN1 knockout caused reduced EIS^{diff} but showed increased EIS^{SC} in concordance with observed parakeratosis and increased *stratum corneum* compaction (Figure 5d). FLG expression was clearly decreased in AHR, TFAP2A and CLDN1 knockout lines and completely absent in the FLG knockout line (Figure 5d). Expression of IVL was decreased in all knockout cell lines, except the FLG knockout. CLDN1 (only fully absent in CLDN1 knockout) and CLDN4 expression appeared unchanged related to the epidermal cell layers which were affected by all genotypes as compared to control (Figure 5d). Hence, we conclude that EIS^{diff} is strongly determined by the degree of epidermal terminal differentiation.

EIS detects therapeutic response in proinflammatory IL–4 + IL–13 epidermis model

Besides detecting or monitoring epidermal defects, reversing these defects is a key component in the treatment of inflammatory skin diseases and an important parameter in the development of potential novel therapeutics. Therefore, we investigated if EIS can measure the reversal of barrier defects for future implementation in pre–clinical drug screening. For this we chose pharmacological molecules known to activate AHR, a key regulator of epidermal differentiation (Figure 5d) and novel target for topical anti–inflammatory treatment [43, 44]. Hereto, IL–4 and IL–13 stimulated HEEs were additionally treated with an array

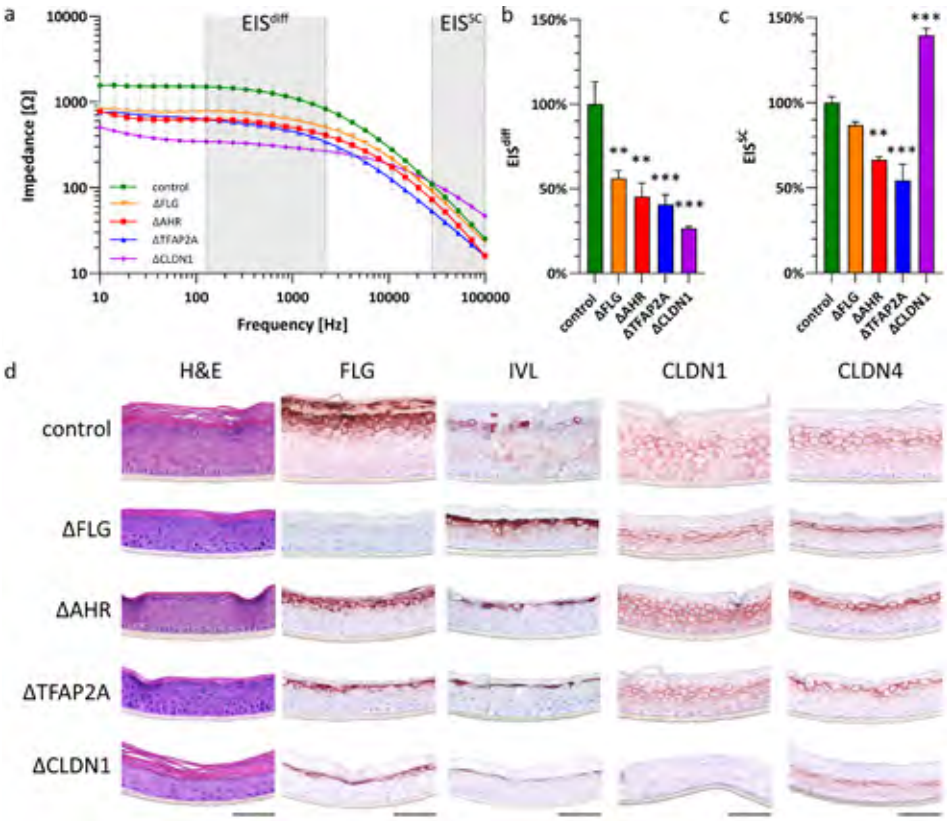

Figure 5: Knockout of genes involved in keratinocyte differentiation and cell–cell adhesion decreases EIS^{diff}. (**A**) Endpoint–measured impedance spectrum, (**B**) EIS^{diff} and (**C**) EIS^{SC} of HEEs with knockout of target gene at day 10 of air exposure. Each condition represents three biological replicates and EIS^{diff} and EIS^{SC} are compared to control. Each (**D**) HEEs stained for differentiation (FLG, IVL) and cell–cell adhesion (CLDN1, CLDN4) proteins. Pictures represent three biological replicates and were taken at 40x magnification. Size bars indicate 100 µm.

of AHR–activating ligands (L1–5) known to have a therapeutic effect, next to structurally–related nonactivating compounds (M1–2) (Table S2). AHR–activating compounds resulted in restored IL–4 + IL–13–impaired EIS^{diff} and EIS^{SC} impedance spectra, indicating capability of EIS to measure the AHR–dependent repair of skin barrier defects (Figure 6a–c). Compounds that do not activate AHR signaling (M1–2) did not restore the cytokine–mediated reduction in EIS (Figure 6a–c). In fact, these compounds known to block endogenous AHR signaling further decreased EIS^{SC} significantly with similar trends in EIS^{diff}. Since we now confidently determined that EIS^{diff} measurements correlate with keratinocyte differentiation, we assumed that expression levels of differentiation proteins FLG and IVL would also correlate with the rescue in EIS^{diff} by AHR ligands. This we could demonstrate clearly for IVL,

as AHR agonists were partially able to restore the dampened IVL expression by IL–4 and IL–13. AHR–binding but nonactivating compounds (M1–2) did not restore IVL expression (Figure S2a). FLG protein levels followed a similar expression pattern as IVL albeit differences were less pronounced. Again, the expression of tight junction protein CLDN4 remained unchanged throughout treatments (Supplemental Figure 2) confirming earlier results.

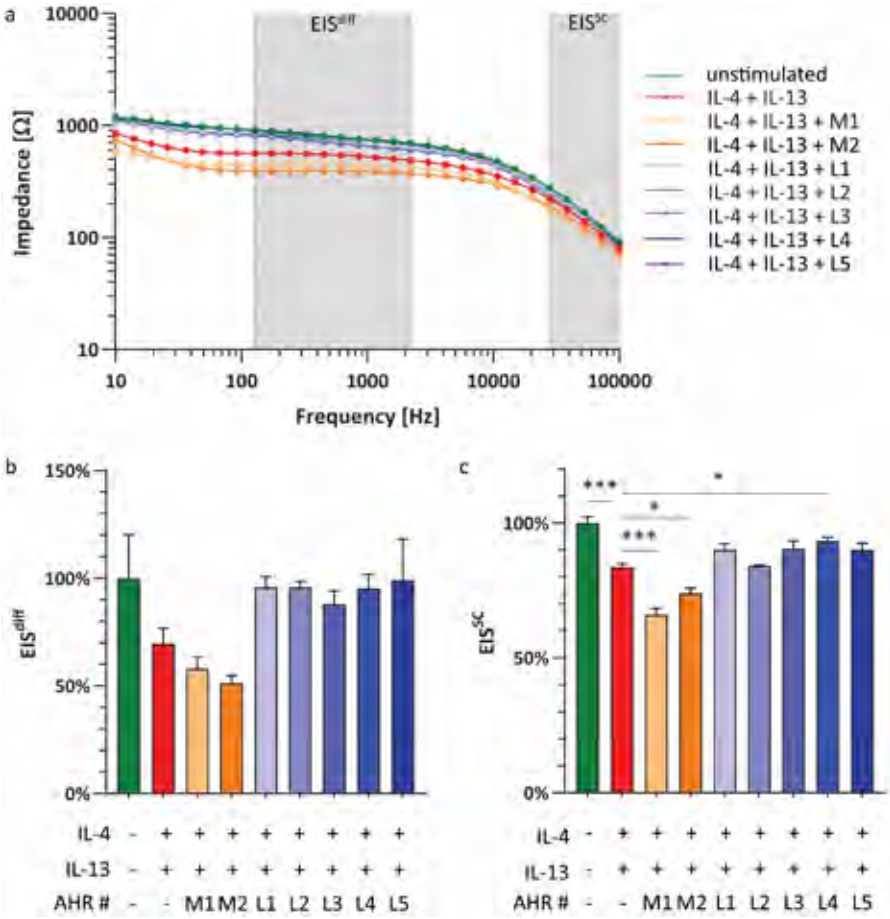

Figure 6: EIS detects therapeutic AHR response in a proinflammatory epidermis model. (**A**) Endpoint–measured impedance spectrum, (**B**) EIS^{diff} and (**C**) EIS^{SC} of HEEs stimulated with IL–4 and IL–13 cytokines alone and in combination with AHR activating therapeutic compounds at day 8 of air exposure. Each condition represents three biological replicates and EIS^{diff} and EIS^{SC} of control conditions and AHR–binding compounds are compared to IL–4 + IL–13 stimulation.

Discussion

In this study, we investigated the applicability of EIS to assess skin barrier function in 3-dimensional HEE *in vitro* organotypic epidermis models. EIS proved an easy to handle and noninvasive system to obtain real–time quantitative readouts correlating to functional barrier properties.

While fit here to the Nunc carrier plate system, the device can be customized to various transwell cell culture platforms. Running costs are low and the measurements are performed in a semiautomated fashion. The fixed electrode setup additionally standardizes the measurements and produced results are highly repeatable when taking into account that electrical impedance readouts depend on cell passage number, culture medium and temperature [39]. Reported readout trends are reproducible while absolute values have been observed to differ between replicated experiments. Sample readouts therefore need to be correlated with controls within the same experiment (see technical recommendations). While endpoint measurements cater to less variance, measurements can be performed and repeated in high quantities at virtually any time during HEE culture without harming tissue integrity. With current functional barrier assessments structurally relying on invasive endpoint measurements (permeation studies, Franz cell diffusion assay) and / or being laborious and sensitive to handling (Franz cell diffusion assay, TEWL, TEER), EIS provides a noninvasive, semiautomated and reproducible alternative.

EIS measures a broad range of frequencies in contrast to single frequency TEER measurements [39, 45] therefore being able to capture different functional skin barrier parameters. For quantitative analysis, experimentally obtained impedance spectra are usually fit to the corresponding electrical circuit model to isolate individual electrical parameters [46]. To aid biologic interpretation, we here chose to correlate the obtained impedance spectra with known biological barrier properties. Theoretical considerations in combination with our own data highlighted two frequency ranges which we described through calculating their area under the curve.

Frequencies on a plateau around 100–2000 Hz were termed EIS^{diff} as they quantified differentiation in viable keratinocytes as assessed by the expression of differentiation markers FLG and IVL, which together predicted 76 % of EIS^{diff} during HEE development. While EIS^{diff} exhibits clear independence of viable epidermis and *stratum corneum* thickness, a correlation with tight junction function remains

uncertain. On the one hand, EIS^{diff} was observed to be independent from CLDN1 and CLDN4 protein expression during HEE development and cytokine stimulations. ΔCLDN1 HEEs exhibit a strongly reduced EIS^{diff}, but this can be explained by a concomitant reduced expression of keratinocyte differentiation markers as CLDN1 knockout is known to alter pro–FLG processing [47]. On the other hand, EIS^{diff} frequencies overlap with R_P impedance contribution, with R_P being the electrical circuit model element to describe the resistance of tight junctions [39]. Furthermore, during IL–17A cytokine stimulation EIS^{diff} increased independent of differentiation protein expression, which could be a result of an IL–17A strengthening effect on tight junction function [42]. In conclusion, EIS^{diff} uniquely quantifies keratinocyte differentiation independent of CLDN1 and CLDN4 protein expression, however a contribution of tight junction function cannot be ruled out since sole protein expression does not entirely mirror tight junction functionality [48, 49].

Frequencies of a higher frequency range between 20,000 Hz and 100,000 Hz were termed EIS^{SC} and overlap with C_{Cell}, a parameter describing ability of a cell to store an electrical charge. EIS^{SC} conclusively quantifies *stratum corneum* rather than complete HEE thickness. However, further experiments should investigate the relationship between EIS^{SC}, lipid organization and *stratum corneum* composition.

This study used EIS to assess HEE skin barrier function during formation, to study the effects of single genes and to assess skin barrier function under inflammatory conditions and treatment. EIS was able to measure the defects induced by knockout of cardinal differentiation–driving transcription factors (AHR and TFAP2A) and differentiation effector genes (FLG). The observed defects were congruent with other barrier function assessments reporting an elevated TEWL in ΔTFAP2A and ΔFLG HEEs and in human FLG loss–of–function variants [31, 33, 50, 51]. Cytokine–induced proinflammatory conditions resulted in keratinocyte differentiation deficiencies and changes in *stratum corneum* thickness, which could be captured and quantified by EIS. The IL–4 + IL–13 induced decrease in EIS^{diff} and EIS^{SC} *in vitro* also replicates the *in vivo* situation where the IL–4 and IL–13 driven skin disease atopic dermatitis is accompanied by elevated TEWL and decreased EIS values measured on *in vivo* patient skin [22, 52-54]. *In vivo*, EIS can also detect therapeutic improvements of atopic dermatitis associated with improvements in clinical scoring and reduced expression of inflammatory biomarkers [22, 55] similar to the detected therapeutic improvements in our *in vitro* atopic dermatitis model.

To conclude, we propose EIS to be a valuable tool to noninvasively study epidermal barrier function in organotypic skin models. The dual viable epidermis/*stratum*

corneum barrier assessment and the quantification of keratinocyte differentiation are, to our knowledge, singular across all barrier evaluation techniques. The proposed semiquantitative EIS analysis is easy to replicate and uniquely correlates impedance readouts with biological barrier properties. We suggest EIS to be especially suited for longitudinal studies of barrier development, keratinocyte differentiation and barrier–disrupting skin diseases including preclinical therapeutic studies. In addition, EIS can be used in multi–cell type models to investigate the interplay between epidermis, extrinsic and intrinsic factors, potentially in combination with patient–derived cells, immune cells and/or bacteria. The possibility to correlate *in vitro* and *in vivo* EIS measurements facilitates a unique translational approach from bedside to bench and back.

Technical recommendations

To ensure optimal, reproducible EIS measurements without compromising culture integrity, we propose several guidelines for implementing EIS in the laboratory:

- Measurements depend on temperature and ion content of the surrounding fluid. To ensure maximum comparability between conditions, use an isotonic buffer solution (e.g. phosphate–buffered saline (PBS)) and allow samples to adjust to room temperature for at least 30 minutes before measurements.
- To minimize variation when performing serial measurements at various days of the cell culture, the time of topical exposure to PBS should be kept minimal and PBS should be carefully removed after measurements to maintain the air–liquid interface as much as possible for proper barrier formation and function.
- Before commencing measurements, blank measurements on PBS only or empty filters should be performed, as this provides information on intrinsic capacitance of the electrodes and the resistance of PBS and filters. When analyzing the results, blanks should be subtracted from measured sample values.
- Previous publications have normalized EIS based on the surface area of the used cell culture system using various methods [56-58]. Considering the lack of consensus, we report uncorrected EIS values and the surface area of HEEs (0.47 cm^2) to aid comparisons.
- Control conditions should be taken along for each individual experiment and measurement time point to interpret relative changes in preference to absolute values.
- EIS^{diff} (127–2212 Hz) and EIS^{SC} (28,072–100,000 Hz) are determined through calculating the area under the curve at respective frequencies.

Data availability

The impedance data related to this article can be found at https://doi.org/10.34973/yfca-cr43, hosted at the Radboud University Data Repository. Pictures of immunohistochemistry staining are available from the corresponding author upon request.

Acknowledgements

We thank Joachim Wegener (University of Regensburg, Germany) for the critical reading of our manuscript and all members of the van den Bogaard group for the lively discussions and suggestions. We thank Ewald Bronkhorst for advice on the correlation analysis. This collaborative work was supported by NIH R35 grant ES028244, PAST4FUTURE grant LSHM20043-HSGF and European Innovation Council (EIC) under grant agreement No. 101098826 (SKINDEV) and the Radboud university medical center (EB). The FLG knockout cells were generated under a LEO Foundation grant LF-OC-22-001056 (JS and EB). SR is CEO and founder of Locsense B.V., which contributed in–kind to this work. The results presented in the study are not influenced nor determined by the views or wishes of Locsense, nor did Locsense provide any financial support for this study that may conflicted with the results interpretation or presentation of data. The contribution of Locsense was limited to the development of the smart lid to fit the cell culture system and to providing technical support. Discussions with Locsense on the data representation and electrical circuit interpretation aided in correlating the data output to biological interpretations. The remaining authors declare no conflicts of interest.

Abbreviations

AHR - aryl hydrocarbon receptor, ANOVA - analysis of variance, C_A, C_B - cellular membrane capacitance, C_{Cell} - cellular capacitance, C_{El} - electrode capacitance, CLDN1 - claudin 1, CLDN4 - claudin 4, CRISPR/Cas9 - clustered regularly interspaced short palindromic repeats / CRISPR–associated protein 9, EIS - electrical impedance spectroscopy, EIS^{diff} - keratinocyte differentiation–attributable electrical impedance, EIS^{SC} - *stratum corneum*–attributable electrical impedance, FLG - filaggrin, H&E - hematoxylin and eosin, HEE - human epidermal equivalents, IL – interleukin, PBS - phosphate–buffered saline, IVL - involucrin, KRT16 - keratin 16, R_A, R_B - cellular membrane resistance, R_{Cell} - cellular resistance, R_{Cyt} - cytoplasmatic resistance, R_{Medium} - culture medium resistance, R_P - paracellular resistance, SKALP - skin–derived antileukoprotease, TEER - transepithelial electrical resistance, TEWL - transepidermal water loss, TFAP2A - transcription factor activating enhancer binding protein 2 alpha

References

1. Natsuga, K., Epidermal barriers. Cold Spring Harb Perspect Med, 2014. **4**(4): p. a018218.
2. Évora, A.S., et al., Corneocytes: Relationship between Structural and Biomechanical Properties. Skin Pharmacol Physiol, 2021. **34**(3): p. 146-161.
3. van Smeden, J., et al., The important role of stratum corneum lipids for the cutaneous barrier function. Biochim Biophys Acta, 2014. **1841**(3): p. 295-313.
4. Eyerich, S., et al., Cutaneous Barriers and Skin Immunity: Differentiating A Connected Network. Trends Immunol, 2018. **39**(4): p. 315-327.
5. Niehues, H., et al., 3D skin models for 3R research: The potential of 3D reconstructed skin models to study skin barrier function. Exp Dermatol, 2018. **27**(5): p. 501-511.
6. Al Kindi, A., et al., Staphylococcus aureus second immunoglobulin-binding protein drives atopic dermatitis via IL-33. J Allergy Clin Immunol, 2021. **147**(4): p. 1354-1368.e3.
7. Orsmond, A., et al., Skin Barrier Dysregulation in Psoriasis. Int J Mol Sci, 2021. **22**(19).
8. Yoshida, T., L.A. Beck, and A. De Benedetto, Skin barrier defects in atopic dermatitis: From old idea to new opportunity. Allergol Int, 2022. **71**(1): p. 3-13.
9. Hadj-Rabia, S., et al., Claudin-1 gene mutations in neonatal sclerosing cholangitis associated with ichthyosis: a tight junction disease. Gastroenterology, 2004. **127**(5): p. 1386-90.
10. van den Bogaard, E.H.J., et al., Deficiency of the human cysteine protease inhibitor cystatin M/E causes hypotrichosis and dry skin. Genet Med, 2019. **21**(7): p. 1559-1567.
11. Celebi Sözener, Z., et al., Environmental factors in epithelial barrier dysfunction. J Allergy Clin Immunol, 2020. **145**(6): p. 1517-1528.
12. El Ghalbzouri, A., et al., Leiden reconstructed human epidermal model as a tool for the evaluation of the skin corrosion and irritation potential according to the ECVAM guidelines. Toxicol In Vitro, 2008. **22**(5): p. 1311-20.
13. Pecoraro, B., et al., Predicting Skin Permeability by Means of Computational Approaches: Reliability and Caveats in Pharmaceutical Studies. J Chem Inf Model, 2019. **59**(5): p. 1759-1771.
14. Roberts, M.S., et al., Topical drug delivery: History, percutaneous absorption, and product development. Adv Drug Deliv Rev, 2021. **177**: p. 113929.
15. Shamaprasad, P., et al., Using molecular simulation to understand the skin barrier. Prog Lipid Res, 2022. **88**: p. 101184.
16. Riethmüller, C., Assessing the skin barrier via corneocyte morphometry. Exp Dermatol, 2018. **27**(8): p. 923-930.
17. van den Bogaard, E., et al., Perspective and Consensus Opinion: Good Practices for Using Organotypic Skin and Epidermal Equivalents in Experimental Dermatology Research. J Invest Dermatol, 2021. **141**(1): p. 203-205.
18. Arık, Y.B., et al., Barriers-on-chips: Measurement of barrier function of tissues in organs-on-chips. Biomicrofluidics, 2018. **12**(4): p. 042218.
19. Neupane, R., et al., Alternatives to Biological Skin in Permeation Studies: Current Trends and Possibilities. Pharmaceutics, 2020. **12**(2).
20. Tárnoki-Zách, J., et al., Development and Evaluation of a Human Skin Equivalent in a Semiautomatic Microfluidic Diffusion Chamber. Pharmaceutics, 2021. **13**(6).
21. Alexander, H., et al., Research Techniques Made Simple: Transepidermal Water Loss Measurement as a Research Tool. J Invest Dermatol, 2018. **138**(11): p. 2295-2300.e1.

22. Rinaldi, A.O., et al., Electrical impedance spectroscopy for the characterization of skin barrier in atopic dermatitis. Allergy, 2021. **76**(10): p. 3066-3079.
23. Fernandes, J., et al., Real-time monitoring of epithelial barrier function by impedance spectroscopy in a microfluidic platform. Lab Chip, 2022. **22**(10): p. 2041-2054.
24. Wegener, J., A. Hakvoort, and H.J. Galla, Barrier function of porcine choroid plexus epithelial cells is modulated by cAMP-dependent pathways in vitro. Brain Res, 2000. **853**(1): p. 115-24.
25. Morin, M., et al., Skin hydration dynamics investigated by electrical impedance techniques in vivo and in vitro. Sci Rep, 2020. **10**(1): p. 17218.
26. Groeber, F., et al., Impedance spectroscopy for the non-destructive evaluation of in vitro epidermal models. Pharm Res, 2015. **32**(5): p. 1845-54.
27. Mannweiler, R., et al., Direct assessment of individual skin barrier components by electrical impedance spectroscopy. Allergy, 2021. **76**(10): p. 3094-3106.
28. Tjabringa, G., et al., Development and validation of human psoriatic skin equivalents. Am J Pathol, 2008. **173**(3): p. 815-23.
29. Dickson, M.A., et al., Human keratinocytes that express hTERT and also bypass a p16(INK4a)-enforced mechanism that limits life span become immortal yet retain normal growth and differentiation characteristics. Mol Cell Biol, 2000. **20**(4): p. 1436-47.
30. Smits, J.P.H., et al., Immortalized N/TERT keratinocytes as an alternative cell source in 3D human epidermal models. Sci Rep, 2017. **7**(1): p. 11838.
31. Smits, J.P.H., et al., Investigations into the FLG Null Phenotype: Showcasing the Methodology for CRISPR/Cas9 Editing of Human Keratinocytes. J Invest Dermatol, 2023. **143**(8): p. 1520-1528.e5.
32. Arnold, K.A., et al., CLDN1 knock out keratinocytes as a model to investigate multiple skin disorders. Exp Dermatol, 2024. **33**(5): p. e15084.
33. Smits, J.P.H., et al., The Aryl Hydrocarbon Receptor Regulates Epidermal Differentiation through Transient Activation of TFAP2A. J Invest Dermatol, 2024. **144**(9): p. 2013-2028.e2.
34. Rikken, G., et al., Lead optimization of aryl hydrocarbon receptor ligands for treatment of inflammatory skin disorders. Biochem Pharmacol, 2023. **208**: p. 115400.
35. Crowe, A.R. and W. Yue, Semi-quantitative Determination of Protein Expression using Immunohistochemistry Staining and Analysis: An Integrated Protocol. Bio Protoc, 2019. **9**(24).
36. R Core Team. R: A language and environment for statistical computing. R foundation for statistical computing. 2023.
37. Fletcher, T.D., Psychometric: Applied Psychometric Theory, in R Package. 2023.
38. Benson, K., S. Cramer, and H.J. Galla, Impedance-based cell monitoring: barrier properties and beyond. Fluids Barriers CNS, 2013. **10**(1): p. 5.
39. Srinivasan, B., et al., TEER measurement techniques for in vitro barrier model systems. J Lab Autom, 2015. **20**(2): p. 107-26.
40. Yeste, J., et al., Engineering and monitoring cellular barrier models. J Biol Eng, 2018. **12**: p. 18.
41. Furue, M., Regulation of Filaggrin, Loricrin, and Involucrin by IL-4, IL-13, IL-17A, IL-22, AHR, and NRF2: Pathogenic Implications in Atopic Dermatitis. Int J Mol Sci, 2020. **21**(15).
42. Brewer, M.G., et al., Antagonistic Effects of IL-4 on IL-17A-Mediated Enhancement of Epidermal Tight Junction Function. Int J Mol Sci, 2019. **20**(17).

43. Bissonnette, R., et al., Tapinarof in the treatment of psoriasis: A review of the unique mechanism of action of a novel therapeutic aryl hydrocarbon receptor-modulating agent. J Am Acad Dermatol, 2021. **84**(4): p. 1059-1067.
44. van den Bogaard, E.H., et al., Coal tar induces AHR-dependent skin barrier repair in atopic dermatitis. J Clin Invest, 2013. **123**(2): p. 917-27.
45. Faway, E., et al., Towards a Standardized Procedure for the Production of Infective Spores to Study the Pathogenesis of Dermatophytosis. J Fungi (Basel), 2021. **7**(12).
46. Magar, H.S., R.Y.A. Hassan, and A. Mulchandani, Electrochemical Impedance Spectroscopy (EIS): Principles, Construction, and Biosensing Applications. Sensors (Basel), 2021. **21**(19).
47. Sugawara, T., et al., Tight junction dysfunction in the stratum granulosum leads to aberrant stratum corneum barrier function in claudin-1-deficient mice. J Dermatol Sci, 2013. **70**(1): p. 12-8.
48. Bäsler, K., et al., The role of tight junctions in skin barrier function and dermal absorption. J Control Release, 2016. **242**: p. 105-118.
49. Kirschner, N., et al., Tight junctions and differentiation--a chicken or the egg question? Exp Dermatol, 2012. **21**(3): p. 171-5.
50. Nemoto-Hasebe, I., et al., Clinical severity correlates with impaired barrier in filaggrin-related eczema. J Invest Dermatol, 2009. **129**(3): p. 682-9.
51. Yang, G., et al., Skin Barrier Abnormalities and Immune Dysfunction in Atopic Dermatitis. Int J Mol Sci, 2020. **21**(8).
52. Chamlin, S.L., et al., Ceramide-dominant barrier repair lipids alleviate childhood atopic dermatitis: changes in barrier function provide a sensitive indicator of disease activity. J Am Acad Dermatol, 2002. **47**(2): p. 198-208.
53. Flohr, C., et al., Filaggrin loss-of-function mutations are associated with early-onset eczema, eczema severity and transepidermal water loss at 3 months of age. Br J Dermatol, 2010. **163**(6): p. 1333-6.
54. Sugarman, J.L., et al., The objective severity assessment of atopic dermatitis score: an objective measure using permeability barrier function and stratum corneum hydration with computer-assisted estimates for extent of disease. Arch Dermatol, 2003. **139**(11): p. 1417-22.
55. Breternitz, M., et al., Placebo-controlled, double-blind, randomized, prospective study of a glycerol-based emollient on eczematous skin in atopic dermatitis: biophysical and clinical evaluation. Skin Pharmacol Physiol, 2008. **21**(1): p. 39-45.
56. Chen, S., R. Einspanier, and J. Schoen, Transepithelial electrical resistance (TEER): a functional parameter to monitor the quality of oviduct epithelial cells cultured on filter supports. Histochem Cell Biol, 2015. **144**(5): p. 509-15.
57. Haorah, J., et al., Activation of protein tyrosine kinases and matrix metalloproteinases causes blood-brain barrier injury: Novel mechanism for neurodegeneration associated with alcohol abuse. Glia, 2008. **56**(1): p. 78-88.
58. Liu, X., et al., A biofabricated vascularized skin model of atopic dermatitis for preclinical studies. Biofabrication, 2020. **12**(3): p. 035002.
59. Luengo, J., et al., Human Skin Permeation Enhancement Using PLGA Nanoparticles Is Mediated by Local pH Changes. Pharmaceutics, 2021. **13**(10).
60. Klotz, T., et al., Devices measuring transepidermal water loss: A systematic review of measurement properties. Skin Res Technol, 2022. **28**(4): p. 497-539.
61. O'Donnell, E.F., et al., The anti-inflammatory drug leflunomide is an agonist of the aryl hydrocarbon receptor. PLoS One, 2010. **5**(10).

62. Rikken, G., et al., Carboxamide Derivatives Are Potential Therapeutic AHR Ligands for Restoring IL-4 Mediated Repression of Epidermal Differentiation Proteins. Int J Mol Sci, 2022. **23**(3).
63. Poland, A., E. Glover, and A.S. Kende, Stereospecific, high affinity binding of 2,3,7,8-tetrachlorodibenzo-p-dioxin by hepatic cytosol. Evidence that the binding species is receptor for induction of aryl hydrocarbon hydroxylase. J Biol Chem, 1976. **251**(16): p. 4936-46.
64. Safe, S.H., Comparative toxicology and mechanism of action of polychlorinated dibenzo-p-dioxins and dibenzofurans. Annu Rev Pharmacol Toxicol, 1986. **26**: p. 371-99.

Supplemental figures

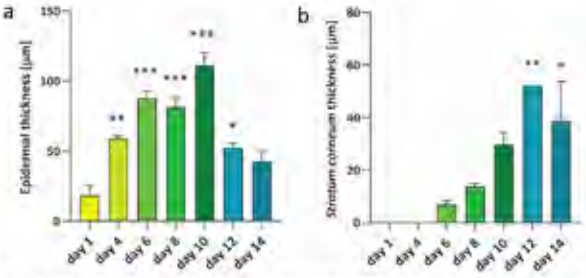

c FLG, IVL, CLDN1, CLDN4 multiple linear regression

	Value	95 % confidence interval		adjusted R^2
R^2	0.58	0.34 – 0.81		0.46
	Value	95 % confidence interval		p-value
Intercept	445111	-485353 –	1375575	0.32
FLG	2.325	-0.738 –	5.388	0.13
IVL	7.191	-0.841 –	13.541	*
CLDN1	0.457	- 2.538 –	3.450	0.75
CLDN4	-1.281	- 7.380 –	4.818	0.66

d FLG, IVL multiple linear regression

	Value	95 % confidence interval		adjusted R^2
R^2	0.57	0.33 – 0.81		0.52
	Value	95 % confidence interval		p-value
Intercept	458173	-227551 –	1143898	n.s.
FLG	1.975	0.417 –	3.533	*
IVL	7.045	2.373 –	11.717	**

e FLG, IVL, FLG x IVL multiple linear regression

	Value	95 % confidence interval		adjusted R^2
R^2	0.76	0.60 – 0.91		0.71
	Value	95 % confidence interval		p-value
Intercept	-232503	-910704 –	445699	n.s.
FLG	4.324	2.455 –	6.194	***
IVL	14.08	8.481 –	19.682	***
FLG x IVL	-2.1×10^{-5}	-3.4×10^{-5} –	-8.3×10^{-5}	**

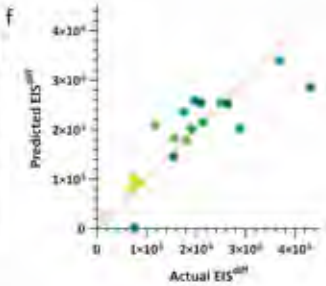

Supplemental Figure S1: FLG, IVL and FLG x IVL interaction significantly influence EIS^{diff} during HEE development. (**A-B**) (**A**) Epidermal thickness and (**B**) *stratum corneum* thickness of during HEE development compared to day 1. Each condition represents three biological replicates. (**C-E**) Multiple linear regression using (**C**) FLG, IVL, CLDN1 and CLDN4, (**D**) FLG and IVL and (**E**) FLG, IVL and FLG x IVL expression to predict EIS^{diff}. Analysis is based on all timepoints and replicates from figure 3. (**F**) Correlation of actual and FLG, IVL, FLG x IVL regressed EIS^{diff}.

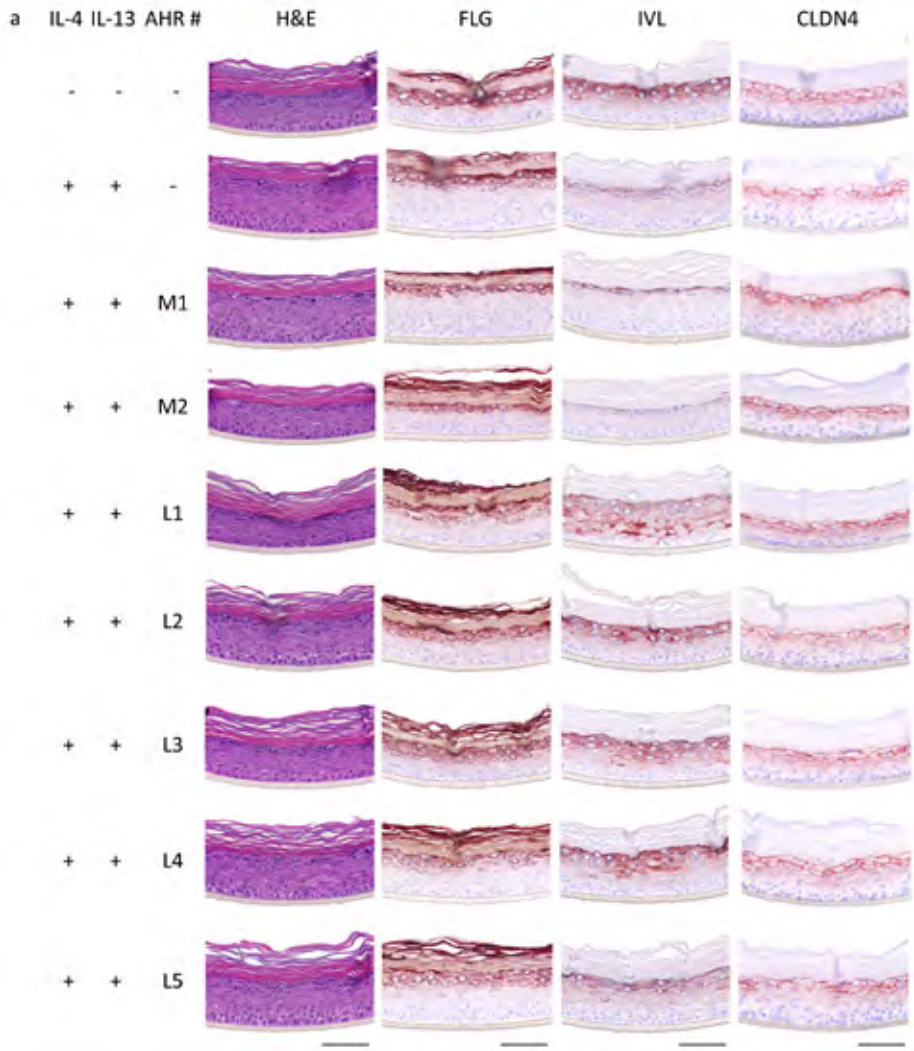

Supplemental Figure S2: AHR activation mediates therapeutic response in a proinflammatory epidermis model. (**A**) HEEs stained for differentiation (FLG, IVL) and cell–cell adhesion (CLDN4) proteins. Pictures represent three biological replicates of HEEs at day 8 of air exposure and were taken with 40x magnification. Size bars indicate 100 µm.

Supplemental tables

Supplemental Table S1. Overview of methodologies used for measurement of *in vitro* epidermal barrier function.

Technique	Principle of analysis	Assessed barrier component	Advantages
Permeation studies	Paracellular diffusion of dyes/tracers of various molecular weights	tight junction pore size, corneodesmosome integrity, lipid barrier	• relatively cheap • easy to implement
Franz cell diffusion assay	Assessment of drug permeation from donor chamber through HEE into acceptor chamber	outside–in barrier function including *stratum corneum* and tight junction barrier function	• gold standard for assessing outside–in barrier • quantitative
Transepidermal water loss (TEWL)	Measurement of changes in air humidity on top of HEE	lipid barrier function in relation to *stratum corneum* thickness	• non–destructive • quantitative
Transepithelial electrical resistance (TEER)	2 electrodes apply low alternating current over the HEE at a single frequency	tight junction ionic conductance ("tight junction tightness")	• non–destructive • quantitative • easy to implement

HEE: human epidermal equivalent; TEER: transepithelial electrical resistance; TEWL: transepidermal water loss

Supplemental Table S2: AHR–binding compounds

Abbreviation	Compound	Concentration	Reference
M1	SGA360	10 nM	[34]
M2	Teriflunomide	10 µM	[61]
L1	coal tar	2 µg/mL	[44]
L2	SGA388	10 nM	[34]
L3	Leflunomide	10 µM	[61]
L4	IMA-7101	1 nM	[62]
L5	TCDD	10 nM	[63, 64]

Disadvantages	References
• destructive end–point parameter • conventionally non–quantitative and not high–throughput	[17, 18]
• destructive end–point parameter • high level of expertise required • model system must stay intact during sampling period after harvest • highly influenced by temperature, sampling frequency and stirring conditions	[19, 59]
• highly influenced by probe type and angle, contact pressure, temperature and atmospheric pressure • high variability between different instruments • high background readings • labor intensive	[21, 60]
• highly influenced by electrode positioning, temperature and medium composition • not designed for complex tissues • labor intensive	[39]

Supplemental Table S3: Antibodies used for immunohistochemical analysis

Antigen	Species	Dilution	Company
FLG	Mouse	1:100	Thermo Fisher
IVL	Mouse	1:20	Mon 150 (own antibody)
CLDN1	Rabbit	1:200	Invitrogen
CLDN4	Mouse	1:200	Invitrogen
Ki67	Rabbit	1:200	Abcam
SKALP	Rabbit	1:4000	Own antibody
KRT16	Mouse	1:200	Santa-Cruz
Goat anti–rabbit	Goat	1:200	Vector laboratories
Horse anti–mouse	Mouse	1:200	Vector laboratories

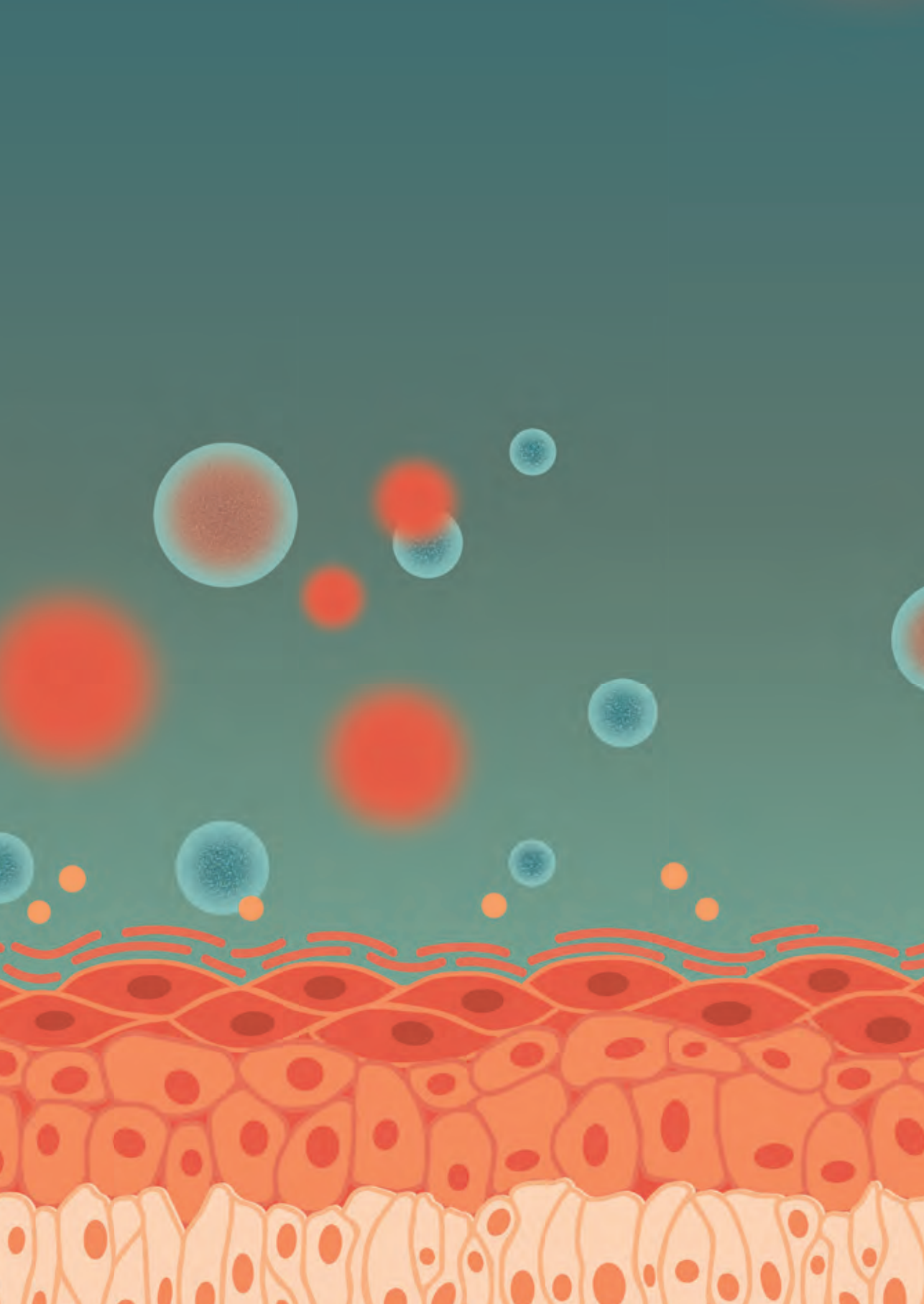

Chapter 6.

Dissecting key contributions of Th2 and Th17 cytokines to atopic dermatitis pathophysiology

Luca D. Meesters[1,2], Janou A.Y. Roubroeks[2], Aranka Gerritsen[1], Niels Velthuijs[3], Jaimy A. Klijnhout[1], Camille Laberthonnière[2,3], Ivonne M. van Vlijmen-Willems[1], Matthias Hübenthal[4], Diana Rodijk-Olthuis[1], Rens H. W. Peters[1], Gijs Rikken[1], Silke Szymczak[5], Nanna Fyhrquist[6,7], Harri Alenius[7,8], Stephan Weidinger[4], Jos P.H. Smits[1,9], Musa Mhlanga[3,10], Huiqing Zhou[2,10], Hanna Niehues[1], Ellen H. van den Bogaard[1]

Affiliations

[1] Department of Dermatology, Radboud University Medical Center (Radboudumc), Nijmegen, The Netherlands

[2] Department of Molecular Developmental Biology, Faculty of Science, Radboud University, Nijmegen, The Netherlands

[3] Department of Cell Biology, Faculty of Science, Radboud University, Nijmegen, The Netherlands

[4] Department of Dermatology, University Hospital Schleswig-Holstein, Kiel, Germany

[5] Institute of Medical Biometry and Statistics, University of Lübeck, Lübeck, Germany

[6] Department of Health Sciences, Karlstad University, Karlstad, Sweden

[7] Institute of Environmental Medicine, Karolinska Institute, Stockholm, Sweden

[8] Human Microbiome Research Program, University of Helsinki, Helsinki, Finland

[9] Department of Dermatology, University Hospital Düsseldorf, Medical Faculty, Heinrich Heine University, Düsseldorf, Germany

[10] Department of Human Genetics, Radboud University Medical Center (Radboudumc), Nijmegen, The Netherlands

Published in

J Allergy Clin Immunol. 2025 May 21:S0091-6749(25)00570-6. doi: 10.1016/j.jaci.2025.05.007.

Online ahead of print.

Abstract

In atopic dermatitis (AD), epidermal disease hallmarks are driven by a complex cutaneous inflammatory milieu that varies between patients. How these variable inflammatory signals affect cellular and molecular epidermal AD phenotypes is difficult to study *in vivo*. We aimed to unravel which AD-associated cytokines drive specific epidermal disease hallmarks. We utilized primary and immortalized keratinocyte-derived human epidermal equivalents stimulated with T helper (Th)2, Th17 and Th22 cytokines. Morphological, functional and transcriptomic analyses revealed that Th2 cytokines interleukin (IL)-4 and IL-13 were main inducers of a pro-inflammatory and hyperproliferative epidermis. The presence of IL-17A or IL-22 in the Th2 milieu, and especially Th2 + IL-22, most closely resembled AD hallmarks including spongiosis, more severe keratinocyte differentiation defects and epidermal barrier dysfunction. Single-cell spatial transcriptomics showed expansion of keratinocytes expressing high levels of proliferation genes, and downregulation of differentiation genes in the upper epidermal layers. The transcriptomic comparison to *in vivo* AD lesional skin indicated that the Th2 + IL-22 AD model demonstrated greatest resemblance and identified AD disease marker genes altered by Th2 + IL-22 such as downregulated *ACER1* and *AKR1C3*. Gene expression levels were restored by combinatory exposure to aryl hydrocarbon receptor (AHR) ligand tapinarof and Janus Kinase (JAK) inhibitor tofacitinib. This combined therapeutic approach also completely restored epidermal barrier function and improved morphological disease hallmarks. Our results reveal the important role of IL-22 in the Th2 driven acute AD pathophysiology and highlight the potential of combinatory medicine in targeted treatment of AD.

Introduction

Atopic dermatitis (AD) is a common chronic inflammatory skin disease, characterized by overactivation of the cutaneous immune system, deregulated epidermal homeostasis and an impaired skin barrier function [1]. The latter can be mainly attributed to epidermal alterations that interfere with the skin's physical, chemical and immunological skin barrier [2]. Typical epidermal hallmarks in AD that relate to skin barrier defects in the acute phase of the disease include keratinocyte hyperproliferation, epidermal differentiation defects and epidermal edema (spongiosis) [3]. Genetically, loss-of-function variants in the *filaggrin* (*FLG*) gene give rise to enhanced risk of AD [4, 5]. Due to the local cytokine milieu in AD lesions, expression of other late keratinocyte differentiation proteins like involucrin (IVL), loricrin (LOR) and hornerin (HRNR), is also hampered [6].

The inflammatory milieu is driven by skin-resident and infiltrating immune cells and their cross-talk with stromal and epidermal cells. T helper (Th)2 cells and mediators are recognized as inducers of keratinocyte proliferation whilst impairing keratinocyte differentiation [7-9]. In AD, Th2 cells and cytokines interleukin (IL)-4, IL-5, IL-13 and IL-31 are highly abundant [10, 11]. In addition to these 'classical' AD cytokines, IL-17A and IL-22 have recently emerged as disease-modifying cytokines in acute AD, albeit initially associated to psoriasis [12-15]. However, the effects of these cytokines on epidermal homeostasis in the AD pathology are less well characterized. Yet, knowledge on which specific cytokines drive the epidermal phenotype in patients may allow for personalized specific and potentially more effective therapies.

Hereto, organotypic skin models provide a valuable experimental platform to investigate disease mechanisms and the effect of disease-associated molecules or targeted drugs, as this is difficult to unravel *in vivo* with the presence of a complex cell and cytokine milieu. Previously, cytokine (combinations) have been linked to epidermal AD hallmarks, as summarized in [16], however these studies used varying experimental set-ups, mainly focused on Th1 and Th2 cytokines, and did not compare data to *in vivo* AD lesional skin. Therefore, we aimed to unravel the effect of individual and combinations of Th2 and Th17/22 cytokines on epidermal barrier development using human epidermal equivalents (HEEs) from primary normal human epidermal keratinocytes (NHEK) and immortalized human N/TERT-2G keratinocytes. We performed functional and molecular characterizations including bulk and single-cell spatial transcriptomic analyses to compare our AD models to *in vivo* lesional AD,

and evaluated the effect of epidermal differentiation and inflammation signaling targeting compounds.

Methods

All details can be found in the Supplemental Methods.

AD human epidermal equivalent (HEE) generation

HEEs were generated as previously described [17] with cytokine stimulation during the last 72 hours. Therapeutic compounds were added simultaneously with the cytokines or 24 hours after.

Morphological and immunohistochemical analysis

HEEs were formalin-fixed and paraffin-embedded. 6µm sections were hematoxylin and eosin stained or used for immunohistochemistry.

Real-time quantitative polymerase chain reaction (RT-qPCR)

Total RNA was isolated using the E.Z.N.A. Total RNA Kit I kit, followed by DNaseI treatment and cDNA synthesis. Real-time quantitative PCR (RT-qPCR) was executed with SYBR Green using the CFX Connect™ Real-Time System. Gene expression was normalized to the expression of *RPLP0* and relative expression levels were calculated using the $2^{-\Delta\Delta CT}$ method.

Bulk RNA-sequencing and analysis *in vitro* models

RNA-seq was performed as previously described [18] with minor adaptations. Data was analyzed using the seq2science RNA-seq workflow. For comparison to *in vivo* data, upregulated differentially expressed genes (DEGs) were defined as having a log2FC > 0, while downregulated genes were defined by a log2FC < 0.

Pseudobulk analysis scRNA-sequencing data *in vivo* samples

Publicly available single-cell RNA sequencing data of skin biopsies from AD patients and healthy controls [19] was analyzed using the R package Seurat and the standard Seurat workflow. Pseudobulk data was generated and DEGs between healthy and AD were identified using DESeq2. P-adjusted < 0.05 filtering was applied to DEGs and up- and downregulated genes were defined as log2FC > 1 or log2FC < -1, respectively.

Bulk RNA-sequencing analysis *in vivo* samples

Differential expression meta-analysis was performed on bulk transcriptomic profiles comparing 188 AD lesional (ADL) and 91 AD non-lesional (ADNL) with 181 healthy control (HC) skin biopsies from public and academic cohorts. Study-wise regression coefficients (corresponding to (log2) FC) were pooled using random effects meta-analysis. P-values were adjusted for multiple testing using the Benjamini-Hochberg procedure and significantly differentially expressed genes were required to meet adjusted p-value < 0.05 and the absolute pooled (log2) FC > 1. Competitive gene set enrichment analysis has been performed, testing the null hypothesis that the members of individual gene sets of interest are uniformly distributed along the list of ranked measures of differential expression, using the differential expressions of cytokine stimulated HEEs compared to controls contrasted to DEGs between AD lesion skin and healthy control skin.

Spatial transcriptomics and analysis

2 mm punch biopsies of HEEs were embedded in OCT, flash frozen in isopentane and cryosectioned, before 4% PFA fixation on cold Rebus Biosystems coverslips. Spatial transcriptomics was performed using the High Fidelity Assay on the Esper from Rebus Biosystems. Using the Esper Analysis software, high resolution images were reconstructed, manual intensity thresholds were set and detected smFISH spots were assigned to their closest nucleus based on DAPI. Further analysis was performed using Scanpy and pyComplexHeatmap.

Electrical impedance spectroscopy (EIS) measurement

The electrical impedance spectra (EIS) were measured as previously described [20].

Statistics

For qPCR, quantified protein and EIS data, one-way analysis of variance followed by Dunnett *post hoc* testing was performed in GraphPad Prism version 9. P-values of <0.05 were considered statistically significant.

Results

Epidermal differentiation and barrier function deregulation upon combined Th2 cytokines and IL-17A or IL-22 exposure

Exposure of HEEs to IL-4 or IL-13 induced epidermal acanthosis and AD-associated gene expression including *CA2*, *NELL2*, *CCL2* and *CCL26* (Figure 1A,C, Supplementary Figure 1A,C). In comparison, IL-17A and IL-22 alone initiated hypogranulosis and

reduced expression of epidermal differentiation markers FLG, IVL, keratin (KRT)2 (IL-17A specific), KRT10 (IL-22 specific), tight junction proteins claudin (CLDN)1 and CLDN4 (IL-17A specific), and the disease-associated marker KRT16 (IL-22 specific) (Table 1) (Figure 1A,B, Supplementary Figure 1A,B).

To model AD *in vitro,* HEEs are typically stimulated with either IL-4 or IL-13, or a combination of both which we hereafter call "Th2 mix" [21-24]. In our model, the Th2 mix showed similar lack of effects to IL-4 and IL-13 alone (Figure 1A-C, Figure 2A, B, Supplementary Figure 2A, B), including absence of spongiosis and keratinocyte differentiation and tight junction protein defects. We then performed electrical impedance spectroscopy (EIS), a quantitative methodology to measure epidermal barrier function in HEEs through transepithelial resistance and capacitance [20]. Two parameters were defined correlating with expression of keratinocyte differentiation proteins (EIS^{diff}) and *stratum corneum* thickness (EIS^{sc}). We did not find any significant reductions in EIS^{diff} and only slight reduction in EIS^{sc} upon exposure of HEEs to the Th2 mix, indicating minimal epidermal barrier defects (Figure 2D).

Before investigating the additional effect of IL-17A and IL-22 on AD features *in vitro*, IL-22 levels were titrated to avoid cytotoxicity when used in the same concentration as Th2 cytokines (Supplementary Figure 3). Supplementation of the Th2 mix with IL-17A or IL-22 initiated spongiosis and hypogranulosis, and strongly reduced differentiation proteins FLG, IVL and KRT2 (Figure 2A). Th2 + IL-22 increased KRT16 expression, whereas CLDN1 and 4 were reduced by Th2 + IL-17A (Figure 2B). EIS^{diff} and EIS^{sc} showed a downward trend by Th2 + IL-17A, but Th2 + IL-22 most significantly reduced EIS^{diff} and EIS^{sc} (Figure 2D). By evaluating different combinations of Th2 cytokines, IL-17A and IL-22, we found that hypogranulosis and spongiosis were present after any combination except for IL-13 + IL-17A; hyperproliferation was present upon combinations with IL-4 or IL-17A; and reduced FLG expression mainly with IL-22 (Supplementary Figure 4A). AD-associated marker gene expression of *CA2*, *CCL26* and *IL1B* was driven by the addition of IL-22 to any of the Th2 cytokines (Supplementary Figure 4B) (Table 1). IL-17A and IL-22 are strong inducers of antimicrobial peptides (AMPs), which are partially suppressed in AD by Th2 cytokines [25, 26]. In our study, addition of IL-17A as compared to Th2 cytokines alone increased the expression of *defensin beta 4* (*DEFB4*), *peptidase inhibitor 3* (*PI3*), *S100 calcium binding protein A7* (*S100A7)* and *cathelicidin antimicrobial peptide (CAMP*) in both cell types, which was less apparent upon addition of IL-22 (Supplementary Figure 2C) which may fit better with AD pathology.

To develop pre-clinical models for AD that are widely reproducible and generalizable among laboratories, the use of validated immortal keratinocyte cell lines, like N/TERT

cells [22, 27], may be preferred over freshly isolated primary cells that show large interindividual donor-dependent responses. HEEs derived from primary NHEKs and immortalized N/TERT-2G cells generally showed similar phenotypes when exposed to Th2 and Th17/22 cytokines. Only minor differences in N/TERT-2G cells were observed (Supplementary Figure 5A-D), including spongiosis in the upper layers of the *stratum spinosum*, and less hyperproliferation and barrier impairment (EIS^{diff}) upon addition of IL-17A or IL-22.

Table 1. Summary of effects of individual and cocktails of AD associated cytokines IL-4, IL-13, IL-17A and IL-22 in NHEK-HEEs.

Cytokine(s)	Morphology	Proliferation	Differentiation	Barrier	Inflammation
IL-4	Acanthosis	↑ Ki67 [7], KRT16	↓ IVL	*EIS not measured*	↑ *CCL2, NELL2*
IL-13	Acanthosis	↑ Ki67 [7]	↓ IVL	*EIS not measured*	↑ *CCL2, NELL2*
IL-17A	Acanthosis, hypogranulosis	↑ Ki67 [7]	↓ IVL, KRT2	↓ CLDN1, CLDN4, *EIS not measured*	↓ *CA2*
IL-22	Acanthosis, hypogranulosis	↑ KRT16	↓ FLG, IVL	*EIS not measured*	↑ *CCL2,* ↓ *CCL26*
Th2	Acanthosis	↑ Ki67, KRT16	↓ IVL	-	↑ *CA2, NELL2, CCL2, CCL26*
Th2 + IL-17A	Acanthosis, hypogranulosis, spongiosis	↑ Ki67, KRT16	↓ FLG, IVL, KRT2	↓ EIS^{diff}, CLDN4	↑ *NELL2, CCL2, CCL26*
Th2 + IL-22	Acanthosis, hypogranulosis, spongiosis	↑ Ki67, KRT16	↓ FLG, IVL, KRT2	↓ EIS^{diff}, EIS^{sc}	↑ *CA2, NELL2, CCL2, CCL26*

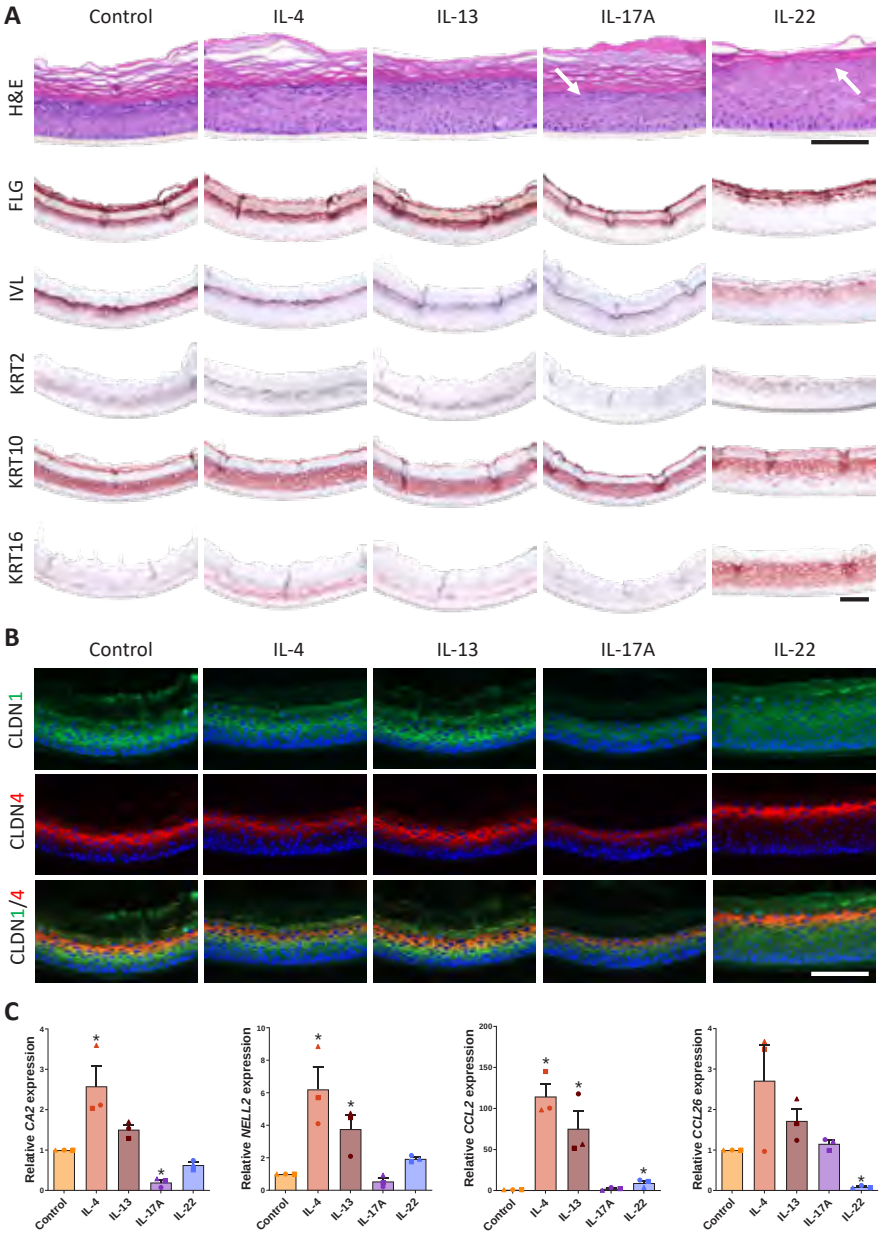

Figure 1. Effect of individual AD associated cytokines IL-4, IL-13, IL-17A and IL-22 on NHEK-HEEs. (**A**) The morphology and differentiation protein expression of FLG, IVL, KRT2, KRT10 and alarmin KRT16. White arrow: hypogranulosis. Scale bar = 100µm. (**B**) Tight junction protein expression of CLDN1 (green) and CLDN4 (red), and DAPI (blue). Scale bar = 100µm. (**C**) The expression of AD associated genes *CA2*, *NELL2*, *CCL2* and *CCL26*. All data is representative for N=3 primary keratinocyte donors, and presented as mean +/- SEM. * = p-value below 0.05 as compared to control.

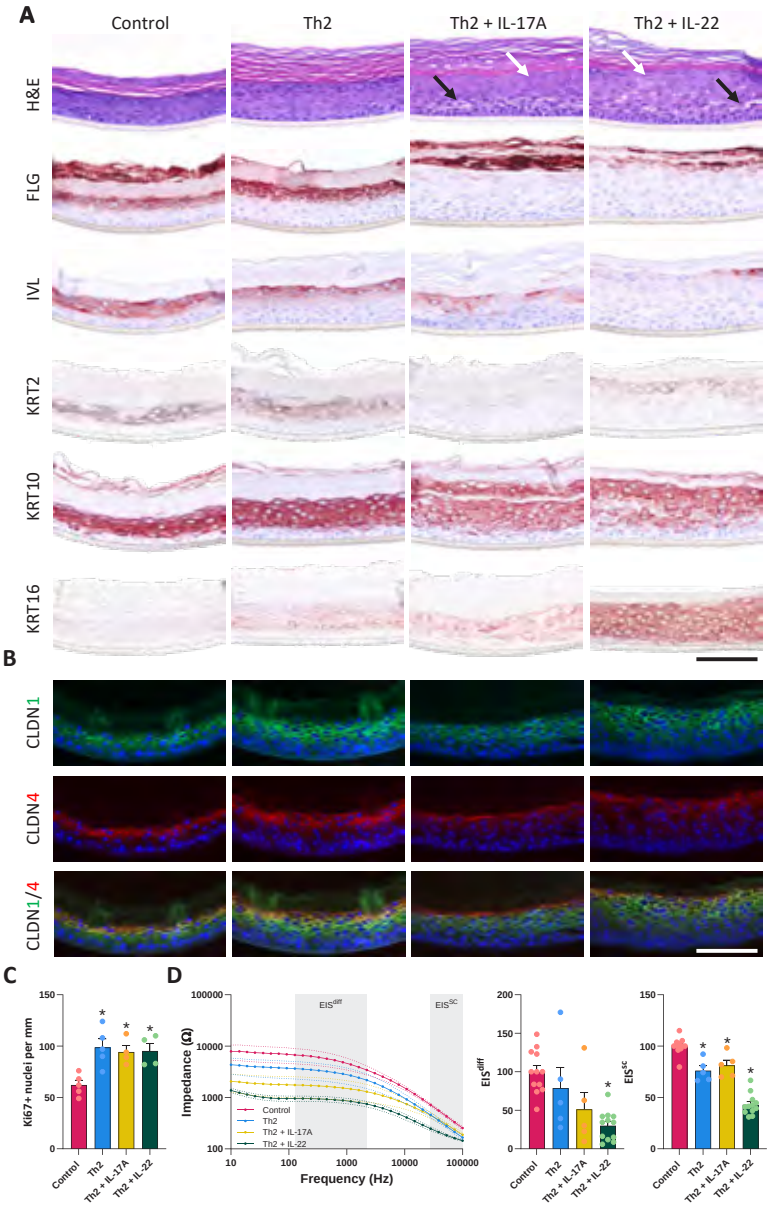

Figure 2. NHEK-HEEs upon stimulation with Th2 cytokines with and without IL-17A or IL-22. (**A**) Morphology and differentiation protein expression of FLG, IVL, KRT2, KRT10 and alarmin KRT16 of HEEs stimulated with the Th2 mix of IL-4 and IL-13 with and without IL-17A or IL-22. White arrow: hypogranulosis. Black arrow: spongiosis. Scale bar = 100µm. (**B**) Tight junction protein expression of CLDN 1 (green) and CLDN4 (red), and DAPI (blue). Scale bar = 100µm. (**C**) Ki67 protein quantification as a measure of proliferating keratinocytes. (**D**) Electrical impedance spectra (EIS), and EIS^{sc} and EIS^{diff} as percentages relative to the unstimulated control. Control and Th2 + IL-22 data is representative for N=12 (five biological replicates) and Th2 and Th2 + IL-17A data for N=5 (three biological replicates). Data is presented as mean +/- SEM. * = p-value below 0.05 as compared to control.

Cytokines induce distinct and overlapping keratinocyte differentiation defects

To identify genes and biological processes underlying the differences in response to Th2 +/- IL-17A or IL-22, we performed RNA-sequencing on HEEs. Principal component analysis (PCA) indicated that the Th2 mix induced a minor transcriptomic change over control, as compared to Th2 + IL-17A or IL-22 (PC1, 74% variance, Figure 3A). To investigate the potential functions of DEGs (Supplementary Table 1), hierarchical clustering yielded six clusters for subsequent Gene Ontology (GO) analysis (Figure 3B, C, Supplementary Table 2). Cluster 1 contained genes that were mainly induced by Th2 cytokines, including inflammatory genes like cytokines *CCL2* and *IL33*. Cluster 2 and 3 genes were specifically induced by either Th2 + IL-17A or IL-22, respectively. "Response to hypoxia" related genes such as *hypoxia-inducible factor 1 alpha* (*HIF1A)* were among the cluster 2 genes, whereas tight junction gene *CLDN1* and viral response genes *IFIH1*, *IFNAR2*, *STAT1* were in cluster 3. Cluster 4 and 5 genes were generally not affected by Th2 cytokines alone, but by both Th2 + IL-17A or IL-22. Cluster 4 genes were upregulated, playing a potential role in "exocytosis" (exocyst complex components), "intrinsic apoptotic signaling pathway" (caspases), "wound healing" (*occludin*), "I-kappaB kinase/NF-kappaB signaling" (*tumor necrosis factor*) and "skin development" (*S100* and *small proline rich* (*SPRR*) genes). Cluster 5 genes were strongly repressed, including epidermis development genes like *FLG*, *IVL* and *LOR*. Cluster 6 gene expression was in general downregulated by all combinations but most strongly by Th2 + IL-22. This cluster also included genes involved in epidermis development processes, such as *hornerin (HRNR)*, *epidermal growth factor receptor (EGFR)* and *CLDN4*. Similar analysis of cytokine treated N/TERT-2G-HEEs demonstrated analogous gene expression patterns highly representing the primary cell-derived models, and with less heterogeneity among replicas (Supplementary Figure 6A-C, Supplementary Table 3, 4).

Single-cell spatial transcriptomes define cytokine-induced gene deregulation in specific epidermal layers

Single molecular FISH based single-cell spatial transcriptomics was performed to identify the spatial localization of cytokine-induced DEGs in HEEs. First, genes that are known to be expressed in specific epidermal layers were selected to validate the methodology. We defined the epidermal layers based on their spatial location and relative similarity: the first layer from the bottom (L1), the second layer (L2), the middle layers (LM) and top layer (LT, last living cell layer). As expected, in control HEEs we observed basal keratinocyte genes such as collagens and integrins in L1, spinous keratinocyte genes such as *DSG1, KRT1, KRT2* in L2 and LM, and granular genes *IVL, FLG* in LT (Figure 4A, B, Supplementary Figure 6D).

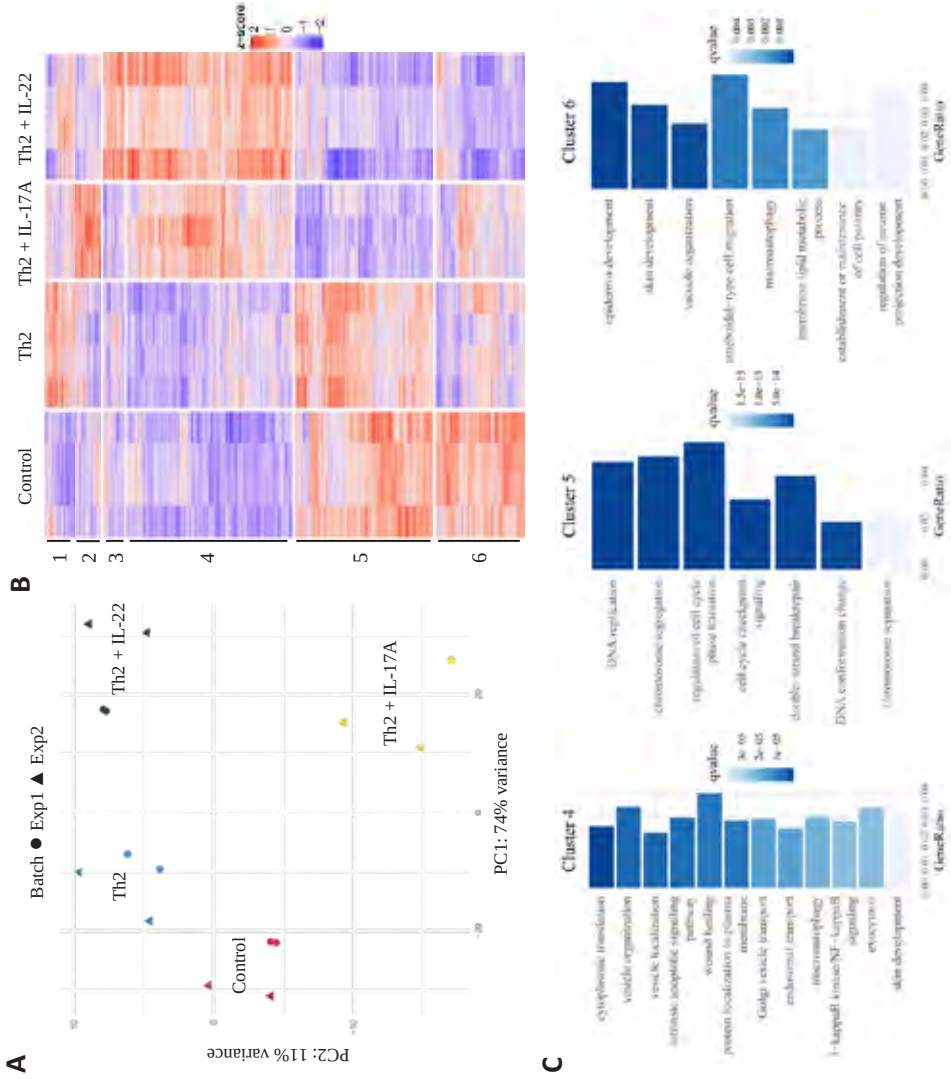

Figure 3. Transcriptomic analysis of NHEK-HEEs upon stimulation with various AD related cytokine cocktails. (**A**) Principal Component Analysis (PCA) plot. Exp=experiment. (**B**) Clustered heatmap, (**C**) Gene Ontology (GO)-term analyses. Data is representative for N=3 or 4 (two biological replicates).

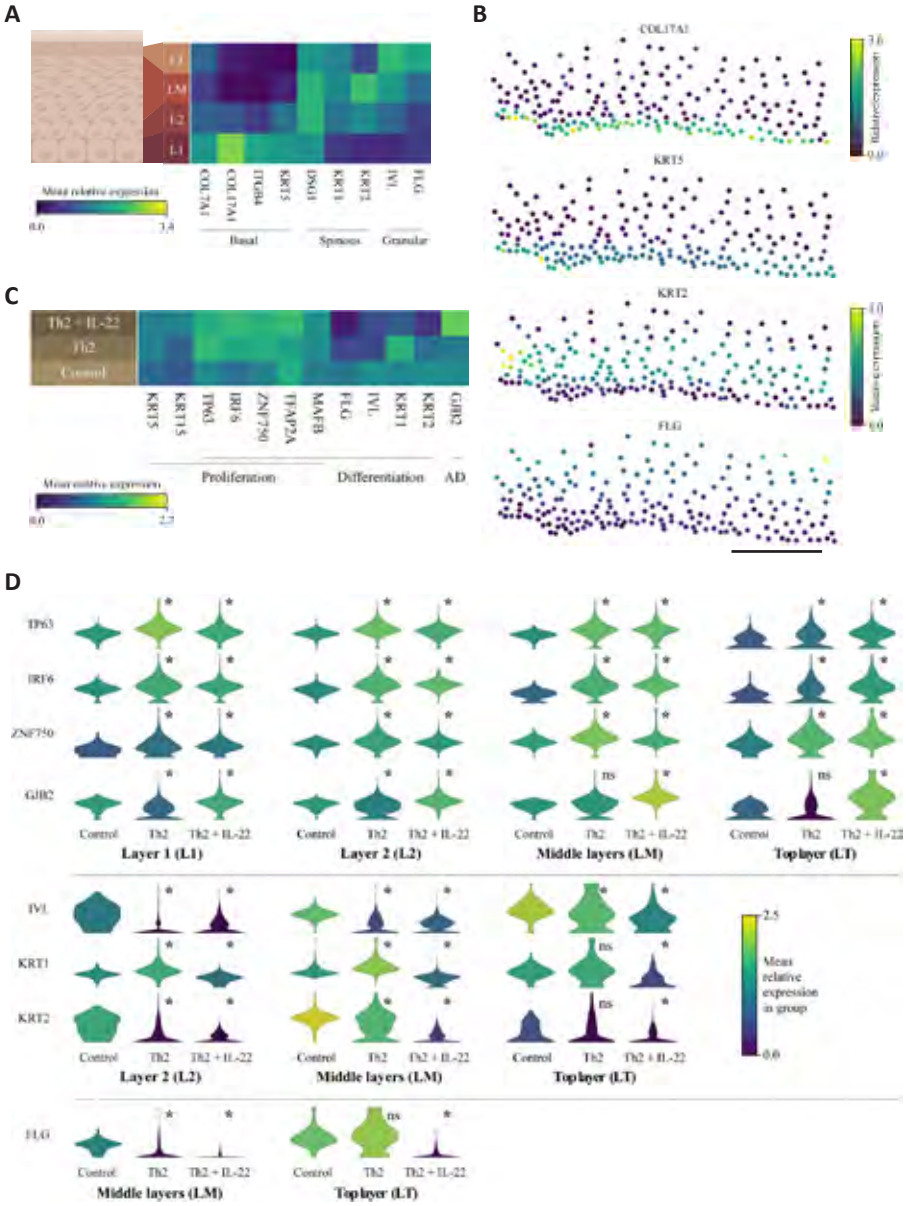

Figure 4. Spatial transcriptomic analysis of NHEK-HEEs in untreated condition and upon stimulation with various AD related cytokine cocktails. (**A**) Heatmap of layer specific genes in layer 1 (L1), layer 2 (L2), middle layers (LM) and the top layer (LT) in the untreated control. (**B**) Cell-specific expression of basal keratinocyte markers *COL17A1* and *KRT5*, spinosum marker *KRT2* and granulosum marker *FLG* in untreated controls (legend from 0 to 5 applies to *KRT5*, *KRT2* and *FLG*). Scale bar = 100µm. (**C**) Heatmap of keratinocyte differentiation and proliferation related genes per condition. (**D**) Violin plots of the gene expression per condition. Data is representative for N=4 (two biological replicates). * = p-value below 0.05 as compared to control.

Subsequently, we selected additional genes previously reported to play roles in keratinocyte proliferation and differentiation. HEEs exposed to Th2 + IL-22 were analyzed in addition to Th2 cytokines alone, representing severe and mild epidermal defects, respectively. Results demonstrate that *tumor protein 63* (*TP63*) known as a master regulator of epidermal proliferation and differentiation [28, 29], and its target genes, *Interferon Regulatory Factor 6* (*IRF6*) and *Zinc Finger Protein 750* (*ZNF750*), exhibited significantly higher expression in an increased number of cells in all epidermal layers upon Th2 +/- IL-22 exposure (Figure 4C, D, Supplementary Figure 6E). Keratinocyte differentiation markers like *IVL*, *FLG* and *KRT2,* were downregulated by Th2 cytokines and more significantly by Th2 + IL-22 in LM and LT. Expression of AD marker *Gap Junction Protein Beta 2 (GJB2)* [30-32] was specifically induced by Th2 + IL-22 in the upper layers LM and LT.

Th2 cytokines + IL-22 induces the most similar transcriptome to lesional AD

To confirm the biological relevance of our findings, we compared our RNA-sequencing data of HEEs to publicly available single-cell RNA sequencing (scRNA-seq) data of skin biopsies from AD patients and healthy volunteers [19]. A pseudobulk of the *in vivo* keratinocyte data was extracted from the complete scRNA-seq (Supplementary Figure 7A) and was used to identify DEGs between AD lesional and healthy keratinocytes. The up- and downregulated genes in AD were compared to DEGs in cytokine stimulated HEEs over controls. A more significant overlap represented by statistical significance was observed between DEGs induced by Th2 + IL-17A or IL-22 in HEEs and *in vivo* DEGs, as compared to Th2 cytokines alone (Supplementary Figure 7B, Supplementary Table 5). In parallel, we performed comparative analysis of our RNA-sequencing data of HEEs with a differential expression meta-analysis of full thickness skin of multiple cohorts of AD patients profiled using microarray or RNA-seq technology. Gene set enrichment analysis (GSEA) showed that cytokine induced gene expressions in HEEs are highly enriched in DEGs detected in AD patient full thickness skin, with Th2 + IL-22 and Th2 alone showing the highest and lowest proportion of associations, respectively (Figure 5A, Supplementary Table 14). Additionally, the highest number of overlapping DEGs were detected between the Th2 + IL-22 condition, as compared to controls, and lesional AD skin, as compared to healthy skin (Figure 5B). GO-term analysis on the overlapping upregulated genes upon Th2 + IL-17A or IL-22 *in vitro* and AD *in vivo* revealed a strong inflammatory response (Supplementary Figure 7C, Supplementary Table 6). The overlapping downregulated genes with Th2 + IL-17A showed processes not specific to the epidermis, while epidermal development was associated with the overlapping downregulated genes upon Th2 + IL-22. In N/TERT-

2G-HEEs, addition of IL-17A or IL-22 to Th2 cytokines increased overlapping DEG numbers with AD *in vivo* associated to similar processes (Supplementary Table 7, 8).

Of the 10 most upregulated genes *in vivo*, *serpin* genes were significantly upregulated in any of the cytokine conditions and *SPRR* and *S100 genes* were only significantly upregulated when IL-17A or IL-22 was added (Supplementary Figure 8A). Of the top 10 most downregulated genes, *HSD11B1* was downregulated by addition of both IL-17A or IL-22, whereas others like *SERPINA12* and *C1orf68* were specifically downregulated in the presence of IL-22 (Supplementary Figure 8B). It is also important to highlight the differences between *in vivo* and *in vitro* pathology. Many interferon responsive genes were among the upregulated genes in AD *in vivo,* but were not induced by Th2 + IL-22 *in vitro*, while multiple claudins were downregulated *in vivo* but not *in vitro*.

Next, we sought to discover the drivers that orchestrate the multiple deregulated processes in AD to devise effective intervention strategies and validate our model. Our search strategy was focused on genes that were involved in multiple deregulated biological processes that we identified by Th2 + IL-22 stimulated NHEK-HEEs and in AD *in vivo*. Seven upregulated genes were associated with minimally five significantly deregulated biological processes: *baculoviral IAP repeat containing 3* (*BIRC3*), *C-type lectin domain family 7 member A* (*CLEC7A*), *interferon-gamma-inducible protein 16* (*IFI16*), *Interleukin 1 Receptor Associated Kinase 2* (*IRAK2*), *Lactotransferrin* (*LTF*), *S100A12* and *WNT5A*. In addition, *alkaline ceramidase 1* (*ACER1*) and *Aldo-keto Reductase 1C3* (*AKR1C3*) were associated to all downregulated epidermal processes. These differential genes are hereafter called 'bridge genes'. Their differential expression between cytokine treatment and control *in vitro* was validated with RT-qPCR (Supplementary Figure 7D, Supplementary Figure 8C). Concordant differential expression could be shown in the meta-analysis comparing AD lesional (ADL) and AD non-lesional (ADNL) to healthy control (HC) skin biopsies, with *ACER1* and *AKR1C3* significantly lower and *BIRC3*, *LTF* and *S100A12* higher in AD as compared to HC (Figure 5C, Supplementary Table 9).

Epidermal defects by Th2 cytokines + IL-22 are restored by a combinatory therapeutic strategy

Of the bridge genes, *AKR1C3* was recognized as a target of aryl hydrocarbon receptor (AHR) signaling [33] which is known to have a role in epidermal development [34, 35] and skin barrier repair in AD [36, 37]. Therefore, we investigated the potential of AHR ligands to normalize the expression of bridge genes and restore tissue function. AHR ligands IMA-06504 [38] and tapinarof [39] effectively targeted AHR signaling illustrated by induced expression of AHR target gene *CYP1A1*. Epidermal integrity,

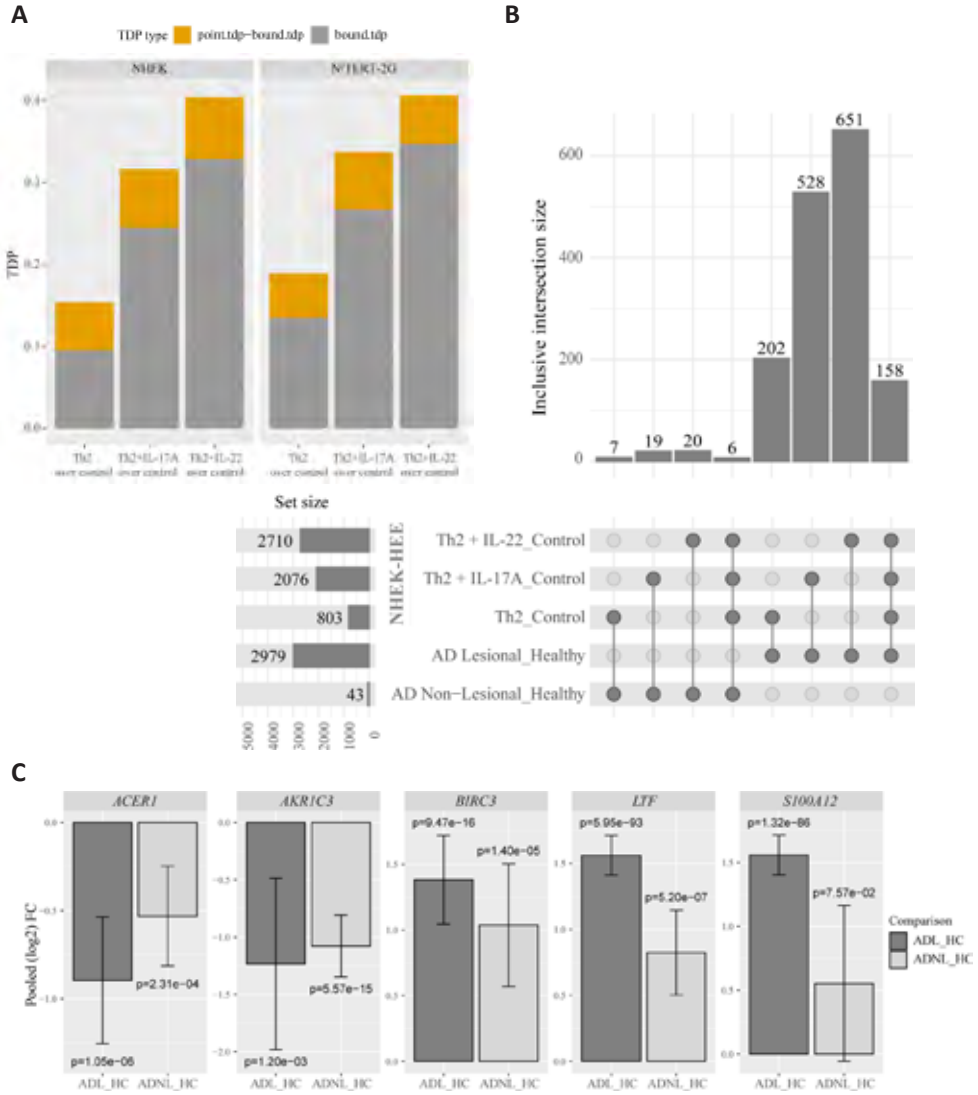

Figure 5. Transcriptomic comparison of *in vitro* AD-HEEs and *in vivo* AD affected epidermis. (**A**) Gene set enrichment analysis comparing gene expression induced in AD-HEEs generated from NHEK and N/TERT-2G with DEGs detected from AD patient affected skin as compared to controls, showing point estimate (point.tdp) and lower bound (bound.tdp) for the proportion of true discoveries (TDP, genes associated to DEGs from ADL_HC) (**B**) UpSet plot to show the number of overlapping genes with lesional and non-lesional full thickness skin biopsies from a larger cohort (meta-analysis) of AD patients and *in vitro* epidermal AD models. (**C**) Meta-analysis results of the bridge genes in the full thickness skin biopsies of the larger cohort of AD patients as compared to healthy controls, with error bars corresponding to the respective 95% confidence intervals. For the meta-analysis, data from N=188 AD lesional (ADL), 91 AD non-lesional (ADNL) and 181 healthy controls (HC) is used. * = p-value below 0.05 as compared to control.

differentiation, hyperproliferation, barrier function and *AKR1C3/ACER1* expression were partially restored in a donor-dependent manner (Supplementary Figure 9A-C, Figure 6A-C, Supplementary Table 15) and correlated to *CYP1A1* expression and therefore AHR activation (Supplementary Figure 9D). Overall, tapinarof demonstrated the strongest therapeutic effects. It is important to note that the disease-initiating cytokines are continuously present at high concentrations in our model system, whereas inflammation and cytokine production by T cells *in vivo* would also be affected by AHR ligands [39]. To better model the combined anti-inflammatory effects and epidermal differentiation induction by AHR activation, and given the recent advances in the development of Janus Kinase inhibitors (JAKi) as treatment for AD [40-42], we evaluated the effect of individual JAK1/3 inhibition (tofacitinib) and combined with AHR activation (tapinarof) on Th2 + IL-22-driven epidermal pathology.

Tofacitinib alone already reduced hypogranulosis and spongiosis, whereas combined with tapinarof also differentiation proteins were enhanced at both timepoints (Figure 6A, Supplementary Figure 10A). In contrast to single drug exposure, both drugs simultaneously applied with cytokines for 72h prevented cytokine-induced reduction of EIS^{diff} (Figure 6B). When applied 24h after the cytokines for 48h, to show restoring effects, the combination of drugs also enhanced EIS^{diff} to control levels. With both timings of the drugs, EIS^{sc} was significantly higher as compared to cytokines alone, but did not fully prevent or restore EIS^{sc} impairment. Finally, the combination of tapinarof and tofacitinib for 72 hours showed an overall greater restoring effect on inflammatory gene *CCL2* and the bridge genes as compared to single therapeutics (Figure 6C). Other genes from the same induced biological processes as the bridge genes, like *IL13RA2*, *SERPINB3/4*, and *DPP4* were also downregulated by tofacitinib alone and in combination with tapinarof (Supplementary Figure 10B).

> **Figure 6. The effect of AHR ligand tapinarof and JAK1/3 inhibitor tofacitinib on Th2 + IL-22-mediated epidermal differentiation and barrier defects.** (**A**) Morphology and differentiation protein expression of IVL and KRT2, and proliferation marker Ki67. Arrow and dashed boxes implicate restoration of the granular layer. Scale bar = 100µm. (**B**) Electrical impedance spectra (EIS), and EIS^{sc} and EIS^{diff} as percentages relative to the unstimulated control. (**C**) Expression of AHR target gene *CYP1A1*, inflammatory gene *CCL2* and bridge genes *ACER1*, *AKR1C3*, *BIRC3*, *S100A12* and *LTF*. All data is representative for N=3 replicates of NHEK-HEEs. Data is presented as mean +/- SEM. * = p-value below 0.05 as compared to Th2 + IL-22.

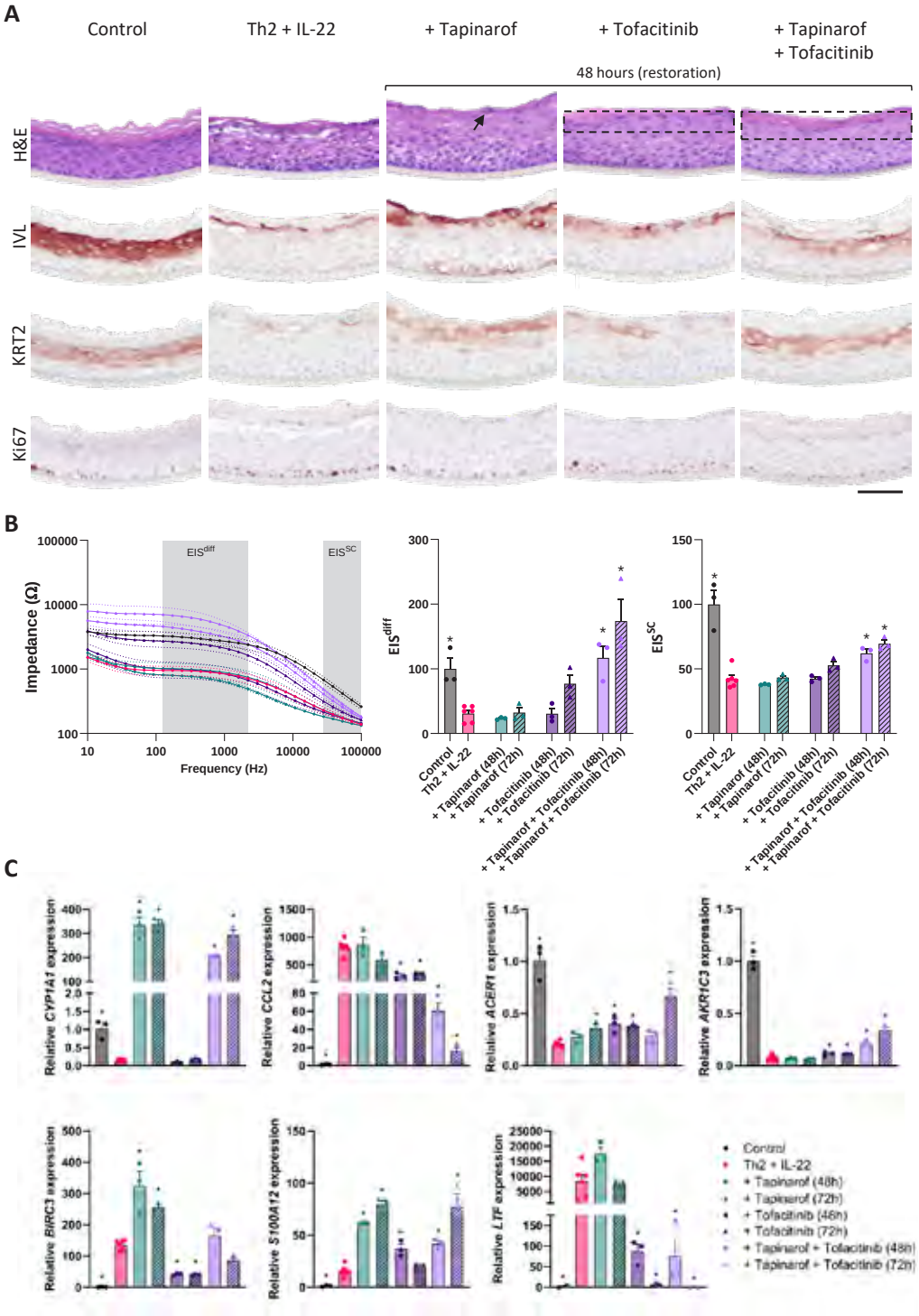
A
Control
Th2 + IL-22
+ Tapinarof
+ Tofacitinib
+ Tapinarof
+ Tofacitinib
48 hours (restoration)
H&E
IVL
KRT2
Ki67
B
Impedance (Ω)
Frequency (Hz)
EIS^diff
EIS^SC
Control
Th2 + IL-22
+ Tapinarof (48h)
+ Tapinarof (72h)
+ Tofacitinib (48h)
+ Tofacitinib (72h)
+ Tapinarof + Tofacitinib (48h)
+ Tapinarof + Tofacitinib (72h)
C
Relative CYP1A1 expression
Relative CCL2 expression
Relative ACER1 expression
Relative AKR1C3 expression
Relative BIRC3 expression
Relative S100A12 expression
Relative LTF expression
Control
Th2 + IL-22
+ Tapinarof (48h)
+ Tapinarof (72h)
+ Tofacitinib (48h)
+ Tofacitinib (72h)
+ Tapinarof + Tofacitinib (48h)
+ Tapinarof + Tofacitinib (72h)

Discussion

We provide experimental evidence to dissect epidermal hallmarks of AD related to specific inflammatory cytokines that dictate the local inflammatory milieu and determine treatment response. Th2 cytokines activated pro-inflammatory signaling and hyperproliferation, whereas addition of IL-17A or IL-22 appeared necessary for epidermal differentiation defects and barrier dysfunction. Th2 + IL-22 also transcriptionally mimicked *in vivo* lesional AD most closely, underscoring the role of IL-22 in AD pathophysiology. Combination therapy by tapinarof and tofacitinib appeared highly effective and abolished the cytokine-induced disturbance of epidermal homeostasis and corroborates other studies showing effective targeting of JAK/STAT signaling in keratinocytes by JAK inhibitors and restored epidermal homeostasis in cytokine-induced AD models [7, 24, 43, 44]. These insights may help to differentiate pathophysiological processes in patients and steer therapeutic developments.

We demonstrate a key role for IL-22 within a Th2 cytokine milieu in AD. Most biological processes were induced or impaired by Th2 + IL-22, which is in line with the Th2/Th22-skewing observed in most AD patients while Th1/Th17 contributions are variable [45, 46]. Moreover, integrative network analysis showed co-expression of IL-4R or IL-13 with IL-22 in AD [47]. Importantly, immunological distinctions between AD phenotypes are influenced by ethnicity and age. Asian AD is marked by heightened Th17 activation, while in chronic phases AD is dominated by a Th1 signature in European/American versus a Th2/Th22 in African/American populations. In pediatric AD, primarily Th2-mediated processes drive the disease [48]. Our observed effects of the cytokine combinations may therefore not generalize to all AD patients, but rather specific patients subgroups.

The role of bridge genes that are involved in multiple disease processes like *BIRC3*, *LTF* and *S100A12* in inflammation [49-51], and their possibility for non-invasive measurement [52] makes them potential AD biomarkers, although their exact contribution to disease is yet unknown. The role of *ACER1* and *AKR1C3* in driving epidermal differentiation defects also needs further investigation, as the downregulation of *AKR1C3* in *in vivo* AD skin and our *in vitro* RNA-seq data was in accordance with a previous study [52] but contrasting another one [53], which could hint towards patient-specific alterations in gene regulation.

Single-cell spatial transcriptomics showed that *TP63* and its targets *ZNF750* [54] and *IRF6* [55] had higher expression in an increased number of cells in various epidermal layers. P63 has been linked to (hyper)proliferation [28, 56, 57] and IL-4 and IL-13-

mediated overexpression of P63 has been linked to keratinocyte differentiation repression [58, 59]. This suggests that, next to its potential role in driving skin inflammation as previously proposed [60, 61], P63 could be an important driver of AD-associated hyperproliferation, and therefore can potentially be targeted to treat AD. Since new P63 targeting treatments are already under investigation for skin cancer [62, 63], repositioning of those may be effective for hyperproliferative inflammatory skin diseases.

The important role of IL-22 in the AD pathophysiology, and effective therapeutic approach when JAK inhibition was included, might explain why JAK1 inhibitors abrocitinib and upadacitinib show a greater disease improvement versus Dupilumab treatment only blocking the IL-4 receptor [64, 65]. We also highlight the value of combinatory therapies towards skin barrier repair and dampening of inflammation. While less severe IL-4-driven AD hallmarks are effectively restored by AHR activation alone [36], more severe epidermal phenotypes upon Th2 + IL-22 seem to require combined therapeutic targeting. Also, the anti-inflammatory effects of AHR ligands and JAK inhibitors on other skin cells than keratinocytes, not included in our model system, might be important for clinical efficacy in AD patients. Thereby, dual targeting by different therapeutics may not be required when multiple cells types involved in the disease pathophysiology are simultaneously targeted and contributing to dampening of the inflammatory process.

Beyond uncovering pathophysiological processes and finding new targets for therapeutic intervention, our data provides directions towards improvement of pre-clinical organotypic AD models. Lack of IFN signaling appeared key in our Th2 + IL-22 model. As IFN-γ has a distinct role in chronic AD [66] and the biopsies included in the data set from Rojahn were presumably taken from chronic AD lesions, this might explain the lack of CLDN1 downregulation upon Th2 + IL-22 [67-69], that was previously related to IFN-γ [70], but also IL-1β [71]. Addition of Th1 cytokines could mimic the transition from acute to chronic AD. Moreover, our model did not include fibroblasts [72, 73], immune cells [74, 75], microbiota [76, 77] or defined AD genotypes [72, 78], which could all influence cytokine responses and improve the translatability to *in vivo* AD mechanisms. Future research should be directed to more complex organotypic models including multi-cellular interactions upon Th2 + IL-22 exposure to untangle AD pathology. For model optimization, immortal N/TERT-2G keratinocytes are better suitable for genetic modification to mimic the genetic predisposition of AD. We showed the potential of N/TERT-2G as alternative to NHEK as both cell types responded mostly similar, besides spongiosis in higher layers and only minor effects on proliferation and EIS^{diff} in N/TERT-2G-HEEs. This

might be caused by their immortal cell state or foreskin origin [79] and should be taken into account in the light of AD hyperproliferation.

Our comprehensive study clearly demonstrated the important contribution of IL-22 to Th2 cytokine-driven AD epidermal pathology. The translation from *in vitro* transcriptomic data to both keratinocyte pseudobulk data derived from scRNA-seq on skin biopsies, as well as to full thickness skin data from a large patient cohort, yielded novel insights into driving pathophysiological processes and target genes that are associated to epidermal disease hallmarks. Differential and synergistic effects of cytokines should be investigated further including transcriptomics data from cohorts of well-defined AD patients (e.g., severity, genotype, disease duration) to identify AD endotype specific cytokines that may explain or predict therapeutic efficacy.

Data availability

Raw RNA-sequencing files generated for this study are deposited in the Gene Expression Omnibus (GEO) database with the accession number GSE282371. Public transcriptomic datasets incorporated in the differential meta-analysis are available from ArrayExpress (accession E-MTAB-8149) and GEO (accession GSE130588 and GSE193309). Data from P2N_clinical will be shared upon reasonable request. Meta-analysis summary statistics are provided in Supplementary Table 9.

Acknowledgements

We would like to acknowledge Marijke P. Baltissen for performing the RNA-sequencing, and Ward F. G. Nijen Twilhaar for pre-processing of the AD lesional scRNA-sequencing data. For critical discussions on the data and reviewing of the manuscript we are grateful to Abdoelwaheb E. G. El Ghalbzouri from the PAST4FUTURE consortium. This work is supported by Health Holland grant PAST4FUTURE, LSHM20043-HSGF to EB and HZ. Further support is provided to EB by Next Generation ImmunoDermatology (NGID) NWA-ORC project NWA.1389.20.182, EIC-Pathfinder project SKINDEV (No.101098826) and LEO Foundation grant LF-OC-22-001056 (to JS and EB). EB, MH and HN are funded by the Innovative Medicines Initiative 2 Joint Undertaking (JU) under grant agreement (No. 821511). The JU receives support from the European Union's Horizon 2020 research and innovation programme and EFPIA. This work reflects only the authors' view and the IMI 2 JU is not responsible for any use that may be made of the information it contains. The authors declare no conflicts of interest.

Abbreviations

ACER1 - Alkaline Ceramidase 1, AD - Atopic dermatitis, AHR - Aryl hydrocarbon receptor, AKR1C3 - Aldo-Keto Reductase Family 1 Member C3, AMP - Antimicrobial peptide, ARG1 - Arginase 1, BIRC3 - Baculoviral IAP Repeat Containing 3, C1orf68 - Chromosome 1 open reading frame 68, CA2 - Carbonic anhydrase II, CAMP - Cathelicidin antimicrobial peptide, CCL - C-C motif chemokine, CLDN – Claudin, CLEC7A - C-Type Lectin Domain Containing 7A, COL – Collagen, CXCL - C-X-C motif ligand chemokine, CYP1A1 - Cytochrome P450 Family 1 Subfamily A Member 1, DEFB4 - Defensin beta 4, DEG - Differentially expressed genes, DSG - Desmoglein, EIS^{diff} - Electrical impedance spectroscopy differentiation, EIS^{sc} - Electrical impedance spectroscopy *stratum corneum*, EGFR - Epidermal Growth Factor Receptor, EV - Extracellular vesicle, FLG – Filaggrin, GBA2 - Glucosylceramidase Beta 2, GJB2 - Gap Junction Protein Beta 2, GO - Gene ontology, HEE - Human epidermal equivalent, HIF1A - Hypoxia-inducible factor 1 alpha, HRNR – Hornerin, HSD11B1 - Hydroxysteroid 11-Beta Dehydrogenase 1, IFI16 - Interferon Gamma Inducible Protein 16, IFIH1 - Interferon Induced with Helicase C Domain 1, IFNAR2 - Interferon Alpha and Beta Receptor Subunit 2, IL – Interleukin, IRAK2 - Interleukin 1 Receptor Associated Kinase 2, IRF6 - Interferon Regulatory Factor 6, ITG – Integrin, JAK - Janus Kinase, IVL – Involucrin, KRT – Keratin, L1 / 2 - Layer 1 / 2, LM - Middle layers, LOR – Loricrin, LT - Top layer, LTF – Lactotransferrin, MAFB - MAF BZIP Transcription Factor B, MCM - Minichromosome maintenance, NELL2 - Neural EGFL like 2, NHEK - Normal human epidermal keratinocytes, PC(A) - Principal component (analysis), PI3 - Peptidase inhibitor 3, S100 - S100 calcium binding protein, SEM - Standard error of the mean, SKALP - Skin-derived antileukoprotease, SPRR - Small Proline Rich Protein, STAT - Signal transducer and activator of transcription, TFAP2A - Transcription Factor AP-2 Alpha, Th - T helper cell, TNF - Tumor necrosis factor, (T)P63 - Tumor protein 63, ZNF750 - Zinc Finger Protein 750

References

1. Montero-Vilchez, T., et al., Skin Barrier Function in Psoriasis and Atopic Dermatitis: Transepidermal Water Loss and Temperature as Useful Tools to Assess Disease Severity. J Clin Med, 2021. **10**(2).
2. Niehues, H., et al., 3D skin models for 3R research: The potential of 3D reconstructed skin models to study skin barrier function. Exp Dermatol, 2018. **27**(5): p. 501-511.
3. Langan, S.M., A.D. Irvine, and S. Weidinger, Atopic dermatitis. Lancet, 2020. **396**(10247): p. 345-360.
4. Palmer, C.N., et al., Common loss-of-function variants of the epidermal barrier protein filaggrin are a major predisposing factor for atopic dermatitis. Nat Genet, 2006. **38**(4): p. 441-6.
5. Barker, J.N., et al., Null mutations in the filaggrin gene (FLG) determine major susceptibility to early-onset atopic dermatitis that persists into adulthood. J Invest Dermatol, 2007. **127**(3): p. 564-7.
6. Kim, B.E., et al., Loricrin and involucrin expression is down-regulated by Th2 cytokines through STAT-6. Clin Immunol, 2008. **126**(3): p. 332-7.
7. Niehues, H., et al., Identification of Keratinocyte Mitogens: Implications for Hyperproliferation in Psoriasis and Atopic Dermatitis. JID Innov, 2022. **2**(1): p. 100066.
8. Bernard, F.X., et al., Keratinocytes under Fire of Proinflammatory Cytokines: Bona Fide Innate Immune Cells Involved in the Physiopathology of Chronic Atopic Dermatitis and Psoriasis. J Allergy (Cairo), 2012. **2012**: p. 718725.
9. Nograles, K.E., et al., Th17 cytokines interleukin (IL)-17 and IL-22 modulate distinct inflammatory and keratinocyte-response pathways. Br J Dermatol, 2008. **159**(5): p. 1092-102.
10. Jeong, C.W., et al., Differential in vivo cytokine mRNA expression in lesional skin of intrinsic vs. extrinsic atopic dermatitis patients using semiquantitative RT-PCR. Clin Exp Allergy, 2003. **33**(12): p. 1717-24.
11. Neis, M.M., et al., Enhanced expression levels of IL-31 correlate with IL-4 and IL-13 in atopic and allergic contact dermatitis. J Allergy Clin Immunol, 2006. **118**(4): p. 930-7.
12. Gittler, J.K., et al., Progressive activation of T(H)2/T(H)22 cytokines and selective epidermal proteins characterizes acute and chronic atopic dermatitis. J Allergy Clin Immunol, 2012. **130**(6): p. 1344-54.
13. Koga, C., et al., Possible pathogenic role of Th17 cells for atopic dermatitis. J Invest Dermatol, 2008. **128**(11): p. 2625-2630.
14. Esaki, H., et al., Early-onset pediatric atopic dermatitis is T(H)2 but also T(H)17 polarized in skin. J Allergy Clin Immunol, 2016. **138**(6): p. 1639-1651.
15. Noda, S., et al., The Asian atopic dermatitis phenotype combines features of atopic dermatitis and psoriasis with increased TH17 polarization. J Allergy Clin Immunol, 2015. **136**(5): p. 1254-64.
16. Quílez, C., et al., Targeting the Complexity of In Vitro Skin Models: A Review of Cutting-Edge Developments. J Invest Dermatol, 2024. **144**(12): p. 2650-2670.
17. Rikken, G., H. Niehues, and E.H. van den Bogaard, Organotypic 3D Skin Models: Human Epidermal Equivalent Cultures from Primary Keratinocytes and Immortalized Keratinocyte Cell Lines. Methods Mol Biol, 2020. **2154**: p. 45-61.
18. Geckin, B., et al., Differences in Immune Responses in Individuals of Indian and European Origin: Relevance for the COVID-19 Pandemic. Microbiol Spectr, 2023. **11**(2): p. e0023123.
19. Rojahn, T.B., et al., Single-cell transcriptomics combined with interstitial fluid proteomics defines cell type-specific immune regulation in atopic dermatitis. J Allergy Clin Immunol, 2020. **146**(5): p. 1056-1069.

20. van den Brink, N.J.M., et al., Electrical Impedance Spectroscopy Quantifies Skin Barrier Function in Organotypic In Vitro Epidermis Models. J Invest Dermatol, 2024. **144**(11): p. 2488-2500.
21. Castex-Rizzi, N., et al., In vitro approaches to pharmacological screening in the field of atopic dermatitis. Br J Dermatol, 2014. **170 Suppl 1**: p. 12-8.
22. Smits, J.P.H., et al., Immortalized N/TERT keratinocytes as an alternative cell source in 3D human epidermal models. Sci Rep, 2017. **7**(1): p. 11838.
23. Lee, S.H., et al., Ameliorating effect of dipotassium glycyrrhizinate on an IL-4- and IL-13-induced atopic dermatitis-like skin-equivalent model. Arch Dermatol Res, 2019. **311**(2): p. 131-140.
24. Clarysse, K., et al., JAK1/3 inhibition preserves epidermal morphology in full-thickness 3D skin models of atopic dermatitis and psoriasis. J Eur Acad Dermatol Venereol, 2019. **33**(2): p. 367-375.
25. Ong, P.Y., et al., Endogenous antimicrobial peptides and skin infections in atopic dermatitis. N Engl J Med, 2002. **347**(15): p. 1151-60.
26. Nomura, I., et al., Cytokine milieu of atopic dermatitis, as compared to psoriasis, skin prevents induction of innate immune response genes. J Immunol, 2003. **171**(6): p. 3262-9.
27. Dickson, M.A., et al., Human keratinocytes that express hTERT and also bypass a p16(INK4a)-enforced mechanism that limits life span become immortal yet retain normal growth and differentiation characteristics. Mol Cell Biol, 2000. **20**(4): p. 1436-47.
28. Truong, A.B., et al., p63 regulates proliferation and differentiation of developmentally mature keratinocytes. Genes Dev, 2006. **20**(22): p. 3185-97.
29. Koster, M.I., et al., p63 is the molecular switch for initiation of an epithelial stratification program. Genes Dev, 2004. **18**(2): p. 126-31.
30. De Benedetto, A., et al., Tight junction defects in patients with atopic dermatitis. J Allergy Clin Immunol, 2011. **127**(3): p. 773-86.e1-7.
31. Albuloushi, A., et al., A heterozygous mutation in GJB2 (Cx26F142L) associated with deafness and recurrent skin rashes results in connexin assembly deficiencies. Exp Dermatol, 2020. **29**(10): p. 970-979.
32. Altunbulakli, C., et al., Relations between epidermal barrier dysregulation and Staphylococcus species-dominated microbiome dysbiosis in patients with atopic dermatitis. J Allergy Clin Immunol, 2018. **142**(5): p. 1643-1647.e12.
33. Vogeley, C., et al., Unraveling the differential impact of PAHs and dioxin-like compounds on AKR1C3 reveals the EGFR extracellular domain as a critical determinant of the AHR response. Environ Int, 2022. **158**: p. 106989.
34. Sutter, C.H., et al., 2,3,7,8-Tetrachlorodibenzo-p-dioxin increases the expression of genes in the human epidermal differentiation complex and accelerates epidermal barrier formation. Toxicol Sci, 2011. **124**(1): p. 128-37.
35. van den Bogaard, E.H., et al., Genetic and pharmacological analysis identifies a physiological role for the AHR in epidermal differentiation. J Invest Dermatol, 2015. **135**(5): p. 1320-1328.
36. van den Bogaard, E.H., et al., Coal tar induces AHR-dependent skin barrier repair in atopic dermatitis. J Clin Invest, 2013. **123**(2): p. 917-27.
37. Bissonnette, R., et al., Tapinarof for psoriasis and atopic dermatitis: 15 years of clinical research. J Eur Acad Dermatol Venereol, 2023. **37**(6): p. 1168-1174.

38. Rikken, G., et al., Carboxamide Derivatives Are Potential Therapeutic AHR Ligands for Restoring IL-4 Mediated Repression of Epidermal Differentiation Proteins. Int J Mol Sci, 2022. **23**(3).
39. Smith, S.H., et al., Tapinarof Is a Natural AhR Agonist that Resolves Skin Inflammation in Mice and Humans. J Invest Dermatol, 2017. **137**(10): p. 2110-2119.
40. Chovatiya, R. and A.S. Paller, JAK inhibitors in the treatment of atopic dermatitis. J Allergy Clin Immunol, 2021. **148**(4): p. 927-940.
41. Miao, M. and L. Ma, The efficacy and safety of JAK inhibitors for atopic dermatitis: a systematic review and meta-analysis. J Dermatolog Treat, 2022. **33**(4): p. 1869-1877.
42. Kogame, T., G. Egawa, and K. Kabashima, Exploring the role of Janus kinase (JAK) in atopic dermatitis: a review of molecular mechanisms and therapeutic strategies. Immunol Med, 2023. **46**(3): p. 112-120.
43. Morelli, M., et al., Selective Immunomodulation of Inflammatory Pathways in Keratinocytes by the Janus Kinase (JAK) Inhibitor Tofacitinib: Implications for the Employment of JAK-Targeting Drugs in Psoriasis. J Immunol Res, 2018. **2018**: p. 7897263.
44. Srivastava, A., et al., Tofacitinib Represses the Janus Kinase-Signal Transducer and Activators of Transcription Signalling Pathway in Keratinocytes. Acta Derm Venereol, 2018. **98**(8): p. 772-775.
45. Glickman, J.W., et al., Comparing cutaneous molecular improvement with different treatments in atopic dermatitis patients. J Allergy Clin Immunol, 2020. **145**(4): p. 1285-1288.
46. Leung, D.Y., Atopic dermatitis: Age and race do matter! J Allergy Clin Immunol, 2015. **136**(5): p. 1265-7.
47. Federico, A., et al., Integrative network analysis suggests prioritised drugs for atopic dermatitis. J Transl Med, 2024. **22**(1): p. 64.
48. Guttman-Yassky, E., Y. Renert-Yuval, and P.M. Brunner, Atopic dermatitis. Lancet, 2025. **405**(10478): p. 583-596.
49. Thorne, A., et al., Differential regulation of BIRC2 and BIRC3 expression by inflammatory cytokines and glucocorticoids in pulmonary epithelial cells. PLoS One, 2023. **18**(6): p. e0286783.
50. Yeom, M., et al., Lactoferrin inhibits the inflammatory and angiogenic activation of bovine aortic endothelial cells. Inflamm Res, 2011. **60**(5): p. 475-82.
51. Pavel, A.B., et al., The proteomic skin profile of moderate-to-severe atopic dermatitis patients shows an inflammatory signature. J Am Acad Dermatol, 2020. **82**(3): p. 690-699.
52. Del Duca, E., et al., Intrapatient comparison of atopic dermatitis skin transcriptome shows differences between tape-strips and biopsies. Allergy, 2024. **79**(1): p. 80-92.
53. Mantel, A., et al., Aldo-keto reductase 1C3 is expressed in differentiated human epidermis, affects keratinocyte differentiation, and is upregulated in atopic dermatitis. J Invest Dermatol, 2012. **132**(4): p. 1103-10.
54. Sen, G.L., et al., ZNF750 is a p63 target gene that induces KLF4 to drive terminal epidermal differentiation. Dev Cell, 2012. **22**(3): p. 669-77.
55. Moretti, F., et al., A regulatory feedback loop involving p63 and IRF6 links the pathogenesis of 2 genetically different human ectodermal dysplasias. J Clin Invest, 2010. **120**(5): p. 1570-7.
56. Parsa, R., et al., Association of p63 with proliferative potential in normal and neoplastic human keratinocytes. J Invest Dermatol, 1999. **113**(6): p. 1099-105.
57. Leonard, M.K., et al., ΔNp63α regulates keratinocyte proliferation by controlling PTEN expression and localization. Cell Death Differ, 2011. **18**(12): p. 1924-33.

58. Kubo, T., et al., IL-13 modulates ΔNp63 levels causing altered expression of barrier- and inflammation-related molecules in human keratinocytes: A possible explanation for chronicity of atopic dermatitis. Immun Inflamm Dis, 2021. **9**(3): p. 734-745.

59. Brauweiler, A.M., D.Y.M. Leung, and E. Goleva, The Transcription Factor p63 Is a Direct Effector of IL-4- and IL-13-Mediated Repression of Keratinocyte Differentiation. J Invest Dermatol, 2021. **141**(4): p. 770-778.

60. Jiménez-Andrade, Y., et al., The Developmental Transcription Factor p63 Is Redeployed to Drive Allergic Skin Inflammation through Phosphorylation by p38α. J Immunol, 2022. **208**(12): p. 2613-2621.

61. Rizzo, J.M., et al., ΔNp63 regulates IL-33 and IL-31 signaling in atopic dermatitis. Cell Death Differ, 2016. **23**(6): p. 1073-85.

62. Patel, A., et al., Targeting p63 Upregulation Abrogates Resistance to MAPK Inhibitors in Melanoma. Cancer Res, 2020. **80**(12): p. 2676-2688.

63. Jiang, Y., et al., Reciprocal inhibition between TP63 and STAT1 regulates anti-tumor immune response through interferon-γ signaling in squamous cancer. Nat Commun, 2024. **15**(1): p. 2484.

64. Reich, K., et al., Efficacy and safety of abrocitinib versus dupilumab in adults with moderate-to-severe atopic dermatitis: a randomised, double-blind, multicentre phase 3 trial. Lancet, 2022. **400**(10348): p. 273-282.

65. Blauvelt, A., et al., Efficacy and Safety of Upadacitinib vs Dupilumab in Adults With Moderate-to-Severe Atopic Dermatitis: A Randomized Clinical Trial. JAMA Dermatol, 2021. **157**(9): p. 1047-1055.

66. Su, C., et al., Differentiation of T-helper cells in distinct phases of atopic dermatitis involves Th1/Th2 and Th17/Treg. European Journal of Inflammation, 2017. **15**(1): p. 46-52.

67. Xia, Y., et al., Claudin-1 Mediated Tight Junction Dysfunction as a Contributor to Atopic March. Front Immunol, 2022. **13**: p. 927465.

68. Bergmann, S., et al., Claudin-1 decrease impacts epidermal barrier function in atopic dermatitis lesions dose-dependently. Scientific Reports, 2020. **10**(1): p. 2024.

69. Gruber, R., et al., Diverse regulation of claudin-1 and claudin-4 in atopic dermatitis. Am J Pathol, 2015. **185**(10): p. 2777-89.

70. Mizutani, Y., et al., Interferon-γ downregulates tight junction function, which is rescued by interleukin-17A. Exp Dermatol, 2021. **30**(12): p. 1754-1763.

71. Watson, R.E., et al., Altered claudin expression is a feature of chronic plaque psoriasis. J Pathol, 2007. **212**(4): p. 450-8.

72. Berroth, A., et al., Role of fibroblasts in the pathogenesis of atopic dermatitis. J Allergy Clin Immunol, 2013. **131**(6): p. 1547-54.

73. Löwa, A., et al., Fibroblasts from atopic dermatitis patients trigger inflammatory processes and hyperproliferation in human skin equivalents. J Eur Acad Dermatol Venereol, 2020. **34**(6): p. e262-e265.

74. van den Bogaard, E.H., et al., Crosstalk between keratinocytes and T cells in a 3D microenvironment: a model to study inflammatory skin diseases. J Invest Dermatol, 2014. **134**(3): p. 719-727.

75. Wallmeyer, L., et al., TSLP is a direct trigger for T cell migration in filaggrin-deficient skin equivalents. Sci Rep, 2017. **7**(1): p. 774.

76. Rikken, G., et al., Novel methodologies for host-microbe interactions and microbiome-targeted therapeutics in 3D organotypic skin models. Microbiome, 2023. **11**(1): p. 227.

77. van der Krieken, D.A., et al., Gram-positive anaerobic cocci guard skin homeostasis by regulating host-defense mechanisms. iScience, 2023. **26**(4): p. 106483.
78. Niehues, H., et al., Epidermal equivalents of filaggrin null keratinocytes do not show impaired skin barrier function. J Allergy Clin Immunol, 2017. **139**(6): p. 1979-1981.e13.
79. McHeik, J.N., et al., Study of proliferation and 3D epidermal reconstruction from foreskin, auricular and trunk keratinocytes in children. Burns, 2015. **41**(2): p. 352-8.
80. van Duijnhoven, J.L., et al., MON-150, a versatile monoclonal antibody against involucrin: characterization and applications. Arch Dermatol Res, 1992. **284**(3): p. 167-72.
81. Schindelin, J., et al., Fiji: an open-source platform for biological-image analysis. Nat Methods, 2012. **9**(7): p. 676-82.
82. Livak, K.J. and T.D. Schmittgen, Analysis of relative gene expression data using real-time quantitative PCR and the 2(-Delta Delta C(T)) Method. Methods, 2001. **25**(4): p. 402-8.
83. van der Sande, M., et al., Seq2science: an end-to-end workflow for functional genomics analysis. PeerJ, 2023. **11**: p. e16380.
84. Chen, S., et al., fastp: an ultra-fast all-in-one FASTQ preprocessor. Bioinformatics, 2018. **34**(17): p. i884-i890.
85. Dobin, A., et al., STAR: ultrafast universal RNA-seq aligner. Bioinformatics, 2013. **29**(1): p. 15-21.
86. Ewels, P., et al., MultiQC: summarize analysis results for multiple tools and samples in a single report. Bioinformatics, 2016. **32**(19): p. 3047-8.
87. Li, H., et al., The Sequence Alignment/Map format and SAMtools. Bioinformatics, 2009. **25**(16): p. 2078-9.
88. Anders, S., P.T. Pyl, and W. Huber, HTSeq--a Python framework to work with high-throughput sequencing data. Bioinformatics, 2015. **31**(2): p. 166-9.
89. Love, M.I., W. Huber, and S. Anders, Moderated estimation of fold change and dispersion for RNA-seq data with DESeq2. Genome Biol, 2014. **15**(12): p. 550.
90. Yoav Benjamini, Y.H., Controlling the False Discovery Rate: A Practical and Powerful Approach to Multiple Testing. Journal of the Royal Statistical Society Series B (Methodological), 1995. **57**(1): p. 289-300.
91. Gu, Z., R. Eils, and M. Schlesner, Complex heatmaps reveal patterns and correlations in multidimensional genomic data. Bioinformatics, 2016. **32**(18): p. 2847-9.
92. Ritchie, M.E., et al., limma powers differential expression analyses for RNA-sequencing and microarray studies. Nucleic Acids Res, 2015. **43**(7): p. e47.
93. Wu, T., et al., clusterProfiler 4.0: A universal enrichment tool for interpreting omics data. Innovation (Camb), 2021. **2**(3): p. 100141.
94. Wickham, H., ggplot2: Elegant Graphics for Data Analysis. 2016, New York: Springer link.
95. Hao, Y., et al., Integrated analysis of multimodal single-cell data. Cell, 2021. **184**(13): p. 3573-3587.e29.
96. Shen L, S.I., GeneOverlap: Test and visualize gene overlaps.. 2024.
97. Piccolo, S.R., et al., A single-sample microarray normalization method to facilitate personalized-medicine workflows. Genomics, 2012. **100**(6): p. 337-44.
98. Krueger, F. TrimGalore version 0.6.6. 2023; Available from: https://github.com/FelixKrueger/TrimGalore.
99. Martin, M., Cutadapt removes adapter sequences from high-throughput sequencing reads. EMBnet, 2011.
100. Andrews, S., FastQC version 0.11.9. 2022.

101. Kim, D., et al., Graph-based genome alignment and genotyping with HISAT2 and HISAT-genotype. Nat Biotechnol, 2019. **37**(8): p. 907-915.

102. Liao, Y., G.K. Smyth, and W. Shi, The R package Rsubread is easier, faster, cheaper and better for alignment and quantification of RNA sequencing reads. Nucleic Acids Res, 2019. **47**(8): p. e47.

103. Robinson, M.D., D.J. McCarthy, and G.K. Smyth, edgeR: a Bioconductor package for differential expression analysis of digital gene expression data. Bioinformatics, 2010. **26**(1): p. 139-40.

104. Silkeszy. HarmonizeGeneExprData. 2022; Available from: https://github.com/szymczak-lab/harmonizeGeneExprData.

105. Silkeszy. QCnormSE. 2020; Available from: https://github.com/szymczak-lab/QCnormSE.

106. Viechtbauer, W., Conducting Meta-Analyses in R with the metafor Package. Journal of Statistical Software, 2010. **36**(3): p. 1-48.

107. Silkeszy. MetaAnalyzeGeneExprData. 2024; Available from: https://github.com/szymczak-lab/metaAnalyzeGeneExprData.

108. Daniel D. Sjoberg, K.W., Michael Curry, Jessica A. Lavery and Joseph Larmarange, Reproducible Summary Tables with the gtsummary Package The R Journal, 2021. **13**(1): p. 570-580.

109. Lex, A., et al., UpSet: Visualization of Intersecting Sets. IEEE Trans Vis Comput Graph, 2014. **20**(12): p. 1983-92.

110. Wolf, F.A., P. Angerer, and F.J. Theis, SCANPY: large-scale single-cell gene expression data analysis. Genome Biol, 2018. **19**(1): p. 15.

111. Gu, Z., Complex heatmap visualization. Imeta, 2022. **1**(3): p. e43.

Supplemental figures

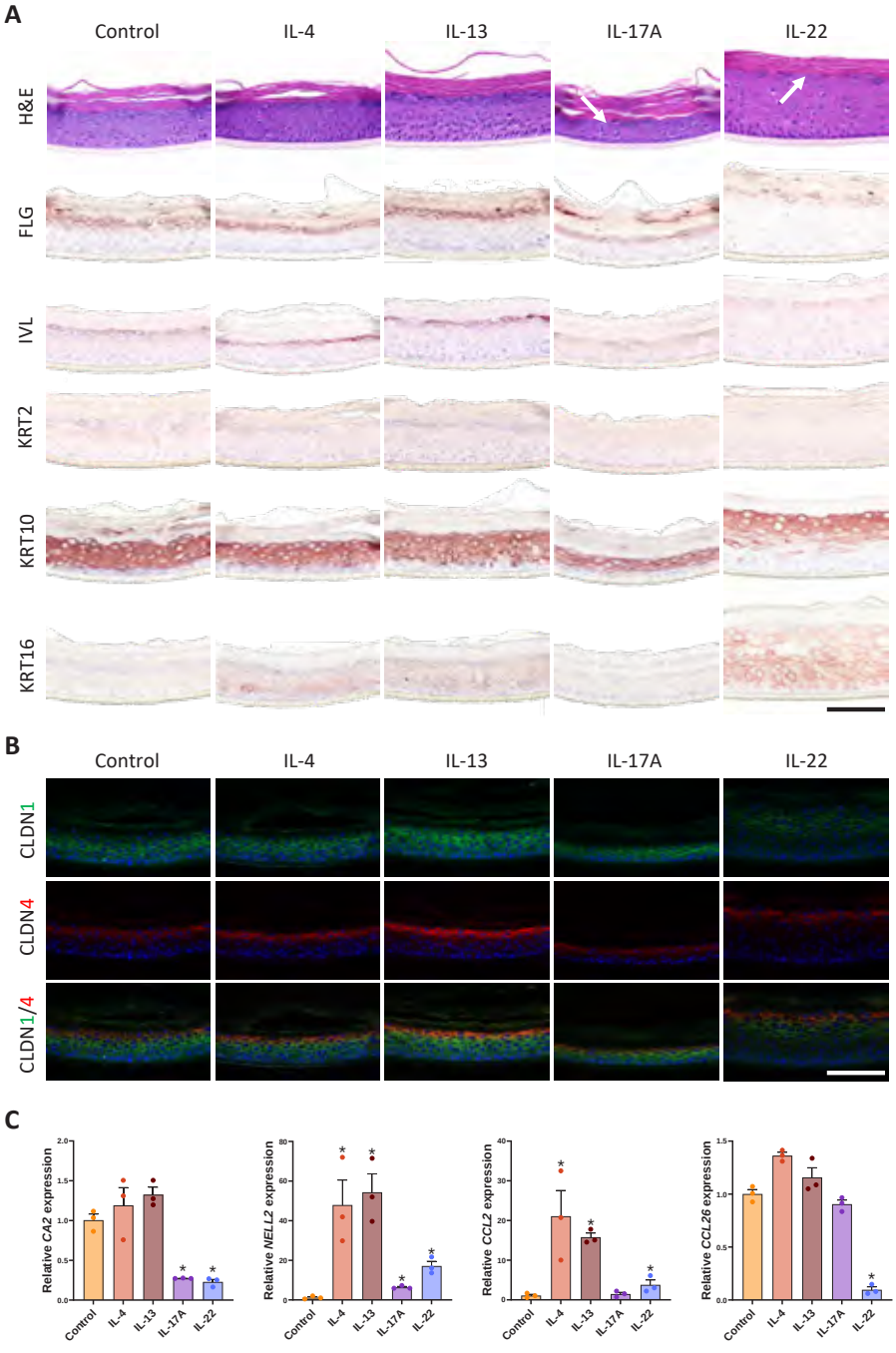

< Supplementary Figure 1. Effect of individual AD associated cytokines IL-4, IL-13, IL-17A and IL-22 on N/TERT-2G-HEEs. (**A**) The morphology and differentiation protein expression of FLG, IVL, KRT2, KRT10 and alarmin KRT16. White arrow: hypogranulosis. Scale bar = 100µm. (**B**) Tight junction protein expression of CLDN1 (green) and CLDN4 (red), and DAPI (blue). Scale bar = 100µm. (**C**) The expression of AD associated genes *CA2*, *NELL2*, *CCL2* and *CCL26*. All data is representative for N=3 N/TERT-2G-HEEs, and presented as mean +/- SEM. * = p-value below 0.05 as compared to control.

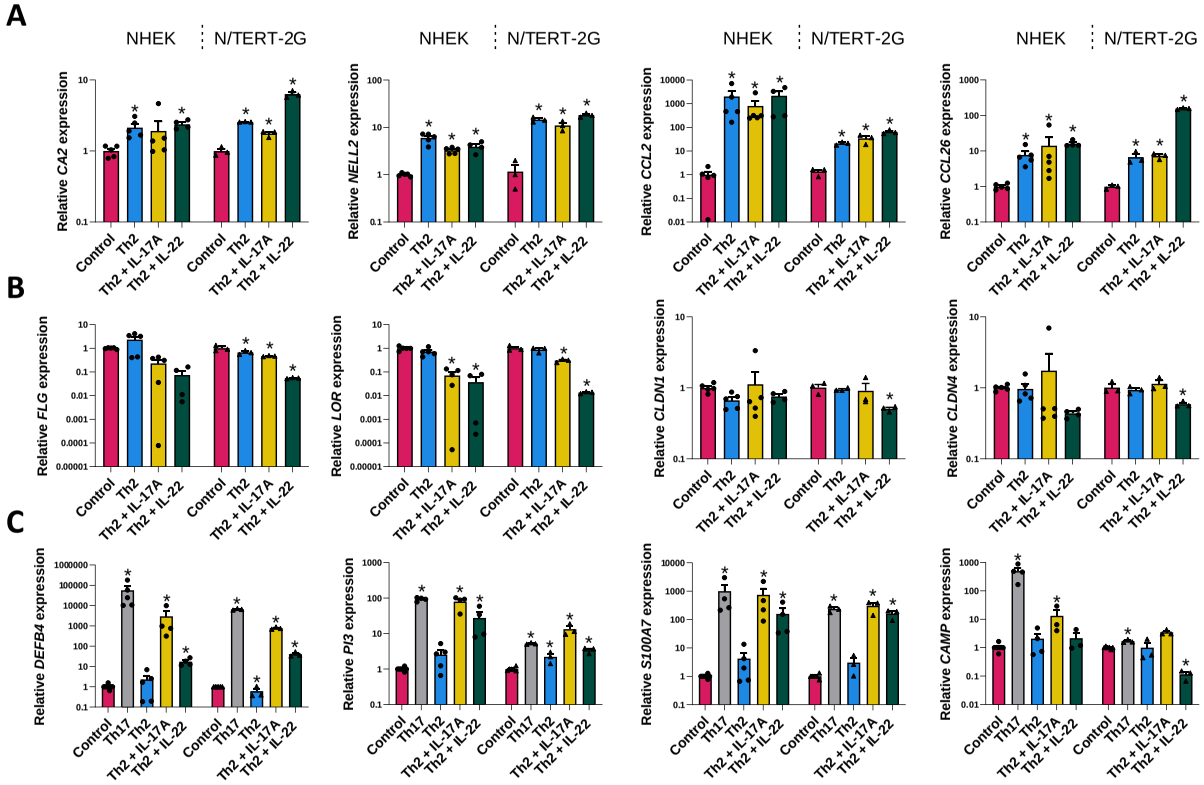

Supplementary Figure 2. Gene expression profiles of HEEs upon stimulation with Th2 cytokines with and without IL-17A or IL-22, and Th17 cytokines IL-17A and IL-22. (**A**) AD-associated (pro-inflammatory) genes, (**B**) Keratinocyte differentiation and tight junction markers, (**C**) Antimicrobial peptides. All data is representative for N=5 for NHEK (three biological replicates) or N=3 N/TERT-2G technical replicates. Data is presented as mean +/- SEM. * = p-value below 0.05 as compared to control.

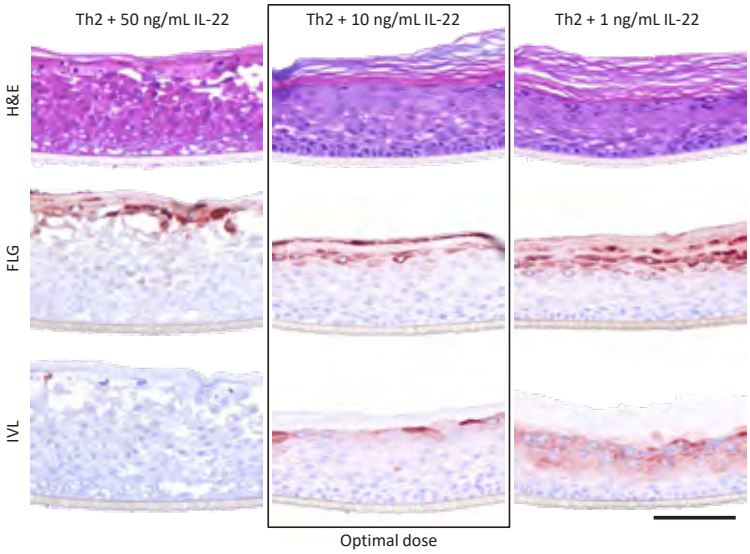

Supplementary Figure 3. Concentration titration series of IL-22 when combined with Th2 cytokines. Morphology is representative for N=2 or 3 replicates. Scale bar= 100µm.

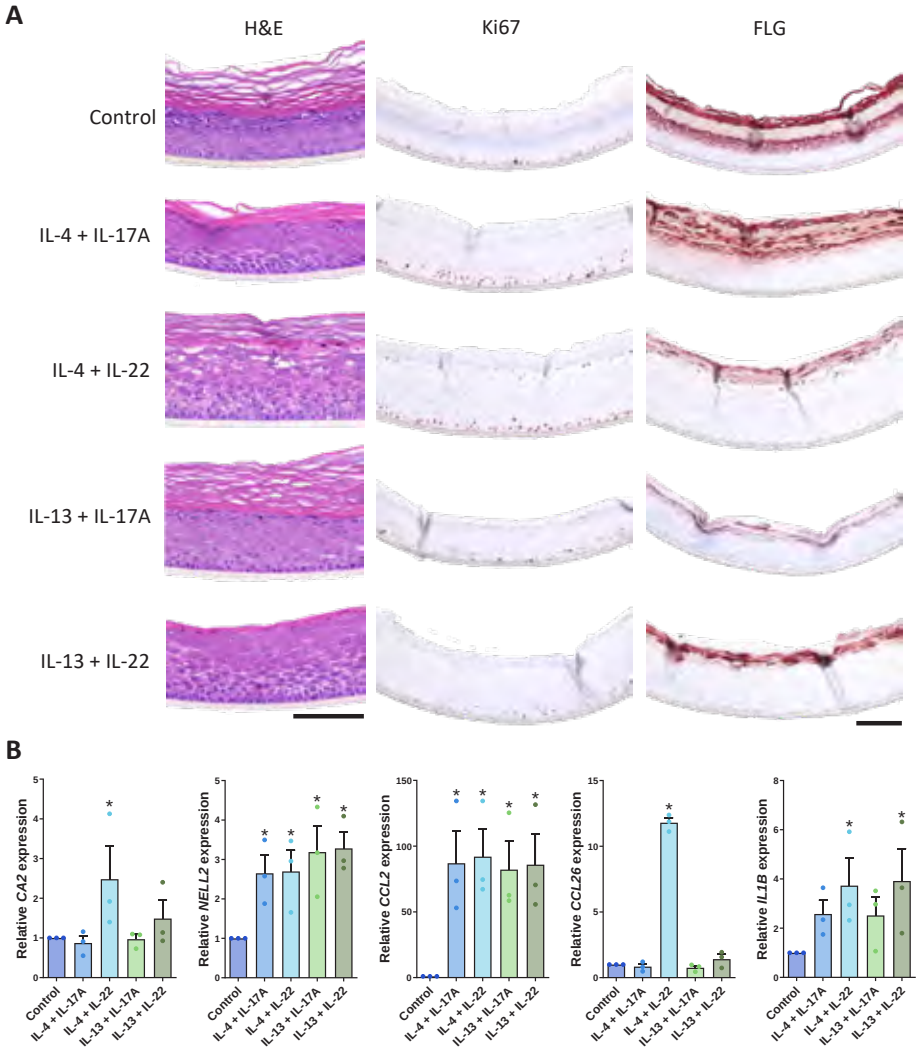

Supplementary Figure 4. Effect of various cytokine combinations of IL-4, IL-13, IL-17A and IL-22 on NHEK-HEEs. (**A**) Morphology, expression of differentiation protein FLG, and expression of proliferation marker Ki67. Scale bar = 100µm. (**B**) Gene expression of AD markers *CA2*, *NELL2*, *CCL2*, *CCL26* and *IL1B*. All data is representative for N=3 primary keratinocyte donors. Data is presented as mean +/- SEM. * = p-value below 0.05 as compared to control.

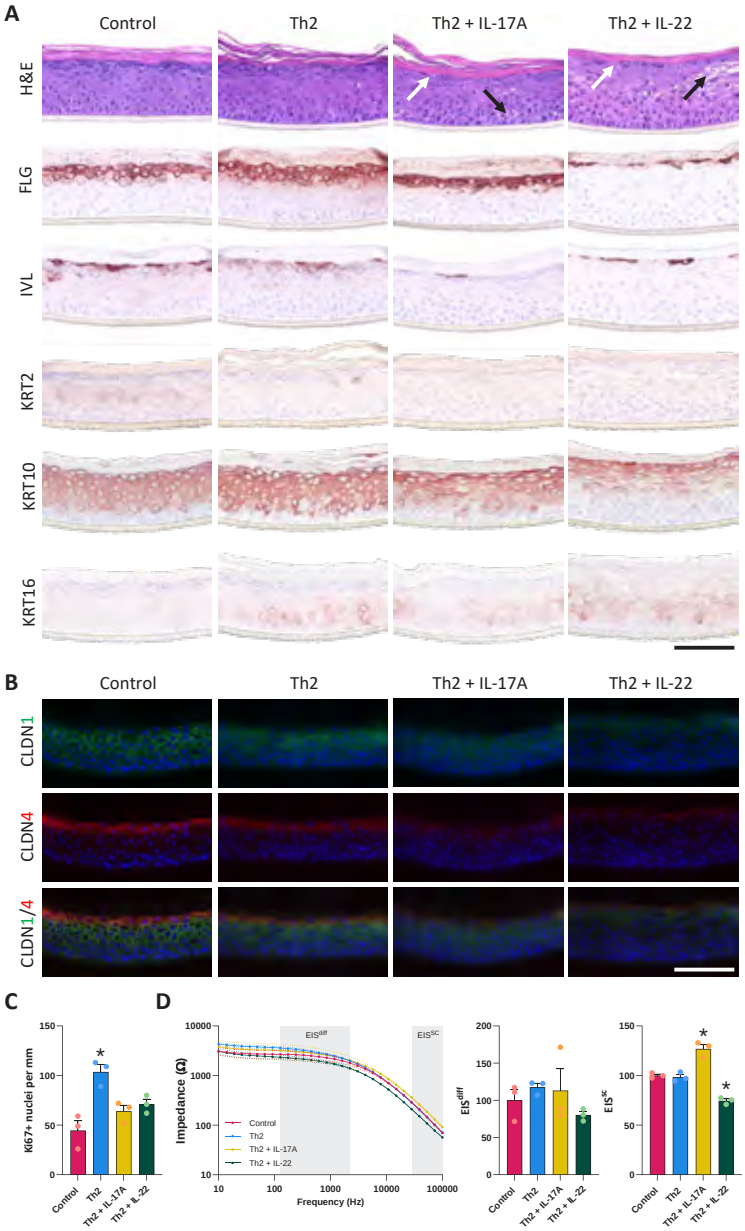

Supplementary Figure 5. N/TERT-2G-HEEs upon stimulation with Th2 cytokines and IL-17A or IL-22. (**A**) Morphology and differentiation protein expression of FLG, IVL, KRT2, KRT10, and alarmin KRT16 of HEEs stimulated with the Th2 mix of IL-4 and IL-13 with and without IL-17A or IL-22. White arrow: hypogranulosis. Black arrow: spongiosis. Scale bar = 100µm. (**B**) Tight junction protein expression of CLDN1 (green) and CLDN4 (red), and DAPI (blue). Scale bar = 100µm. (**C**) Ki67 quantification as a measure of proliferating keratinocytes. (**D**) Electrical impedance spectra (EIS), and EIS^{sc} and EIS^{diff} as percentages relative to the unstimulated control. All data is representative for N=3 N/TERT-2G-HEEs. Data is presented as mean +/- SEM. * = p-value below 0.05 as compared to control.

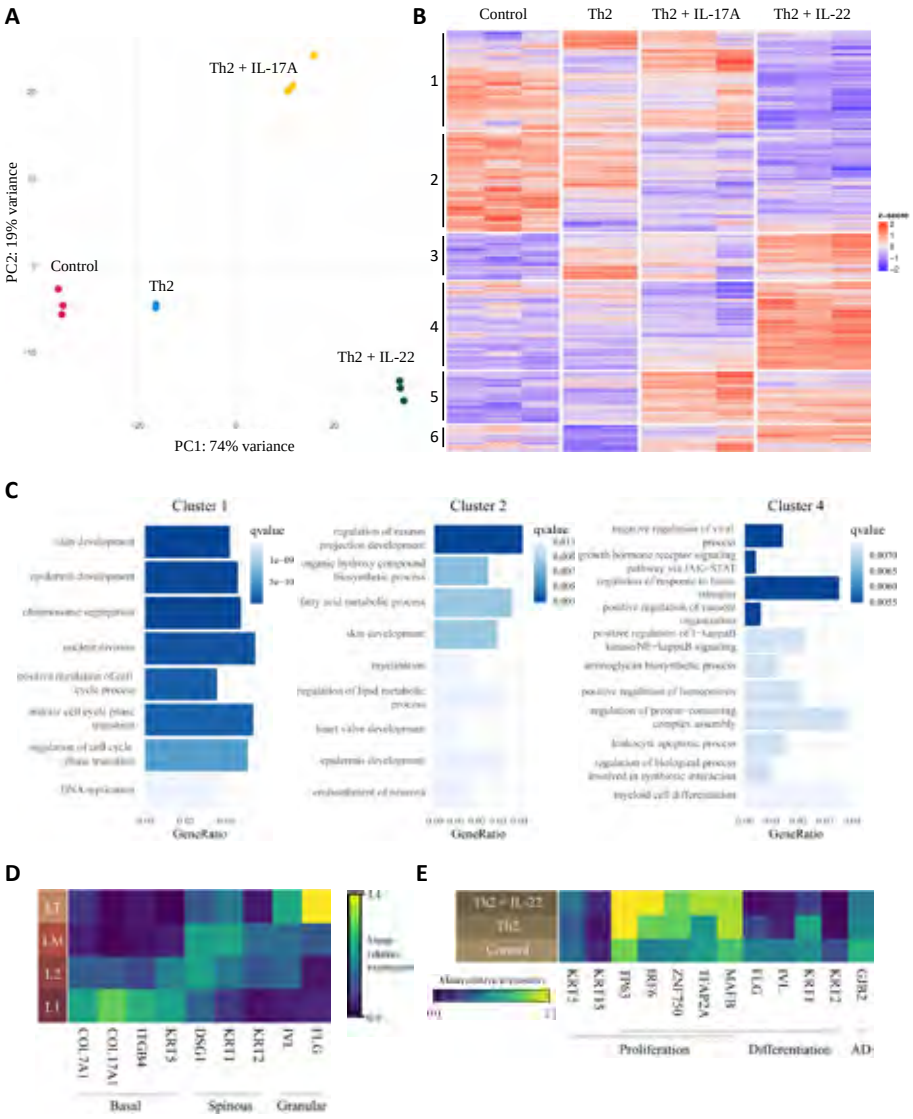

Supplementary Figure 6. Transcriptomic analysis of N/TERT-2G-HEEs upon stimulation with various AD related cytokine cocktails. (**A**) Principal Component Analysis (PCA) plot. (**B**) Clustered heatmap. (**C**) Gene Ontology (GO)-term analyses. (**D**) Heatmap of layer specific genes in layer 1 (L1), layer 2 (L2), middle layers (LM) and the top layer (LT) in the untreated control. (**E**) Heatmap of keratinocyte differentiation and proliferation related genes per condition. Data is representative for N=2 or 3 N/TERT-2G-HEEs.

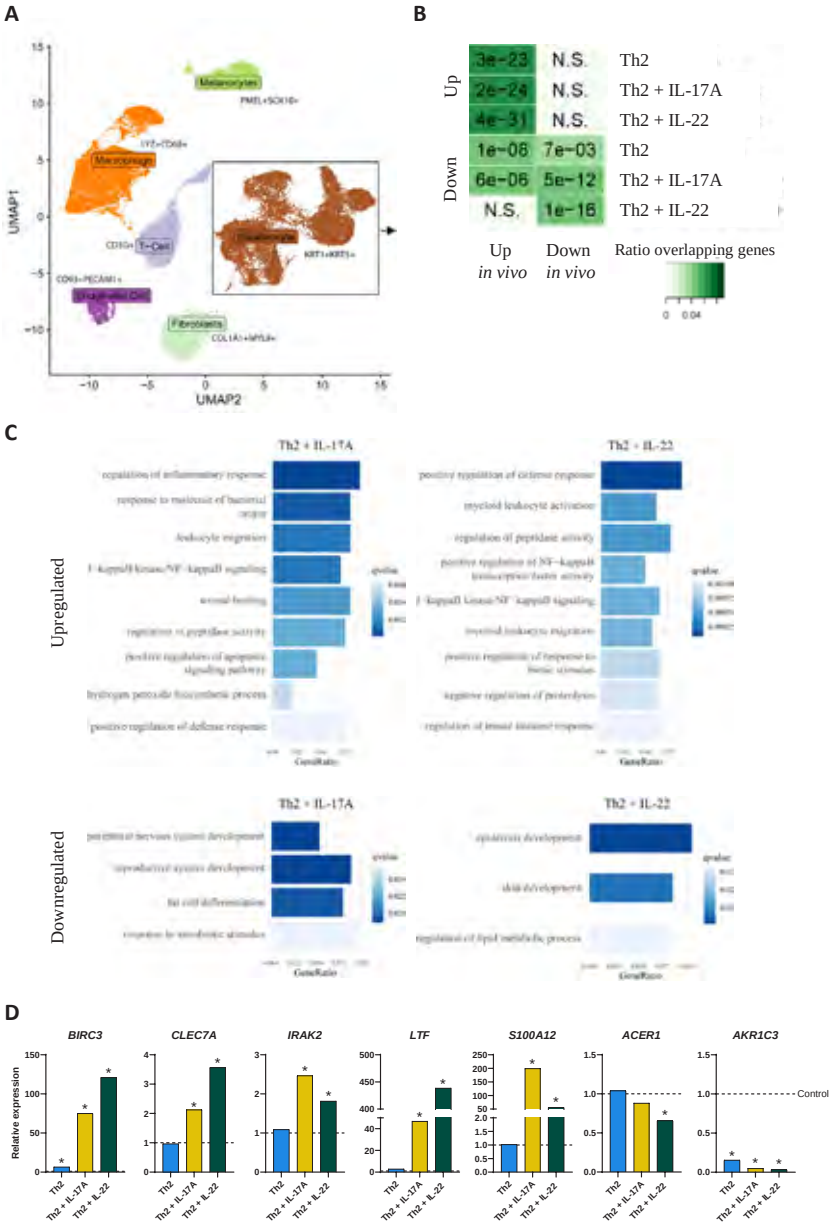

Supplementary Figure 7. Transcriptomic comparison of *in vitro* AD-HEEs and *in vivo* AD lesional. (**A**) UMAP of *in vivo* single-cell RNA-sequencing data by Rojahn et al. including marker expression of subpopulations. (**B**) Jaccardian grids of the overlap in up- and downregulated genes in the epidermis of AD patients (dataset Rojahn et al.) and in NHEK-HEEs stimulated with cytokine cocktails. The color represents the overlapping ratio and the number the significance. (**C**) GO-term analyses on genes overlapping between *in vivo* and *in vitro* data. (**D**) RNA-seq fold changes of genes that were categorized in minimally five (upregulated genes) or three (downregulated genes) GO-terms that overlap in the epidermis of AD patients (dataset Rojahn et al.) and in NHEK-HEEs. *In vitro* data is representative for N=3 or 4 (two biological replicates), and Rojahn's *in vivo* data for N=4 AD patients and N=2 healthy controls.

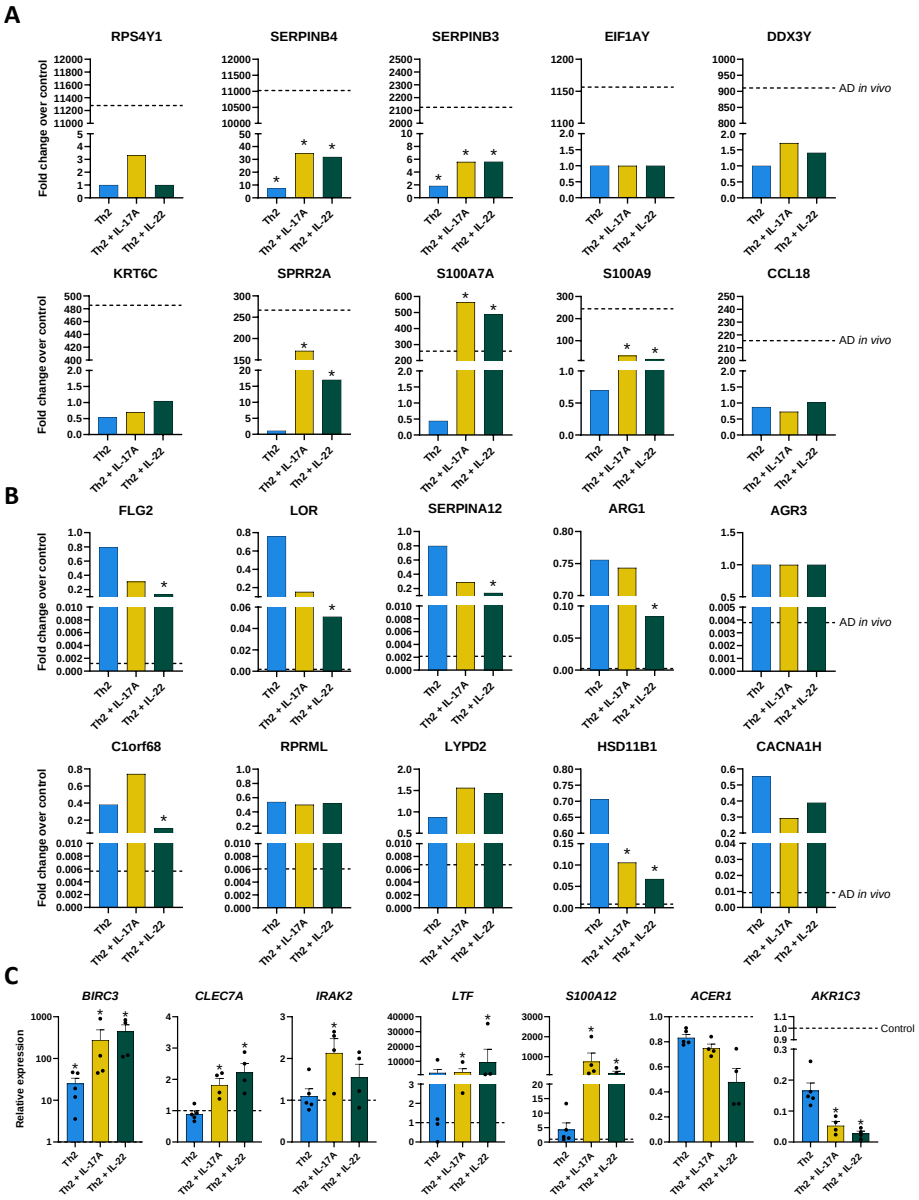

Supplementary Figure 8. The expression of the most differential genes in AD over healthy controls in *in vitro* AD-HEEs. (**A**) The fold changes of cytokine stimulated HEEs over untreated controls of the top 10 highest induced genes in AD *in vivo*. (**B**) The fold changes of cytokine stimulated HEEs over untreated controls of the top 10 most reduced genes in AD *in vivo*. (**C**) qPCR validation of bridge genes. *In vitro* data is representative for N=3 or 4 (two biological replicates), and *in vivo* data for N=4 AD patients and N=2 healthy controls. * = p-value below 0.05 as compared to control.

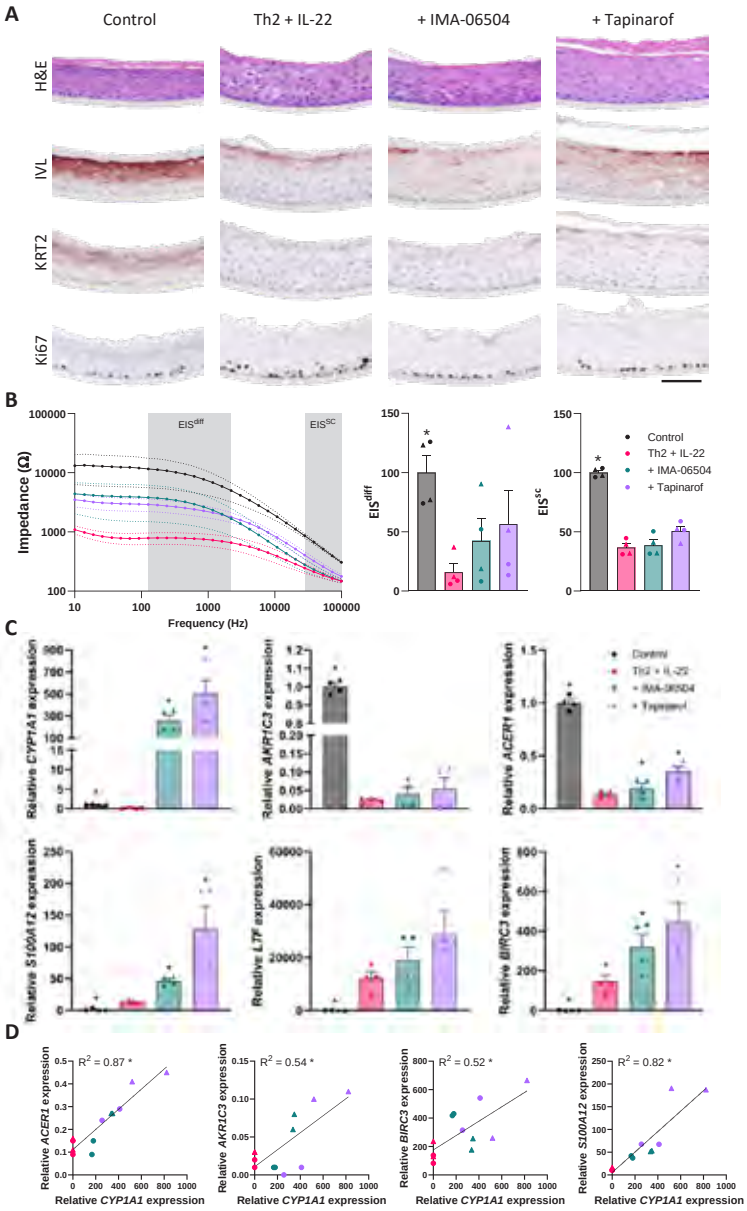

Supplementary Figure 9. The effect of AHR ligands on Th2 + IL-22-mediated epidermal differentiation and barrier defects. (**A**) Morphology and differentiation protein expression of IVL and KRT2, and proliferation marker Ki67. Scale bar = 100µm. (**B**) Electrical impedance spectra (EIS), and EIS^{sc} and EIS^{diff} as percentages relative to the unstimulated control. (**C**) Expression of AHR target gene *CYP1A1*, and bridge genes *AKR1C3* and *WNT5A*, and correlation of *CYP1A1* expression with EIS^{diff}, *AKR1C3* and *WNT5A*. (**D**) Correlation analyses between AHR activation (measured by *CYP1A1* expression) and *ACER1*, *AKR1C3*, *BIRC3* and *S100A12* expression. All data is representative for N=4 replicates of NHEK-HEEs. Data is presented as mean +/- SEM. * = p-value below 0.05 as compared to Th2 + IL-22. Note: *LTF* was not measured in controls and therefore the CT value was set at 40.

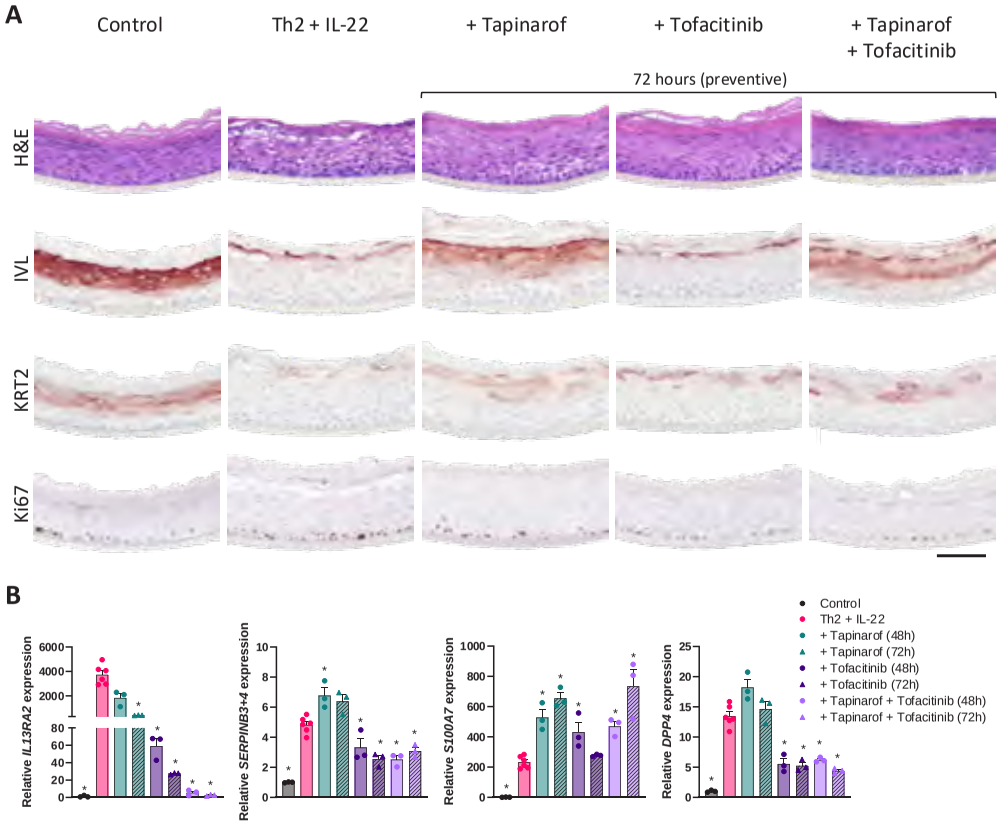

Supplementary Figure 10. The effect of AHR ligand tapinarof and JAK1/3 inhibitor tofacitinib on Th2 + IL-22-mediated epidermal differentiation. (**A**) Morphology and differentiation protein expression of IVL and KRT2, and proliferation marker Ki67. Scale bar = 100µm. (**B**) Expression of *IL13RA2*, *SERPINB3+4*, *S100A7* and *DPP4*. All data is representative for N=3 replicates of NHEK-HEEs. Data is presented as mean +/- SEM. * = p-value below 0.05 as compared to Th2 + IL-22.

Supplemental tables

(The tables are available upon request via the Radboud Data Repository: ru.rumc.p4fcyto_r0005499a_dsc_385)

Supplementary Table 1. Differential expression of *in vitro* cytokine-stimulated NHEK models as compared to control. A) Th2 cytokine stimulated HEEs. **B**) Th2 + IL-17A stimulated HEEs. **C**) Th2 + IL-22 stimulated HEEs.

Supplementary Table 2. Genes per heatmap cluster and GO-terms per cluster of cytokine stimulated and control NHEK-HEEs. A) Genes per heatmap cluster. **B**) Genes per GO-term from cluster 1. **C**) Genes per GO-term from cluster 2. **D**) Genes per GO-term from cluster 3. **E**) Genes per GO-term from cluster 4. **F**) Genes per GO-term from cluster 5. **G**) Genes per GO-term from cluster 6.

Supplementary Table 3. Differential expression of *in vitro* cytokine-stimulated N/TERT-2G models as compared to control. A) Th2 cytokine stimulated HEEs. **B**) Th2 + IL-17A stimulated HEEs. **C**) Th2 + IL-22 stimulated HEEs.

Supplementary Table 4. Genes per heatmap cluster and GO-terms per cluster of cytokine stimulated and control N/TERT-2G-HEEs. A) Genes per heatmap cluster. **B**) Genes per GO-term from cluster 1. **C**) Genes per GO-term from cluster 2. **D**) Genes per GO-term from cluster 3. **E**) Genes per GO-term from cluster 4. **F**) Genes per GO-term from cluster 5. **G**) Genes per GO-term from cluster 6.

Supplementary Table 5. Overlapping and missing differential genes in *in vitro* cytokine-stimulated NHEK models as compared to *in vivo* AD. A) Th2 cytokine stimulated HEEs. **B**) Th2 + IL-17A stimulated HEEs. **C**) Th2 + IL-22 stimulated HEEs.

Supplementary Table 6. GO-terms of the overlapping differential genes in *in vitro* cytokine-stimulated NHEK models as compared to *in vivo* AD. A) Upregulated genes in Th2 cytokine stimulated HEEs. **B**) Upregulated genes in Th2 + IL-17A stimulated HEEs. **C**) Upregulated genes in Th2 + IL-22 stimulated HEEs. **D**) Downregulated genes in Th2 cytokine stimulated HEEs. **E**) Downregulated genes in Th2 + IL-17A stimulated HEEs. **F**) Downregulated genes in Th2 + IL-22 stimulated HEEs.

Supplementary Table 7. Overlapping and missing differential genes in *in vitro* cytokine-stimulated N/TERT-2G models as compared to *in vivo* AD. A) Th2 cytokine stimulated HEEs. **B**) Th2 + IL-17A stimulated HEEs. **C**) Th2 + IL-22 stimulated HEEs.

Supplementary Table 8. GO-terms of the overlapping differential genes in *in vitro* cytokine-stimulated N/TERT-2G models as compared to *in vivo* AD. A) Upregulated genes in Th2 cytokine stimulated HEEs. **B**) Upregulated genes in Th2 + IL-17A stimulated HEEs. **C**) Upregulated genes in Th2 + IL-22 stimulated HEEs. **D**) Downregulated genes in Th2 cytokine stimulated HEEs. **E**) Downregulated genes in Th2 + IL-17A stimulated HEEs. **F**) Downregulated genes in Th2 + IL-22 stimulated HEEs.

Supplementary Table 9. Differential meta-analysis of bulk RNA-seq data. A) Clinical characteristics (sex, age, SCORAD, EASI) of cohorts incorporated in the meta-analysis. Categorical variables are reported in terms of absolute counts and percentages per category. Continuous variables are reported in terms of median, lower quartile and upper quartile. **B**) Profiling platforms used for generating transcriptomic data. **C**) Summary statistics of differential meta-analysis comparing ADL and HC. **D**) Summary statistics of differential meta-analysis comparing ADNL and HC. **E**) Summary statistics of differential meta-analysis for bridge genes *ACER1*, *AKR1C3*, *BIRC3*, *LTF* and *S100A12*, comparing ADL and HC as well as ADNL and HC (ci.l and ci.u representing the lower and upper bounds of the corresponding 95% confidence interval).

Supplementary Table 10. Cytokine concentrations used to stimulation human epidermal equivalents.

Cytokine	Manufacturer	Concentration
IL-4	Peprotech	50 ng/mL
IL-13	Peprotech	50 ng/mL
IL-17A	Peprotech	50 ng/mL
IL-22	Peprotech	50 ng/mL
Cocktail	**Concentration**	
Th2	IL-4: 50 ng/mL + IL-13: 50 ng/mL	
Th2 + IL-17A	IL-4: 50 ng/mL + IL-13: 50 ng/mL + IL-17A: 50 ng/mL	
Th2 + IL-22	IL-4: 50 ng/mL + IL-13: 50 ng/mL + IL-22: 10 ng/mL	
Th17	IL-17A: 50 ng/mL + IL-22: 50 ng/mL	

Supplementary Table 11. Antibody dilutions used for immunohistochemical analysis.

Antibody target	Catalog number	Manufacturer	Dilution
Ki67	ab16667	Abcam	1:200
Filaggrin	MA5-13440	Thermo Fisher Scientific	1:100
Involucrin	Mon 150	[80]	1:20
Keratin 2	65191	Progen	1:200
Keratin 10	MK10	Euro-diagnostica	1:100
Keratin 16	sc-53255	Santa-Cruz	1:200
Claudin 1	51-9000	Thermo Fisher Scientific	1:400
Claudin 4	32-9400	Thermo Fisher Scientific	1:400

Supplementary Table 12. Primer sequences used for RT-qPCR analysis.

Primer target	Forward primer (5'-3')	Reverse primer (3'-5')
RPLP0	caccattgaaatcctgagtgatgt	tgaccagcccaaaggagaag
CCL26	cctgggtgcgaagctatgaa	ttgcctcttttggtagtgaatatcac
CA2	aacaatggtcatgctttcaacg	tgtccatcaagtgaaccccag
CCL2	gaagaatcaccagcagcaagtg	gatctccttggccacaatgg
NELL2	cagaattgtcaacagtgcc	attcacactccacatctgg
IL1B	aatctgtacctgtcctgcgtgtt	tgggtaatttttgggatctacactct
FLG	acttcactgagtttcttctgatggtatt	tccagacttgagggtctttttctg
LOR	aggttaagacatgaaggatttgcaa	ggcaccgatgggcttagag
CLDN1	ccagtcaatgccaggtacga	ttggatagggccttggtgtt
CLDN4	gctgtaaacaggtttgggca	tcagaggggatcagtctcca
DEFB4	gatgcctcttccaggtgttttt	ggatgacatatggctccactctt
PI3	catgagggccagcagctt	tttaacaggaactcccgtgaca
S100A7	cttccttagtgcctgtgacaaaaa	aaggacagaaactcagaaaaatcaatct
CAMP	ccaggcccacgatggat	accagcccgtccttcttga

6

Supplementary Table 13. Overview of transcriptomic data and analyses that were used for specific figures.

Figure	Samples	Sequencing and/or analysis
3A-C	*In vitro* HEEs	Bulk RNA-sequencing
4A-D	*In vitro* HEEs	Spatial transcriptomics
5A-B	*In vitro* HEEs	Bulk RNA-sequencing
	In vivo full skin	Meta-analysis of micro-array or bulk RNA-sequencing of full thickness skin biopsies (lesional and non-lesional AD vs. healthy controls)
5C	*In vivo* full skin	Meta-analysis of micro-array or bulk RNA-sequencing of full thickness skin biopsies (lesional and non-lesional AD vs. healthy controls)
Supplementary 6A-C	*In vitro* HEEs	Bulk RNA-sequencing
Supplementary 6D-E	*In vitro* HEEs	Spatial transcriptomics
Supplementary 7A	*In vivo* full skin	Publicly available scRNA-sequencing of full thickness skin biopsies [19]
Supplementary 7B-C	*In vitro* HEEs	Bulk RNA-sequencing
	In vivo epidermis	Pseudobulk of epidermis data from publicly available scRNA-sequencing of full thickness skin biopsies (lesional AD vs. healthy controls) [19]
Supplementary 7D	*In vitro* HEEs	Bulk RNA-sequencing
Supplementary 8A-C	*In vitro* HEEs	Bulk RNA-sequencing

Supplementary Table 14. Gene set enrichment analysis of gene expression signature of TH2_Ctl, TH2IL17_Ctl, TH2IL22_Ctl generated from NHEK and N/TERT. Size, the size of the reference gene set, ADL_HC; Coverage, proportion of genes from the reference gene set present in the expression signature of HEEs; Bound.tdp, the lower bound for the proportion of associations (true discoveries); Point.tdp, the point estimate for the proportion of associations (true discoveries); Bound.tdn, the lower bound for the number of associations (Bound.tdn=Size*Coverage*Bound.tdp); Point.tdn, the point estimate for the number of associations (Point.tdn=Size*Coverage*Estimate.tdp); Padj, BH-adjusted competitive enrichment p-value.

Comparison	Gene set name	Size	Coverage	Bound .tdp	Estimate. tdp	Bound .tdn	Estimate .tdn	Padj
NHEK_ Th2_Control	ADL_HC	2979	0,84	0.10	0.15	238.37	384.98	9.74E-03
NHEK_ Th2+IL-17A_ Control	ADL_HC	2979	0,84	0.25	0.32	613.37	792.90	8.05E-04
NHEK_ Th2+IL-22_ Control	ADL_HC	2979	0,84	0.33	0.40	822.82	1011.32	1.59E-03
N/TERT-2G_ Th2_Control	ADL_HC	2979	0,83	0.13	0.19	332.69	468.38	1.50E-03
N/TERT-2G_ Th2+IL-17A_ Control	ADL_HC	2979	0,83	0.27	0.34	661.36	834.24	2.82E-06
N/TERT-2G_ Th2+IL-22_ Control	ADL_HC	2979	0,83	0.35	0.41	858.36	1006.11	1.51E-05

Supplementary Table 15. Ki67 immunostaining quantification for the effect of therapeutics on cytokine-induced hyperproliferation. The upper table presents the quantification corresponding to Supplementary Figure 9, and the lower table to Figure 6.

Supplemental methods

Supplementary table 13 summarizes which transcriptomic data was used per (supplementary) figure.

AD human epidermal equivalent (HEE) generation

Isolation of primary human keratinocytes *(FLG wildtype)* was performed according to the principles of the Declaration of Helsinki, as described previously [17]. N/TERT-2G immortalized keratinocytes from Rheinwald laboratory [27] were cultured in CnT-PR medium (CELLnTEC) with 1% Penicillin-Streptomycin (Sigma-Aldrich) before HEE generation as previously described [17]. In brief, human keratinocytes were seeded in a Nunc 24-transwell system (Thermo Fisher Scientific) and cultured submerged for two days in CnT-PR proliferation medium (CELLnTEC) followed by one day submerged culture in 60/40 CnT-PR-3D differentiation medium (CELLnTEC) and DMEM medium (Sigma-Aldrich). Next, cultures were lifted to the air-liquid interface and medium was refreshed every other day. To mimic AD *in vitro,* the medium was supplemented with cytokines in different concentrations (Supplementary Table 10) during the last 72 hours before harvesting. AHR ligands tapinarof (1µM, Benvitimod, SML3430, Sigma-Aldrich), IMA-06504 (1 nM, [38]) and JAK1/3 inhibitor tofacitinib (450nM, PZ0017, Sigma-Aldrich) were added simultaneously with the cytokines (for preventive effects), or for the last 48 hours of the culture (for restoring effects). Primary keratinocyte HEEs were harvested at day 8 and N/TERT-2G HEEs at day 10 of the air-liquid interface [17, 22].

Morphological and immunohistochemical analysis

HEEs were fixed in 4% formalin (Sigma-Aldrich) for 1 hour and embedded in paraffin (Leica). 6µm sections were hematoxylin and eosin (H&E) stained or used for immunohistochemistry analysis. Sections were blocked for 15 minutes with 5% normal donkey (CLDN1/4) (SouthernBiotech), horse (FLG, IVL, KRT2, KRT10, KRT16) (Vector laboratories) or goat (Ki67) (SouthernBiotech) serum in PBS and incubated for 1 hour with the primary antibodies as listed in Supplementary Table 11. Next, sections were incubated for 30 minutes with biotinylated secondary antibodies (Vector laboratories), Donkey-anti rabbit AF488 (CLDN1) (Abcam) or donkey anti-mouse AF647 (CLDN4) (Invitrogen) and for 30 minutes with avidin-biotin complex (Vector Laboratories). Protein expression was visualized using 3-Amino-9-ethylcarbazole (AEC) (Merck Millipore) and sections were mounted with glycerol gelatin (Sigma Aldrich) or Fluoromount-G with DAPI (ThermoFisher) (CLDN1/4).. For Ki67 quantification, two images were taken per HEE using the ZEISS Axio Imager equipped with a ZEISS Axiocam 105 color Digital Camera with the x20 objective.

Analysis was performed with CellProfiler version 4.2.1 or Fiji version 1.54f [81] and image analysis pipelines are available on request.

RNA isolation and real-time quantitative polymerase chain reaction (RT-qPCR) analysis

Total RNA was isolated using the E.Z.N.A. Total RNA Kit I (Omega Bio-Tek) kit according to manufacturer's protocol. After DNAse I (Invitrogen, Thermo Fisher Scientific) treatment and cDNA synthesis (PCR Biosystems), real-time quantitative PCR (RT-qPCR) was executed with primers listed in Supplementary Table 12 and SYBR Green (Bio-Rad) using the CFX Connect™ Real-Time System (Bio-Rad). If nothing could be detected, the CT value was set at 40, which is the number of cycles run. Gene expression was normalized to the expression of *human acidic ribosomal phosphoprotein P0* (*RPLP0*) and relative expression levels were calculated using the $2^{-\Delta\Delta CT}$ method [82].

Bulk RNA-sequencing of *in vitro* models

For preparation of RNA sequencing libraries, 400ng of RNA per sample and the KAPA RNA HyperPrep kit with RiboErase (human/mouse/rat [HMR]) (Kapa Biosystems) were used. Oligonucleotide hybridization, rRNA depletion and cleanup, DNase digestion and cleanup, and RNA elution were performed according to manufacturer's protocol. Fragmentation and priming was executed at 94°C for 6 min. First- and second-strand synthesis, and A-tailing were performed according to manufacturer's protocol. A 1.5-µM stock (NEXTflex DNA barcodes; Bio Scientific) was used for adapter ligation. Post-ligation cleanups were executed according to manufacturer's protocol, followed by eight cycles of library amplification and a 0.8× bead-based cleanup. High-sensitivity DNA bioanalyzer (Agilent Technologies) was used to determine the library size, and to measure the library concentration the DeNovix double-stranded DNA (dsDNA) high-sensitivity assay was performed. Sequencing was done with the Illumina NextSeq 500 instrument and 42bp-paired end reads were generated.

Bulk RNA-sequencing data analysis from *in vitro* models

RNA-sequencing data was analyzed using the seq2science RNA-seq workflow version 0.9.5 [83]. Paired-end reads were trimmed with fastp version 0.20.1 [84], using default options. Reads were subsequently aligned to the GRCh38.p13 reference assembly using the default options provided with STAR version 2.7.6a [85]. In order to assess the quality of the samples, several quality control metrics were generated as described below (data not shown), and inspected using MultiQC version 1.11 [86]. Duplicate reads were marked and inspected with Picard

MarkDuplicates version 2.23.8, and alignment statistics were collected using samtools stats version 1.14 [87]. All samples were found to be of sufficient quality, and reads were counted and summarized to gene-level from filtered bam-files using HTSeq-count version 0.12.4 [88].

Subsequent analyses were performed in the R statistical environment version 4.2.2. DEGs were defined using DESeq2 version 1.38.2 [89], comparing conditions of cytokine cocktail concentrations (controls, Th2, Th2 + IL-17A, and Th2 + IL-22) within each HEE model (NHEK and N/TERT-2G). Batch corrections were performed for the NHEK-HEEs, and a multiple testing correction was performed using the Benjamini-Hochberg method [90].

Heatmaps were generated using ComplexHeatmap version 2.14.0 [91] based on genes that were significant (p-adjusted < 0.05) in at least one within-HEE model comparison. Clustering was performed based on z-scores of count values, with a batch correction applied to the NHEK-HEE count values using limma version 3.54.2 [92]. For each cluster, a Gene Ontology enrichment analysis for biological processes was performed using the *enrichGO* function from the R package clusterProfiler version 4.6.0 [93]. Only terms with a q-value < 0.05 were examined. If any parent/child terms were significant, only the parent terms were plotted using the *ggplot2* package version 3.4.0 [94].

Pseudobulk analysis of scRNA-sequencing data from *in vivo* samples

Publicly available single-cell RNA sequencing data of skin biopsies from four AD patients and two healthy controls was downloaded from the Gene Expression Omnibus (GEO, accession number GSE153760), and pre-processed as described in Rojahn et al. [19]. Briefly, Cell Ranger version 3.0.2 (10x Genomics) was used to demultiplex, align, and count the scRNA-seq data. The reference genome GRCh38 was used for the alignment of reads. The R package Seurat version 4.0.0 [95] was used to analyze the data and a filtering criterion was applied which excluded cells that had fewer than 100 or more than 5000 genes, more than 20000 counts, or a mitochondrial count percentage >10%. Mitochondrial genes were also removed from the dataset. The standard Seurat workflow was subsequently applied, including normalization, identification of variable genes, data scaling, and principal component analysis. We then executed the *FindNeighbours()* and *FindClusters()* functions within the Seurat package along with Uniform Manifold Approximation and Projection (UMAP) to identify and visualize clusters. Skin biopsy keratinocyte populations were selected based on marker expression of *KRT1*, *KRT5*, *KRT10* and *KRT14*, including only cells with at least 1000 genes. Pseudobulk data was then

generated through the aggregation (sum) of gene counts in individual cells across samples, and DEGs were identified using DESeq2 by comparing healthy controls to AD biopsy samples.

In order to examine the similarities between our *in vitro* models and the *in vivo* pseudobulk data, the overlap between up- and down-regulated pseudobulk DEGs and DEGs in the *in vitro* cytokine cocktail conditions (Th2, Th2 + IL-17A, Th2 + IL-22) relative to untreated controls was examined. Overlaps were assessed using the GeneOverlap R package [96] and a Jaccard index was used to measure similarity between two lists of DEGs. In order to test the significance of the overlap, a contingency table was created (in/not in list 1 versus in/not in list 2) and a Fisher's exact test was applied. For these overlap analyses, a p-value threshold of p-adjusted < 0.05 was applied to all DEGs. For the *in vitro* data, upregulated DEGs were defined as having a log2FC > 0, while downregulated genes were defined by a log2FC < 0. In the *in vivo* data, up- and downregulated genes were defined by a log2FC > 1 or log2FC < -1, respectively. Gene Ontology enrichment analyses for biological processes were performed on DEG overlaps using *enrichGO* as described previously.

Bulk RNA-sequencing data analysis of *in vivo* samples

Transcriptomic profiles based on 188 AD lesional, 91 AD non-lesional as well as 181 healthy control biopsies have been acquired from public (E-MTAB-8149, GSE130588, GSE193309) or academic sources (P2N_clinical). For cohort characteristics, see Supplementary Table 9 (sheet "cohort characteristics"). Punch biopsies have been profiled using microarray (E-MTAB-8149, Affymetrix Human Gene 2.1 ST Array; GSE130588, Affymetrix Human Genome U133 Plus 2.0 Array) or RNA-seq technology (GSE193309, Illumina NovaSeq 6000; P2N_clinical, Illumina NovaSeq 6000/HiSeq 2500). For further details see Supplementary Table 9 (sheet "profiling"). Raw microarray data (Affymetrix CEL files) has been processed using single-channel array normalization (SCAN) employing the R package SCAN.UPC version 2.30.0 [97]. Raw sequencing data has been processed using TrimGalore version 0.6.6 [98], Cutadapt version 4.4 [99], FastQC version 0.11.9 [100], HISAT2 version 2.2.1 [101], SAMtools version 1.11 [87] and Rsubread version 2.2.6 [102] and annotated according to Ensembl release 103 (GRCh38). Sequencing count data has been converted to the logarithmic scale using the voom transformation provided with R packages limma version 3.52.3 [92] with scaling factors to normalize library size calculated using R package edgeR version 3.30.3 [103]. Harmonization of molecular and clinical data (sex, age, SCOring Atopic Dermatitis (SCORAD), Eczema Area and Severity Index (EASI)) incorporated in the meta-analyses has been performed using the R package harmonizeGeneExprData, available at GitHub [104]. Subsequent quality control

of the resulting datasets has been performed using the R Package QCnormSE, available at GitHub [105]. For each study, expression values of each gene have been standardized to mean of zero and standard deviation of 1 to increase comparability across profiling technologies.

Single-cohort differential expression analysis has been performed using linear models as implemented in R package limma version 3.54.2 [92] with gene expression as dependent and sample type (AD lesional, AD non-lesional, healthy skin) as independent variable. The subsequent cross-cohort analysis pooled the regression coefficients (corresponding to (log2) FC) using random effects meta-analysis as implemented by the R package metafor version 3.8-1 [106]. Meta-analysis p-values were adjusted for multiple testing using the Benjamini-Hochberg procedure [90] and significantly differentially expressed genes were required to meet adjusted p-value < 0.05 and the absolute pooled (log2) FC > 1. With the R package metaAnalyzeGeneExprData [107] the authors provide wrapper functions implementing the employed meta-analysis workflow. Visual and tabular summaries of analysis results have been generated using R packages tidyr version 1.3.1, gtsummary version 1.7.2 [108], and ComplexUpset version 1.3.3 [109].

Competitive gene set enrichment analysis has been performed using R package rSEA (version 2.1.1), testing the null hypothesis that the members of individual gene sets of interest are uniformly distributed along the list of ranked measures of differential expression. Using this approach differential expression signatures of cytokine stimulated HEEs generated from primary keratinocytes compared to controls (NHEK_Th2_Control, NHEK_Th2+IL-17A_Control, NHEK_Th2+IL-22_Control), as well as those generated from immortalized keratinocytes compared to controls (N/TERT-2G_Th2_Control, N/TERT-2G_Th2+IL-17A_Control, N/TERT-2G_Th2+IL-22_Control) are contrasted to a set of DEGs derived from the differential expression meta-analysis comparing AD lesion skin to healthy control skin (ADL_HC, significance criterion: pvalue.random.adj<0.05 and abs(estimate.random)>1). Associations between the *in vitro* signatures and the *in vivo* gene set are considered significant for BH-adjusted competitive enrichment p-values <0.05.

HEE harvesting, cryosectioning and fixation for spatial transcriptomics

Per HEE, three 2 mm punch biopsies were taken and a total of 9 punch biopsies were threaded on a single hypodermic needle. Two needles were sunk in chilled OCT (Thermo Scientific) per cryomold to align all punch biopsies. Embedded punch biopsies were flash frozen in partially frozen isopentane (Thermo Scientific) until frozen solid and immediately stored at -80˚C. Blocks were mounted in the cryostat

(Epredia Cryostar), sectioned at 6 µm thickness and directly mounted on cold Rebus Biosystems coverslips for spatial transcriptomics as well as glass slides for morphology assessment through H&E staining (as described before). Single sections from three different blocks were mounted on the same coverslip. Coverslips were air dried for 5 minutes after mounting the final section and fixed for 10 minutes at room temperature in 4% PFA (Sigma-Aldrich) in PBS, followed by two 10 minute washes in PBS and two 5 minute washes in 70% ethanol. Coverslips were stored submerged in 70% ethanol at -20˚C until performing spatial transcriptomics.

Spatial transcriptomics

Spatial transcriptomics was performed using the High Fidelity Assay on the Esper from Rebus Biosystems using a panel of 30 genes: *ABCA12*, *AHR*, *CHUCK*, *CLDN1*, *COL17A1*, *COL7A1*, *CYP1A1*, *DCN*, *DSG1*, *FLG*, *GJB2*, *HRNR*, *IGFBP5*, *IRF6*, *ITGB4*, *IVL*, *KLF4*, *KRT15*, *KRT1*, *KRT2*, *KRT5*, *MAFB*, *MCM3*, *MKI67*, *NIPAL4*, *RPLP0*, *TFAP2A*, *TGM1*, *TP63* and *ZNF750*. For validation of the methodology in control HEEs, the marker genes for basal keratinocytes were *collagen (COL)7A1, COL17A1, integrin (ITG)B4, KRT5*, for spinous keratinocytes *desmoglein* (*DSG)1, KRT1, KRT2* and for granular keratinocytes *IVL, FLG*. The flow cell was assembled and reagents were prepared and loaded onto the machine following manufacturer instructions. After tubing priming and a flow cell wash, a quick scan was made of the entire imageable area, after which all areas containing properly mounted HEEs were selected for imaging. The High Fidelity Assay performs tissue pretreatment, DAPI staining and primary probe hybridization, followed by 10 cycles of secondary probe hybridization, imaging of three targets and probe stripping.

Image processing and bioinformatic analysis for spatial transcriptomics

Using the Esper Analysis software, high resolution images were constructed from the raw Synthetic Aperture Optics data. For the intensity in both low and high resolution images as well as the intensity variation between single low resolution images, manual thresholds were set to allow for detection of smFISH spots. This was followed by generation of nuclear masks from the DAPI images using StarDist and assignment of spots to the closest nuclei within a maximum distance of 80 pixels from each spot. The resulting cellxgene matrix, including spatial coordinates of every cell, was analyzed using Scanpy version 1.8.2 [110]. Cells were filtered based on nuclear perimeter (200–600 pixels) and number of spots per cell (20–800) leaving a total of 11,672 cells. Spot counts were log transformed, normalized per cell and scaled. Coordinates of cells per HEE were transformed to allow for horizontal visualization of each HEE. Per HEE, cells were assigned to a layer by iterating in 400 pixel intervals through the equivalent from left to right and assigning cells within 100 pixels from

the bottom cell to layer 1 (L1) and all cells between 100 and 200 pixels from the bottom cell to layer 2 (L2). All cells within 150 pixels of the top cell per iteration were assigned to the top layer (LT). All remaining cells were assigned to the middle layer (LM). Mean relative expression per layer and/or cell type and treatment was plotted using pyComplexHeatmap version 1.6.1 [111].

Electrical impedance spectroscopy (EIS) measurement

The electrical impedance spectra (EIS) were measured as previously described [20]. Briefly, HEEs were acclimatized to room temperature and submerged in PBS in the 24-transwell system. After calibration, a range 30 of electrical pulses from 10Hz to 100,000Hz was run through the HEEs and the impedance (Ω) was measured using the Locsense Artemis device with SmartSense lid (Locsense). The impedances were corrected for the impedance of blank filters. The area under the curves (AUC) between 127Hz and 2212Hz were calculated and presented as percentages relative to the untreated condition of the same donor and experiment, as measure for differentiation protein expression (EIS^{diff}). The AUC between 28,072Hz and 100,000Hz are presented as percentages relative to the untreated condition of the same donor and experiment, as measure for *stratum corneum* resistance (EIS^{sc}).

Statistical analysis of qPCR and EIS data

For qPCR results, data is represented as mean +/- standard error of the team (SEM) of at least 3 biological or technical replicates. Raw ΔCT values were used to test for statistical significance of RT-qPCR data. One-way analysis of variance followed by Dunnett *post hoc* testing was performed in GraphPad Prism version 9. For EIS data, statistical analyses were performed similarly on AUC values. For correlation analyses, simple linear regression modeling was performed in GraphPad and a correlation was considered significant when the slope significantly deviated from zero. P-values of <0.05 were considered statistically significant.

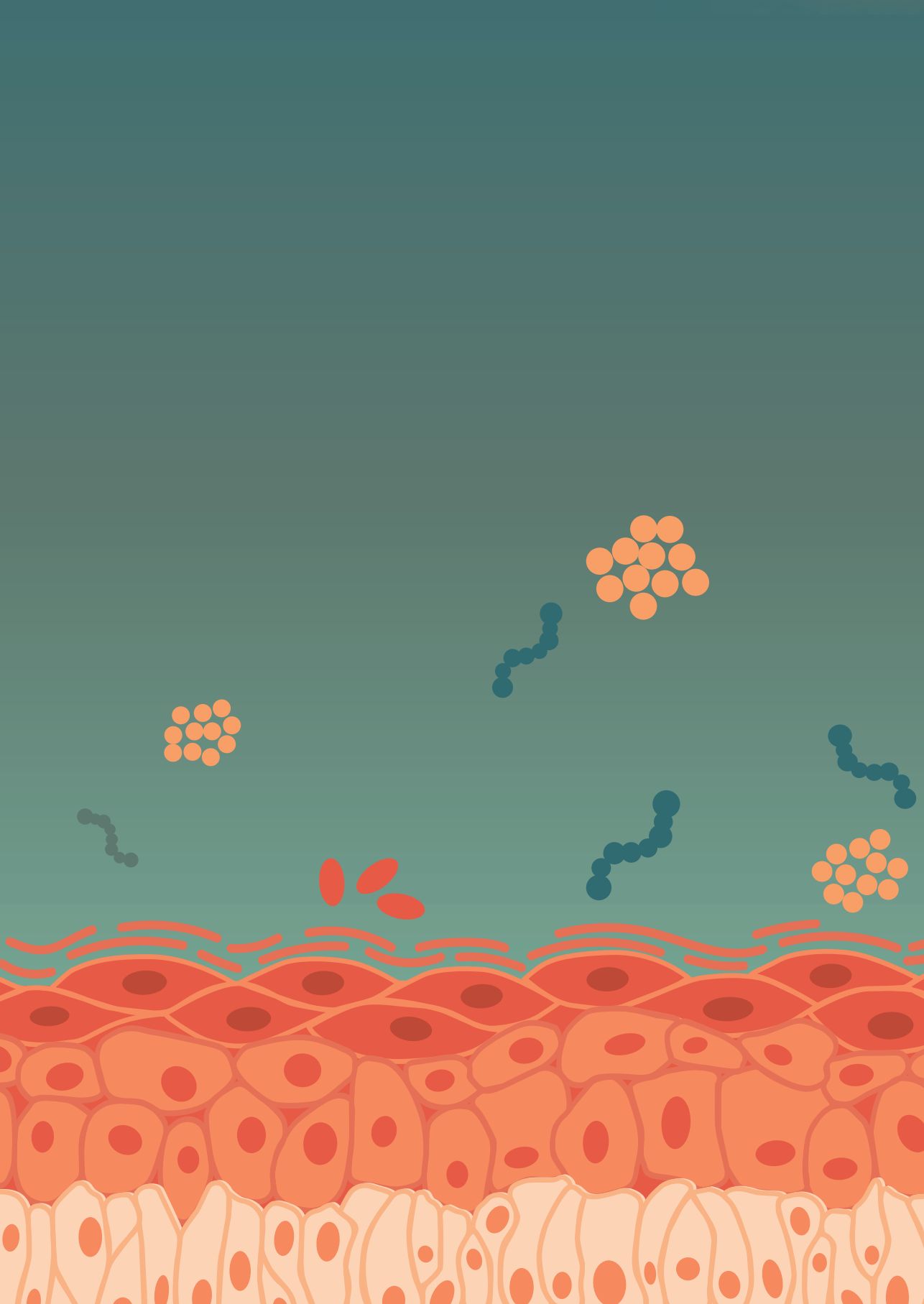

Chapter 7.

Novel methodologies for host-microbe interactions and microbiome targeted therapeutics in 3D organotypic skin models

Gijs Rikken[1], Luca D. Meesters[1], Patrick A.M. Jansen[1] Diana Rodijk-Olthuis[1], Ivonne M.J.J. van Vlijmen-Willems[1], Hanna Niehues[1], Jos P.H.Smits[1,2], Peter Oláh[2], Bernhard Homey[2], Joost Schalkwijk[1], Patrick L.J.M. Zeeuwen[1] and Ellen H. van den Bogaard[1]

Affiliations

[1] Department of Dermatology, Radboud University Medical Center (Radboudumc), Nijmegen, The Netherlands

[2] Department of Dermatology, University Hospital Düsseldorf, Medical Faculty, Heinrich-Heine-University Düsseldorf, Düsseldorf, Germany

Published in

Microbiome. 2023 Oct 17;11(1):227. doi: 10.1186/s40168-023-01668-x.

Abstract

Following descriptive studies on skin microbiota in health and disease, mechanistic studies on the interplay between skin and microbes are on the rise, for which experimental models are in great demand. Here, we present a novel methodology for microbial colonization of organotypic skin and analysis thereof. An inoculation device ensured a standardized application area on the *stratum corneum* and a homogenous distribution of bacteria, while preventing infection of the basolateral culture medium even during prolonged culture periods for up to two weeks at a specific culture temperature and humidity. Hereby, host-microbe interactions and antibiotic interventions could be studied, revealing diverse host responses to various skin-related bacteria and pathogens. Our methodology is easily transferable to a wide variety of organotypic skin or mucosal models and different microbes at every cell culture facility at low costs. We envision that this study will kick-start skin microbiome studies using human organotypic skin cultures, providing a powerful alternative to experimental animal models in pre-clinical research.

Introduction

The skin is a multi-faceted barrier organ that hosts a diversity of commensal microbial communities, composing the human skin microbiota. Over the past decade, we have witnessed a scientific breakthrough with respect to our knowledge and understanding of these microorganisms due to advances in sequencing technologies and the initiation of the human microbiome project [1]. Skin microbiome composition and diversity varies between body sites and individuals and is affected by environmental influences [2, 3]. The most abundant bacteria identified at the genus level are *Corynebacterium*, *Cutibacterium* and *Staphylococcus* [2, 4], along with the most common fungal commensal *Malassezia* [4-6]. These microbes play an important role in skin health by educating the immune system [7-9], preventing the colonization by pathogens [10, 11] and promoting skin barrier function [12, 13].

Alterations in skin microbiome composition, called dysbiosis, are nowadays associated with a plethora of skin conditions, such as atopic dermatitis (AD), psoriasis and acne [14-21]. Colonization and infection of the skin by *Staphylococcus aureus* (*S. aureus*) has been under investigation for decades [22, 23], but recent studies also suggest other *Staphylococcus* species like *S. epidermidis* [24] and *S. capitis* [25] to contribute to skin pathologies. The question remains whether dysbiosis is the cause or consequence of skin diseases and to what extent the microbiome can be leveraged as a therapeutic target [26-28]. Following initial descriptive studies on the skin microbiome [4, 29], investigative mechanistic studies using biologically relevant experimental models are of utmost importance to dissect the cause or contribution of microbial dysbiosis to health and disease [27, 30, 31].

Notwithstanding the importance and utility of widely used *in vivo*-animal models [32-34], the skin microbiome of rodents is significantly different from humans and the instability of the microbiome in laboratory animals is known to affect the experimental outcome [30]. Alternatively, human skin cell cultures (*e.g.,* keratinocyte monolayer cultures) allow investigations on the direct interaction between keratinocytes and microbes [35, 36]. Herein, cultures inoculated with live bacteria are restricted to be short-term as cell viability will be compromised upon the bacterial overgrowth within a few hours [37, 38]. Optionally, heat-killed bacteria, bacterial components or the bacterial culture supernatant can be used [39-41]. However, these do not mimic the actual colonization onto the protective *stratum corneum*, which acts as a physical barrier and filter for microbial metabolites [42]. Investigative studies on these metabolites and potential quorum sensing molecules [43, 44] that interact with bacterial or host cell receptors to activate signal transduction pathways [13, 45, 46],

would benefit from models in which live bacteria are grown under biologically relevant culture conditions, such as a natural growth substrate (the *stratum corneum*) with a viable epidermis underneath.

Advanced organotypic skin models (either full thickness skin or epidermal equivalents) have recently been used more often in host-microbe interaction studies. Next to bacterial infection models, microbial colonization is reported for a variety of skin-related bacteria and fungi. To summarize the current state-of-the-art, we provide a literature overview including experimental details and read-out parameters in Supplemental Table S1. These studies clearly indicate the utility of organotypic skin models for skin microbiome research, but also highlight a lack of standardization, relatively short culture periods of up to 24 hours, the high risk of basolateral culture infections and low assay throughput at high costs. Furthermore, the common use of standard cell culture conditions (37°C at a high relative humidity) in these microbial exposed culture studies favors the growth of aerobic bacteria which will affect the bacterial diversity of *in vitro* cultured skin microbiome samples [47].

In an attempt to overcome these limitations, we here present a low cost and easy to use technical advance for microbial colonization of 3D human epidermal equivalents (HEEs). This may enable standardization of microbiome research using organotypic skin models and facilitate multi-parameter analytics from one single culture. Using this model system we provide proof-of-concept for differential host defense responses by skin commensals and pathogens, establish long-term culture periods up to two weeks and implement effective intervention studies by topical antibiotics.

Methods

Primary keratinocyte isolation

Surplus human skin was obtained from plastic surgery (according to the principles of the Declaration of Helsinki). Human primary keratinocytes were isolated as previously described [48]. Briefly, 6 mm full-thickness biopsy punches of the freshly excised skin tissue were taken and placed into antibiotic/antimycotic medium for 4 hours at 4°C. Thereafter, 0.25% trypsin in phosphate buffered saline (PBS) was added and incubated overnight (o/n) at 4°C. Next, the enzymatic reaction was stopped by the addition of 10% (v/v) fetal bovine serum (GE Healthcare Life Sciences). A pair of tweezers was used to scrape the surface of the biopsy for

harvesting of the keratinocytes. The keratinocytes were counted and seeded onto feeder cells at a density of 50.000 cells/cm^2 in keratinocyte growth medium. The cells were harvested at 95% confluency with a final DMSO concentration of 10% and the cryovials were placed o/n into a freezing container at -70°C, after which the cells were stored in liquid nitrogen.

3D human epidermal equivalent (HEE) culture

HEEs were generated according to the protocols previously described by Rikken *et al*. 2020. Briefly, cell culture inserts (24-wells, 0.4 µm pore size filters; Thermo Fisher Scientific, Nunc) were coated with 150 µL of rat tail collagen in sterile cold PBS (100 µg/mL, BD Biosciences, Bedford, USA) at 4°C for 1 hour. Thereafter, excessive collagen solutions were carefully aspirated and the filters were washed with sterile cold PBS. Then, 150.000 primary human keratinocytes were seeded submerged in 150 µL CnT-prime medium (CELLnTEC, Bern, Switzerland). 900 µL of CnT-prime was added to the basolateral chamber, after which the cultures were incubated at 37°C and 5% CO_2. After 48 hours, cultures were switched to 3D differentiation medium, which consists of 60% CnT-Prime 3D Barrier medium (CELLnTEC, Bern, Switzerland) and 40% High Glucose Dulbecco's Modified Eagle's Medium (DMEM, D6546, Sigma-Aldrich). 24 hours later, the HEEs were lifted to the air-liquid interface (ALI) using 1600 µL of 3D differentiation medium, which was refreshed every other day. The HEE culture schedule is depicted in Figure 1F (created with Adobe Illustrator, https://www.adobe.com/illustrator).

For the N/TERT-2G cells [49, 50], EpiLife medium (Gibco) or CnT-prime (CELLnTEC) was used (based on availability) for seeding the cells and during the first 48 hours of submerged culture. The N/TERT-2G HEEs were generated from N/TERT-2G keratinocytes at passage 3.

Bacterial cultures

Bacterial strains (see Supplemental Table S2) were obtained from the Department of Medical Microbiology of the Radboud University Medical Center and the Department of Dermatology of the Heinrich-Heine-University in Düsseldorf (clinical isolate of AD skin, SA-DUS-011). *S. aureus*, *S. epidermidis*, *S. capitis* and *Corynebacterium aurimucosum* (*C. aurimucosum*) strains were grown o/n on Columbia agar with 5% sheep blood (Becton, Dickinson and Co.) under aerobic conditions at 37°C. Single colonies were used to inoculate cultures in 3 mL brain heart infusion (BHI) medium (Mediaproducts BV) in a 14 mL round bottom tube with snap cap (Cat#352057, Falcon, Corning) and incubated o/n at 37°C while shaking (225 rpm). Thereafter, bacterial cultures were diluted 100 times (30 µL in

3 mL BHI medium) and grown for another 2.5 hours in a shaking incubator to reach exponential growth. *Cutibacterium acnes* (*C. acnes*) was grown on Columbia agar with 5% sheep blood for 2 days at 37°C under anaerobic conditions (anaerobic jar system with an Oxoid Anaerogen 3.5L sachet (Cat#AN0035A, Thermo Fisher Scientific)), after which a single colony was picked and cultured o/n in 3 mL BHI medium at 37°C under anaerobic conditions. Thereafter, the bacteria were collected by centrifugation. The pellets containing the bacteria were washed twice in PBS and finally resuspended in PBS to reach the desired amount of colony forming units (CFU)/mL.

Glass cylinder methodology for topical application of bacteria

After resuspension, the bacterial strains were topically applied on the *stratum corneum* of the organotypic cultures using a glass cloning cylinder (Cat#070303-04, Bioptechs, Pennsylvania, USA) with an outer diameter of 6 mm (inner diameter of 4 mm). Cylinders were first washed with soap followed by disinfection with 70% and 100% ethanol (air-dried in flow cabinet). The cylinder was placed on top of the HEE, with the raw surface facing downwards in the middle of the insert, using forceps, leaving approximately 1 mm space at the edge of the culture area. 25 µL of bacterial suspension (or PBS only) was carefully pipetted inside the cylinder. During 4-5 hours, the cultures were placed on a heated plate (37°C) in the flow cabinet (without the lid) to allow the surface to become dry again. Afterwards, the cylinder was carefully removed and additional supplementation of culture medium (approximately 100 µL) in the basolateral compartment was required before returning cultures to the incubator at 37°C and 5% CO_2. A macroscopic view of the glass cylinder on top of the HEE is shown in Figure 1B, whereas a schematic overview of the HEE culture schedule with bacterial exposure is depicted in Figure 1F. During the culture experiments, samples of the culture medium were brought onto blood agar plates and incubated o/n at 37°C to check for sterility.

Depending on the experimental design, the bacteria were applied at different time points of the ALI (day 7, 8 and 11) and HEEs were harvested after 6 hours up to 13 days of culture. For the N/TERT-2G culture experiment, *S. aureus* ATCC 29213 was colonized at day 9 of the ALI.

To mimic the *in vivo* skin environment and to optimize culture conditions, HEEs inoculated with the SA-DUS-011 strain were also cultured at 32°C (at the start of colonization, up to 10 days) at low relative humidity (dry atmosphere). This was accomplished by removing the water tray from the incubator. Of note, the culture medium in the basolateral chamber thereby evaporated faster requiring additional

culture medium supplementation of 200 µL every day. Alternatively, the medium level could be increased with 500 µL to account for the evaporation and prevent the HEEs from running dry o/n.

The glass cylinder methodology was compared to a small droplet application (5 µL volume of bacterial suspension (SA-DUS-011 strain)) without the cylinder. The droplet was pipetted in the middle of the HEE (to minimize the risk of basolateral infections) and thereafter subjected to the same protocol as described above (37°C and 32°C).

Topical application of antibiotics

Fusidic acid (FA, F0881, Sigma-Aldrich) was used as a narrow spectrum antibiotic known to combat *S. aureus* infections. Both *S. aureus* ATCC 29213 and the SA-DUS-011 strain were analyzed after the addition of FA in a concentration series. Immediately after the colonization of *S. aureus* (~4 hours later, complete evaporation of PBS), 25 µL of FA (1% DMSO in water) was applied inside the same cylinder as used for the application of *S. aureus*. Again, the liquid was allowed to evaporate inside the flow cabinet (without lid on a heated plate, 37°C) and the cylinders were carefully removed afterwards. The HEEs with *S. aureus* ATCC 29213 were subjected to 1, 10 and 100 µg/mL FA, incubated at 37°C and 5% CO_2 and harvested after 24 hours (technical triplicates).

For a prolonged HEE culture experiment with the SA-DUS-011 strain, FA (10 and 100 µg/mL) was applied every other day using the sterile glass cloning cylinder on top of the HEE. Cultures were incubated at 32°C (dry incubator) with 5% CO_2 and harvested after 24 hours (technical triplicates) and 8 days (technical quadruplicates) of colonization.

Multi-parameter end point analysis of organotypic cultures exposed to bacteria

The polycarbonate filter supporting the organotypic culture was gently pressed out of the transwell by placing it up-side-down and using a 8 mm biopsy punch (BP-80F, KAI Medical). A 6 mm biopsy punch was used to sample the area that had been covered by the glass cylinder. The bacterial colonization area was macroscopically visible to the naked eye, which allowed the precise excision using the biopsy punch. Of this 6 mm sample, a 3 mm biopsy was punched and fixed for 4 hours in 4% formalin (Sigma-Aldrich) for histological processing. The remainder of the sample was divided in two, with one part placed in 350 µL lysis buffer for total RNA isolation and the remainder in 250 µL PBS for CFU count, or in 500 µL PBS

for microbial genomic DNA isolation for 16S rRNA gene sequencing. In summary, also depicted in the schematic image in Supplemental Figure S2B, samples were obtained for i) tissue morphology and/or protein expression ii) bacterial growth and iii) host gene expression from one single HEE to minimize batch effects and increase assay throughput.

Immunohistochemistry and confocal microscopy

6 µm paraffin sections were stained with hematoxylin and eosin (Sigma-Aldrich) or mounted with DAPI (4′,6-diamidino-2-phenylindole) fluoromount-G (Thermo Fisher Scientific) after deparaffinization. For immunohistochemical analysis, sections were first blocked with 5% normal goat, rabbit or horse serum in PBS for 15 minutes and incubated with the primary antibody for 1 hour at room temperature or o/n at 4°C (Supplemental Table S3). Thereafter, the sections were washed in PBS and subsequently incubated with biotinylated secondary antibodies for 30 minutes. Next, sections were washed again in PBS and incubated with avidin-biotin complex (1:50 avidin, 1:50 biotin in 1% BSA/PBS (v/v)) (Vector laboratories) for 30 minutes. Protein expression was visualized by color change due to the peroxidase activity of 3-amino-9-ethylcarbazole (AEC). The tissue was counterstained with hematoxylin, after which the sections were mounted with glycerol gelatin (Sigma-Aldrich, Cat No. 1002946952). For confocal microscopy, the primary antibodies goat anti-hBD2 and rabbit anti-SKALP were used in 1% BSA/PBS. As secondary antibodies, a donkey anti-goat Alexa Fluor 647 was used for hBD2 and a donkey anti-rabbit Alexa Fluor 594 was used for SKALP/elafin. All secondary antibodies (Molecular Probes, Eugene, OR) were diluted 1:200 in 1% BSA/PBS. 6 µm paraffin sections were mounted in fluoromount-G (Thermo Fisher Scientific, US) with DAPI (4′,6-diamidino-2-phenylindole). Image acquisition of immunofluorescence-stained tissue sections was performed by a ZEISS Axio Imager equipped with a ZEISS Axiocam 105 Color Digital Camera (Zeiss, Oberkochen, Germany). The ZEISS Axiocam 105 color is a compact five-megapixel camera (2560 x 1920 pixels) for high-resolution images with a 1/2.5″ sensor. For confocal microscopy, the Zeiss LSM900 confocal laser scanning microscope objective 63 x numerical aperture 1.4, focal plane 1 mm, was used. Images were chosen as representative of the whole culture or biopsies and stored in CZI format.

Keratinocyte RNA isolation and RT-qPCR analysis

RNA from the epidermal cells was isolated with the E.Z.N.A. Total RNA Kit I (OMEGA bio-tek) according to the manufacturer's protocol. Isolated RNA was treated with DNaseI (Invitrogen) and used for cDNA synthesis using SuperScript IV VILO Master Mix (Invitrogen) and UltraScript 2.0 (PCR Biosystems) according to the

manufacturer's protocols. Subsequent real-time quantitative PCR (RT-qPCR) was performed using SYBR Green (Bio-Rad). qPCR primers were obtained from Biolegio (Nijmegen, The Netherlands) and depicted in Supplemental Table S4. Target gene expression levels were normalized using the house keeping gene human acidic ribosomal phosphoprotein P0 (RPLP0). The ΔΔCt method was used to calculate relative mRNA expression levels [51].

Bacterial analysis

To isolate the bacteria from the organotypic cultures, the sample was homogenized/disintegrated in 250 µL PBS using a plastic micro pestle (Bel-Art, USA) in a 1.5 mL Eppendorf tube with convex bottom, by turning it around 10 times. Then, the suspension was completely homogenized using a needle (BD Microlance, 0.8 mm x 50 mm) and syringe (Henke-Ject, Tuberculin, 1 mL) by passing it 10 times. The homogenate was used to prepare a 10x dilution series and plated out on Columbia agar with 5% sheep blood. Plates were incubated at 37°C either o/n at aerobic conditions or for 2 days at anaerobic conditions. CFUs were counted and corrected for dilution and harvesting method, considering that only a part (3/8) of the culture was used for counting.

Dye penetration assay

To determine the time point of *stratum corneum* formation allowing bacterial colonization, 25 µL of 1 mM lucifer yellow (LY, Sigma-Aldrich) was applied inside a glass cylinder on top of the HEEs at various time points of the ALI culture (day 5 till day 8) and incubated for 2.5 hours at 37°C. After routine formalin fixation and embedding in paraffin, 6 µm sections were counterstained and mounted using DAPI Fluoromount-G (Thermo Fisher Scientific). LY was visualized at excitation wavelength of 488 nm using the ZEISS Axiocam 305 mono and a 10x or 40x objective.

Statistical analysis

Statistical analysis was performed using GraphPad Prism 9.0 (https://www.graphpad.com). Each HEE culture experiment includes technical replicates from a single keratinocyte donor, unless specified otherwise in the figure legend.

For the RT-qPCR gene expression analysis, the raw ΔCt values were used. An unpaired t-test was performed to determine statistical significance between two groups. Paired (biological replicates) and unpaired one-way analysis of variance (ANOVA) was used for comparison between multiple groups followed by Tukey's multiple comparison post hoc test.

To determine statistical significance for the CFU count data, unpaired nonparametric one-sided Mann-Whitney U test was used.

Ethics approval and Consent to participate

The primary cells used in this study were obtained from surplus material from plastic surgeries according to the Declaration of Helsinki. Patients consent was documented in electronic patient records on the use of biological material that remained after treatment for scientific research (Code of Good Conduct). Bacterial isolates were obtained from non-invasive skin swabs patients after informed consent.

Results

The prerequisites for bacterial colonization of organotypic skin *in vitro*

For bacterial colonization of organotypic skin and the study of host-microbe interactions, prevention of cell culture infection is crucial. Like in native intact skin, the *stratum corneum* of organotypic skin models should form a barrier preventing bacteria from penetrating the epidermis. Therefore, bacterial inoculation should occur subsequent to robust *stratum corneum* formation of the organotypic HEEs to discriminate bacterial colonization versus an invasive infection. The first appearance of lipid-rich *stratum corneum* layers that marks the time point of inoculation can be easily visualized by a tracer molecule, lucifer yellow (LY). For all primary keratinocyte donors (N=8), LY was retained in the *stratum corneum* at day 7 of the air-liquid interface (ALI) culture, which was therefore considered as the starting point for bacterial colonization of HEEs in further experiments (Supplemental Figure S1A). To address the suitability of the HEE model for long-term bacterial exposed culture studies, the lifespan of the HEEs was monitored. Expression patterns of the proliferation marker Ki-67, differentiation markers keratin 10 (K10) and filaggrin (FLG) and antimicrobial peptide (AMP) SKALP/elafin remained normal [52] for 25 days. The number of *stratum corneum* layers, however, increased due to lack of desquamation *in vitro* (Supplemental Figure S1B). After 30 days, a reduced number of epidermal layers and loss of the granular layer was seen (Supplemental Figure S1C). Therefore, the window of opportunity for studying host-microbe interactions or intervention strategies in the herein presented HEE model system was estimated being 18 days: from the start point of bacterial inoculation at day 7 of the ALI to maximally day 25.

Glass cylinder methodology for standardized topical inoculation of HEEs

In our efforts to optimize the bacterial application method for inoculating HEEs (from small to larger bacterial suspension droplets or complete coverage of the HEE), we were challenged by the labor-intensiveness, lack in reproducibility of bacterial colonization, high inter-individual variation between researchers, detrimental effects on epidermal morphology and most importantly frequent immediate infections (<24 hours of bacterial exposed culture) of the basolateral culture medium via the edges of the HEE. We therefore considered the utility of a glass cloning cylinder for topical application of the bacteria. The inert material minimally interacts with the bacteria or epidermis and allows easy sterilization. To quickly monitor the containment of liquid inside the cylinder at macroscopic level, we visualized the distribution of trypan blue on the HEE without and with the glass cylinder (Figure 1A-B, respectively). Microscopic analysis after LY application indicated an equal distribution over the *stratum corneum*, containment of liquid within the cylinder area and foremost clean edges of the HEE (Figure 1C).

Next, we investigated the effects of the glass cylinder and proposed vehicle (PBS) on the viability and structural integrity of the HEE. Prolonged immersion of organotypic epidermis is less desirable considering the detrimental effects on skin barrier formation and function [53, 54]. Indeed, covering HEEs with PBS for 24 hours changed the expression of markers for epidermal proliferation (Ki-67) and terminal differentiation (FLG) (Figure 1D). To reduce the time of liquid coverage of the *stratum corneum*, the cultures were placed on a laboratory hot plate (set at 37°C) without the lid of the transwell culture plate in the laminar flow hood to accelerate PBS evaporation. Thereby, the glass cylinder could be removed within 4-5 hours before returning the culture plates to the incubator. After careful morphological analysis (Figure 1E), this culture setup as depicted in Figure 1F was used as the basis for all further experiments.

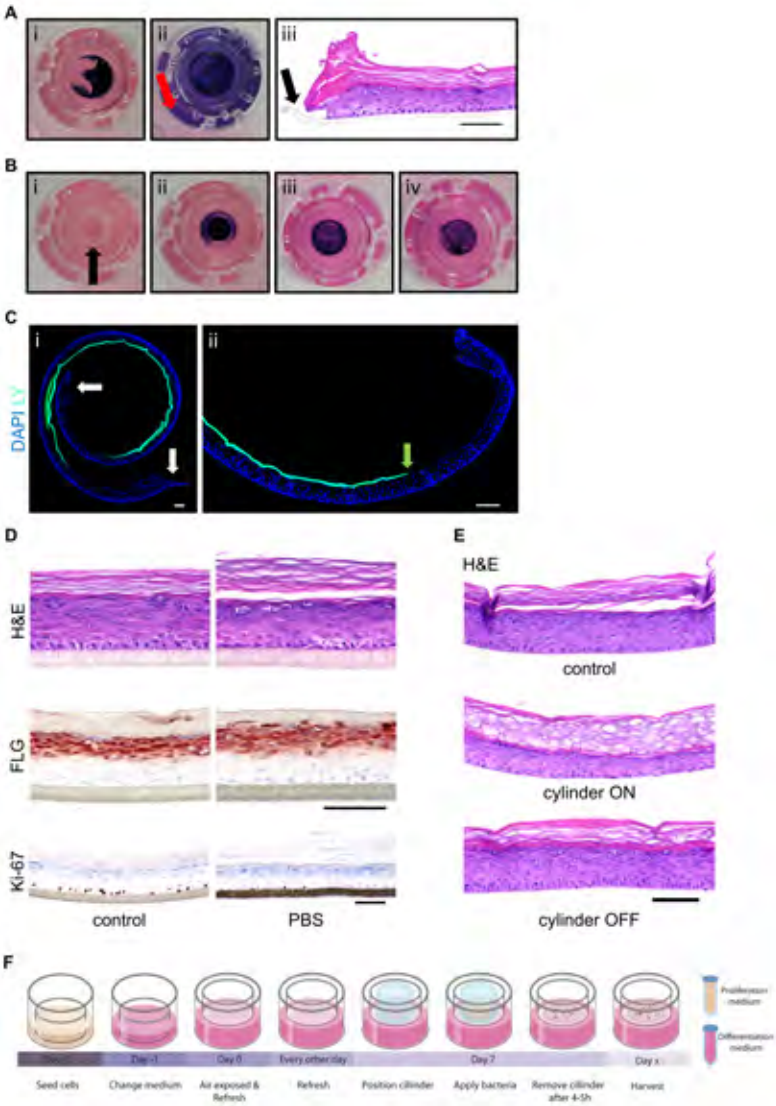

Figure 1. Validation of glass cylinder methodology. (**A**) i) 25 µL drop of trypan blue in PBS applied on top of the HEE, ii) the basolateral penetration of trypan blue after 4 hours of incubation (red arrow) and iii) H&E staining showing the open edges of the HEE (black arrow). (**B**) i) Glass cloning cylinder on top of the HEE indicated with the black arrow, ii) 25 µL of trypan blue in PBS was pipetted inside the cylinder, iii) the PBS was evaporated 4 hours later (in flow cabinet on heated plate at 37°C, without lid) and iv) the removal of the cylinder revealed a blue colonized circle without basolateral penetration. (**C**) Lucifer yellow (LY) added inside the glass cylinder and harvested after 2.5 hours of incubation. DAPI staining and fluorescent imaging (10x magnification) shows i) the distribution of LY onto the whole HEE and ii) clean edges. (**D**) H&E, Ki-67 and filaggrin (FLG) staining of HEE with a drop of PBS on top for 24 hours to analyze the morphological changes and protein expression patterns compared to the control. (**E**) Difference in morphology between the removal of the cylinder after PBS evaporation or leaving it on top of the HEE for 48 hours shown with an H&E staining. (**F**) Schematic overview of HEE culture and the topical application of bacteria using a glass cylinder. Scale bar = 100 µm.

Inoculation of HEE with pathogens and skin commensals

For acquiring first proof-of-concept on our methodology, a bacterial suspension of the pathogen *S. aureus* (ATCC 29213, 10^4 CFU in PBS) was added inside the glass cylinder, followed by a colonization period of 24 hours. Whole epidermal tissue analysis (8 mm biopsy punch) showed a homogenous distribution of the bacteria on the *stratum corneum* in the middle part, whilst keeping the edges of the HEEs free from bacteria (Supplemental Figure S2A). Next, we used one single HEE for multi-parameter readout analysis (Supplemental Figure S2B). After 24 hours of culture with two *S. aureus* strains (ATCC 29213 and a clinical isolate from an AD patient (SA-DUS-011)), CFU analysis indicated exponential bacterial growth reaching similar CFUs for both strains, with unaffected epidermal morphology (Figure 2A, Supplemental Figure S2C). Remarkably, marker gene expression analysis of AMPs (*DEFB4, S100A9* and *PI3*), revealed a strong induction after culture with SA-DUS-011 (Figure 2B). Also inflammatory mediators, here illustrated by *CCL20* and *IL1B*, were highly upregulated (Supplemental Figure S2D) in contrast to the laboratory ATCC strain.

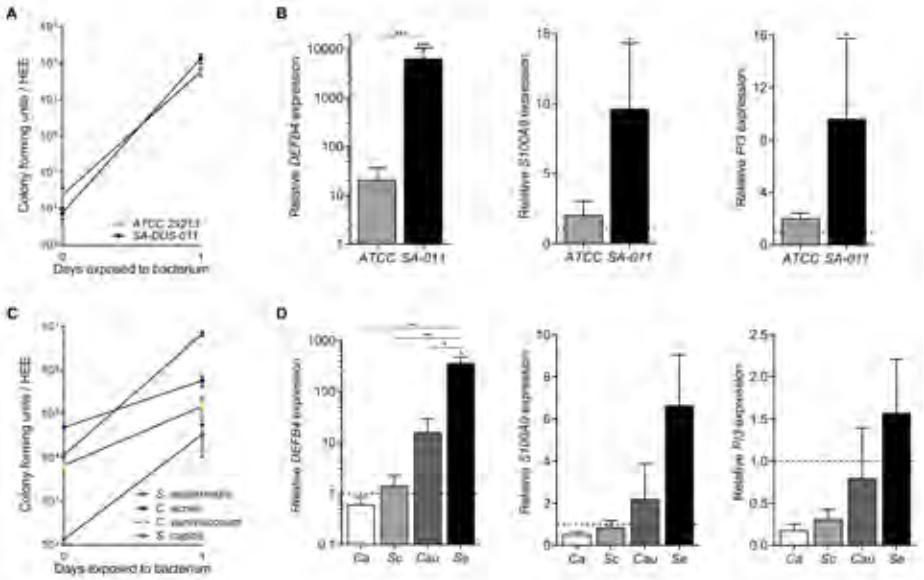

Figure 2. Colonization of HEEs with skin pathogens and commensals. (**A**) Growth and viability analysis by means of colony forming unit (CFU) count (input at 0 hours) (biological N=4) and (**B**) gene expression analysis of the antimicrobial peptides *DEFB4* (gene encoding hBD2), *S100A9* (MRP14) and *PI3* (SKALP/elafin) after 24 hours of exposure to two *S. aureus* strains (ATCC 29213 and the clinical isolate SA-DUS-011) (biological N=4, all controls set at 1). (**C**) CFU count (input at 0 hours) (N=3) and (**D**) gene analysis of *DEFB4, S100A9* and *PI3* after 24 hours of culture with skin related bacteria (*S. epidermidis* = *Se, C. acnes* = *Ca, C. aurimucosum* = *Cau, S. capitis* = *Sc*) (N=3, control set at 1 (dashed line)). *p<0.05, **p<0.01. Mean ± SEM.

To study the capability of aerobic, aerotolerant or facultative anaerobic skin commensals to colonize HEEs, *S. epidermidis*, *S. capitis*, *C. aurimucosum* and *C. acnes* were applied and cultured for 24 hours. CFU analysis indicated overall bacterial growth (Figure 2C), albeit at different growth rates between the tested strains (Supplemental Figure S2E). No differences were observed in the morphological appearance of the HEEs exposed to different bacterial strains (Supplemental Figure S2F), yet expression levels of host defense marker genes were significantly different, and mostly highly induced by *S. epidermidis* (Figure 2D, Supplemental Figure S2E and S2G). Importantly, no basolateral infections occurred during all HEE cultures as confirmed by plating culture medium onto blood agar plates.

Prolonged HEE culture with *S. aureus* ATCC 29213

Considering the favorable aerobic growth conditions for *Staphylococci* in HEE models and cell cultures in general, infections are expected upon long-term cultures if the glass cylinder does not effectively constrain the bacteria from leaking via the HEE edges, or when bacteria actively penetrate the *stratum corneum*. Being a commonly used human pathogenic strain, *S. aureus* ATCC 29213 was first selected for a prolonged two week culture period on top of the HEE. *S. aureus* quickly reached a maximum of approximately 10^8 CFU within 24 hours followed by a plateau phase during 13 days of culture (Figure 3A). The growth and survival of *S. aureus* on the HEE was irrespective of the start inoculum, reaching maximum levels between 10^7 and 10^8 CFU after 20 hours in all conditions (Supplemental Figure S3A). The epidermal morphology and protein marker expression for keratinocyte proliferation (Ki-67) and differentiation (FLG, involucrin (IVL)) of the HEEs cultured with *S. aureus* were comparable to control HEEs (Figure 3B, Supplemental Figure S3B). Induction of SKALP/elafin protein expression was observed after 24 hours of bacterial exposure and remained stable over time (Figure 3C).

Accumulating *stratum corneum* layers due to lack of desquamation *in vitro* (Figure 3B) could in principle hamper potential host-microbe interactions at later stages of the culture period. However, *stratum corneum* thickness did not influence bacterial growth and viability (Supplemental Figure S3C), nor did it hamper the induction of SKALP/elafin (Supplemental Figure S3D) when applying *S. aureus* at later stages of the ALI (day 11). Considering the popularity of the immortalized N/TERT keratinocytes in skin science as an alternative cell source for primary keratinocytes, we generated HEEs from the N/TERT-2G cell line which resulted in similar colonization rates as observed for primary keratinocytes (Supplemental Figure S4A-B). Again, in all experiments, no infections occurred during the short-term culture period.

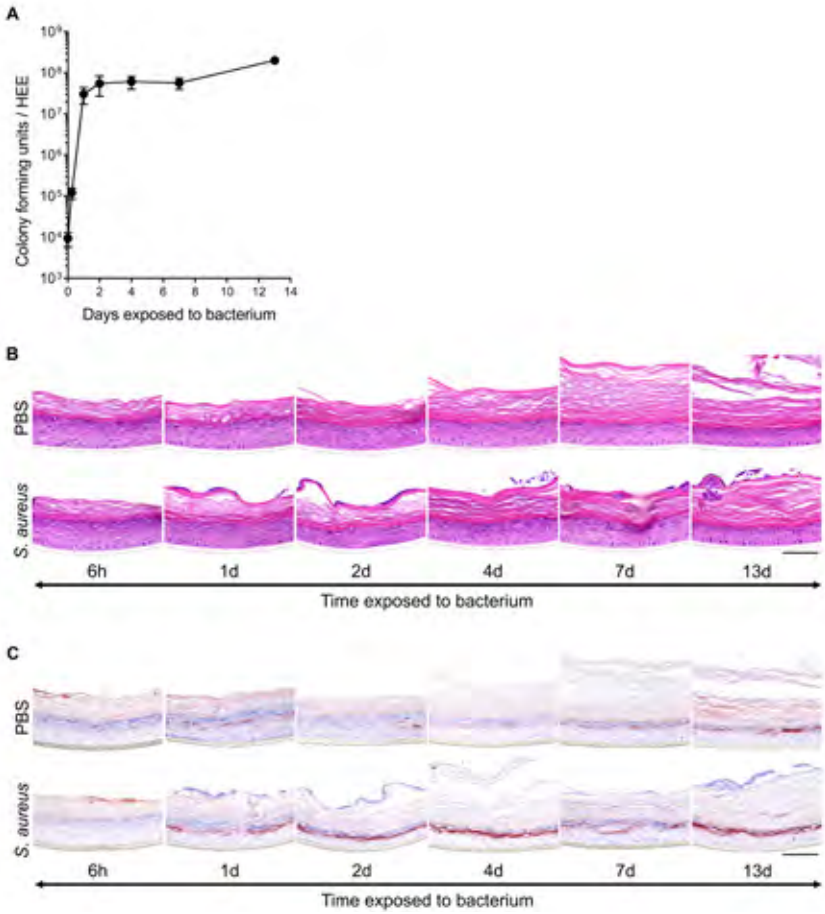

Figure 3. Prolonged HEE culture analysis after *S. aureus* ATCC 29213 colonization. (**A**) Colony forming unit (CFU) analysis of HEEs inoculated with *S. aureus* ATCC 29213 and harvested at different time points of culture up to 13 days (input at day 0). All data points represent N=4 biological keratinocyte donor replicates, except for the 13 days culture (N=1). (**B**) H&E and (**C**) SKALP/elafin staining of the HEE donor cultured for 13 days with *S. aureus* and its vehicle (PBS). Scale bar = 100 µm.

Epidermal infections after prolonged colonization by *S. epidermidis* and *S. aureus*

Commensal bacteria like *S. epidermidis* can become opportunistic pathogens causing skin infections [55] and may induce AD-like disease at high abundances [56]. Considering the strong host defense response we observed already after 24 hours of HEE colonization (Figure 2D, Supplemental Figure S2G), we evaluated the effects of a more prolonged culture with *S. epidermidis*. Epidermal infections occurred within 96 hours, even at a minimal input inoculum of 10^2 CFU. Structural damage of the epidermis, including loss of the granular layer, parakeratosis and reduced

epidermal layers was observed (Figure 4A). Strong induction of hBD2 and SKALP/elafin protein expression after 96 hours (Figure 4B) was subsequently accompanied by the confirmed presence of bacteria in the culture medium. Of note, no basolateral infections were observed after 24 hours. However, the already high AMP levels at 24 hours may have resulted from intracellular or invading bacteria in the epidermis not visible by light microscopy. However, confocal microscopy of immunofluorescent stainings did not reveal any presence of either *S. epidermidis* or *S. aureus* in the lower layers of the *stratum corneum* nor the living cells beneath in the epidermis (Supplemental Figure S5) at this time point, confirming a host defense response by bacteria-secreted factors through the *stratum corneum*.

Since the *S. aureus* clinical isolate (SA-DUS-011*)* also showed strong induction of host defense gene expression at 24 hours, we also prolonged this culture, resulting in basolateral cell culture infections within 96 hours (Figure 4C). Prior to bacterial growth in the basolateral compartment, yellow colonies typical for *S. aureus* were macroscopically visible on the HEE surface after 48 hours. Harvesting the SA-DUS-011 HEEs at different time points indicated various degrees of infection by upregulated AMP expression (hDB2 and SKALP/elafin) at the start of infection followed by structural damage to the epidermis (Figure 4D). Similar results were obtained using N/TERT HEEs. Herein, epidermal infections were seen in 5/6 replicates after 72 hours with concomitant upregulation of *DEFB4* (Supplemental Figure S4C). The induction of AMPs upon microbial exposure may thus be considered as an indicator for epidermal infections *in vitro* at later days, even when the epidermal morphology is still unaffected and basolateral culture medium and epidermis shows no signs of infection.

Bacterial infections related to culture conditions

To address the influence of potential experimental artefacts (*e.g.*, *stratum corneum* defects) from the cylinder application, the glass cylinder methodology was head-to-head compared with the application of a small volume of SA-DUS-011 in the middle of the HEEs [57-59]. In addition, to better mimic the natural growth conditions of bacteria on skin, physiologically relevant culture conditions (32°C, dry atmosphere) were compared to the traditional cell culture conditions (37°C, high humidity; warm and humid).

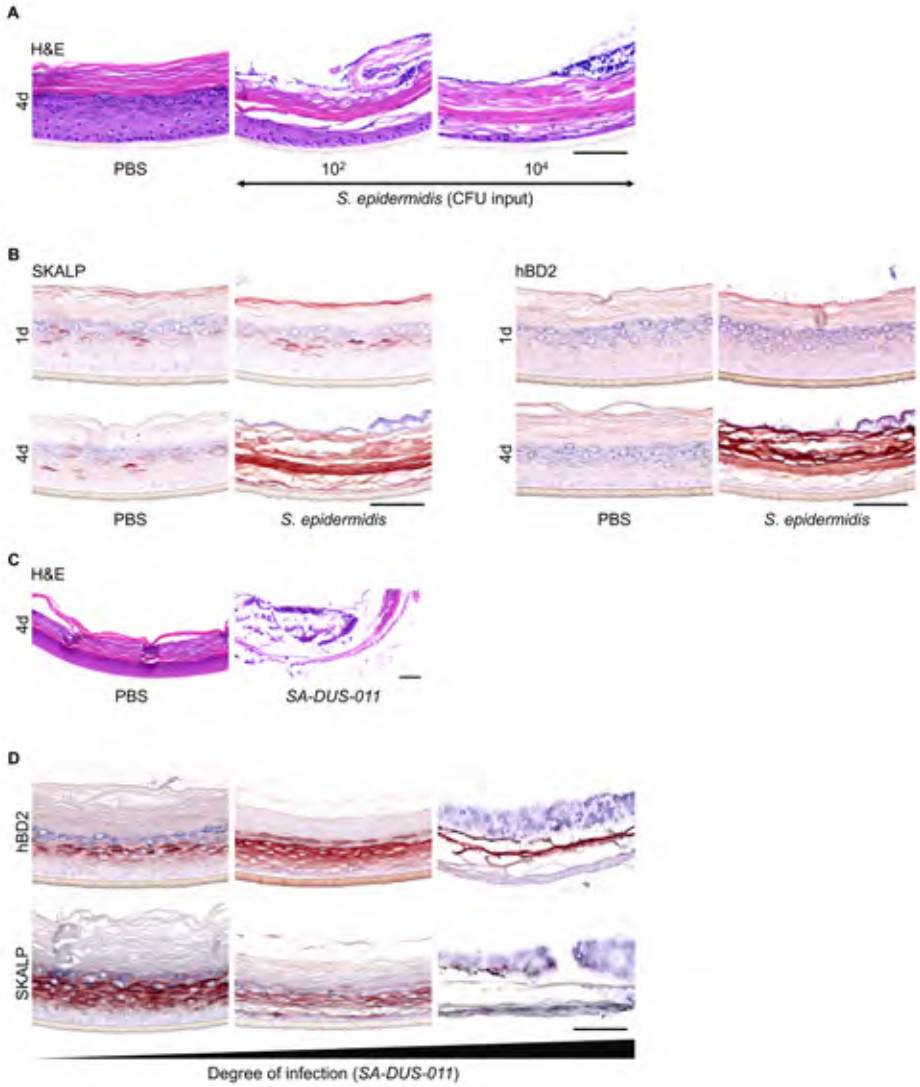

Figure 4. Epidermal infections caused by *S. epidermidis* and *S. aureus*. (**A**) *S. epidermidis* (10^2 and 10^4 CFU input) caused epidermal infections within 96 hours of culture, visualized with H&E staining that revealed the structural damage and loss of granular layer compared to the control HEE (PBS). (**B**) Immunostainings of the AMPs SKALP/elafin and hBD2 showed induction of protein expression in case of an epidermal infection. (**C**) H&E staining of HEE colonized with the *S. aureus* clinical isolate SA-DUS-011 (10^4 CFU input) for 96 hours compared to the control HEE (PBS). (**D**) HEEs inoculated with SA-DUS-011, harvested at different time points of infection and stained for the AMPs SKALP/elafin and hBD2. All HEEs had multiple visible large yellow colonies on top of the *stratum corneum*. Only the culture medium of the first HEE was not infected yet, analyzed with a blood agar plate and o/n incubation at 37°C. Scale bar = 100 µm.

The large bacterial surface area in the cylinder in warm and humid conditions conferred significantly higher CFU count and relative growth than the droplet area and reached similar CFU counts as in previous experiments (10^7-10^8 CFU) (Figure 5A-B). At 32°C and dry conditions, a maximum CFU of 10^6 per HEE was reached at both the droplet and cylinder application method, albeit the number of HEEs that became infected significantly differed between both application methods (Figure 5C). Briefly, the smaller droplet area delayed infection onset in a warm and humid environment by at least 4 days, but could not prevent all HEEs becoming infected within 7 days after bacterial inoculation. At 32°C and dry conditions delayed infection onset using the cylinder and even prevented infections in 80% of HEEs with a small (droplet) application area.

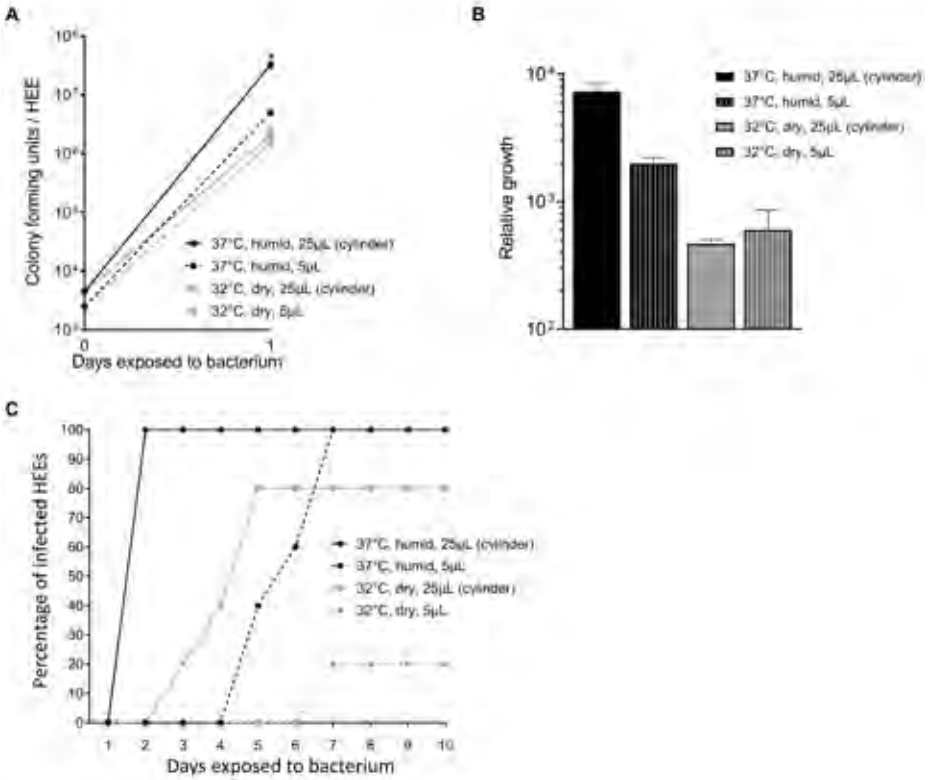

Figure 5. Bacterial infections using different culture conditions. (**A**) Colony forming unit (CFU) analysis and (**B**) relative growth of the *S. aureus* clinical isolate SA-DUS-011 after 24 hours of colonization applying four different methods (glass cylinder methodology (25 µL) *versus* small droplet (5 µL) and 37°C (humid) *versus* 32°C (dry)) (N=3 per method) (input at 0 hours), *p<0.05 (Mann-Whitney U test, CFU outcome of 37°C glass cylinder method compared to the other methods). (**C**) Percentage of infected HEEs (N=5 per method), cultured and exposed for up to 10 days with SA-DUS-011 applied using the four different methods.

To further dissect the influence of temperature versus humidity on bacterial growth and infection rate, HEEs were also cultured at 32°C in a humid environment. After 48 hours, SA-DUS-011 caused epidermal infections in all HEEs that were incubated in humid conditions (of note: the infections started earlier at 37°C compared to 32°C). At 32°C and dry conditions, only 3 out of 8 HEEs became infected.

Topical antibiotic inhibits the growth of *S. aureus*

Next to more fundamental studies on skin host-microbe interactions, organotypic 3D skin microbiome models could be of importance for research and development of pre-, pro- and antibiotics to modulate the skin microbiome for therapeutic purposes. We implemented the cylinder methodology for the topical application of antibiotics using readout parameters for both host and microbe. Fusidic acid (FA) is used in clinical practice for the treatment of *Staphylococci* skin infections and herein chosen as a proof-of-principle intervention.

Inhibition of *S. aureus* ATCC 29213 growth was observed in a dose dependent manner after a single dose of FA was added inside the cylinder directly after the initiation of *S. aureus* colonization, indicating the bacteriostatic effect of FA (Figure 6A). In the morphological analysis, the lower amount of *S. aureus* colonies on top of the *stratum corneum* relate to the effective FA treatment. At the effective FA concentrations of 10 and 100 µg/mL, no morphological changes of the HEE were observed (Figure 6B). Based on the aforementioned optimal culture conditions, FA efficacy was tested (10 and 100 µg/mL) on the *S. aureus* clinical isolate SA-DUS-011 using the glass cylinder and culturing at 32°C and in a dry environment up to 8 days. At day 1, CFU analysis showed a strong reduction of *S. aureus* (Figure 6C) indicative of the effective bacteriostatic effects of FA (bacteria were not completely killed, resulting in 10^5 CFU on day 8 upon FA treatment every other day). During the following 7 days, 50% of the untreated *S. aureus*-colonized HEEs became infected after 4 days. The remainder of the untreated *S. aureus*-colonized HEEs that were harvested at day 8 showed severe epidermal damage (Figure 6D) with high CFU counts (Figure 6C) indicative of epidermal infections. FA treatment not only limited the bacterial growth, but also completely prevented infections and epidermal damage caused by *S. aureus* in HEEs.

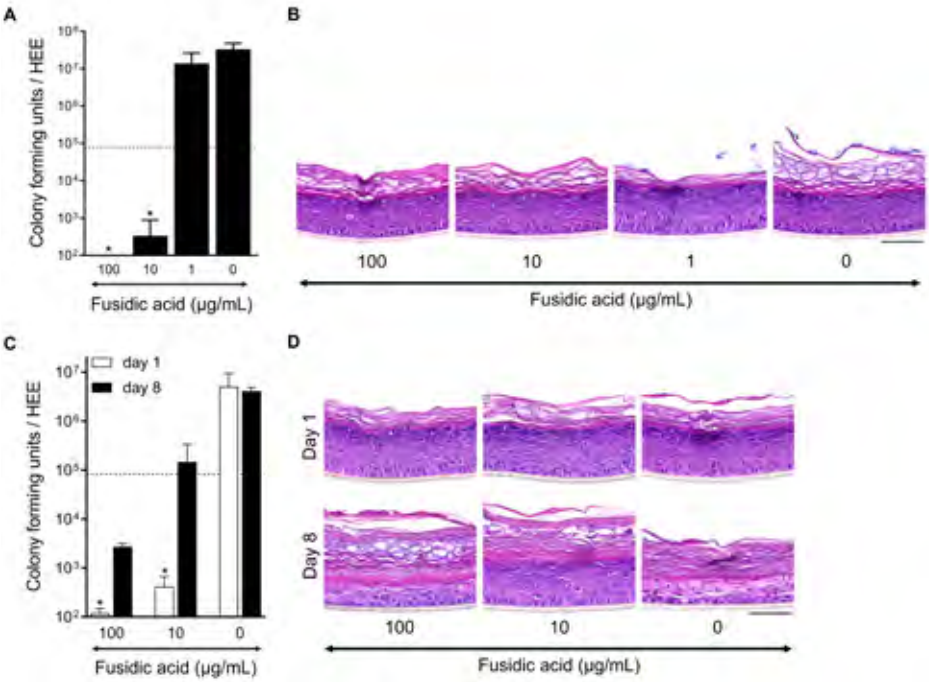

Figure 6. Fusidic acid inhibits the growth of *S. aureus* on HEEs. (**A**) Dose inhibiting effect via colony forming unit (CFU analysis) of HEEs topically applied with fusidic acid (FA, 1-10-100 µg/mL, 1% DMSO in water (0 µg/mL, vehicle)) 4 hours after *S. aureus* ATCC 29213 colonization (dotted line: amount of CFUs at start of treatment) and harvested 24 hours later (N=3), and (**B**) H&E staining thereof. (**C**) CFU analysis on day 1 (N=3 per treatment) and day 8 (0 µg/mL (N=2) and 10-100 µg/mL (N=4)), and (**D**) H&E staining of HEEs colonized with the *S. aureus* clinical isolate SA-DUS-011 subjected to the FA treatment protocol (10 and 100 µg/mL). HEEs were analyzed with a prolonged culture up to 8 days to study epidermal infections; 50% (2 out of 4) *S. aureus* HEEs infected after 96 hours (FA applied at day 0, 2, 4 and 6) (of note, cultured at 32°C (dry)). *$p<0.05$ (Mann-Whitney U test, CFU outcome of fusidic acid dosages compared to the vehicle (0 µg/mL)). Mean ± SEM. Scale bar = 100 µm.

Discussion

We here present a technical advance for the topical bacterial inoculation of a 3D human epidermal equivalent (HEE) with a minimal risk of basolateral infections, whilst allowing *in vitro* studies on infectious virulent strains. This methodology using glass cylinders will be easily transferable to a wide variety of advanced organotypic skin [60, 61] or mucosal models [62], would be amenable for the application of diverse microbiota (bacteria [63, 64], viruses [65-67] and fungi [68, 69]) and can be used in every cell culture facility considering the various sizes and commercial availability, at low costs. We were able to increase the assay throughput by the large bacterial exposure area and thus obtaining multiple samples for various endpoint

analysis from one single HEE. Furthermore, our model allows us to influence the cell culture environment to study infection *vs*. colonization. However, to more closely mimic the *in vivo* situation, more complex models involving immune cells and fibroblasts (full-thickness skin, *ex vivo*) and genetic predisposing factors need to be taken into account to fully comprehend biological mechanisms that underly host-microbe interactions in health and disease.

We generated both a colonization and infection model based on the single strain exposure of a fully developed epidermal model. While other bacterial exposed culture models to date induce an infection by making a wound [59, 61, 70, 71], we here showed that the *S. aureus* clinical isolate (SA-DUS-011) caused epidermal infections after colonizing an intact skin. Albeit similar growth rates and a high CFU output (10^7-10^8), the *S. aureus* strain ATCC 29213 did not infect the HEE within two weeks of culture nor did it induce the expression levels of any of the host defense markers. Based on these results we consider the inoculum not being related to the AMP response, but rather depending on a strain specific effect and its secreted factors. Therefore, screening of various skin related bacterial species and using more than one strain per bacterium, ideally isolated from individual patients or volunteers, followed by whole genome sequencing [47], could relate virulence factors to the clinical features of the patient and host-microbe responses *in vitro*.

While here we present the model characteristics using single bacterial strains, the ultimate goal would be the application of whole skin microbiome samples or pre-designed microbial communities, as used in experimental animal models [13]. Yet, *in vitro* cell culture conditions have been shown to affect the stability of the commensal communities, skewing towards a dominance of aerobic bacteria after the culture period [47] and 16S or shotgun sequencing only includes information on relative abundancies whilst lacking information on bacterial viability. Methods to exclude bacterial DNA from dead cells, like propidium monoazide (PMA) [72], may provide a solution but require a labor-intense multi-step protocol and will be difficult to validate for the correct dosing of complex bacterial mixtures to avoid killing of microbes due to treatment.

The major advantage of a glass cylinder is the large colonization surface, allowing the collection of multiple samples, that we called "*multiple parameter endpoint analysis*". A small droplet, as commonly used, prevents infection of the basolateral chamber, but will require multiple transwell inserts, large experimental setups or cell culture formats (6-12well), [57, 60, 63, 64, 73-75]. Others completely cover the cell culture surface with bacterial suspension, but this requires immediate analysis

or removal of non-adherent bacteria [69, 76-79]. Furthermore, when the set-up of experiments require multiple treatment steps of the equivalents, the cylinder provides a defined area wherein treatments can be applied after each other by equally distributed evaporation of the solutions, as we here showed for fusidic acid. This antibiotic prevented infections and maintained the epidermal morphology for at least 8 days of treatment, which is a novel finding compared to other antibiotic organotypic models [57, 76, 78, 80]. Although we found that the glass cylinder does accelerate the start of epidermal infections, a small droplet application also resulted in infections. Therefore, we value the utility of the glass cylinder and changed the culture environmental conditions (32°C in a dry atmosphere) to delay the onset of infections and maximize the culture period and window of opportunity for interventions. By changing the cell culture environmental conditions and varying the application area of bacteria we leverage the opportunity to either study skin infection or colonization. Interestingly, we observed that under dry culture conditions, cultures located in the middle of the culture plate infected earlier than those in the outer rows, presumably due to higher humidity in the middle of the culture plate. Hence, only controlling the humidity in the cell culture incubator is not sufficient to fully standardize environmental conditions within the culture plate.

Modulation of microbiome composition and its effects might also be accomplished by changing host factors. We here showed that the use of the N/TERT-2G immortalized keratinocyte cell line is a suitable alternative for microbial colonization of HEEs since the epidermal structure is similar to that of primary keratinocytes [50]. In addition, it is the preferred cell type for genome editing and the use of a cell line instead of primary cells will reduce the biological variation. For example, knockdown of the differentiation protein filaggrin (*FLG*) showed increased colonization of *S. aureus* on top of the organotypic N/TERT model [77]. This correlation between FLG and microbial colonization is also observed *in vivo* for *S. aureus* [81, 82]. In addition, specific commensal species are underrepresented on *FLG*-deficient skin showing a reduction of gram positive anaerobic cocci [37], that appear to harbor important AMP-inducing capabilities [41]. Furthermore, continued efforts in the optimization of culture conditions and protocols to better mimic the *in vitro* skin barrier to that of native skin [83, 84] will also affect the interaction between microbes and epidermal keratinocytes in organotypic model systems and as such, it will remain a challenge to compare results obtained between various models. Detailed information on the model characteristics (morphology, skin barrier function, cell sources, culture medium, microbial strain selection) are pre-requisites for studies that aim to investigate cell-host-microbe interactions in organotypic skin models.

In conclusion, our developed model system allows for easy utilization of organotypic human epidermal models for investigative skin microbiome research. This opens avenues into the application of more complex microbial cultures, the evaluation of specific pathogens in genotype-defined organotypic human skin models, and the screening of pre-, pro- or antibiotic treatments therein.

Acknowledgements

The authors thank undergraduate students Berber Maste, Priscilla Faas, Laura Edo Aceña, Blanca Gonzalez Melarde and Jaimy Klijnhout for technical assistance during their research internships which all contributed to the evolvement of the final model system. Danique van der Krieken assisted with the microbiological techniques, and Priscilla Faas created the schematic figures using Adobe Illustrator. This study was funded by the Dutch Research Council, Meer Kennis met Minder Dieren program (No.114021503 to EvdB and PZ) and the the Innovative Medicines Initiative 2 Joint Undertaking (JU) under grant agreement (No. 821511 to EvdB and BH). The JU receives support from the European Union's Horizon 2020 research and innovation programme and EFPIA. The authors declare no competing interests.

Abbreviations

AD - atopic dermatitis, ALI - air-liquid interface, AMP - antimicrobial peptide, BHI - brain heart infusion, CFU - colony forming units, DAPI - 4',6-diamidino-2-phenylindole, FA - fusidic acid, H&E - hematoxylin and eosin, HEE - human epidermal equivalent, IL – interleukin, LY - lucifer yellow, o/n – overnight, PBS - phosphate buffered saline, RT-qPCR - real-time quantitative PCR

References

1. Turnbaugh, P.J., et al., The human microbiome project. Nature, 2007. **449**(7164): p. 804-10.
2. Costello, E.K., et al., Bacterial community variation in human body habitats across space and time. Science, 2009. **326**(5960): p. 1694-7.
3. Findley, K., et al., Topographic diversity of fungal and bacterial communities in human skin. Nature, 2013. **498**(7454): p. 367-70.
4. Grice, E.A., et al., Topographical and temporal diversity of the human skin microbiome. Science, 2009. **324**(5931): p. 1190-2.
5. Gao, Z., et al., Quantitation of major human cutaneous bacterial and fungal populations. J Clin Microbiol, 2010. **48**(10): p. 3575-81.
6. Chng, K.R., et al., Whole metagenome profiling reveals skin microbiome-dependent susceptibility to atopic dermatitis flare. Nat Microbiol, 2016. **1**(9): p. 16106.
7. Naik, S., et al., Commensal-dendritic-cell interaction specifies a unique protective skin immune signature. Nature, 2015. **520**(7545): p. 104-8.
8. Lai, Y., et al., Commensal bacteria regulate Toll-like receptor 3-dependent inflammation after skin injury. Nat Med, 2009. **15**(12): p. 1377-82.
9. Naik, S., et al., Compartmentalized control of skin immunity by resident commensals. Science, 2012. **337**(6098): p. 1115-9.
10. Nakatsuji, T., et al., Antimicrobials from human skin commensal bacteria protect against Staphylococcus aureus and are deficient in atopic dermatitis. Sci Transl Med, 2017. **9**(378).
11. Iwase, T., et al., Staphylococcus epidermidis Esp inhibits Staphylococcus aureus biofilm formation and nasal colonization. Nature, 2010. **465**(7296): p. 346-9.
12. Yuki, T., et al., Activation of TLR2 enhances tight junction barrier in epidermal keratinocytes. J Immunol, 2011. **187**(6): p. 3230-7.
13. Uberoi, A., et al., Commensal microbiota regulates skin barrier function and repair via signaling through the aryl hydrocarbon receptor. Cell Host Microbe, 2021. **29**(8): p. 1235-1248 e8.
14. Grice, E.A. and J.A. Segre, The skin microbiome. Nat Rev Microbiol, 2011. **9**(4): p. 244-53.
15. Tauber, M., et al., Staphylococcus aureus density on lesional and nonlesional skin is strongly associated with disease severity in atopic dermatitis. J Allergy Clin Immunol, 2016. **137**(4): p. 1272-1274 e3.
16. Kong, H.H., et al., Temporal shifts in the skin microbiome associated with disease flares and treatment in children with atopic dermatitis. Genome Res, 2012. **22**(5): p. 850-9.
17. Zeeuwen, P.L., et al., Microbiome and skin diseases. Curr Opin Allergy Clin Immunol, 2013. **13**(5): p. 514-20.
18. Gao, Z., et al., Substantial alterations of the cutaneous bacterial biota in psoriatic lesions. PLoS One, 2008. **3**(7): p. e2719.
19. Alekseyenko, A.V., et al., Community differentiation of the cutaneous microbiota in psoriasis. Microbiome, 2013. **1**(1): p. 31.
20. Dessinioti, C. and A.D. Katsambas, The role of Propionibacterium acnes in acne pathogenesis: facts and controversies. Clin Dermatol, 2010. **28**(1): p. 2-7.
21. Frank, D.N., et al., Microbial diversity in chronic open wounds. Wound Repair Regen, 2009. **17**(2): p. 163-72.

22. Tong, S.Y., et al., Staphylococcus aureus infections: epidemiology, pathophysiology, clinical manifestations, and management. Clin Microbiol Rev, 2015. **28**(3): p. 603-61.
23. Leyden, J.J., R.R. Marples, and A.M. Kligman, Staphylococcus aureus in the lesions of atopic dermatitis. Br J Dermatol, 1974. **90**(5): p. 525-30.
24. Gallo, R.L., S. epidermidis influence on host immunity: more than skin deep. Cell Host Microbe, 2015. **17**(2): p. 143-4.
25. Ederveen, T.H.A., et al., A generic workflow for Single Locus Sequence Typing (SLST) design and subspecies characterization of microbiota. Sci Rep, 2019. **9**(1): p. 19834.
26. Rigon, R.B., et al., Skin microbiota as a therapeutic target for psoriasis treatment: Trends and perspectives. J Cosmet Dermatol, 2021. **20**(4): p. 1066-1072.
27. Ruff, W.E., T.M. Greiling, and M.A. Kriegel, Host-microbiota interactions in immune-mediated diseases. Nat Rev Microbiol, 2020. **18**(9): p. 521-538.
28. Dreno, B., et al., The Skin Microbiome: A New Actor in Inflammatory Acne. Am J Clin Dermatol, 2020. **21**(Suppl 1): p. 18-24.
29. Zeeuwen, P.L., et al., Microbiome dynamics of human epidermis following skin barrier disruption. Genome Biol, 2012. **13**(11): p. R101.
30. Emmert, H., et al., Skin microbiota analysis in human 3D skin models-"Free your mice". Exp Dermatol, 2020. **29**(11): p. 1133-1139.
31. Last, A., et al., In vitro infection models to study fungal-host interactions. FEMS Microbiol Rev, 2021.
32. Kokai-Kun, J.F., et al., Lysostaphin cream eradicates Staphylococcus aureus nasal colonization in a cotton rat model. Antimicrob Agents Chemother, 2003. **47**(5): p. 1589-97.
33. Liu, H., et al., Staphylococcus aureus Epicutaneous Exposure Drives Skin Inflammation via IL-36-Mediated T Cell Responses. Cell Host Microbe, 2017. **22**(5): p. 653-666 e5.
34. Triplett, K.D., et al., GPER activation protects against epithelial barrier disruption by Staphylococcus aureus alpha-toxin. Sci Rep, 2019. **9**(1): p. 1343.
35. Nagy, I., et al., Distinct strains of Propionibacterium acnes induce selective human beta-defensin-2 and interleukin-8 expression in human keratinocytes through toll-like receptors. J Invest Dermatol, 2005. **124**(5): p. 931-8.
36. Wickersham, M., et al., Metabolic Stress Drives Keratinocyte Defenses against Staphylococcus aureus Infection. Cell Rep, 2017. **18**(11): p. 2742-2751.
37. Zeeuwen, P.L., et al., Gram-positive anaerobe cocci are underrepresented in the microbiome of filaggrin-deficient human skin. J Allergy Clin Immunol, 2017. **139**(4): p. 1368-1371.
38. Wu, X., et al., Interferon-Lambda 1 Inhibits Staphylococcus aureus Colonization in Human Primary Keratinocytes. Front Pharmacol, 2021. **12**: p. 652302.
39. Moriwaki, M., et al., Staphylococcus aureus from atopic dermatitis skin accumulates in the lysosomes of keratinocytes with induction of IL-1alpha secretion via TLR9. Allergy, 2019. **74**(3): p. 560-571.
40. Igawa, S., et al., Human Keratinocytes Use Sphingosine 1-Phosphate and its Receptors to Communicate Staphylococcus aureus Invasion and Activate Host Defense. J Invest Dermatol, 2019. **139**(8): p. 1743-1752 e5.
41. van der Krieken, D.A., et al., Gram-positive anaerobic cocci guard skin homeostasis by regulating host-defense mechanisms. iScience, 2023. **26**(4): p. 106483.

42. Niehues, H., et al., 3D skin models for 3R research: The potential of 3D reconstructed skin models to study skin barrier function. Exp Dermatol, 2018. **27**(5): p. 501-511.
43. Paharik, A.E., et al., Coagulase-Negative Staphylococcal Strain Prevents Staphylococcus aureus Colonization and Skin Infection by Blocking Quorum Sensing. Cell Host Microbe, 2017. **22**(6): p. 746-756 e5.
44. Williams, M.R., et al., Quorum sensing between bacterial species on the skin protects against epidermal injury in atopic dermatitis. Sci Transl Med, 2019. **11**(490).
45. Leung, M.H.Y., et al., Changes of the human skin microbiota upon chronic exposure to polycyclic aromatic hydrocarbon pollutants. Microbiome, 2020. **8**(1): p. 100.
46. Rademacher, F., et al., Staphylococcus epidermidis Activates Aryl Hydrocarbon Receptor Signaling in Human Keratinocytes: Implications for Cutaneous Defense. J Innate Immun, 2019. **11**(2): p. 125-135.
47. Larson, P.J., et al., Challenges in Developing a Human Model System for Skin Microbiome Research. J Invest Dermatol, 2021. **141**(1): p. 228-231 e4.
48. Rikken, G., H. Niehues, and E.H. van den Bogaard, Organotypic 3D Skin Models: Human Epidermal Equivalent Cultures from Primary Keratinocytes and Immortalized Keratinocyte Cell Lines. Methods Mol Biol, 2020. **2154**: p. 45-61.
49. Dickson, M.A., et al., Human keratinocytes that express hTERT and also bypass a p16(INK4a)-enforced mechanism that limits life span become immortal yet retain normal growth and differentiation characteristics. Mol Cell Biol, 2000. **20**(4): p. 1436-47.
50. Smits, J.P.H., et al., Immortalized N/TERT keratinocytes as an alternative cell source in 3D human epidermal models. Sci Rep, 2017. **7**(1): p. 11838.
51. Livak, K.J. and T.D. Schmittgen, Analysis of relative gene expression data using real-time quantitative PCR and the 2– ΔΔCT method. methods, 2001. **25**(4): p. 402-408.
52. Niehues, H., et al., Epidermal equivalents of filaggrin null keratinocytes do not show impaired skin barrier function. J Allergy Clin Immunol, 2017. **139**(6): p. 1979-1981 e13.
53. Mayrovitz, H.N. and N. Sims, Biophysical effects of water and synthetic urine on skin. Adv Skin Wound Care, 2001. **14**(6): p. 302-8.
54. Woo, K.Y., D. Beeckman, and D. Chakravarthy, Management of Moisture-Associated Skin Damage: A Scoping Review. Adv Skin Wound Care, 2017. **30**(11): p. 494-501.
55. Otto, M., Staphylococcus epidermidis--the 'accidental' pathogen. Nat Rev Microbiol, 2009. **7**(8): p. 555-67.
56. Cau, L., et al., Staphylococcus epidermidis protease EcpA can be a deleterious component of the skin microbiome in atopic dermatitis. J Allergy Clin Immunol, 2021. **147**(3): p. 955-966 e16.
57. Reddersen, K., et al., Three-dimensional human skin model infected with Staphylococcus aureus as a tool for evaluation of bioactivity and biocompatibility of antiseptics. Int J Antimicrob Agents, 2019. **54**(3): p. 283-291.
58. Duckney, P., et al., The role of the skin barrier in modulating the effects of common skin microbial species on the inflammation, differentiation and proliferation status of epidermal keratinocytes. BMC Res Notes, 2013. **6**: p. 474.
59. Charles, C.A., et al., Use of tissue-engineered skin to study in vitro biofilm development. Dermatol Surg, 2009. **35**(9): p. 1334-41.
60. Bolle, E.C.L., et al., An in vitro Reconstructed Human Skin Equivalent Model to Study the Role of Skin Integration Around Percutaneous Devices Against Bacterial Infection. Front Microbiol, 2020. **11**: p. 670.

61. Corzo-Leon, D.E., D.M. MacCallum, and C.A. Munro, Host Responses in an Ex Vivo Human Skin Model Challenged With Malassezia sympodialis. Front Cell Infect Microbiol, 2020. **10**: p. 561382.
62. Shang, L., et al., Multi-species oral biofilm promotes reconstructed human gingiva epithelial barrier function. Sci Rep, 2018. **8**(1): p. 16061.
63. Kohda, K., et al., An In Vitro Mixed Infection Model With Commensal and Pathogenic Staphylococci for the Exploration of Interspecific Interactions and Their Impacts on Skin Physiology. Front Cell Infect Microbiol, 2021. **11**: p. 712360.
64. Laclaverie, M., et al., Development and characterization of a 3D in vitro model mimicking acneic skin. Exp Dermatol, 2021. **30**(3): p. 347-357.
65. Tamosiunaite, A., et al., Histopathological and Immunohistochemical Studies of Cowpox Virus Replication in a Three-Dimensional Skin Model. J Comp Pathol, 2016. **155**(1): p. 55-61.
66. Muhsen, M., et al., Orf virus (ORFV) infection in a three-dimensional human skin model: Characteristic cellular alterations and interference with keratinocyte differentiation. PLoS One, 2019. **14**(1): p. e0210504.
67. Loke, A.S.W., et al., A Novel In Vitro Culture Model System to Study Merkel Cell Polyomavirus-Associated MCC Using Three-Dimensional Organotypic Raft Equivalents of Human Skin. Viruses, 2021. **13**(1).
68. Faway, E., et al., Modeling dermatophytosis in reconstructed human epidermis: A new tool to study infection mechanisms and to test antifungal agents. Med Mycol, 2017. **55**(5): p. 485-494.
69. Kitisin, T., et al., Utilization of an in vitro biofabricated 3D skin as a pathological model of cutaneous candidiasis. New Microbiol, 2020. **43**(4): p. 171-179.
70. Shepherd, J., et al., Development of three-dimensional tissue-engineered models of bacterial infected human skin wounds. Tissue Eng Part C Methods, 2009. **15**(3): p. 475-84.
71. Havlikova, J., et al., Direct identification of bacterial and human proteins from infected wounds in living 3D skin models. Sci Rep, 2020. **10**(1): p. 11900.
72. van der Krieken, D.A., et al., An In vitro Model for Bacterial Growth on Human Stratum Corneum. Acta Derm Venereol, 2016. **96**(7): p. 873-879.
73. Lemoine, L., et al., Microbially competent 3D skin: a test system that reveals insight into host-microbe interactions and their potential toxicological impact. Arch Toxicol, 2020. **94**(10): p. 3487-3502.
74. Loomis, K.H., et al., A mixed community of skin microbiome representatives influences cutaneous processes more than individual members. Microbiome, 2021. **9**(1): p. 22.
75. Barua, N., et al., Comparative Study of Two-Dimensional (2D) vs. Three-Dimensional (3D) Organotypic Kertatinocyte-Fibroblast Skin Models for Staphylococcus aureus (MRSA) Infection. Int J Mol Sci, 2021. **23**(1).
76. Park, A.Y., et al., Modulation of Gene Expression in a Sterile Atopic Dermatitis Model and Inhibition of Staphylococcus aureus Adhesion by Fucoidan. Dermatopathology (Basel), 2021. **8**(2): p. 69-83.
77. van Drongelen, V., et al., Reduced filaggrin expression is accompanied by increased Staphylococcus aureus colonization of epidermal skin models. Clin Exp Allergy, 2014. **44**(12): p. 1515-24.
78. Haisma, E.M., et al., Inflammatory and antimicrobial responses to methicillin-resistant Staphylococcus aureus in an in vitro wound infection model. PLoS One, 2013. **8**(12): p. e82800.
79. de Breij, A., et al., Three-dimensional human skin equivalent as a tool to study Acinetobacter baumannii colonization. Antimicrob Agents Chemother, 2012. **56**(5): p. 2459-64.
80. Muller, G., et al., Residual antimicrobial effect of chlorhexidine digluconate and octenidine dihydrochloride on reconstructed human epidermis. Skin Pharmacol Physiol, 2014. **27**(1): p. 1-8.

81. Towell, A.M., et al., Staphylococcus aureus binds to the N-terminal region of corneodesmosin to adhere to the stratum corneum in atopic dermatitis. Proc Natl Acad Sci U S A, 2021. **118**(1).
82. Emmert, H., et al., Stratum corneum lipidomics analysis reveals altered ceramide profile in atopic dermatitis patients across body sites with correlated changes in skin microbiome. Exp Dermatol, 2021. **30**(10): p. 1398-1408.
83. Mieremet, A., et al., Multitargeted Approach for the Optimization of Morphogenesis and Barrier Formation in Human Skin Equivalents. Int J Mol Sci, 2021. **22**(11).
84. Helder, R.W.J., et al., Improved organotypic skin model with reduced quantity of monounsaturated ceramides by inhibiting stearoyl-CoA desaturase-1. Biochim Biophys Acta Mol Cell Biol Lipids, 2021. **1866**(4): p. 158885.
85. Holland, D.B., et al., Microbial colonization of an in vitro model of a tissue engineered human skin equivalent--a novel approach. FEMS Microbiol Lett, 2008. **279**(1): p. 110-5.
86. Holland, D.B., et al., Differential innate immune responses of a living skin equivalent model colonized by Staphylococcus epidermidis or Staphylococcus aureus. FEMS Microbiol Lett, 2009. **290**(2): p. 149-55.
87. Maboni, G., et al., A Novel 3D Skin Explant Model to Study Anaerobic Bacterial Infection. Front Cell Infect Microbiol, 2017. **7**: p. 404.
88. Chaudhari, A.A., et al., A three-dimensional human skin model to evaluate the inhibition of Staphylococcus aureus by antimicrobial peptide-functionalized silver carbon nanotubes. J Biomater Appl, 2019. **33**(7): p. 924-934.
89. Meloni, M., et al., Reproducing the scalp microbiota community: co-colonization of a 3D reconstructed human epidermis with C. acnes and M. restricta. Int J Cosmet Sci, 2021. **43**(2): p. 235-245.
90. Brown, J.L., et al., Assessing the inflammatory response to in vitro polymicrobial wound biofilms in a skin epidermis model. NPJ Biofilms Microbiomes, 2022. **8**(1): p. 19.
91. Holzknecht, J., et al., Small, Cationic Antifungal Proteins from Filamentous Fungi Inhibit Candida albicans Growth in 3D Skin Infection Models. Microbiol Spectr, 2022. **10**(3): p. e0029922.
92. Baede, V.O., et al., The survival of epidemic and sporadic MRSA on human skin mimics is determined by both host and bacterial factors. Epidemiol Infect, 2022. **150**: p. e203.

Supplemental figures

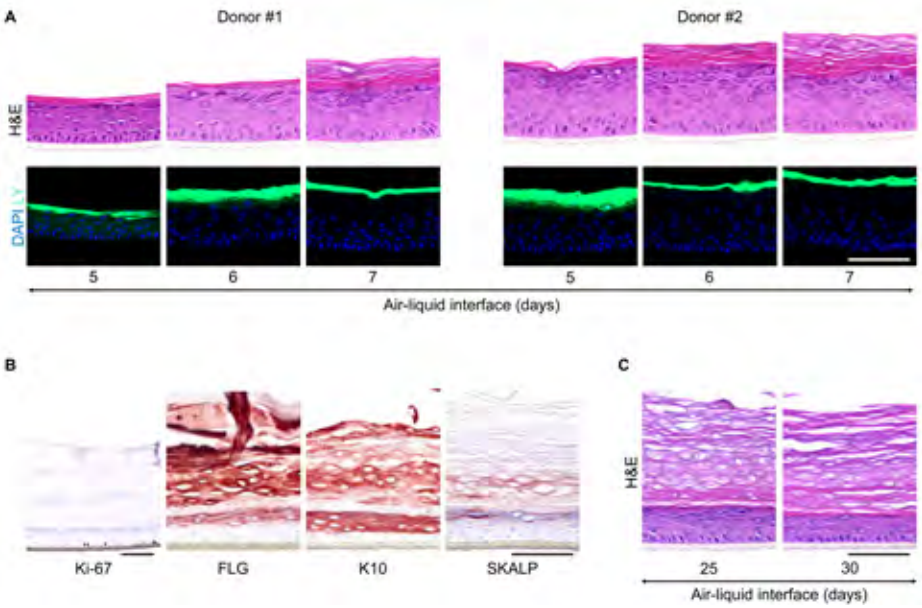

Supplemental Figure S1. *Stratum corneum* formation and lifespan of HEEs. (**A**) H&E and DAPI staining of two HEE donors that were topically applied with LY for 2.5 hours on different days of the air-liquid interface (ALI) to evaluate *stratum corneum* penetration (images represent eight biological keratinocyte donors). (**B**) Protein expression of the proliferation marker Ki-67, differentiation markers filaggrin (FLG) and keratin 10 (K10) and the AMP SKALP/elafin of a HEE at day 25 of the ALI. (**C**) H&E staining of HEEs harvested at day 25 and 30 of the ALI to investigate the lifespan of the culture. Scale bar = 100 µm.

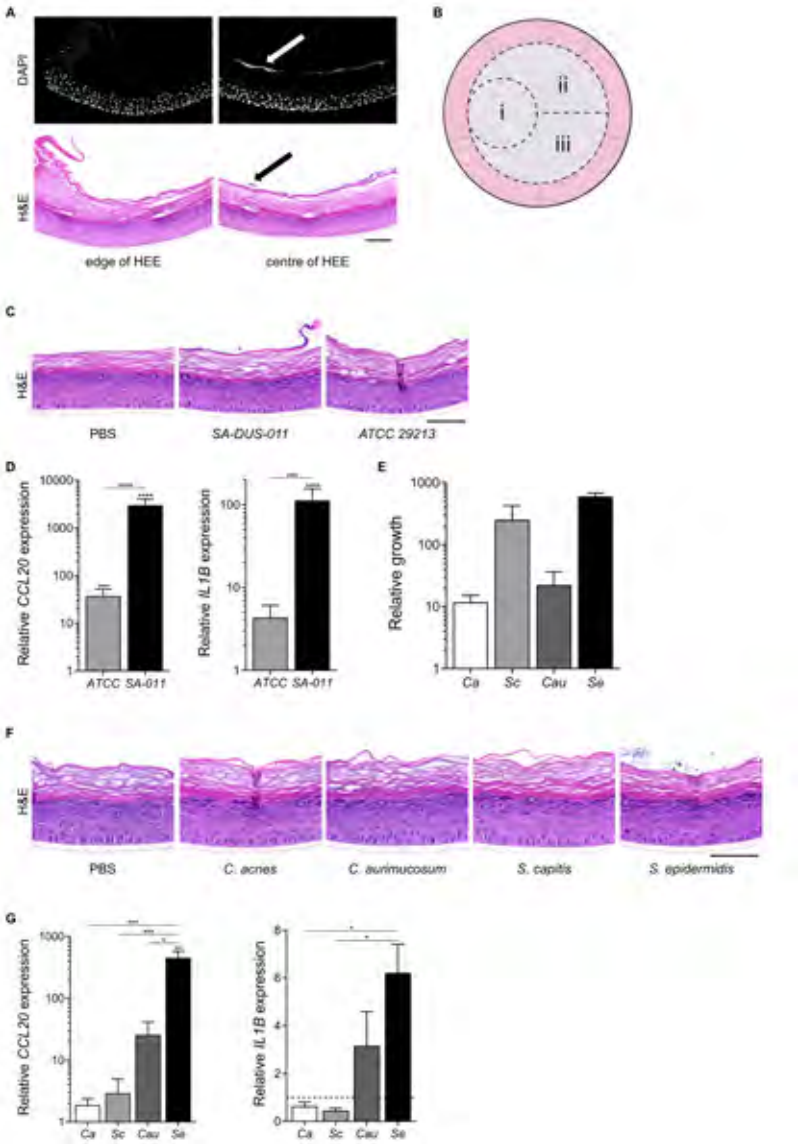

Supplemental Figure S2. Multi-parameter endpoint analysis, bacterial colonization, growth and host defense response. (**A**) DAPI (white nuclei and colonies (white arrow)) and H&E (colonies indicated with black arrow) staining of HEE cultured for 24 hours with 10^4 colony forming units (CFU) of *S. aureus* ATCC 29213 to visualize bacterial colonization and clean edges of the HEE. (**B**) Multi-parameter analysis for i) morphology and/or protein expression, ii) host gene expression and iii) bacterial growth. (**C**) H&E staining and (**D**) inflammatory gene expression (*CCL20* and *IL1B*) of HEEs colonized with *S. aureus* ATCC 29213 and the *S. aureus* clinical isolate SA-DUS-011 for 24 hours to analyze epidermal morphology (biological N=4, controls set at 1). (**E**) Logarithmic growth, (**F**) H&E staining and (**G**) inflammatory gene expression (*CCL20* and *IL1B*) after 24 hours of culture with skin related bacteria (*S. epidermidis* = *Se, C. acnes* = *Ca, C. aurimucosum* = *Cau, S. capitis* = *Sc)* (N=3, control set at 1). *p<0.05, ***p<0.001. Mean ± SEM. Scale bar = 100 µm.

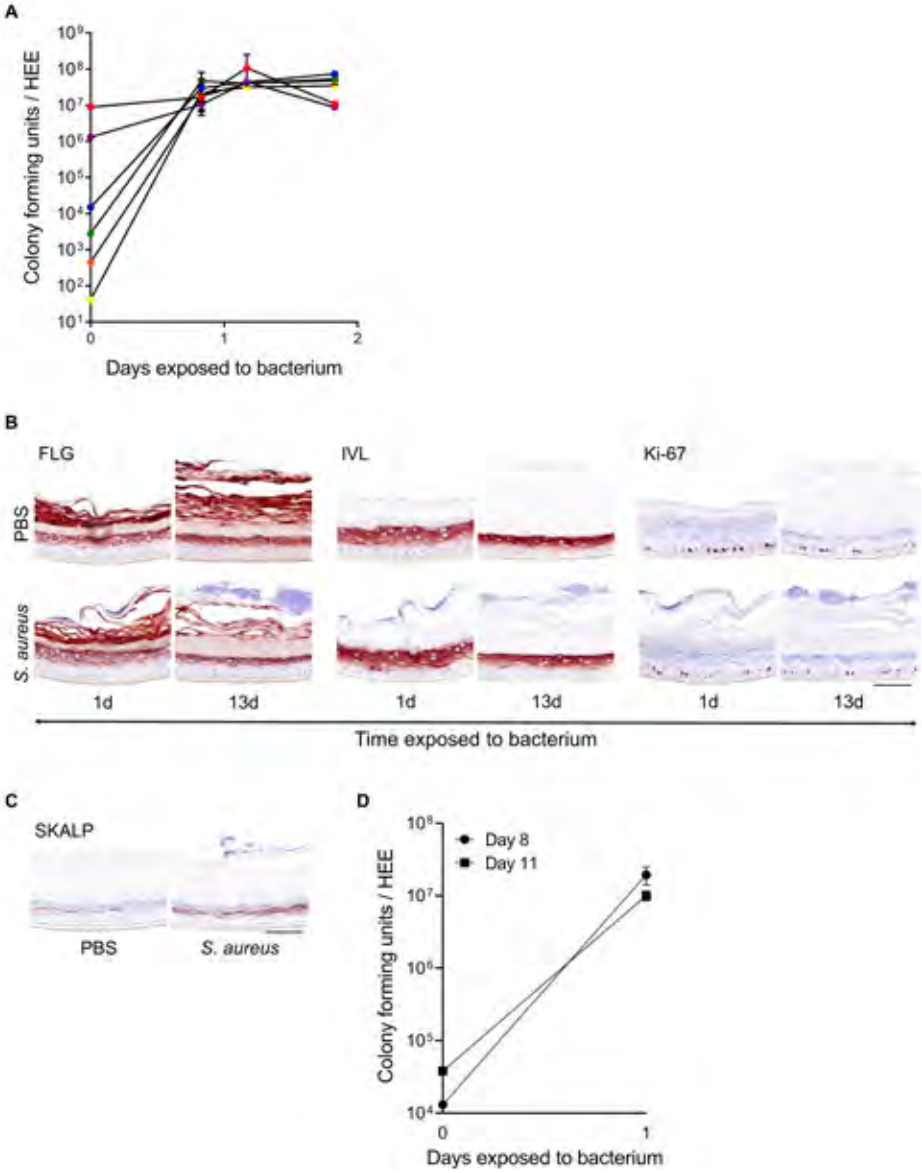

Supplemental Figure S3. Inoculum and *stratum corneum* thickness do not influence growth of *S. aureus* ATCC 29213. (**A**) Colony forming unit (CFU) count of HEEs inoculated with a concentration series (10^1, 10^2, 10^3, 10^4, 10^6 and 10^7 CFU) of *S. aureus* and harvested after 20, 28 and 44 hours of culture (N=2). (**B**) Normal epidermal protein expression after *S. aureus* colonization up to 13 days compared to the control HEE (PBS) shown with the proliferation marker Ki-67 and the differentiation markers filaggrin (FLG) and involucrin (IVL). (**C**) CFU analysis of *S. aureus* colonized at day 8 and day 11 (thick layer of *stratum corneum*) of the air-liquid interface (ALI) for 24 hours (biological N=5, input at day 0). (**D**) SKALP/elafin protein expression of HEE inoculated with *S. aureus* at day 11 of the ALI (thick layer of *stratum corneum*) in comparison with the control HEE (PBS) and cultured for 24 hours. Images represent N=5 biological keratinocyte donors. Scale bar = 100 µm.

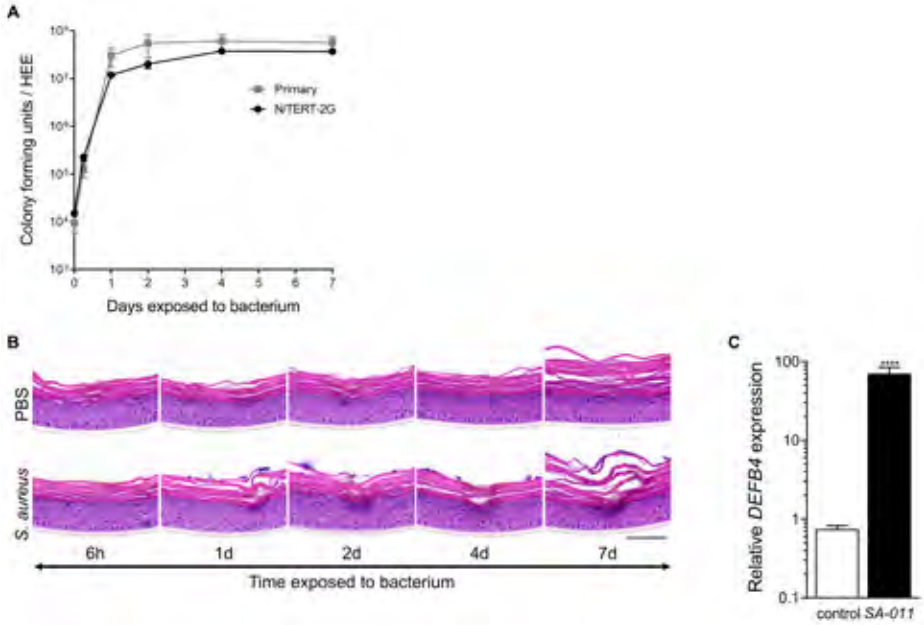

Supplemental Figure S4. HEEs generated with immortalized N/TERT cells and colonized with *S. aureus* strains. (**A**) Colony forming unit (CFU) analysis of N/TERT HEEs colonized with *S. aureus* ATCC 29213 and harvested after different time points of culture up to 7 days (each data point N=3), in comparison with primary human keratinocytes (grey line, biological N=4) and (**B**) H&E staining thereof. (**C**) Gene expression analysis of the antimicrobial peptide *DEFB4* after 72 hours of culture with the *S. aureus* clinical isolate SA-DUS-011 (N=6). ****p<0.0001. Mean ± SEM. Scale bar = 100 µm.

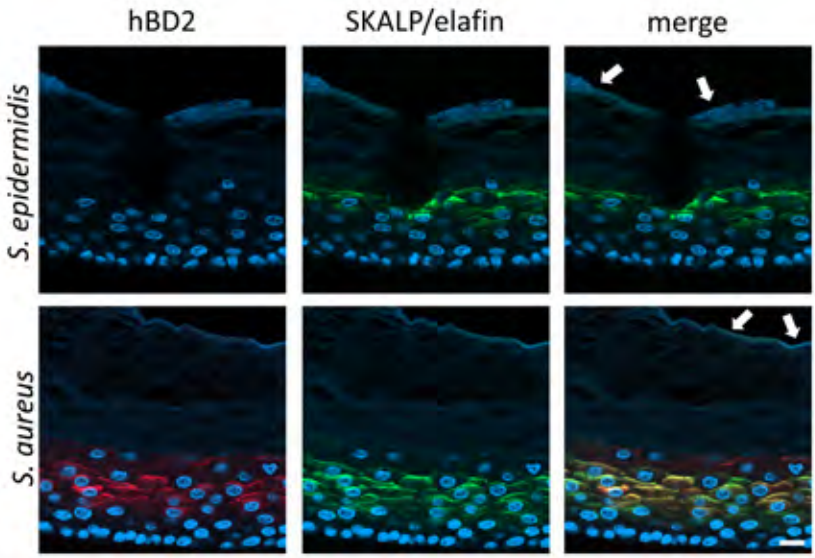

Supplemental Figure S5. Antimicrobial protein expression in HEEs colonized with *S. aureus* clinical isolate SA-DUS-011. Immunofluorescence detection of hBD2 (red signal) and SKALP/elafin (green signal) in HEEs using confocal microscopy. Nuclei of keratinocytes as well as bacteria are stained with DAPI (blue signal). Bacteria on top of the *stratum corneum* (upper panel *S. epidermidis*; lower panel *S. aureus*) are indicated with white arrows. Colocalization of hBD2 and SKALP/elafin in the upper layers of the epidermis is detected as a yellow signal in the merge column (only in HEEs colonized with *S. aureus*). HEEs were grown at 37°C and high humidity.

Supplemental tables

Supplemental Table S1. Studies that used 3D organotypic skin models to investigate bacterial colonization, infection and host-microbe interactions.

Model	Cell source	Microbe(s)	Inoculation	Culture	Analysis	Ref
HSE, colonization	NHEK (foreskin)	*S. epidermidis* *C. acnes* *M. furfur* *S. aureus*	10^2 - 10^6	72, 120 hours	CFUs, histology and TEWL	[85]
HSE, colonization	NHEK (foreskin)	*S. epidermidis* *S. aureus*	10^4	24 hours	RNA (microarray)	[86]
HSE, wound	NHEK	*P. aeruginosa* *S. aureus*	10^7	24 - 72 hours	CFUs and histology	[70]
HSE, wound	NHEK (neonatal)	*P. aeruginosa* *S. aureus*	10^6	3, 5, 7, 10, 24 hours	Histology	[59]
HEE, colonization	NHEK	*A. baumannii* *A. junii*	10^5	72 hours	CFUs, histology and RNA (qPCR)	[79]
HSE, wound, antibiotic	NHEK	*S. aureus*	10^5	24, 48 hours	CFUs, histology, IHC, RNA (qPCR) and ELISA	[78]
HEE, colonization	Skinethic	*S. aureus* *S. epidermidis* *C. acnes*	10^7 – 10^9	24 hours	Biochemical assays, RNA (qPCR)	[58]
HEE, colonization	N/TERT	*S. aureus*	10^5	24 hours	CFUs, histology, IHC, RNA (qPCR) and ELISA	[77]
HEE, colonization	NHEK	*P. aeruginosa* *S. aureus*	10^6	2, 24 hours	CFU, MTT	[80]
Ex vivo, colonization	Ovine biopsy	*D. nodosus*	10^4	28 hours (anaerobic)	Histology, FISH and ELISA	[87]
HSE, infection, antibiotic	NHEK	*S. aureus*	10^7	24 hours	CFUs, Histology, LDH, RNA (qPCR) and ELISA	[57]
HSE, wound	NHEK	*S. aureus*	10^4	2 hours	SEM, CFU	[88]
HSE, infection	NHEK	*S. aureus*	10^7	24 hours	CFUs, histology, IF	[60]
HSE, wound	Labskin	*E. faecium* *S. aureus* *K. pneumoniae* *A. baumannii* *P. aeruginosa*	10^5	24, 48, 72, 96 hours	LESA mass spectra	[71]

Supplemental Table S1. Continued

Model	Cell source	Microbe(s)	Inoculation	Culture	Analysis	Ref
HSE, Infection, antibiotic	NHEK	*C. albicans*	10^5	24 hours	Histology, TEM, XTT assay, WB and immunoassay	[69]
Ex vivo, wound	Human biopsy	*M. sympodialis*	10^6	6 days	Histology, SEM, TUNEL, RNA, Immunoassay	[61]
HSE, colonization	MatTek EpiDerm	*M. luteus* *P. oleovorans*	10^4 – 10^6	4, 8 days	CFUs, Gram stain, ELISA, RNA (qPCR, microarray), WB	[73]
HEE, colonization	Episkin	*C. acnes* *M. restricta*	10^5 – 10^7	72 hours	CFUs, histology, TEER, IF and SEM	[89]
HEE, colonization	NHEK (foreskin)	*C. acnes*	10^5	24, 48 hours	Histology, IF, LY, TEER, RNA and ELISA	[64]
HSE, colonization	EpiDerm	*S. aureus* *P. aeruginosa* *Microbiome*	10^5	18 hours	16S and RNA sequencing, histology and IF	[74]
HEE, colonization, antibiotic	NHEK (foreskin)	*S. aureus* *C. acnes* *S. epidermidis*	10^4	1 hour	CFUs, histology, RNA (qPCR)	[76]
HEE, colonization	LabCyte Epi-Model (foreskin)	*S. aureus* *S. epidermidis*	10^3 – 10^5	48 hours	CFUs, LDH, ELISA, IF	[63]
HSE, infection	NHEK (foreskin)	*S. aureus*	10^7	2, 24, 48 hours	CFUs, histology, TUNEL	[75]
HEE, colonization, therapeutics	Episkin	Microbial biofilm	10^7	24 hours	Histology, RNA (qPCR), Proteomics	[90]
HSE, colonization, therapeutics	Phenion (foreskin)	*C. albicans*	10^2	24, 48 hours	CFUs, LY, histology, TUNEL, IF, ELISA	[91]
HEE, colonization	N/TERT, NHEK	*S. aureus*	10^5	24, 48 hours, 8 days	CFUs, ELISA, Luminex	[92]

CFU - colony forming units, ELISA - enzyme-linked immunosorbent assay, FISH - fluorescence in situ hybridization, HEE - human epidermal equivalent, HSE - human skin equivalent, IF - immunofluorescence, IHC - immunohistochemistry, LDH - lactate dehydrogenase, LESA - liquid extraction surface analysis, LY - lucifer yellow, NHEK - normal human epidermal keratinocytes, qPCR - quantitative polymerase chain reaction, SEM - scanning electron microscope, TEER - Transepithelial electrical resistance, TEM - transmission electron microscopy, TEWL - transepidermal water loss, TUNEL - terminal deoxynucleotidyl transferase biotin-dUTP nick end labelling, WB - western blot.

Supplemental Table S2. Antibodies used for immunohistochemistry

Target	Antibody clone	Antigen retrieval	Dilution
Filaggrin (FLG)	FLG01, Thermo Fisher	Yes	1:100
Ki-67	SP-6, Abcam	Yes	1:200 (o/n 4°C)
Involucrin (IVL)	Mon150, van Duijnhoven *et al*. 1992	Yes	1:20
Keratin 10 (K10)	DE-K10, Abcam	Yes	1:100
SKALP/elafin	92-1, Schalkwijk *et al*.1993	No	1:500
Human β-Defensin-2 (hBD2)	ab9871, Abcam	No	1:100

Supplemental Table S3. Bacterial strains

Strain	Identification number	Gram	Growth conditions
Cutibacterium acnes	ATCC-6919	positive	anaerobe
Staphylococcus epidermidis	ATCC-12228	positive	aerobe
Staphylococcus capitis	Clinical isolate	positive	aerobe
Corynebacterium aurimucosum	Clinical isolate	positive	aerobe
Staphylococcus aureus	ATCC-29213	positive	aerobe
Staphylococcus aureus	Clinical isolate	positive	aerobe

Supplemental Table S4. Primers for qPCR

HUGO gene symbol	Protein	Forward primer (5′ → 3′)	Reverse primer (5′ → 3′)
RPLP0	ribosomal phospoprotein P0	caccattgaaatcctgagtgatgt	tgaccagcccaaaggagaag
DEFB4	human defensin-2, hBD2	gatgcctcttccaggtgttttt	ggatgacatatggctccactctt
CCL20	chemokine (C-C motif) ligand 20	tggccaatgaaggctgtga	gatttgcgcacacagacaactt
IL1B	interleukin-1β	aatctgtacctgtcctgcgtgtt	tgggtaatttttgggatctacactct
S100A9	S100 calcium-binding protein A9	tgtggctcctcggctttg	gcgttccagctgcgacat

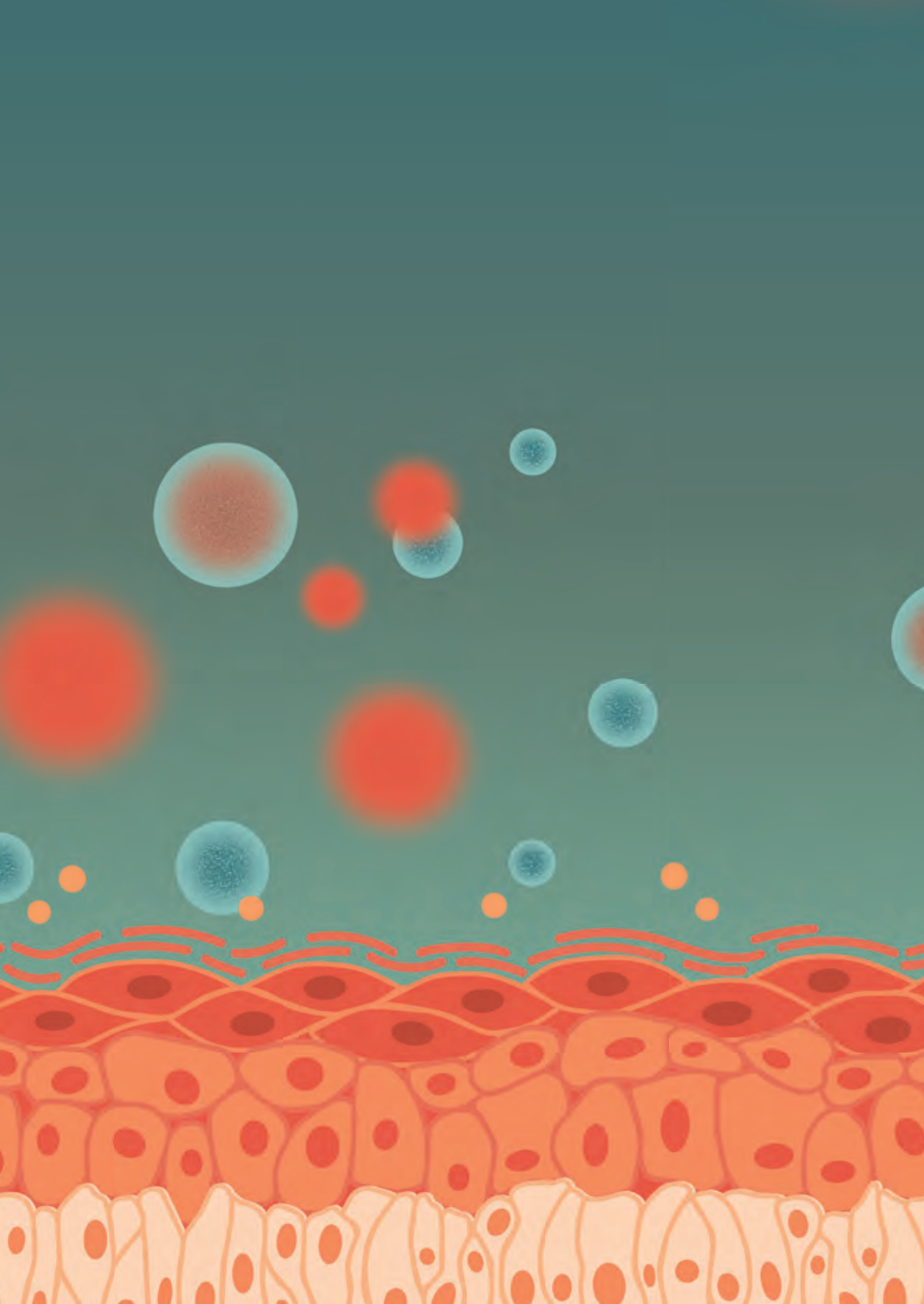

Chapter 8.

Deriving keratinocytes from iPSC to model epidermal differentiation and inflammatory skin diseases

Luca D. Meesters[1,2], Camille Laberthonnière[2], Julian Arts[2], Yavuz Kilic[2], Roos Simons[2], Bram Raaben[2], Wietske Kieboom[2], Ivonne M. van Vlijmen-Willems[1], Diana Rodijk-Olthuis[1], Dulce Lima Cunha[2], Hanna Niehues[1], Ellen H. van den Bogaard[1], Huiqing Zhou[2,3]

Affiliations

[1] Department of Dermatology, Radboud University Medical Center (Radboudumc), Nijmegen, The Netherlands

[2] Department of Molecular Developmental Biology, Faculty of Science, Radboud University, Nijmegen, The Netherlands.

[3] Department of Human Genetics, Radboud University Medical Center (Radboudumc), Nijmegen, The Netherlands.

Published in

Manuscript in preparation.

Abstract

The versatility of induced pluripotent stem cell (iPSC)-derived, also called induced, keratinocytes (iKC) enables developing personalized disease models for drug target discovery and therapeutic screening. However, the overall poor proliferation capacity and heterogeneity of iKC has hampered modeling of the epidermis, such as in air-liquid interface cultures that are the gold standard 3D human model for studying inflammatory skin diseases. Here, we optimized iPSC to keratinocyte differentiation conditions and the subculturing of iKC for generation of human epidermis equivalents (HEEs). While addition of ROCK inhibitor and the choice of coating were imperative for cell survival and proliferation, change to CELLnTEC-30 medium greatly increased the iKC homogeneity as compared to commonly used keratinocyte serum free medium. Single-cell RNA sequencing of iKC cultures revealed different cell populations including a large population of keratinocytes that were similar to primary keratinocytes (pKC). Subculturing of iKC enhanced overall keratinocyte marker gene expression, while sustaining proliferation rates necessary for cell banking. Upon induction of epidermal differentiation in monolayer cultures, iKC showed a flattened morphology and increased expression of suprabasal keratinocyte maker genes. Epidermal differentiation defects typical for chronic inflammatory skin diseases were mimicked using atopic dermatitis (AD)-associated cytokines interleukin (IL)-4, IL-13 and IL-22 in iKC monolayers. Finally, iKC-derived air-liquid interface cultures demonstrated key features of epidermal stratification, including basal Ki67 expression, suprabasal involucrin and filaggrin expression, and terminal differentiation including cornified layers. iKC-HEEs also presented parakeratosis and a weaker epidermal barrier, measured by electrical impedance spectroscopy, as compared to pKC-HEEs, requiring further optimization. Altogether, our improved methodology to generate iPSC-derived keratinocytes facilitates future applications of the iKC to investigate epidermal biology and related diseases.

Introduction

The discovery of induced pluripotent stem cells (iPSC) has revolutionized regenerative medicine. Any somatic cell can be reprogrammed into iPSC with an indefinite *in vitro* lifespan by introducing the four Yamanaka factors [1], providing an unlimited supply of cells that can be genetically modified and differentiated into any cell type. iPSC have been used in numerous studies on disease modeling, drug screening and developing cell therapies, especially in a personalized manner due to their versatile nature [2]. For instance, in investigative dermatology, generating fibroblasts, keratinocytes and other skin cell types from the same donor iPSC facilitates the development of complex skin models in a personalized manner. iPSC-derived skin cells may be preferred over primary cells for availability or accessibility reasons, and to easily introduce or correct genetic disease-associated variants, potentially useful for gene/cell therapies. iPSC are also of interest when studying the developmental process of pluripotent stem cells into skin cell lineages, related to developmental disorders or genodermatoses. Various studies have applied iPSC-derived keratinocytes to unravel molecular mechanisms in genodermatoses, among others epidermolysis bullosa (Table 1). By genetic correction of patient-derived iPSC, *COL7A1* expression was restored in cells with a *COL7A1* patient variant, making cells suitable for regenerative medicine [3].

Next to the huge potential of iPSC for regenerative medicine in genodermatoses, iPSC provide an unlimited cell supply for monolayer cultures and 3D air-liquid interface cultures like human epidermal or skin equivalents (HEE or HSE). 3D cultures are required when studying important features of the epidermis, like stratification and skin barrier formation, and thereby to model epidermal biology and function in health and disease [4]. These key processes are often disturbed in common chronic inflammatory skin diseases, like atopic dermatitis (AD). In AD, the complex interplay between epidermal barrier defects, the overactive immune system and skin microbiome dysbiosis drives disease pathology [5]. Epidermal barrier defects in AD are often displayed by reduced expression of epidermal differentiation proteins like involucrin (IVL) and filaggrin (FLG). This can be a result of genetic predisposition [6] or the presence of inflammatory mediators [7], including T helper (Th)2 derived cytokines interleukin (IL)-4 and IL-13 and Th17/22-derived IL-22 [8]. These disease-associated cytokines have demonstrated to induce different AD hallmarks through *in vitro* studies [9]. Specifically, the presence of IL-22 in a Th2 cytokine milieu appeared crucial to drive epidermal differentiation and barrier defects [10].

Box 1. Differentiation terminology

(iPSC) differentiation	iPSC differentiation toward keratinocytes
Epidermal differentiation	Keratinocyte differentiation (= stratification)
Early epidermal differentiation	Basal keratinocyte differentiation toward spinous keratinocytes
Terminal (epidermal) differentiation	Spinous keratinocyte differentiation toward granular and corneal keratinocytes

Despite the previously mentioned benefits of iPSC for disease modeling, iPSC-derived keratinocytes, also called induced, keratinocytes (iKC) need to meet specific criteria to replace primary keratinocytes (pKC), like the ability to undergo epidermal stratification, terminal differentiation and skin barrier formation. To discriminate between the various types of differentiation or stratification, Box 1 shows the terminology used in this study. So far, immaturity (e.g., low keratinocyte marker expression), heterogeneity and limited proliferation potential have hampered the use of iKC in 3D air-liquid interface cultures. In Table 1 studies are summarized demonstrating the use of iKC in investigative dermatology, that mainly focused on proof-of-concept for the system or on genodermatoses. The morphological description in Table 1 highlights that HEE and HSE cultures from iKC are often less well formed as compared to pKC-derived counterparts. Noteworthy, only two studies applied iKC for inflammatory skin diseases AD or psoriasis with emphasis on genotype-transcriptome correlations rather than 3D models [11, 12]. However, especially for modeling inflammatory skin diseases wherein epidermal proliferation and differentiation malfunction is a key hallmark and target for intervention, homogenous, mature, a proliferative and stratifying iKC cultures are required. Therefore, we here aimed to improve differentiation conditions that can steer iPSC to keratinocytes to better resemble pKC. Retinoic acid (RA) and bone morphogenetic protein 4 (BMP-4)-supplemented keratinocyte serum free medium (KSFM) is commonly used for iPSC to keratinocyte differentiation, and was used as a starting point for optimization (Supplementary Table 1). We compared various seeding densities, coatings, media and timings to add ROCK inhibitor. The reproducibility of iKC differentiation was tested in 2D and 3D culture systems with multiple iPSC lines. Furthermore, the response of iKC to AD cytokines IL-4, IL-13 and IL-22, was investigated to demonstrate the applicability for future studies on disease mechanisms and therapeutic screening.

Table 1. Overview of studies utilizing iPSC derived keratinocytes for dermatological research. Only studies using 2D iPSC to keratinocyte differentiation protocols were included (no 3D organoid differentiations). * Poor resolution of microscopic images in respective publication hampers qualification.

Application	iPSC-derived cells	Type of 3D culture	Epidermal morphology	Reference
Recessive dystrophic epidermolysis bullosa	Keratinocytes	HSE with collagen I and primary fibroblasts	- Multiple cell layers - No stratified epidermis	[13]
Proof-of-concept 3D skin modeling	Keratinocytes, fibroblasts	HSE with collagen I and induced fibroblasts	- Multiple cell layers - Stratified epidermis *NB: no granulosum* *NB: parakeratosis*	[14]
Ectodermal dysplasia	Keratinocytes	-	-	[15]
Unravel pathways regulating epithelial commitment	Keratinocytes	-	-	[16]
Epidermal barrier function	Keratinocytes	HEE	- Multiple cell layers - Stratified epidermis	[17]
Recessive dystrophic epidermolysis bullosa	Keratinocytes	Xenograft	*Xenografts are out of scope here*	[18]
Epidermolysis bullosa	Keratinocytes	HSE with collagen I and primary fibroblasts	- Multiple cell layers - Stratified epidermis* *NB: no granulosum?*	[19]
Proof-of-concept iPSC to keratinocyte differentiation	Keratinocytes	-	-	[20]
Melanin production	Keratinocytes, fibroblasts, melanocytes	HSE with collagen I and induced fibroblasts	- Multiple cell layers - Stratified epidermis *NB: minimal granulosum*	[21]
Recessive dystrophic epidermolysis bullosa	Keratinocytes, mesenchymal stem cells, haematopoietic progenitor cells	-	-	[22]
Genetic and epigenetic footprint during epidermal differentiation	Keratinocytes	HEE	*No H&E available*	[23]
Myelomeningocele	Keratinocytes	HSE with collagen I and primary fibroblasts	- Multiple cell layers - No stratified epidermis *Note: no healthy iPSC were used, so twin-twin transfusion syndrome iPSC-HSE qualified.*	[24]

Table 1. Continued

Application	iPSC-derived cells	Type of 3D culture	Epidermal morphology	Reference
Regenerative medicine	Keratinocytes, fibroblasts	HSE with collagen I and induced fibroblasts	- Minimal cell layers* - No stratified epidermis*	[25]
Atopic dermatitis (genotype)	Keratinocytes	-	-	[11]
Regenerative medicine	Keratinocytes, fibroblasts	HSE with collagen I and induced fibroblasts	- Minimal cell layers* - No stratified epidermis*	[26]
Transdermal drug permeation	Keratinocytes, fibroblasts	HSE with collagen I and induced fibroblasts	- Multiple cell layers - No stratified epidermis	[27]
Recessive dystrophic epidermolysis bullosa	Keratinocytes, fibroblasts	Xenograft	*Xenografts are out of scope here*	[28]
Metabolic plasticity	Keratinocytes, fibroblasts	-	-	[29]
Psoriasis (genotype)	Keratinocytes	-	-	[12]
Proof-of-concept iPSC to keratinocyte differentiation and 3D modeling	Keratinocytes	HEE	- Multiple cell layers - No stratified epidermis	[30]
Regenerative medicine	Keratinocytes, fibroblasts, endothelial cells	Xenograft of spheroids	*Xenografts are out of scope here*	[31]
Fanconi anemia and squamous cell carcinoma susceptibility	Keratinocytes	HSE with collagen I and primary fibroblasts	- Multiple cell layers - Stratified epidermis* *NB: no granulosum?*	[32]
Congenital ichthyosis	Keratinocytes	-	-	[33]
Proof-of-concept iPSC to keratinocyte differentiation and 3D modeling	Keratinocytes, fibroblasts	HSE with primary fibroblasts in polystyrene scaffold	- Multiple cell layers - Stratified epidermis* *NB: no granulosum?* *NB: no continuous corneum?*	[34]
Dystrophic Epidermolysis Bullosa	Keratinocytes, fibroblasts, melanocytes	Xenograft	*Xenografts are out of scope here*	[3]

Methods

iPSC culture

iPSC line 1 (Supplementary Table 2) was cultured on vitronectin XF (Stem cell technologies)-coated plates in E8F plus medium (Gibco). iPSC line 2 and 3 (Supplementary Table 2) were kindly provided by the LUMC hiPSC core facility and cultured on vitronectin XF (Stem cell technologies)-coated plates in mTESR plus medium (Stem cell technologies). All iPSC lines were cultured at 37 °C with 5% CO_2 with fresh medium every other day.

iPSC to keratinocyte differentiation

For directed differentiation, iPSC were singularized using Accutase (Gibco) and seeded onto geltrex (Gibco)-coated plates with or without rat tail collagen type I (from rat tail, Sigma-Aldrich) (Figure 1A). iPSC were cultured in E8F plus (Gibco) (iPSC1) or mTESR plus medium (Stem cell technologies) (iPSC2 and 3) including 1x Revitacell (Gibco) or 10 µM Y-27632 (MedChem) for the first day. After two days, medium was switched to KSFM (Gibco) or CnT-30 (CELLnTEC), with 1 µM all-trans RA (Sigma-Aldrich) and 10 ng/mL BMP-4 (Peprotech). When KSFM was used, cells were split at day 7 using Accutase onto geltrex-collagen I coated plates. 10 µM ROCK inhibitor Y-27632 (MedChem) was added from day 7 (KSFM) or 8 (CnT-30) onwards. The following small molecule compounds were tested: 100 nM JAK inhibitor I (Sigma Aldrich), 1 µM kenpaullone (KLF4 inhibition, StemPro) and 10 µM LY294002 (PI3K inhibition, MedChem). Between day 27 and 30 of differentiation, iPSC-derived keratinocytes were stimulated or stored in liquid nitrogen until further use. For storage, iKC were dissociated using 5 mg/ml dispase (grade II, Sigma-Aldrich) and frozen in DMEM (Sigma-Aldrich) + 10% fetal bovine serum (FBS) (Cytiva) + 10% DMSO (Sigma-Aldrich). All reagents that were tested to passage iKC are listed in Supplementary Table 3.

To induce 2D epidermal differentiation, 2mM $CaCl_2$ (Fluka) or 10% FBS (Cytiva) was added to CnT-30 medium. To induce 2D inflammatory signaling, iKC were treated with a cytokine cocktail containing 50 ng/mL IL-4, 50 ng/mL IL-13 and 10 ng/mL IL-22 (all Peprotech).

iKC culture and human epidermal equivalent (HEE) generation

iKC were seeded onto 1 µg/cm^2 collagen IV (from human placenta, Sigma-Aldrich)-coated plates in CnT-30 with 10 µM ROCK inhibitor Y-27632. Cultures were maintained at 37 °C with 5% CO_2, refreshed every other day and split using 5mg/mL dispase (grade II, Sigma-Aldrich). For HEE generation, dispase-dissociated cells were

counted and 150,000 iKC were seeded per transwell as previously described [35] with the following modification: 24-wells transwell inserts (Nunc) were coated with 4 µg/insert collagen IV and cells were grown in CnT-30 with 10 µM ROCK inhibitor Y-27632 in the submerged phase. The number of cells seeded or the duration of the submerged phase were according to this protocol unless stated otherwise.

Electrical impedance spectroscopy (EIS) measurement

The electrical impedance spectra were measured according to previously determined protocol [36]. In brief, HEEs were acclimatized to room temperature and brought to the middle position of the 24-transwell system with 1600 µL PBS underneath and 500 µL on top. After calibration using PBS in a regular 24-wells plate (PBS blank), 30 electrical pulses ranging from 10 Hz to 100,000 Hz were run through the HEEs and the impedance (Ω) was measured using the Artemis device with SmartSense lid (Locsense). Impedances were corrected for the PBS blank, and the area under the curves (AUC) were calculated between 127Hz and 2212Hz as a proxy for the differentiation status (EIS^{diff}) and between 28,072Hz and 100,000Hz for *stratum corneum* thickness (EIS^{sc}). Next, the percentages of EIS^{diff} and EIS^{sc} relative to the pKC were calculated and visualized.

RNA isolation and real-time quantitative polymerase chain reaction (RT-qPCR) analysis

Total RNA was isolated using the Quick-RNA Microprep Kit (ZYMO research) according to manufacturer's protocol. cDNA synthesis was performed with UltraScript reverse transcriptase (PCRBiosystems), followed by real-time quantitative PCR (RT-qPCR) with Sybr Green (Bio-Rad) and the primers listed in Supplementary Table 4. Raw ct values measured by the CFX Connect™ Real-Time System (Bio-Rad) were normalized to the expression of Ribosomal Protein Lateral Stalk Subunit P0 (RPLP0). The $2^{-\Delta\Delta CT}$ method [37] was used to calculate relative expression levels.

Morphological and immunohistochemical analysis

For immunostaining of monolayer cell cultures, iKC were passaged onto collagen I (rat tail, Sigma-Aldrich)-coated coverslips and fixed upon confluency using 4% formaldehyde solution (Sigma-Aldrich). Cells were permeabilized for 15 minutes with 0.1% TritonX (ThermoFisher) and antigen retrieval was performed for 10 min in boiling citrate buffer (1.8 mM citric acid and 8.2 mM sodium citrate). Coverslips were blocked for 1 hour with 5% normal donkey serum (SouthernBiotech). Primary antibodies (Supplementary Table 5a) in 1% BSA/PBS were incubated overnight in 1% BSA (ThermoFisher) in PBS at 4°C. Secondary antibodies (diluted 1:200 in 1% BSA/PBS) donkey anti-mouse IgG (Alexa Fluor 647, ThermoFisher) and donkey

anti-rabbit IgG (Alexa Fluor 488, Abcam) were applied for 1 hour. Coverslips were mounted with Fluoromount-G with DAPI (ThermoFisher).

For hematoxylin and eosin (H&E) or immunostaining of HEEs, samples were fixed in 4% formaldehyde solution (Sigma-Aldrich) for 1 hour and paraffin (Leica) embedded. 6 µm paraffin sections were H&E stained or used for immunohistochemistry as follows: sections were blocked with 5% normal horse serum (FLG, IVL, KRT10) (Vector laboratories), normal goat serum (Ki67) (SouthernBiotech) or normal donkey serum (claudin (CLDN)1/4) (SouthernBiotech) in PBS for 15 minutes. Primary antibodies (listed in Supplementary Table 5b) were diluted in 1% BSA/PBS (all except CLDN1/4) or 3% BSA/PBS (CLDN1/4) and incubated for 1 hour at room temperature, followed by biotinylated secondary antibodies (Vector laboratories) 1:200 dilution in 1% BSA/PBS, donkey-anti rabbit AF488 (CLDN1) (Abcam) or donkey anti-mouse AF647 (CLDN4) (Invitrogen) in 3%BSA/PBS for 30 minutes. Next, all sections except for CLDN1/4 were incubated with avidin-biotin complex (Vector Laboratories) for 30 minutes and protein expression was visualized using 3-Amino-9-ethylcarbazole (AEC) (Merck Millipore) and nuclei were counterstained with heamatoxylin. Sections were mounted with glycerol gelatin (Sigma Aldrich). For CLDN1/4, sections were enclosed in Fluoromount-G™ met DAPI (Invitrogen).

Bulk RNA-sequencing

To prepare RNA sequencing libraries, 400 ng of RNA was used in combination with the KAPA RNA HyperPrep kit with RiboErase (human/mouse/rat [HMR]) (Kapa Biosystems). Oligonucleotide hybridization, rRNA depletion and cleanup, DNase digestion and cleanup, and RNA elution were executed according to manufacturer's protocol. Fragmentation and priming was performed at 94°C for 6 minutes. First- and second-strand synthesis, and A-tailing were executed according to manufacturer's protocol. For adapter ligation, a 1.5 µM stock (NEXTflex DNA barcodes; Bio Scientific) was used. Post-ligation cleanups were performed according to manufacturer's protocol, with eight cycles of library amplification and a 0.8× bead-based cleanup. To determine the library size, high-sensitivity DNA bioanalyzer (Agilent Technologies) was used. To measure the library concentration, the DeNovix double-stranded DNA (dsDNA) high-sensitivity assay was executed. The Illumina NextSeq 500 instrument was used for sequencing and 42bp-paired end reads were generated.

Bulk RNA-sequencing analysis

RNA-sequencing data was analyzed using the seq2science RNA-seq workflow [38] version 0.9.5, like previously described [39]. GRCh38.p13 was used for mapping bulk RNA-seq reads to the genome.

KEGG pathway analysis of differentially expressed genes (DEG) between pKC and iKC from CnT-30 medium (p adjusted below 0.05, Log2FC below 0.5 or above 2) was performed with the online tool DAVID Bioinformatics [40].

Single-cell (sc)RNA-sequencing

To generate scRNA-seq libraries from iKC and pKC, the GEXSCOPE® Single Cell RNA Library Kit Cell V2 (4180011, Singleron) was used. In brief, the SCOPE-chip SD was primed with absolute ethanol (Merck) and 0.02% v/v Tween-20 (Sigma-Aldrich) in PBS, and barcode beads and lysis mix were prepared according to manufacturer's protocol. Next, 0.25% trypsin-EDTA (Gibco) was used to detach cells and make single cell suspensions of iKC and pKC for scRNA-sequencing. Blocking of trypsin-EDTA was performed with 10% FBS (Cytiva) in DMEM (Sigma-Aldrich), and cells were washed in DPBS (Gibco) and counted. The cell suspension was filtered through a 30 µm cell strainer (CellTrics) and diluted until 350000 cells/mL. The SCOPE-chip was washed with PBS before loading of 100 µL cell suspension. Cells in the microwells were washed twice with PBS and barcode beads were loaded before washing again. 100 µL lysis mix was injected and incubated at room temperature for 20 minutes to allow mRNA binding to barcode beads. The singleron magnetic rack was placed under the SCOPE-chip and the chip was washed with wash buffer A (Singleron). Retrieval of cells in wash buffer A was performed by placing the magnetic rack on top of the chip. Reverse transcription, cDNA amplification and purification were performed according to manufacturer's protocol. cDNA concentrations were measured with the DeNovix dsDNA High Sensitivity Assay for Thermo Fisher Qubit™ 3.0 / 4 Fluorometers and the fragment size profiles with the Agilent 2100 Bioanalyzer Instrument High Sensitivity DNA kit. After manufacturer's cDNA quality control criteria where met, libraries were prepared and amplified according to manufacturer's protocol. Library quality control was performed using the DeNovix dsDNA High Sensitivity Assay and Agilent 2100 Bioanalyzer Instrument High Sensitivity DNA kit. The Illumina NovaSeq X instrument was used for sequencing and 150bp paired-end reads were generated.

ScRNA-sequencing analysis

GRCh38.p14 was used for mapping scRNA-seq reads to the genome.

Pre-processing and quality control of scRNA-seq

The CeleScope v2.0.7 pipeline [41] was run with default parameters described in GSE285034 [42] to retrieve the matrix, barcodes and features files necessary for downstream analysis. scRNA-seq datasets were analyzed in Python with Scanpy version 1.9.6 [43], as described in the GitHub repository. scRNA-seq cells were

selected with a minimum count of 2000, a maximum count of 100000, a feature number higher than 1000 and lower than 10000 as well as a mitochondrial percentage lower than 30 percent. Expected doublets were removed with Scrublet 0.2.3 [44]. Only cells with a mitochondrial ratio lower than 30 percent were selected.

Clustering and integration of scRNA-seq datasets

Clustering in each dataset was conducted with specific parameters from dimension numbers (Elbow plot) and with clustering resolution using Clustree version 0.5.0 [45]. Clustering of scRNA-seq data on the two conditions: iKC separate vs. iKC + pKC integrated, was performed with Leiden clustering [46], using 30 dimensions and 10 for the neighbors parameter. The most optimal clustering resolutions were determined by analyzing the clustering scores for the silhouette index [47], Davies-Bouldin index [48] and Calinski-Harabasz index [47], resulting in final clustering resolutions of 0.1 (iKC separate) and 0.05 (iKC + pKC integrated). iKC integrated with pKC datasets were first clustered on marker genes in individual datasets and were then integrated with scVI [49] (scvi-tools version 1.0.0). The parameters for the Variational Autoencoder were selected as 2 for “n_layers”, 30 for “n_latent” and "nb" for “gene_likelihood”.

Statistical analysis of RT-qPCR and EIS data

Data are presented as mean +/- SEM. Raw ΔCt values were used to test for statistical significance of RT-qPCR data, and AUC values for EIS data. One-way analysis of variance followed by Tukey, Dunnett or Bonferroni (indicated in figure legends) *post hoc* testing was performed in GraphPad Prism version 10. P-values of <0.05 were considered statistically significant, with * = p-value below 0.05, **= p-value below 0.01, ***=p-value below 0.001 and ****=p-value below 0.0001.

Results

Optimized pluripotent stem cell differentiation into iKC by defined cell culture conditions

To improve iPSC to keratinocyte differentiation, we used a previously established protocol [50, 51] and tested i) various seeding densities (500/cm2 to 4000/cm2), ii) coatings after splitting at day 7 (geltrex, collagen I, collagen IV), and iii) timings of adding ROCK inhibitor Y-27632 (not at all or starting between day 7 and 14) using iPSC1 (Supplementary Table 2, Supplementary Figure 1A). In KSFM, we observed the most optimal attachment, proliferation/viability and keratinocyte marker expression when the following culture conditions were applied: 1000/cm2 iPSC

were seeded; splitting onto collagen IV coated plates at day 7; and ROCK inhibitor added from day 7 onwards (Figure 1A, orange box). However, morphological heterogeneity was still apparent (Figure 1B, left). To increase cell culture homogeneity and remove fibroblast-like cells, EDTA washing before splitting or removal of non-adherent cells after 30 minutes during splitting was performed, but unfortunately proven unsuccessful.

Next, we compared the use of KSFM to CnT-30 medium in the differentiation protocol, the latter being a chemically defined medium specifically developed for differentiation of pluripotent stem cells into epithelial lineages. Differentiating cells grew slower in CnT-30, as compared to those in KSFM. In KSFM, differentiating cells became fully confluent and needed to be passaged after one week, whereas in CnT-30 passaging was not necessary. Therefore, to accommodate growth and differentiation of iPSC in becoming iKC, we designed a combination coating of geltrex and collagen I for the complete iPSC to iKC differentiation when CnT-30 was used (Figure 1A, red box). Under this condition, cultures were more homogeneous with a majority of cobblestone-like cells (Figure 1B, right, indicative for epithelial cell fate) and showed higher keratinocyte marker expression levels at day 30 (Figure 1C). To assess the similarities and differences between iKC and pKC bulk RNA-sequencing was performed. In this analysis, we also included RNA-seq data of a pluripotent stem cell (PSC) line for comparison. Principal component analysis demonstrated that the cell state of day 30 iKC in both KSFM and CnT-30 was closer to pKC than to PSC, mainly shown by PC1 (57% variance, Figure 1D). As compared to PSC, iKC showed reduced expression of pluripotency genes including *POU5F1* encoding OCT4, and increased expression of epithelium and keratinocyte genes like *TP63*, *KRT5*, *KRT14* and *ITGB6* (Figure 1E, F). As compared to pKC, marker genes for early epithelial cells such as *TP63* and *ITGB6* reached similar levels in iKC from both media, showing that the commitment to the epithelial lineage was overall successful. Basal keratinocyte marker gene expression, *KRT5* and *KRT14,* was lower in iKC than pKC. Yet, expression levels were higher in CnT-30 than in KSFM, corroborating the cellular morphology and confirming that CnT-30 medium improved the differentiation protocol and iKC outcome (Figure 1F). Therefore, the CnT-30 condition was selected for further data analyses and follow up experiments.

Data- and hypothesis-driven small molecule compounds do not improve iKC generation

To identify potential pathways which could be targeted in further optimization strategies to push iKC to a cell state being more similar to pKC, differentially expressed genes (DEG) between iKC from CnT-30 and pKC (PC2, Figure 1D) were

used. iKC showed higher expression of inflammatory (GO "response to virus") genes like CXCL10 and lower expression of basal keratinocyte (GO "epidermis development") genes as compared to pKC (Figure 1F, Supplementary Figure 1B, C). KEGG analyses indicated underlying pathways, like increased JAK/STAT pathway-related genes, as well as PI3K/Akt/mTOR genes, in iKC than in pKC (Supplementary Table 6). We therefore targeted these pathways by JAK inhibitor I and LY294002 from day 7 onwards, in previously determined concentrations. PI3K inhibitor led to major cell death, also when added later or only for a short time period, indicating this pathway is crucial for cell survival as previously suggested [52]. JAK inhibition did not induce any morphological changes, nor improved keratinocyte gene expression in iKC (Supplementary Figure 1D). Being suggested to promote expansion of functional keratinocyte precursors [53], kenpaullone was supplemented from day 20 onwards for KLF4 inhibition. Kenpaullone did not affect the morphology, proliferation rates nor change epithelial and keratinocyte marker gene expression levels (Supplementary Figure 1D). Target gene expression of *CCL5*/*CXCL10* for JAKi (unpublished data, [54]) and *CYP1A1*/*CYP1B1* for KLF4i (unpublished data, [55]) was not majorly altered by the inhibitors (Supplementary Figure 1E). Altogether, the selected small molecule compounds did not benefit the iKC differentiation in the tested conditions (concentration, timing).

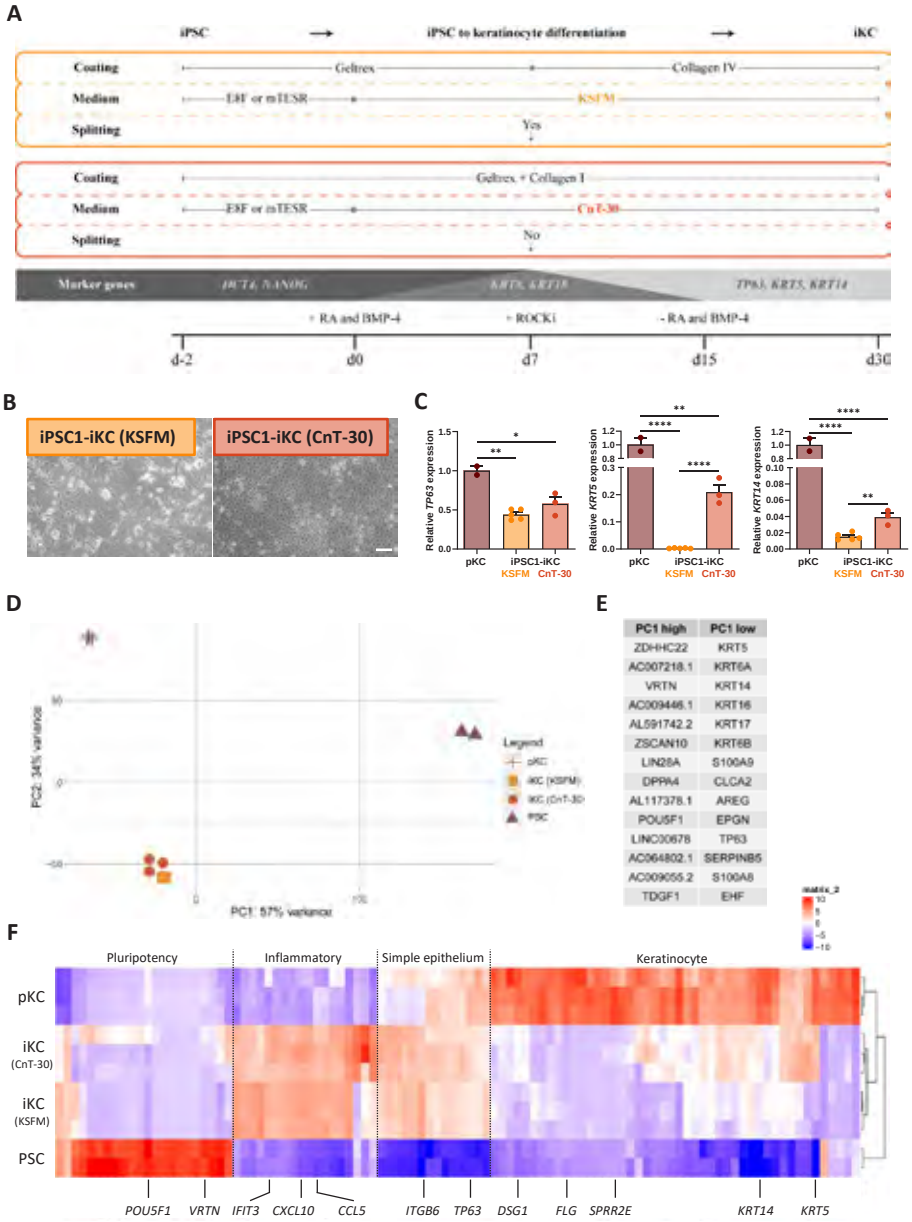

Figure 1. Comparison of iPSC to keratinocyte differentiation in KSFM and CnT-30 medium. **A**) Schematic overview of the cell culture protocols. **B**) Phase contrast image of iKC cultures. Scale bar = 100 µm. **C**) mRNA expression of epithelium (*TP63*) and keratinocyte (*KRT5/14*) marker genes. Data is presented as mean +/- SEM and all conditions were statistically compared by one-way ANOVA with Tukey's *post hoc* correction. **D**) Principal Component Analysis (PCA) on bulk transcriptomes of PSC, pKC and iKC differentiated in KSFM and CnT-30. **E**) Genes that drive PC1 in the PCA. **F**) Heatmap of the 100 most differential genes between PSC, iKC and pKC. All iPSC1-iKC data is representative for N=3 technical replicates.

Reproducibility of iPSC to keratinocyte differentiation with multiple iPSC lines

Since (epithelial) commitment across experiments and iPSC lines can be irreproducible [56], we addressed the robustness of our optimized differentiation protocol by differentiating three independent iPSC lines established from different donors (Supplementary Table 2) into iKC. All iPSC lines showed epithelial commitment based on cobblestone-morphology and high expression of early epithelium markers *KRT18* and *TP63*, keratinocyte markers *KRT5* and *KRT14*, and low expression of fibroblast marker *VIM* (Figure 2A-C). Protein expression of P63 and KRT14 validated the mRNA data, but interestingly, not all P63 positive cells were KRT14 positive, indicating culture heterogeneity issues (Figure 2D). Noteworthy, more cell death was observed in iPSC1-derived cultures yielding fewer cells for analysis or subculturing experiments. Hence, for further experiments only iPSC2 and iPSC3-iKC were used.

scRNA-sequencing reveals three cell populations in the iKC culture

Notwithstanding the reproducibility of our differentiation protocol, heterogeneity issues remained. To investigate the degree of cell heterogeneity in the iKC culture, we performed single-cell (sc)RNA-sequencing on iPSC2-iKC and pKC. After quality control analysis (Supplementary Figure 2A-F), 1618 iKC cells and 25785 pKC cells were further analyzed. Using Uniform Manifold Approximation and Projection (UMAP) visualization, data integration of iKC and pKC (Figure 3A) revealed three cell clusters (Figure 3B). Cluster 1 and 3 clustered separately and mainly consisted of iKC, whereas cluster 2 was a mixture of iKC and pKC. Highly variable gene analysis demonstrated that cluster 1 contained cells expressing early epithelium genes *KRT8* and *KRT18* (Figure 3C). Cells from cluster 2 expressed high levels of *TP63*, *KRT5*, *KRT15*, *COL17A1*, *ITGA6* and *DSG3* that are typical for basal keratinocytes. In cluster 3, cells expressed genes like fibroblast markers *VIM* and *FAP*, and neuronal markers *NCAM1*, *DCX*, *ENO2* and *NEFL*. That iKC were clustered into three distinct groups was consistent with the analysis of iKC only, showing similar marker gene expression (Supplementary Figure 3A, Table 2). Overall, iKC in cluster 2 most closely resembled the transcriptome of pKC. Interestingly, among the highly variable genes between the clusters, cell surface markers like *ITGA6* were enriched in iKC cluster 2 and pKC (Figure 3D, Supplementary Figure 3B). In contrast, *V-Set Domain Containing T Cell Activation Inhibitor 1* (*VTCN1*) was highly expressed in cluster 1 only and *platelet-derived growth factor receptor alpha* (*PDGFRA*) in cluster 3 (Figure 3E, F, Supplementary Figure 3C, D). This suggests that positive and/or negative sorting strategies could be applied to enrich keratinocyte-like cells from the iKC population.

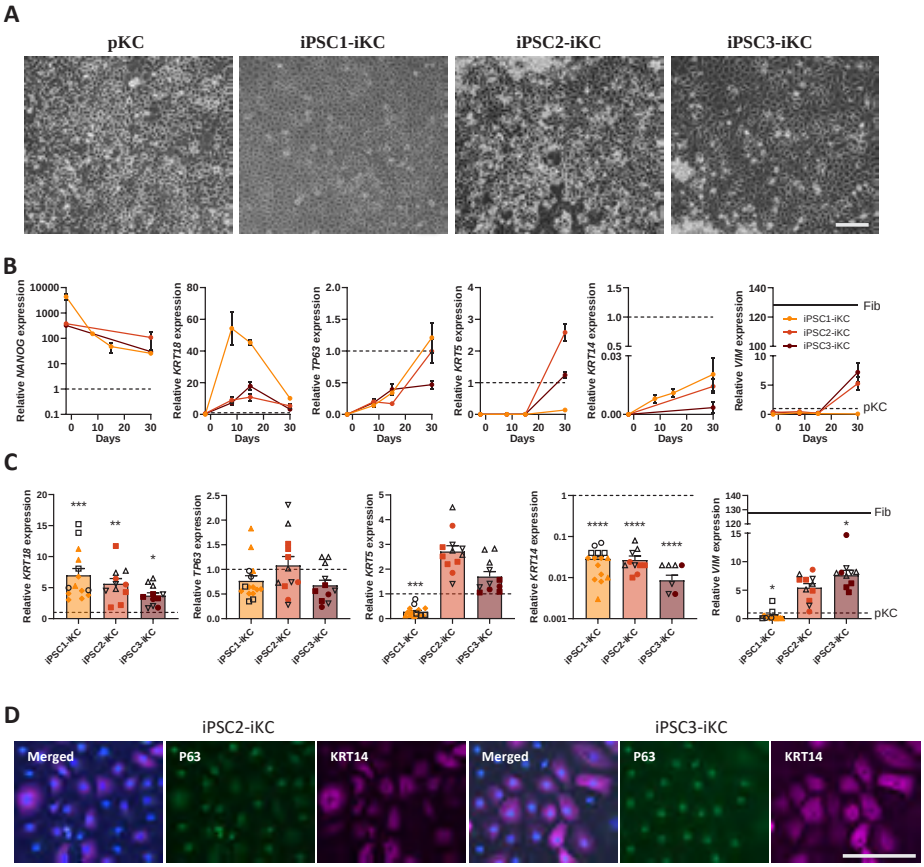

Figure 2. Reproducibility of iPSC to keratinocyte differentiation using the optimized protocol with various iPSC lines. (**A**) Phase contrast image of iKC and pKC. (**B**) mRNA expression levels of pluripotency (*NANOG*), early epithelium (*KRT18*), epithelium (*TP63*), keratinocyte (*KRT5, KRT14*) and fibroblast (*VIM*) marker genes over time. Dashed line indicates pKC expression levels, straight line is representative of primary fibroblast cultures (Fib). (**C**) mRNA expression levels of early epithelium (*KRT18*), epithelium (*TP63*), keratinocyte (*KRT5, KRT14*) and fibroblast (*VIM*) marker genes. iKC were statistically compared to pKC by one-way ANOVA with Dunnett's *post hoc* correction. (**D**) Protein expression of P63 and KRT14 after differentiation. Scale bar = 100µm. All day 30 iKC data is representative for N=2 or more technical replica per biological replica (iPSC1, 2 and 3). Data is presented as mean +/- SEM.

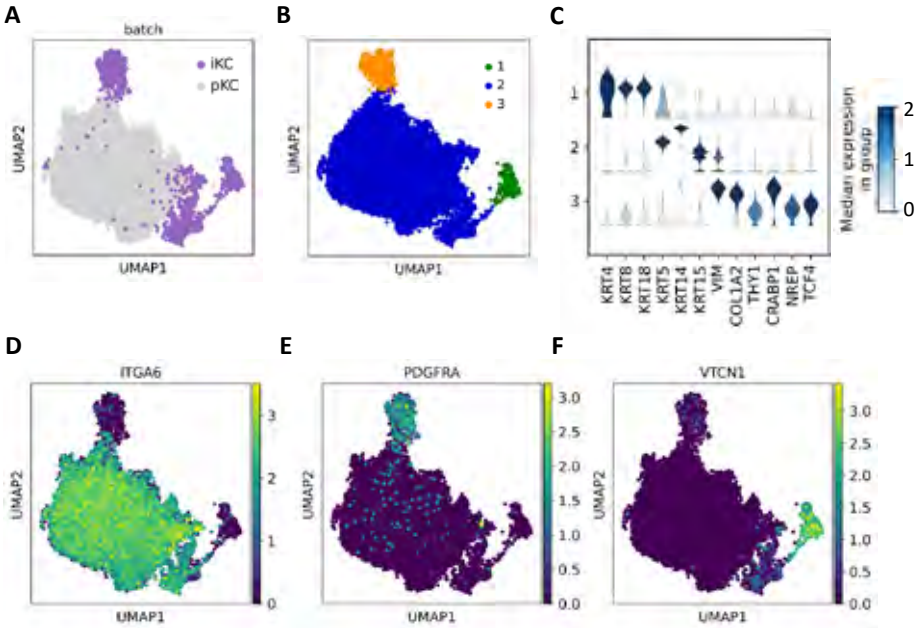

Figure 3. Clustering of iPSC2-iKC and pKC based on single-cell RNA-sequencing. (**A**) UMAP visualization of iKC and pKC, (**B**) UMAP clustering of the integrated population of iKC and pKC, (**C**) Highly variable genes between the three clusters, (**D**) Expression of keratinocyte-related cell surface marker gene *ITGA6*, (**E**) Expression of fibroblast-related cell surface marker gene *PDGFRA*, **F**) Expression of epithelium-related cell surface marker gene *VTCN1*.

Table 2. Highly variable genes per cluster of iPSC2-iKC only. *(This table is available upon request via the Radboud Data Repository: ru.rumc.p4fikc_r0005499a_dsc_696)*

Subculturing of iKC improves their resemblance to primary keratinocytes

Aside from reproducible protocols and cell culture homogeneity, we examined the proliferative potential of iKC as an important parameter for successful expansion of the desired cell populations. We also hypothesized that expansion by subculturing on collagen IV-coated plates could enrich for the keratinocyte-like cells (cluster 2), given the presence of collagen IV in the basement membrane that basal keratinocytes adhere to [57]. In addition, the extended culture time could potentially further mature the early epithelial-like cells (cluster 3). To detach iKC, we tested five different reagents (Supplementary Table 3). From these, dispase yielded the best detachment with least cell death and optimal re-attachment after passaging, and was used to subculture iPSC2- and iPSC3-iKC from passage (P)0 to P9. Remarkably, expression levels of *TP63*, *KRT5* and *KRT14* greatly increased during the first four passages reaching levels similar to pKC (Figure 4A). The cobblestone morphology of iKC was maintained up till passage (P)8/9 (Figure 4B, dashed line) but also many enlarged senescent cells appeared at these later passages (Figure 4B,

solid line). Since *KRT14* expression in iKC already peaks around P5/6 and minimal enlarged cells were present, these passages were used for follow-up experiments.

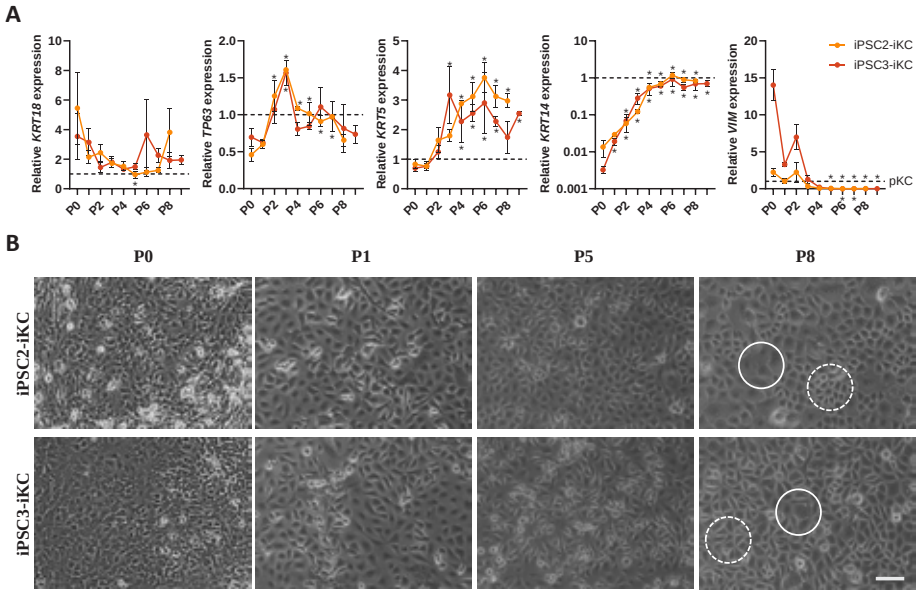

Figure 4. Subculturing of induced keratinocytes derived from IPSC2 and 3. (**A**) mRNA expression levels of early epithelium (*KRT18*), epithelium (*TP63*), keratinocyte (*KRT5*, *KRT14*) and fibroblast (*VIM*) marker genes. Data is presented as mean +/- SEM. iKC were statistically compared to P0 by one-way ANOVA with Dunnett's *post hoc* correction. (**B**) Phase contrast image of iKC cultures, solid line: enlarged cells, dashed line: cobblestone cells. Scale bar = 100µm. All iKC data is representative for N=2 or more technical replica per biological replica (iPSC2 and 3). * = p-value below 0.05.

iKC are capable of early epidermal differentiation

To test the functionality of iKC and their ability to epidermally differentiate (see Box 1 for differentiation terminology), we applied known protocols to induce epidermal differentiation in monolayers by addition of calcium (Ca^{2+}, 96 hours) [58, 59] or fetal bovine serum (FBS, 72 hours) [51, 60]. Both protocols resulted in cell flattening of P0 and P5/6 iKC (Figure 5A, B), a feature in keratinocyte monolayers which typically mimics characteristics of suprabasal (differentiated) keratinocytes in the epidermis [61]. Epidermal differentiation marker expression of *KRT1* was significantly decreased upon FBS in P0 iKC and even much stronger in P6 iKC (Figure 5C). However, upon Ca^{2+}, *KRT1* expression was significantly increased in P5 iPSC3-iKC. Epidermal differentiation marker *IVL* was increased during FBS-induced epidermal differentiation of both P0 and P6 iKC, with a stronger induction in P6 as compared to P0 iKC (Figure 5C). Interestingly, contact inhibition upon confluency was potent

enough to elevate *IVL* expression levels in P5 iKC (Figure 5D), a phenomena observed in pKC as well [62, 63]. Thus, subcultured iKC cultures function more similar to pKC and are better suitable for epidermal differentiation experiments than P0 iKC.

iKC can model epidermal differentiation defects by inflammatory skin disease cytokines

Given the capacity of iKC to mimic (early) epidermal differentiation, we questioned the applicability of iKC to study defects in the epidermal differentiation program as typically seen in inflammatory skin diseases resulting in skin barrier defects [6-8]. We differentiated P0 and P6 iKC with FBS in presence or absence of AD-associated cytokines. The effect of the Th2 cytokine mix entailing IL-4 and IL-13 was compared to the added effect of IL-22 to the Th2 mix, which is known to exert additive effects in pKC [10]. While morphological flattening was not prevented by the cytokines in both P0 and P6 iKC (Figure 6A, B), expression of epidermal differentiation genes *KRT1* and *IVL* in P0 iPSC2-iKC (but not iPSC3-iKC) treated with Th2 + IL-22 appeared reduced (Figure 6C). Stronger effects were observed in P6 iKC, where inhibition of *KRT1* and *IVL* expression by the Th2 mix was already significant and even more by Th2 + IL-22 (Figure 6D). Next to epidermal differentiation defects, *Carbonic Anhydrase-2* (*CA2*) is an AD-specific marker gene known to be elevated in AD lesional skin and Th2-induced AD monolayer cultures [64]. In P0 and even more significant in P6 iKC, *CA2* expression was increased upon stimulation with AD-associated cytokines (Figure 6C, D). Inflammatory gene *CCL2* was significantly increased by Th2 cytokines (3 to 9-fold) and even stronger by Th2 + IL-22 (5 to 21-fold) in P6 iKC (Supplementary Figure 4A). *CCL20* was significantly but not substantially altered by Th2 + IL-22 as compared to FBS alone (2-fold up in iPSC2-iKC and not even 2-fold down in iPSC3-iKC). P0 iKC did not show effects upon cytokines on *CCL* expression, again suggesting they are less similar to pKC than the P6 iKC. This minor inflammatory response to cytokines could not be explained by the level of IL-4 and IL-13 receptor expression, which was low in iPSC but at similar levels in iKC as in pKC (Supplementary Figure 4B).

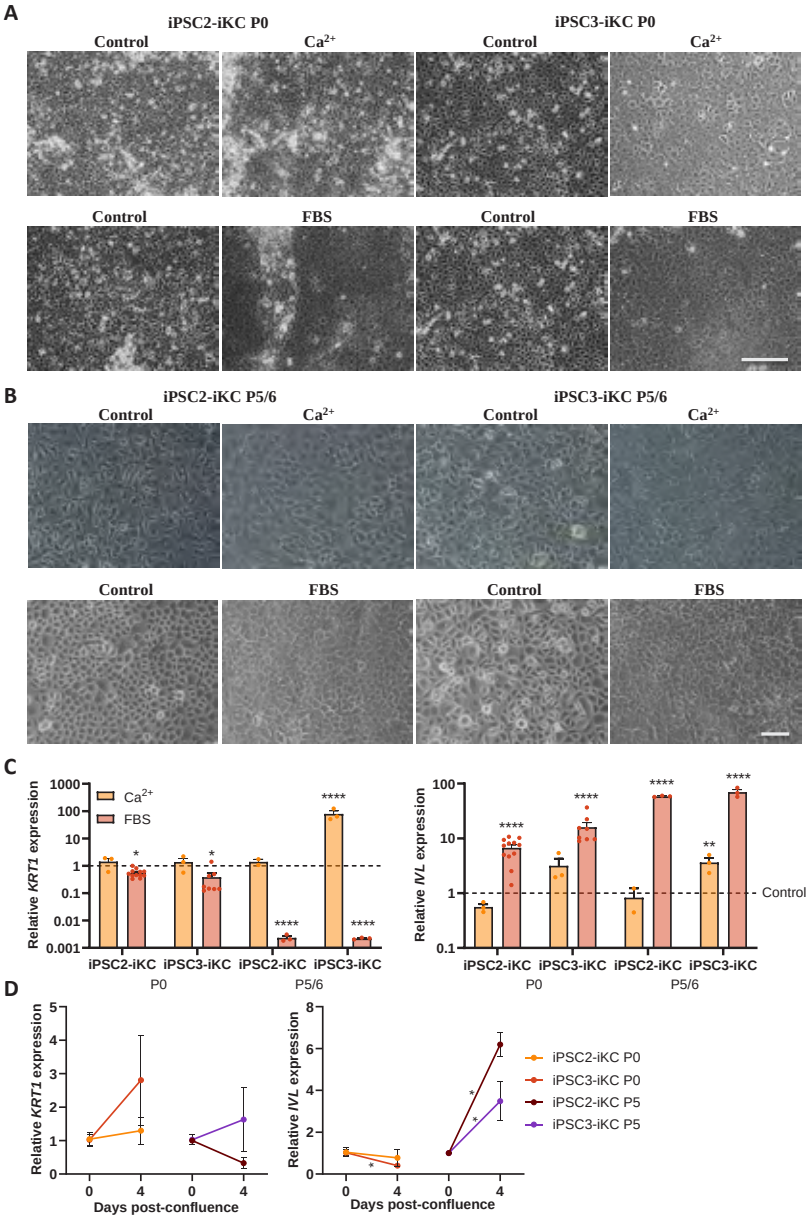

Figure 5. The response of iKC to epidermal differentiation inducers calcium (Ca^{2+}), fetal bovine serum (FBS) and contact inhibition (confluency). (**A**) Phase contrast images of P0 iKC upon Ca^{2+} and FBS. (**B**) Phase contrast images of P5 iKC upon Ca^{2+} and P6 iKC upon FBS. (**C**) mRNA expression levels of epidermal differentiation marker genes *KRT1* and *IVL* in P0 and P5/6 iKC upon Ca^{2+} and FBS. (**D**) mRNA expression levels of *KRT1* and *IVL* over time in P0 and P5 iKC upon contact inhibition. All data is representative for N=2 or more technical replica per biological replica (iPSC2 and 3), and presented as mean +/- SEM. iKC were statistically compared to the control (for C) or to timepoint 0 (for D) by one-way ANOVA with Dunnett *post hoc* correction. Scale bar = 100µm.

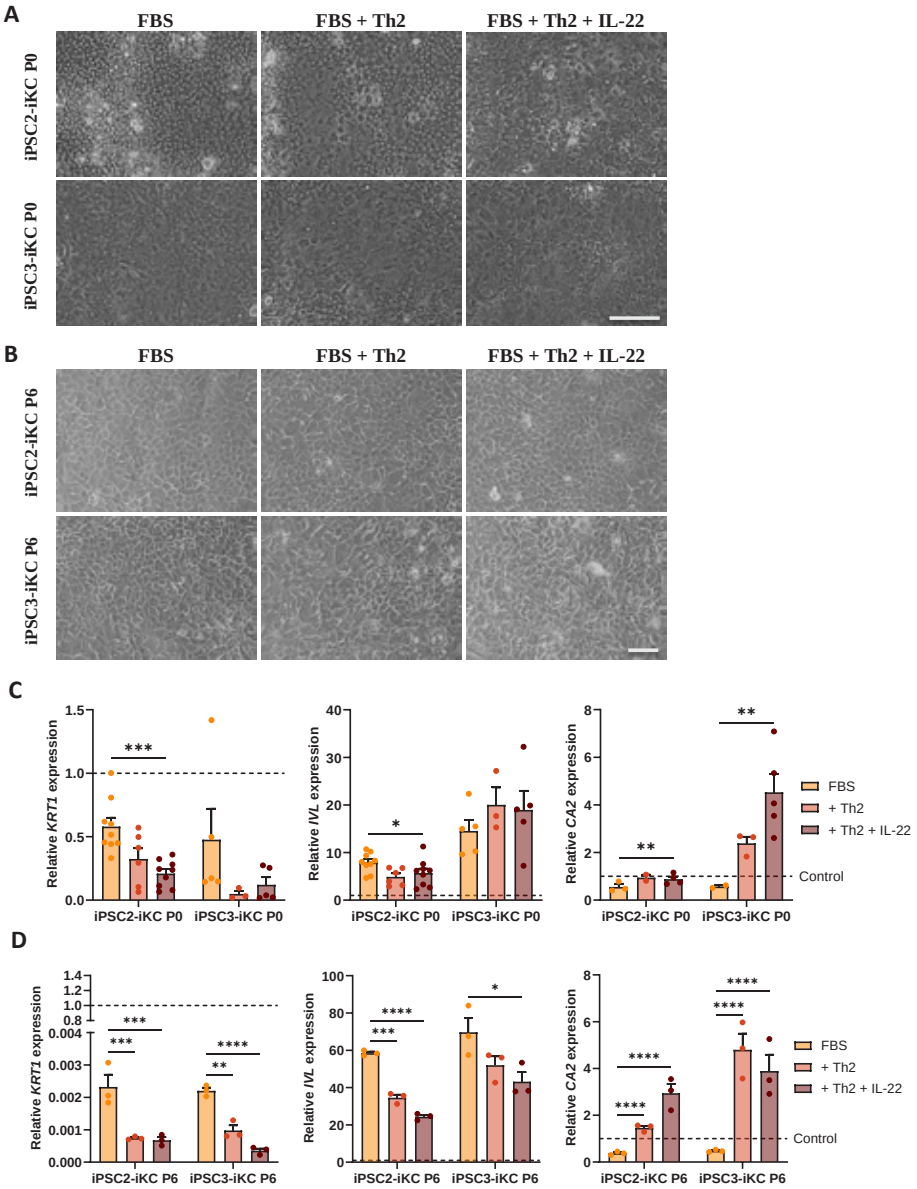

Figure 6. The effect of AD cytokines on FBS-driven iKC responses. (**A**) Phase contrast image of P0 iKC upon FBS and AD cytokines. (**B**) Phase contrast image of P6 iKC upon FBS and AD cytokines. (**C**) mRNA expression levels of epidermal differentiation marker genes *KRT1* and *IVL* and AD marker *CA2* upon FBS and AD cytokines in P0 iKC. (**D**) mRNA expression levels of *KRT1*, *IVL* and *CA2* upon FBS and AD cytokines in P6 iKC. All iKC data is representative for N=2 or more technical replica per biological replica (iPSC2 and 3), and presented as mean +/- SEM. Conditions were statistically compared to FBS by one-way ANOVA with Dunnett's *post hoc* correction. Scale bar = 100µm.

iKC are suitable for human epidermal equivalent generation

Given that 3D human epidermal equivalents (HEE) are preferred over monolayer cultures to model terminal epidermal differentiation and epidermal barrier function, we applied iKC in our air-liquid interface culture system. While P1 iPSC3-iKC did not form any suprabasal layers within 4 days of the air-liquid interface (ALI) culture, P1 iPSC2-iKC formed multiple epidermal layers (Figure 7A). Again, subcultured iKC demonstrated improved epidermal differentiation, mainly for iPSC3-iKC which presented suprabasal layers when used at P6 (Figure 7B). Whereas P1 iPSC2-iKC expressed minor levels of KRT10 and barely any IVL, P6 iPSC3-iKC showed higher expression levels of both (Figure 7C, D). The proliferation capacity in the basal layer measured by Ki67 expression was maintained with any of the iKC. We also compared the presence and absence of ROCKi Y-27632 in the air exposed phase, and found ROCKi to induce swelling of HEEs and to reduce the epidermal thickness (Figure 7E). ROCKi treated HEEs were therefore not further analyzed.

By extending the ALI phase to the regular 8 days, P6 iPSC2-iKC showed improved KRT10 and IVL expression, and slight expression of late epidermal differentiation protein FLG (Figure 8). P6 iPSC3-iKC even generated all epidermal strata, including *stratum granulosum* and *corneum*, with prominent expression of KRT10 and IVL in suprabasal layers and FLG in the granular layer, while maintaining proliferative Ki67+ cells in the basal layer. However, in contrast to pKC, the orientation of basal iKC appeared more horizontal and parakeratosis was present in the *stratum corneum*. With respect to epidermal barrier formation, tight junction proteins claudin CLDN1 and 4 were expressed in iPSC3-iKC-HEEs similar to pKC-HEEs (Figure 8).

To investigate whether the basal keratinocyte orientation and parakeratosis could be a result of low numbers of basal iKC, we increased the number of cells for HEE seeding (250,000 versus 150,000 cells per insert) and the duration of the submerged phase (five days versus three days) to hypothetically allow for a better monolayer formation before the ALI. Both interventions did not improve HEE morphology, with horizontal basal keratinocyte orientation and parakeratosis still present (Supplementary Figure 5A). In addition, expression of IVL, FLG and CLDN1/4 did not seem to increase (Supplementary Figure 5B). To better study the epidermis formation, we quantified the barrier function of iKC and pKC-HEEs by electrical impedance spectroscopy (EIS) [36]. Under the standard culture protocol (150,000 cells, submerged for three days), iKC-HEEs demonstrated an 87% lower EIS corresponding to the differentiation status (EIS^{diff}) and 46% lower EIS corresponding to *stratum corneum* thickness (EIS^{sc}) as compared to pKC (Supplementary Figure 5C).

In accordance with the morphological analysis, EIS^{diff} did not improve by seeding more cells or extending the submerged phase.

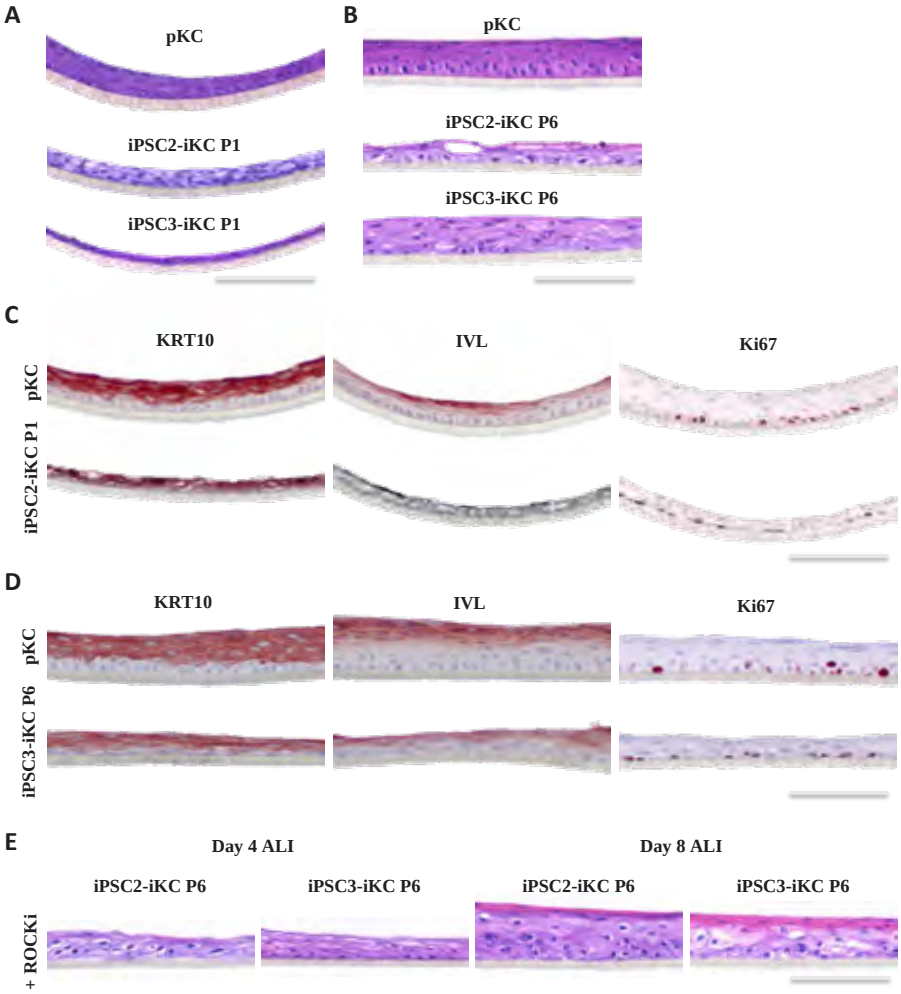

Figure 7. Human epidermal equivalents derived from P1 and P6 iKC and pKC. (**A**) Morphology of epidermis day 4 ALI generated from P1 iKC and pKC. (**B**) Protein expression levels of KRT10, IVL and Ki67 expression in epidermis day 4 ALI generated from P1 iPSC2-iKC and pKC. (**C**) Morphology at day 4 ALI when P6 iKC are used. (**D**) Protein expression levels of KRT10, IVL and Ki67 expression at day 4 ALI when P6 iKC are used. (**E**) Morphology of epidermis day 4 and 8 ALI generated from P6 iKC with continuous ROCK inhibitor supplementation to the medium. Scale bar = 100µm.

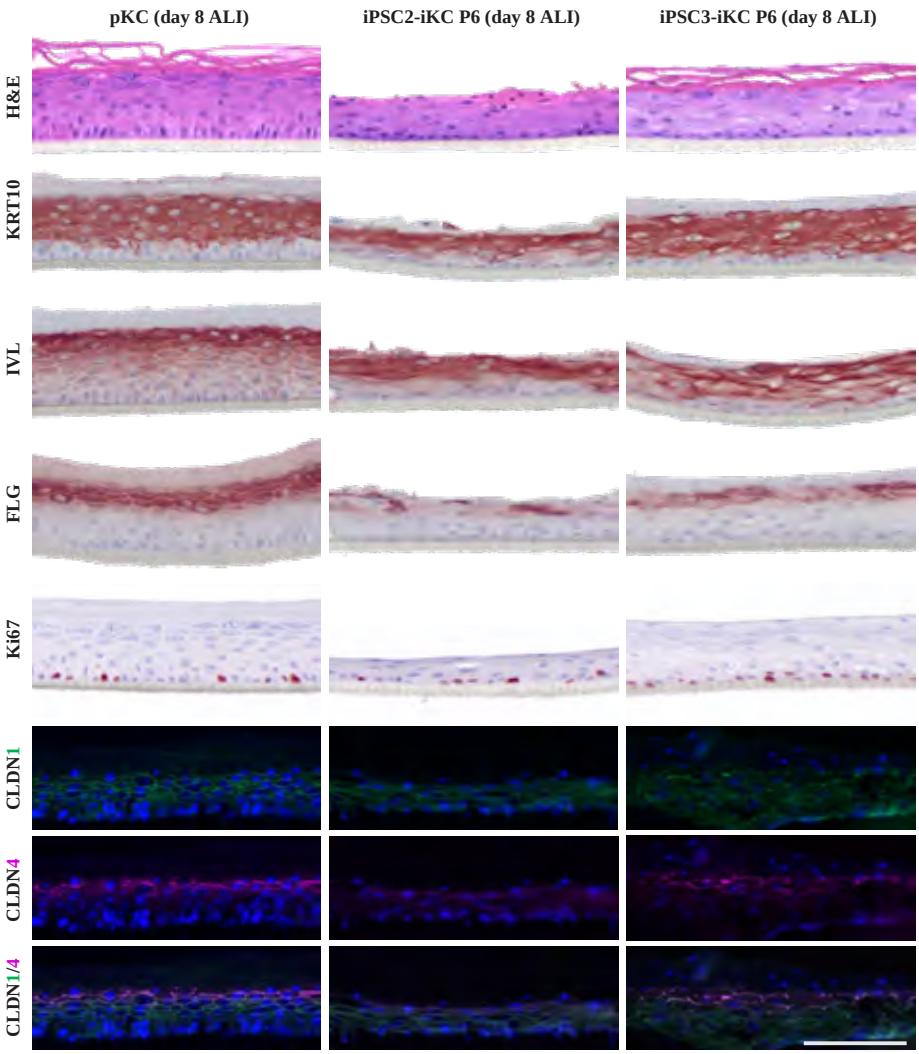

Figure 8. Human epidermal equivalents derived from P6 iKC and pKC at day 8 ALI. Morphology and protein expression of KRT10, IVL, FLG, Ki67 and CLDN1/4. Scale bar = 100µm.

Discussion

There is limited evidence that iPSC-derived keratinocytes can be consistently obtained with sufficient quality (mature, homogeneous) to study epidermal biology and inflammatory skin diseases. To our knowledge, we are the first to reproducibly generate iKC with similar morphology and keratinocyte marker gene expression as pKC. To get there, we pinpointed crucial culture conditions for successful iPSC

to keratinocyte differentiation, including the use of defined CnT-30 medium that is not commonly used by others (Supplementary Table 1) and subculturing of iKC to gain a more mature keratinocyte phenotype. The obtained iKC were capable of epidermal differentiation in 2D and 3D systems, and showed potential to mimic epidermal differentiation defects in 2D upon AD-related cytokines. This provides good reason to further explore the utility of iKC in personalized modeling and unraveling of chronic inflammatory skin diseases and beyond.

The heterogeneous nature of *in vitro* 2D iPSC differentiations, as here demonstrated by scRNA-seq data, might be caused by the simplicity of culture protocols as compared to embryonic development. For example, *in vitro* differentiation into keratinocytes is often initiated only by RA and BMP-4 (Supplementary Table 1), while *in vivo* a 3D micro-environment of cells and their secreted factors is present [65]. Therefore, strategies to push differentiation in the right direction or enrich keratinocyte-like cells after differentiation can be useful. As a quick approach we tested small molecule compounds, based on the bulk RNA-seq data that we already obtained and literature, which were not effective for iKC in the concentrations that were competent enough in pKC (unpublished data). In addition, with the heterogeneity in the iKC culture, scRNA-seq would be better suitable to identify pathways that are differential between keratinocyte-like iKC and pKC. On the other hand, our data indicated that subculturing of iKC did improve the overall keratinocyte marker expression, yet scRNA-sequencing of lower and higher passage iKC will have to reveal if subculturing induced maturation of early epithelial cells or selected for keratinocyte-like cells. Alternatively, implementation of fluorescence-activated cell sorting (FACS) has shown success for pluripotent stem cell-derived corneal limbal stem cells [66], and for pluripotent stem cell-derived keratinocytes [3]. The latter study used ITGA6 for sorting, which we here also demonstrate to be expressed in iKC most closely resembling pKC. In addition, negative selection of unwanted cells [66] could be a complementary approach to remove fibroblast and neuron-like cells from the total iKC population, for instance using PDGFR as presented in our study. Alternatives to overcome viability and time issues with FACS, could be the faster "magnetic-activated cell sorting" (MACS) [67, 68] or more gentle "buoyancy-activated cell sorting" (BACS) [69].

While iKC showed impaired FBS-driven differentiation upon Th2 + IL-22 similar to pKC [10], also differences between the cell types could be observed. For instance, *KRT1* was reduced in iKC upon FBS, which is hypothesized to be a timing issue, since *KRT1* is expressed earlier in differentiation as IVL and the latter did increase. Extending the panel of epidermal differentiation markers could potentially confirm

or reject this hypothesis. With regard to inflammatory cytokine production, FBS significantly induced *CCL20* expression, which opts against using FBS to model inflammatory diseases with iKC in monolayer cultures. By optimizing ALI cultures, this could indeed be prevented. Moreover, the substantial induction of *CCL2* (more than 1000-fold [10]) and *CCL20* (10-fold [10]) by Th2 + IL-22 in pKC was only partially resembled in iKC, while IL-4 and IL-13 receptors were expressed. This could potentially in part be explained by a higher baseline expression of CCL20 in iPSC2-iKC as compared to pKC (Supplementary Table 7), similar to their overall greater inflammatory signature as shown in Figure 1F. Additionally, the culture system was different (2D iKC and 3D pKC) and therefore the differentiation status (more advanced in 3D) as well as the stimulus of differentiation (FBS versus air exposure), so side-by-side comparisons are required to show the resemblance of cell types.

For future personalized disease modeling, we optimized human epidermal equivalent development by testing subcultured iKC, the presence versus absence of ROCK inhibitor, seeding more cells or extending the submerged phase. Our data confirms previous research demonstrating that ROCKi can negatively affect epidermal morphology when supplemented during the ALI culture phase [70]. Our EIS data show that the epidermal barrier function of iKC-HEEs was still impaired as compared to pKC-HEEs, in contrast to previous results [17]. Since many epidermal components and proteins important for barrier functioning were present in our iKC-HEE (*stratum granulosum*, *stratum corneum*, IVL/FLG expression, CLDN1/4 expression), the missing link should be further explored. Besides assessment of more barrier proteins (e.g., loricrin, transglutaminase 3) and lipids (e.g., ceramides) [71], other inside-out and outside-in barrier measurements could be performed to localize the impairment [35]. Potentially, heterogeneity in epidermis development across the HEE could have caused the lower EIS, because the current follows the "quickest route". This could be investigated by H&E staining at multiple sites across the culture. The impaired barrier of iKC-HEEs despite clear stratification also implies that protein stainings most studies summarized in Table 1 use to show the epidermis development might not be enough to state the HEEs formed equally well to pKC-HEEs. For further optimization, seeding of FACS, MACS or BACS enriched keratinocyte-like cells from the subcultured iKC population, or applying the iKC on top of a fibroblast-populated dermal layer, might improve the barrier formation and function. Fibroblasts (and their excreted products like keratinocyte growth factor [72]) are suggested to influence epidermal development including expression of activation markers KRT6/16/17 [73, 74] that are associated to the inflammatory skin disease psoriasis in which parakeratosis is also observed [75, 76]. Therefore, it would be interesting to observe if parakeratosis can be reduced by addition of fibroblasts.

Fibroblasts also seem to contribute to the localization of involucrin [73, 74], of which the latter was expressed suprabasal in iKC-HEEs but more gradually increased during differentiation of pKC-HEEs. If the barrier function of iKC-HEEs would still not be improved, this iKC-HEE model could be used to screen epidermal barrier improving drugs like aryl hydrocarbon receptor ligands [10, 36].

Future investigation could focus on subjecting the optimized iKC-HEEs to the AD cytokines to show whether epidermal differentiation and barrier function defects can be studied using this alternative cell source. This would also open doors for genetic-inflammation interaction studies by comparing iKC from AD patients with FLG variants [11] to genetically corrected iKC in their response to AD cytokines. AD patient-derived iPSC could also be used to generate not only keratinocytes but also fibroblasts and other skin cell types for full thickness skin equivalents. Finally, our protocol for the reproducible generation of iKC and proposed plans for enrichment of the keratinocyte-like population also fuels regenerative medicine and disease modeling of genodermatoses.

Data and code availability

Bulk RNA-seq datasets used in this study are available in the Gene Expression Omnibus (GEO) with accession number GSE287810, and scRNA-seq datasets under GSE285034. The full processing workflow and documentation of code used for scRNA-seq analysis in Python is available in the GitHub repository [77]. An interactive web app was developed to visualize scRNA-seq datasets interactively, and is available at: https://huggingface.co/spaces/Arts-of-coding/singleronkeratinocytes.

Acknowledgements

We would like to thank Marijke Baltissen for performing the RNA-sequencing, and Stefan Baertschi from CELLnTEC for the discussions on the comparison of media. We are also grateful to Christian Freund and colleagues for providing iPSC2 and 3 and supporting with iPSC cultures. This work was supported by a grant from Health-Holland (PAST4FUTURE LSHM20043-HSGF to EvdB and HZ). The authors declare no conflicts of interest.

Abbreviations

AD - atopic dermatitis, AEC - 3-amino-9-ethylcarbazole, ALI – air liquid interface, AUC - area under the curve, BMP-4 - bone morphogenetic protein 4, BSA - bovine serum albumin, CA2 - carbonic anhydrase II, CA^{2+} - calcium, CCL - C-C motif chemokine ligand, CLDN - claudin, CnT - CELLnTEC, COL7A1 - collagen type 7 alpha 1 chain, DAPI - 4′,6-diamidino-2-phenylindole, DEG - differentially expressed genes, (D)PBS

- (Dulbecco's) phosphate-buffered saline, EDTA - ethylenediaminetetraacetic acid, EIS - electrical impedance spectroscopy, FBS - fetal bovine serum, FLG - filaggrin, H&E - hematoxylin and eosin, HEE - human epidermal equivalent, HSE - human skin equivalent, HVG - highly variable genes, iKC - induced keratinocyte, (i)PSC - (induced) pluripotent stem cell, JAK - janus kinase, IL - interleukin, IVL - involucrin, Ki-67 - Kiel 67, KLF4 - krüppel-like factor 4, KRT - keratin, KSFM - keratinocyte serum free medium, P - passage, PCA - principal component analysis, PI3K - phosphatidylinositol 3 kinase, pKC - primary keratinocyte, RA - retinoic acid, RPLP0 - ribosomal protein lateral stalk subunit P0, RT-qPCR - real time quantitative PCR, sc - single-cell, SEM - standard error of the mean, STAT - signal transducer and activator of transcription, Th - T helper cell, (T)P63 - (tumor) protein 63, UMAP - uniform manifold approximation and projection, VIM - vimentin, 2D - two dimensional, 3D - three dimensional

References

1. Takahashi, K., et al., Induction of pluripotent stem cells from adult human fibroblasts by defined factors. Cell, 2007. **131**(5): p. 861-72.
2. Cerneckis, J., H. Cai, and Y. Shi, Induced pluripotent stem cells (iPSCs): molecular mechanisms of induction and applications. Signal Transduct Target Ther, 2024. **9**(1): p. 112.
3. Neumayer, G., et al., A scalable and cGMP-compatible autologous organotypic cell therapy for Dystrophic Epidermolysis Bullosa. Nat Commun, 2024. **15**(1): p. 5834.
4. Niehues, H., et al., 3D skin models for 3R research: The potential of 3D reconstructed skin models to study skin barrier function. Exp Dermatol, 2018. **27**(5): p. 501-511.
5. Weidinger, S., et al., Atopic dermatitis. Nat Rev Dis Primers, 2018. **4**(1): p. 1.
6. Palmer, C.N., et al., Common loss-of-function variants of the epidermal barrier protein filaggrin are a major predisposing factor for atopic dermatitis. Nat Genet, 2006. **38**(4): p. 441-6.
7. Kim, B.E., et al., Loricrin and involucrin expression is down-regulated by Th2 cytokines through STAT-6. Clin Immunol, 2008. **126**(3): p. 332-7.
8. Renert-Yuval, Y., et al., The molecular features of normal and atopic dermatitis skin in infants, children, adolescents, and adults. J Allergy Clin Immunol, 2021. **148**(1): p. 148-163.
9. Quílez, C., et al., Targeting the Complexity of In Vitro Skin Models: A Review of Cutting-Edge Developments. J Invest Dermatol, 2024. **144**(12): p. 2650-2670.
10. Meesters, L.D., et al., Dissecting key contributions of Th2 and Th17 cytokines to atopic dermatitis pathophysiology. J Allergy Clin Immunol, 2025.
11. Devito, L., et al., Induced pluripotent stem cell line from an atopic dermatitis patient heterozygous for c.2282del4 mutation in filaggrin: KCLi001-A. Stem Cell Res, 2018. **31**: p. 122-126.
12. Ali, G., et al., Keratinocytes Derived from Patient-Specific Induced Pluripotent Stem Cells Recapitulate the Genetic Signature of Psoriasis Disease. Stem Cells Dev, 2020. **29**(7): p. 383-400.
13. Itoh, M., et al., Generation of keratinocytes from normal and recessive dystrophic epidermolysis bullosa-induced pluripotent stem cells. Proc Natl Acad Sci U S A, 2011. **108**(21): p. 8797-802.
14. Itoh, M., et al., Generation of 3D skin equivalents fully reconstituted from human induced pluripotent stem cells (iPSCs). PLoS One, 2013. **8**(10): p. e77673.
15. Shalom-Feuerstein, R., et al., Impaired epithelial differentiation of induced pluripotent stem cells from ectodermal dysplasia-related patients is rescued by the small compound APR-246/PRIMA-1MET. Proc Natl Acad Sci U S A, 2013. **110**(6): p. 2152-6.
16. Lian, X., et al., A small molecule inhibitor of SRC family kinases promotes simple epithelial differentiation of human pluripotent stem cells. PLoS One, 2013. **8**(3): p. e60016.
17. Petrova, A., et al., 3D In vitro model of a functional epidermal permeability barrier from human embryonic stem cells and induced pluripotent stem cells. Stem Cell Reports, 2014. **2**(5): p. 675-89.
18. Sebastiano, V., et al., Human COL7A1-corrected induced pluripotent stem cells for the treatment of recessive dystrophic epidermolysis bullosa. Sci Transl Med, 2014. **6**(264): p. 264ra163.
19. Umegaki-Arao, N., et al., Induced pluripotent stem cells from human revertant keratinocytes for the treatment of epidermolysis bullosa. Sci Transl Med, 2014. **6**(264): p. 264ra164.
20. Kogut, I., D.R. Roop, and G. Bilousova, Differentiation of human induced pluripotent stem cells into a keratinocyte lineage. Methods Mol Biol, 2014. **1195**: p. 1-12.
21. Gledhill, K., et al., Melanin Transfer in Human 3D Skin Equivalents Generated Exclusively from Induced Pluripotent Stem Cells. PLoS One, 2015. **10**(8): p. e0136713.

22. Webber, B.R., et al., CRISPR/Cas9-based genetic correction for recessive dystrophic epidermolysis bullosa. NPJ Regen Med, 2016. **1**: p. 16014-.
23. Petrova, A., et al., Induced Pluripotent Stem Cell Differentiation and Three-Dimensional Tissue Formation Attenuate Clonal Epigenetic Differences in Trichohyalin. Stem Cells Dev, 2016. **25**(18): p. 1366-75.
24. Kajiwara, K., et al., Fetal Therapy Model of Myelomeningocele with Three-Dimensional Skin Using Amniotic Fluid Cell-Derived Induced Pluripotent Stem Cells. Stem Cell Reports, 2017. **8**(6): p. 1701-1713.
25. Kim, Y., et al., Establishment of a complex skin structure via layered co-culture of keratinocytes and fibroblasts derived from induced pluripotent stem cells. Stem Cell Res Ther, 2018. **9**(1): p. 217.
26. Kim, Y. and J.H. Ju, Generation of 3D Skin Organoid from Cord Blood-derived Induced Pluripotent Stem Cells. J Vis Exp, 2019 (146).
27. Naito, C., et al., Utility of Three-Dimensional Skin From Human-Induced Pluripotent Stem Cells as a Tool to Evaluate Transdermal Drug Permeation. J Pharm Sci, 2019. **108**(11): p. 3524-3527.
28. Jacków, J., et al., CRISPR/Cas9-based targeted genome editing for correction of recessive dystrophic epidermolysis bullosa using iPS cells. Proc Natl Acad Sci U S A, 2019. **116**(52): p. 26846-26852.
29. Rodimova, S.A., et al., Metabolic activity and intracellular pH in induced pluripotent stem cells differentiating in dermal and epidermal directions. Methods Appl Fluoresc, 2019. **7**(4): p. 044002.
30. Ruiz-Torres, S., et al., Directed differentiation of human pluripotent stem cells into epidermal stem and progenitor cells. Mol Biol Rep, 2021. **48**(8): p. 6213-6222.
31. Ebner-Peking, P., et al., Self-assembly of differentiated progenitor cells facilitates spheroid human skin organoid formation and planar skin regeneration. Theranostics, 2021. **11**(17): p. 8430-8447.
32. Ruiz-Torres, S., et al., Inherited DNA Repair Defects Disrupt the Structure and Function of Human Skin. Cell Stem Cell, 2021. **28**(3): p. 424-435.e6.
33. Lima Cunha, D., et al., hiPSC-Derived Epidermal Keratinocytes from Ichthyosis Patients Show Altered Expression of Cornification Markers. Int J Mol Sci, 2021. **22**(4).
34. Sah, S.K., et al., Generation of Keratinocytes from Human Induced Pluripotent Stem Cells Under Defined Culture Conditions. Cell Reprogram, 2021. **23**(1): p. 1-13.
35. Rikken, G., H. Niehues, and E.H. van den Bogaard, Organotypic 3D Skin Models: Human Epidermal Equivalent Cultures from Primary Keratinocytes and Immortalized Keratinocyte Cell Lines. Methods Mol Biol, 2020. **2154**: p. 45-61.
36. van den Brink, N.J.M., et al., Electrical Impedance Spectroscopy Quantifies Skin Barrier Function in Organotypic In Vitro Epidermis Models. J Invest Dermatol, 2024. **144**(11): p. 2488-2500.e4.
37. Livak, K.J. and T.D. Schmittgen, Analysis of relative gene expression data using real-time quantitative PCR and the 2(-Delta Delta C(T)) Method. Methods, 2001. **25**(4): p. 402-8.
38. van der Sande, M., et al., Seq2science: an end-to-end workflow for functional genomics analysis. PeerJ, 2023. **11**: p. e16380.
39. Smits, J.G.A., et al., Identification of the regulatory circuit governing corneal epithelial fate determination and disease. PLoS Biol, 2023. **21**(10): p. e3002336.
40. NationalInstitutesofHealth(NIH). Available from: https://davidbioinformatics.nih.gov/tools.jsp.
41. Singleron-RD. CeleScope. 2023; Available from: https://github.com/singleron-RD/CeleScope.
42. Edgar, R., M. Domrachev, and A.E. Lash, Gene Expression Omnibus: NCBI gene expression and hybridization array data repository. Nucleic Acids Res, 2002. **30**(1): p. 207-10.

43. Wolf, F.A., P. Angerer, and F.J. Theis, SCANPY: large-scale single-cell gene expression data analysis. Genome Biol, 2018. **19**(1): p. 15.
44. Wolock, S.L., R. Lopez, and A.M. Klein, Scrublet: Computational Identification of Cell Doublets in Single-Cell Transcriptomic Data. Cell Syst, 2019. **8**(4): p. 281-291.e9.
45. Zappia, L. and A. Oshlack, Clustering trees: a visualization for evaluating clusterings at multiple resolutions. Gigascience, 2018. **7**(7).
46. Traag, V.A., L. Waltman, and N.J. van Eck, From Louvain to Leiden: guaranteeing well-connected communities. Sci Rep, 2019. **9**(1): p. 5233.
47. Xu, X.W.a.Y., An improved index for clustering validation based on Silhouette index and Calinski-Harabasz index. IOP Conference Series: Materials Science and Engineering, 2019. **569**(5).
48. Bouldin, D.L.D.a.D.W., A Cluster Separation Measure. IEEE, 2009. **PAMI-1**(2): p. 224 - 227.
49. Svensson, V., et al., Interpretable factor models of single-cell RNA-seq via variational autoencoders. Bioinformatics, 2020. **36**(11): p. 3418-3421.
50. Soares, E., et al., Single-cell RNA-seq identifies a reversible mesodermal activation in abnormally specified epithelia of p63 EEC syndrome. Proc Natl Acad Sci U S A, 2019. **116**(35): p. 17361-17370.
51. Soares, E. and H. Zhou, Pluripotent Stem Cell Differentiation Toward Functional Basal Stratified Epithelial Cells. Methods Mol Biol, 2022. **2454**: p. 297-304.
52. Hossini, A.M., et al., PI3K/AKT Signaling Pathway Is Essential for Survival of Induced Pluripotent Stem Cells. PLoS One, 2016. **11**(5): p. e0154770.
53. Fortunel, N.O., et al., KLF4 inhibition promotes the expansion of keratinocyte precursors from adult human skin and of embryonic-stem-cell-derived keratinocytes. Nat Biomed Eng, 2019. **3**(12): p. 985-997.
54. Rashighi, M. and J.E. Harris, Interfering with the IFN-γ/CXCL10 pathway to develop new targeted treatments for vitiligo. Ann Transl Med, 2015. **3**(21): p. 343.
55. Zhang, W., et al., The gut-enriched Krüppel-like factor suppresses the activity of the CYP1A1 promoter in an Sp1-dependent fashion. J Biol Chem, 1998. **273**(28): p. 17917-25.
56. Volpato, V. and C. Webber, Addressing variability in iPSC-derived models of human disease: guidelines to promote reproducibility. Dis Model Mech, 2020. **13**(1).
57. Kim, T.I., et al., Basement Membrane Status Is Intact in Urticarial Dermatitis vs. Adult-Onset Atopic Dermatitis. Ann Dermatol, 2018. **30**(2): p. 258-261.
58. Boyce, S.T. and R.G. Ham, Calcium-regulated differentiation of normal human epidermal keratinocytes in chemically defined clonal culture and serum-free serial culture. J Invest Dermatol, 1983. **81**(1 Suppl): p. 33s-40s.
59. Wong, C.W., et al., In Vitro Expansion of Keratinocytes on Human Dermal Fibroblast-Derived Matrix Retains Their Stem-Like Characteristics. Sci Rep, 2019. **9**(1): p. 18561.
60. Alkemade, J.A., et al., SKALP/elafin is an inducible proteinase inhibitor in human epidermal keratinocytes. J Cell Sci, 1994. **107** (Pt 8): p. 2335-42.
61. Simpson, C.L., D.M. Patel, and K.J. Green, Deconstructing the skin: cytoarchitectural determinants of epidermal morphogenesis. Nat Rev Mol Cell Biol, 2011. **12**(9): p. 565-80.
62. Smits, J.G.A., et al., Characterization of In Vitro Differentiation of Human Primary Keratinocytes by RNA-Seq Analysis. J Vis Exp, 2020 (159).
63. Poumay, Y. and M.R. Pittelkow, Cell density and culture factors regulate keratinocyte commitment to differentiation and expression of suprabasal K1/K10 keratins. J Invest Dermatol, 1995. **104**(2): p. 271-6.

64. Kamsteeg, M., et al., Increased expression of carbonic anhydrase II (CA II) in lesional skin of atopic dermatitis: regulation by Th2 cytokines. J Invest Dermatol, 2007. **127**(7): p. 1786-9.
65. Hu, M.S., et al., Embryonic skin development and repair. Organogenesis, 2018. **14**(1): p. 46-63.
66. Vattulainen, M., et al., Deciphering the heterogeneity of differentiating hPSC-derived corneal limbal stem cells through single-cell RNA sequencing. Stem Cell Reports, 2024. **19**(7): p. 1010-1023.
67. Pan, J. and J. Wan, Methodological comparison of FACS and MACS isolation of enriched microglia and astrocytes from mouse brain. J Immunol Methods, 2020. **486**: p. 112834.
68. Sutermaster, B.A. and E.M. Darling, Considerations for high-yield, high-throughput cell enrichment: fluorescence versus magnetic sorting. Sci Rep, 2019. **9**(1): p. 227.
69. Liou, Y.R., et al., Buoyancy-activated cell sorting using targeted biotinylated albumin microbubbles. PLoS One, 2015. **10**(5): p. e0125036.
70. van den Bogaard, E.H., et al., Rho kinase inhibitor Y-27632 prolongs the life span of adult human keratinocytes, enhances skin equivalent development, and facilitates lentiviral transduction. Tissue Eng Part A, 2012. **18**(17-18): p. 1827-36.
71. Lefèvre-Utile, A., et al., Five Functional Aspects of the Epidermal Barrier. Int J Mol Sci, 2021. **22**(21).
72. Russo, B., N.C. Brembilla, and C. Chizzolini, Interplay Between Keratinocytes and Fibroblasts: A Systematic Review Providing a New Angle for Understanding Skin Fibrotic Disorders. Front Immunol, 2020. **11**: p. 648.
73. el-Ghalbzouri, A., et al., Effect of fibroblasts on epidermal regeneration. Br J Dermatol, 2002. **147**(2): p. 230-43.
74. El Ghalbzouri, A., E. Lamme, and M. Ponec, Crucial role of fibroblasts in regulating epidermal morphogenesis. Cell Tissue Res, 2002. **310**(2): p. 189-99.
75. Tirumalae, R., Psoriasiform dermatoses: microscopic approach. Indian J Dermatol, 2013. **58**(4): p. 290-3.
76. Yang, L., et al., Nrf2 Promotes Keratinocyte Proliferation in Psoriasis through Up-Regulation of Keratin 6, Keratin 16, and Keratin 17. J Invest Dermatol, 2017. **137**(10): p. 2168-2176.
77. Ewels, P., et al., MultiQC: summarize analysis results for multiple tools and samples in a single report. Bioinformatics, 2016. **32**(19): p. 3047-8.
78. Ali, G. and E.M. Abdelalim, Directed differentiation of human pluripotent stem cells into epidermal keratinocyte-like cells. STAR Protoc, 2022. **3**(3): p. 101613.
79. van Duijnhoven, J.L., et al., MON-150, a versatile monoclonal antibody against involucrin: characterization and applications. Arch Dermatol Res, 1992. **284**(3): p. 167-72.

Supplemental figures

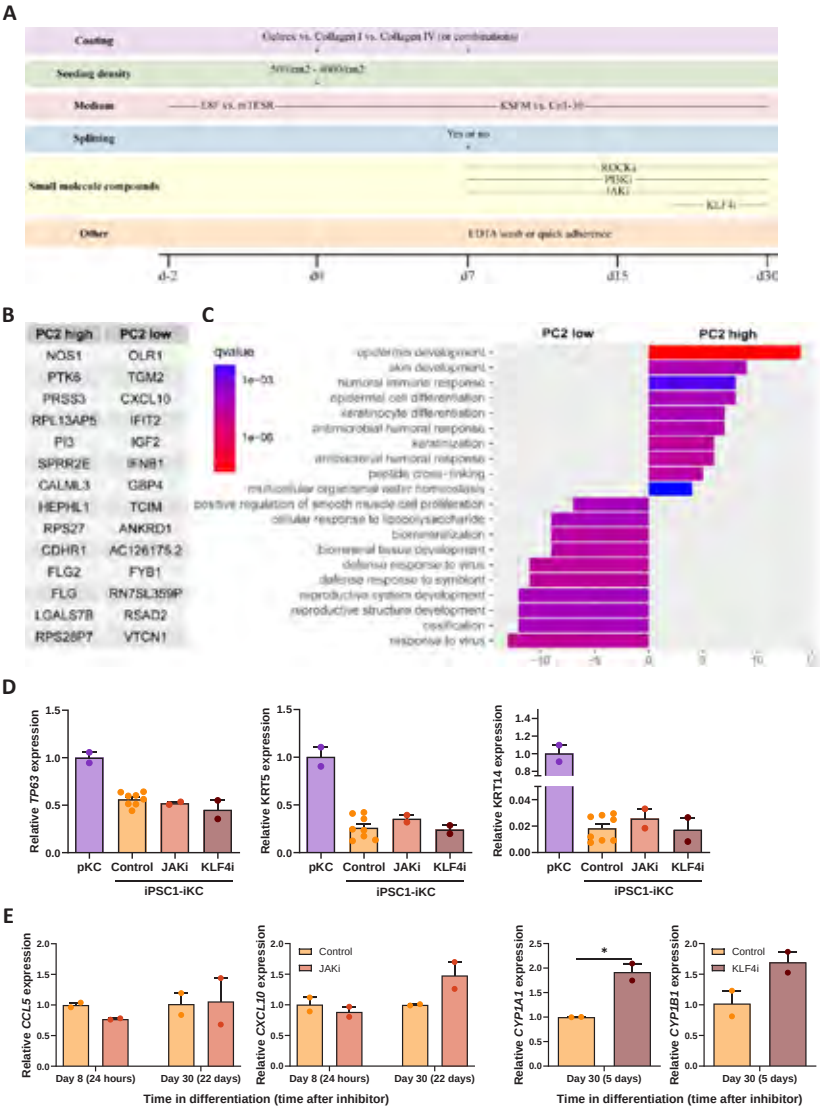

Supplementary Figure 1. Overview of optimization strategies and the effect of small molecule inhibitors on iPSC to keratinocyte differentiation. (**A**) Schematic overview of cell culture optimization strategies. (**B**) Genes that drive PC2 in the PCA plot from Figure 1D. (**C**) Gene Ontology (GO)-term analysis on genes driving PC2. (**D**) mRNA expression levels of epithelium (*TP63*) and keratinocyte (*KRT5/14*) marker genes. (**E**) Target gene expression of *CCL5* and *CXCL10* for JAK inhibition, and of *CYP1A1* and *CYP1B1* for KLF4 inhibition. Data is presented as mean +/- SEM, and conditions were statistically compared to control by one-way ANOVA with Dunnett's (subfigure D) or Bonferroni (subfigure E, left) *post hoc* correction or unpaired t-tests (subfigure E, right). All iPSC1-iKC data is representative for N=2 or more technical replica.

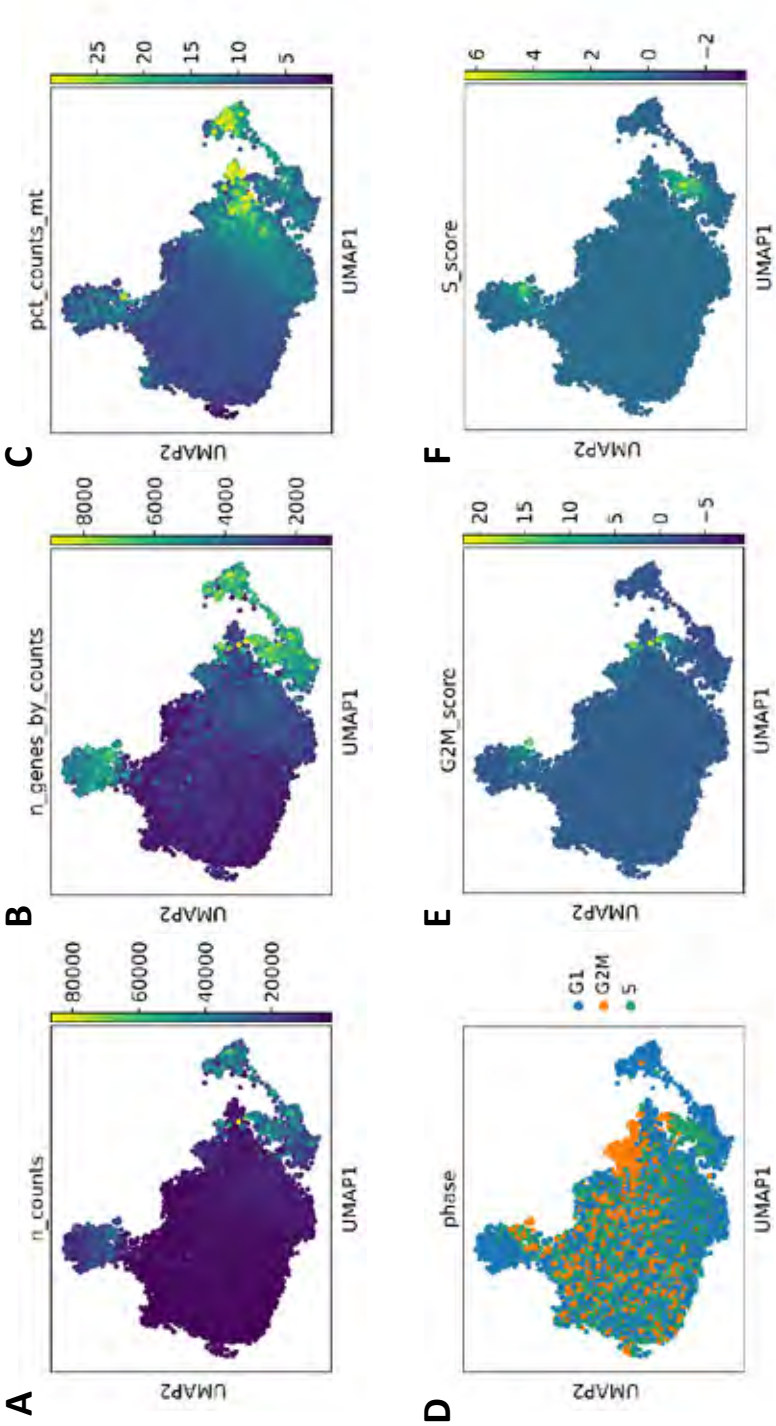

Supplementary Figure 2. Quality control of scRNA-sequencing data from iPSC2-iKC and pKC. (**A**) The total read counts per well, (**B**) Estimated number of genes based on counts per cell, (**C**) mitochondrial percentage of reads per cell, (**D**) Cell cycle phase per cell, (**E**) G2M score, (**F**) S score.

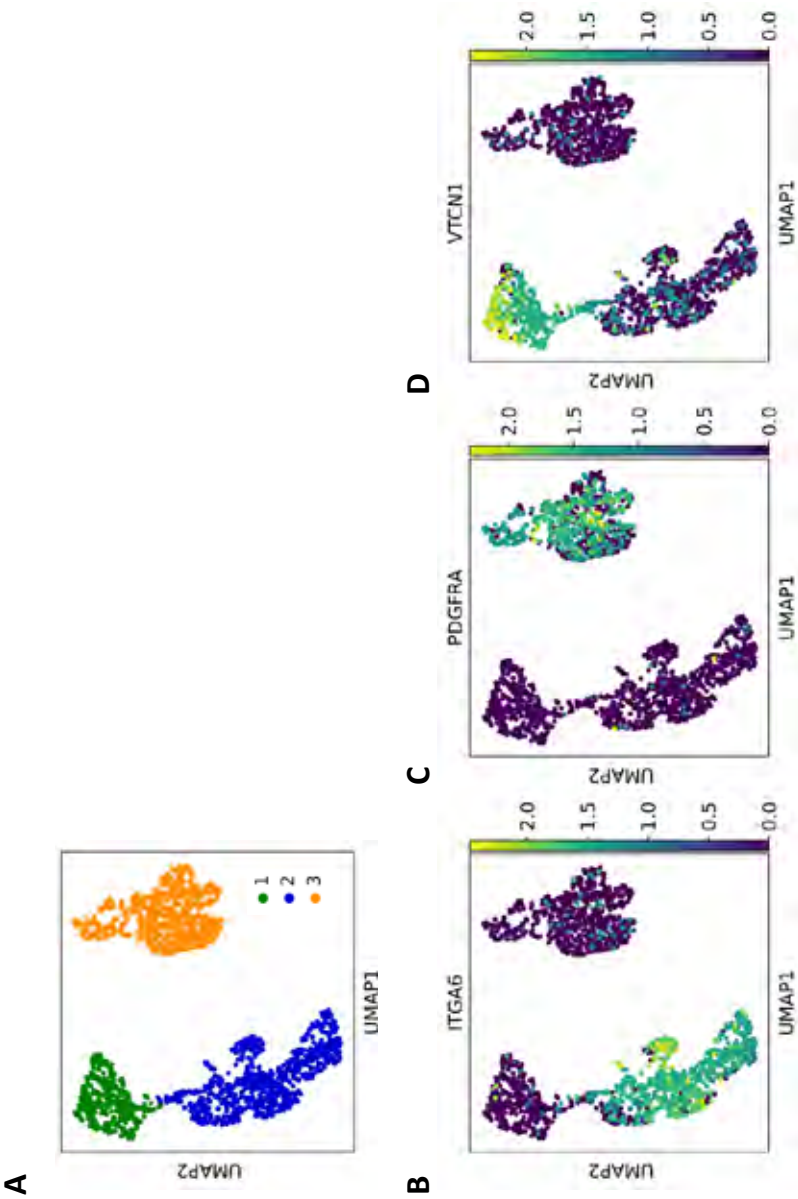

Supplementary Figure 3. Clustering of iPSC2-iKC only based on single cell RNA-sequencing. (**A**) UMAP clustering of iKC, (**B**) Expression of keratinocyte-related cell surface marker gene *ITGA6*, (**C**) Expression of fibroblast-related cell surface marker gene *PDGFRA*, (**D**) Expression of epithelium-related cell surface marker gene *VTCN1*.

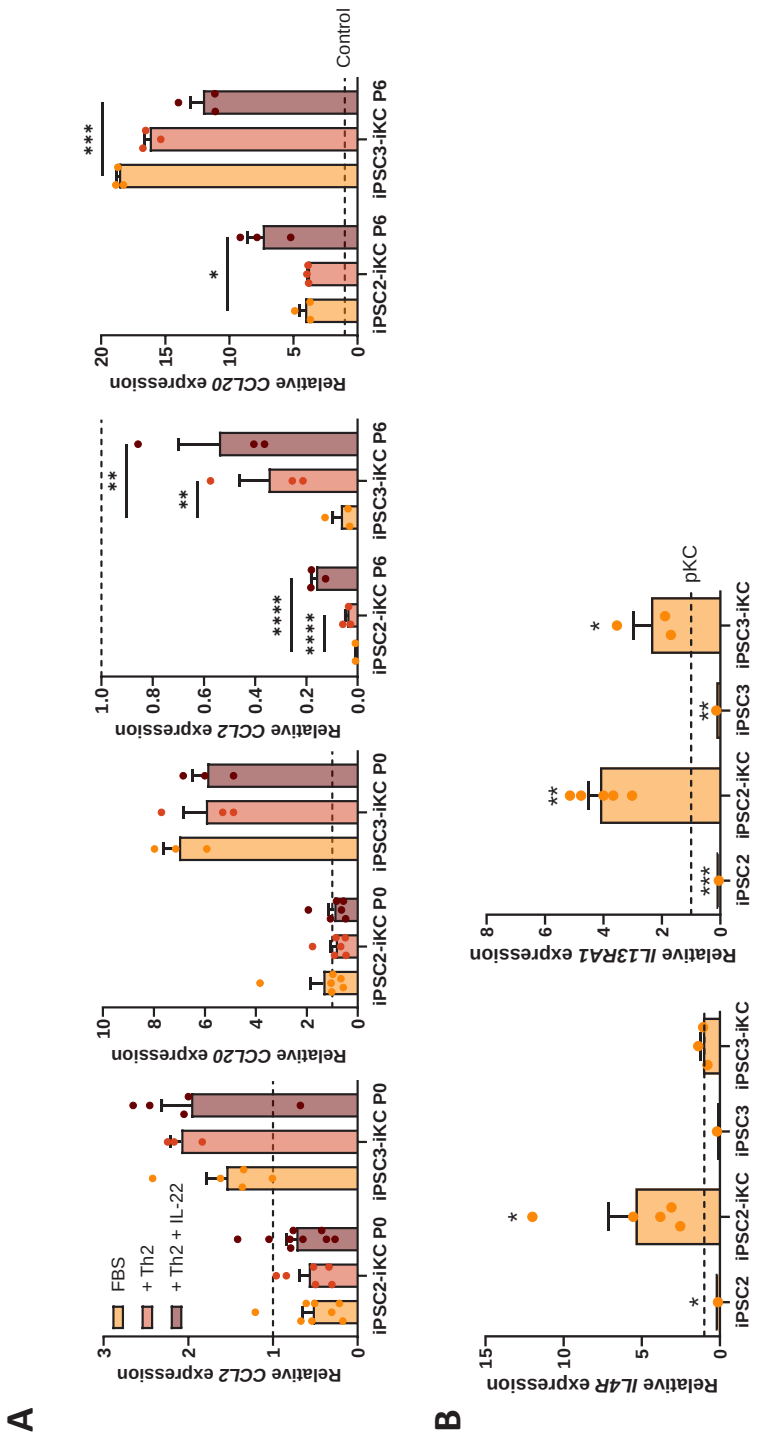

Supplementary Figure 4. The effect of AD cytokines on FBS-driven iKC responses. (**A**) mRNA expression levels of inflammatory AD marker genes *CCL2* and *CCL20* in P0 and P6 iKC. (**B**) mRNA expression levels of *IL-4* and *IL-13 receptor* in iPSC and unstimulated P0 iKC. All iKC data is representative for N=2 or more technical replica per biological replica (iPSC2 and 3), and presented as mean +/- SEM. For subfigure A, conditions were statistically compared to FBS by one-way ANOVA with Dunnett's *post hoc* correction. For B, iPSC and iKC were compared to pKC by one-way ANOVA with Dunnett's *post hoc* correction.

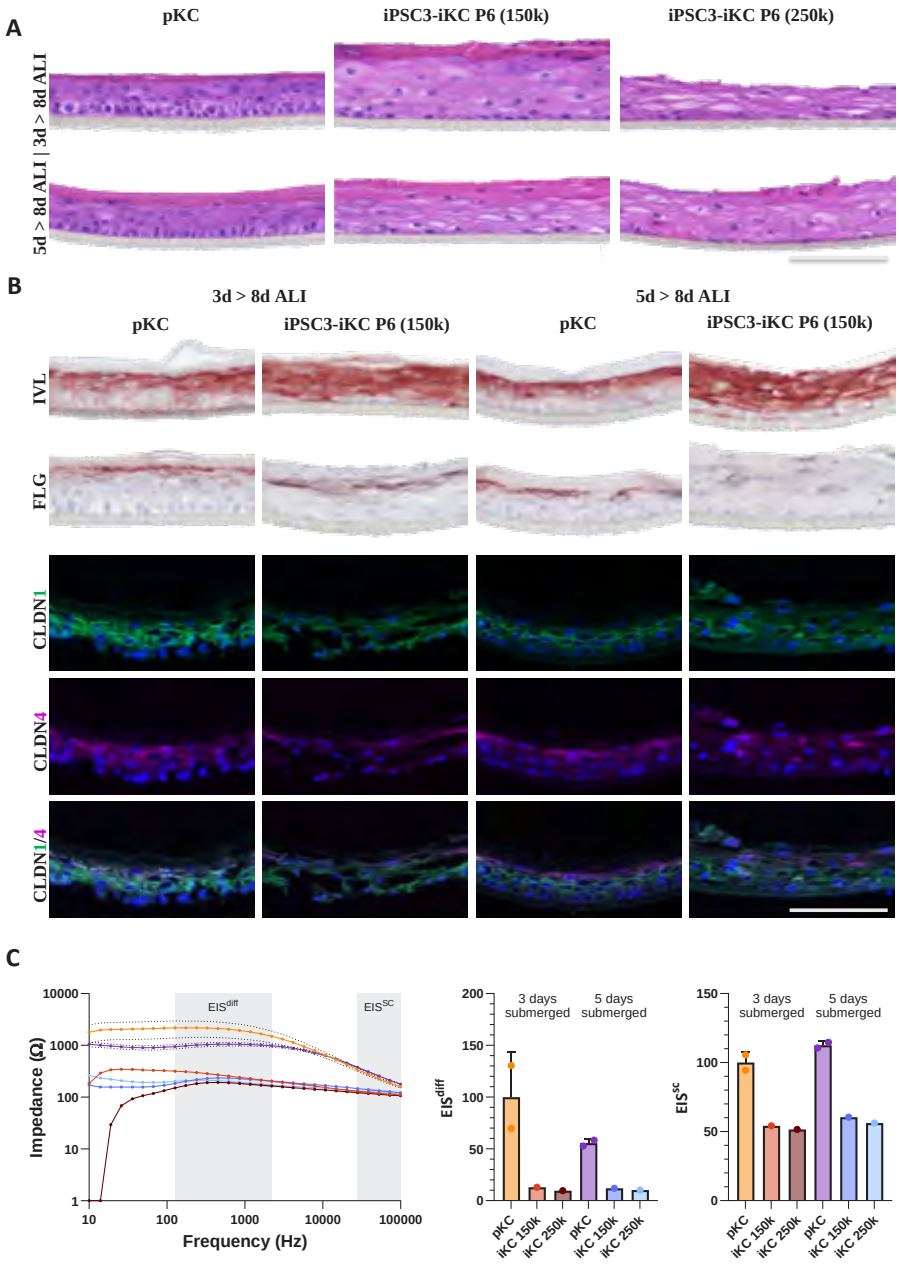

Supplementary Figure 5. Human epidermal equivalents derived from P6 iPSC3-iKC and pKC at day 8 ALI. (**A**) Morphology of epidermis when 150k or 250k cells were seeded after 3 or 5 days of submerged culture and 8 days at the ALI. (**B**) Protein expression of IVL, FLG and CLDN1/4. (**C**) Electrical impedance spectra (EIS) and EIS^{diff}/EIS^{sc} relative to pKC 3 days submerged condition. iKC-HEE were statistically compared to pKC-HEE, and 5 days submerged conditions to 3 days submerged conditions within the same cell type by one-way ANOVA with Bonferroni *post hoc* correction. Scale bar = 100µm.

Supplemental tables

Supplementary Table 1. Culture details of studies utilizing iPSC derived keratinocytes. Only studies using 2D iPSC to keratinocyte differentiation protocols were included (so no 3D organoid differentiations). SB431542: TGF-β inhibitor.

Coating	Medium	Supplements	Reference
Matrigel → fibronectin and collagen	DM or FAD or KSFM → KSFM	1 μM RA, 10 ng/mL BMP-4	[13]
Matrigel	KSFM → CnT-07	1 μM RA, 10 ng/mL BMP-4	[14]
Mitomycin-treated 3T3-G2 feeders	DMEM/F12-based → Green	25 ng/mL BMP-4, 0.3 mM ascorbic acid, 10 μM SB431542	[15]
Matrigel or Synthemax	DMEM/F12-based → KSFM	SU6656 → 1 μM RA, 10 ng/ml BMP-4	[16]
Matrigel → decellularized 3D ECM → Collagen IV	mTESR1 → DMEM/F12-based → KSFM → Epilife	1 μM RA, 25 ng/ml BMP-4	[17]
Gelatin	FAD → N2 → N2 or KSFM	1 μg/ml RA, 25 ng/ml BMP-4	[18]
Protocol of Itoh et al. 2011	*Protocol of Itoh et al. 2011 with following modifications:* CnT-07 or KSFM → CnT-57	*Protocol of Itoh et al. 2011*	[19]
Geltrex and collagen I → rapid attachment on collagen I and collagen IV	N2B27 → KSFM → CnT-07	1 μM RA, 25 ng/mL BMP-4	[20]
Protocol of Itoh et al. 2011	*Protocol of Itoh et al. 2011 with following modifications:* KSFM → CnT-07	*Protocol of Itoh et al. 2011*	[21]
Geltrex → rapid attachment on collagen I and collagen IV	KSFM → CnT-07	1 μM RA, 25 ng/ml BMP-4 → 10 μM ROCK inhibitor	[22]
Protocol of Petrova et al. 2014	*Protocol of Petrova et al. 2014*	*Protocol of Petrova et al. 2014*	[23]
VTN → Collagen I and fibronectin	KSFM	1 μM RA, 10 ng/mL BMP-4 → 20 ng/mL EGF → 10 μM Y-27632, 20 ng/mL EGF	[24]

Supplementary Table 1. Continued

Coating	Medium	Supplements	Reference
Collagen IV	DMEM/F12-based → KSFM	1 µg/ml RA, 25 ng/ml BMP-4, 20 ng/ml EGF → 25 ng/ml BMP-4, 20 ng/ml EGF	[25]
Based on protocol of Petrova et al. 2014 with following modifications: VTN XF	*Based on protocol of Petrova et al. 2014 with following modifications:* KSFM	*Based on protocol of Petrova et al. 2014 with following modifications:* 1 µM RA, 10 ng/µl BMP-4	[11]
Protocol of Kim et al. 2018	*Protocol of Kim et al. 2018*	*Protocol of Kim et al. 2018*	[26]
Matrigel → fibronectin and collagen I	KSFM	1 µM RA, 25 ng/mL BMP-4 → 20ng/ml EGF → 10 µM Y-27632, 20ng/ml EGF	[27]
Protocol of Itoh et al. 2011 with following modifications: VTN	*Protocol of Itoh et al. 2011 with following modifications:* E8 → KSFM	*Protocol of Itoh et al. 2011*	[28]
Protocol of Kogut et al. 2014	*Protocol of Kogut et al. 2014*	*Protocol of Kogut et al. 2014*	[29]
Protocol of Sebastiano et al. 2014 with following modifications: Geltrex	*Protocol of Sebastiano et al. 2014 with following modifications:*DMEM/F12-based → N2	*Protocol of Sebastiano et al. 2014 with following modifications:* 1 µM RA, 20 ng/mL BMP-4 → 10 ng/mL EGF, 1 µM RA, 20 ng/mL BMP-4 → 10 ng/mL EGF	[12, 78]
Matrigel → Collagen IV	KSFM → CnT-07	1 µM RA, 25 ng/mL BMP-4 → 10 µM ROCK inhibitor Y-27362	[30]
Protocol of Kogut et al. 2014 with following modifications: Matrigel	*Protocol of Kogut et al. 2014 with following modifications:* KSFM → CnT-PR	*Protocol of Kogut et al. 2014*	[31]
Matrigel → Collagen IV	KSFM → CnT-07	1 µM RA, 25 ng/mL BMP-4 → 10 µM ROCK inhibitor Y-27632	[32]
Gelatin with 3T3 J2 MEFs	KCM	10 ng/mL KGF/FGF7, 1 µM RA, 25 ng/mL BMP-4 → 10 ng/mL KGF/FGF7	[33]

Supplementary Table 1. Continued

Coating	Medium	Supplements	Reference
Matrigel	KSFM → CnT-07	1 µM RA, 10 ng/mL BMP-4	[34]
VTN	E6 → KSFM	1 µM RA, 5 ng/mL BMP-4	[3]
Geltrex and collagen I	CnT-30	1 µM RA, 10 ng/mL BMP-4 → 1 µM RA, 10 ng/mL BMP-4, 10 µM ROCK inhibitor Y-27632 → 10 µM ROCK inhibitor Y-27632	**This study**

Supplementary Table 2. iPSC lines

iPSC number	Full name	Origin cell type	Reprogramming method	Reference
1	*29.3*	Fibroblast	Lentivirus	[50]
2	*LUMC0004iCTRL10*	Fibroblast	Polycistronic lentivirus	LUMC hiPSC core facility
3	*LUMC0030iCTRL12*	Fibroblast	Polycistronic lentivirus	LUMC hiPSC core facility

Supplementary Table 3. Reagents tested for passaging iKC and their success in detaching iKC

Reagent	Concentration	Manufacturer	Outcome
Dispase	5 mg/mL	Sigma-Aldrich	Cells detach and survive
EDTA	0.5 mM	Sigma-Aldrich	Minimal cell detachment
Accutase	-	Stem cell technologies	Major cell death
Trypsin-EDTA	0.25 or 0.05%	Gibco	Major cell death
Gentle cell dissociation reagent	-	Stem cell technologies	Minimal cell detachment

Supplementary Table 4. Primer sequences

Primer target	Forward primer (5'-3')	Reverse primer (3'-5')
RPLP0	CACCATTGAAATCCTGAGTGATGT	TGACCAGCCCAAAGGAGAAG
NANOG	CCTATGCCTGTGATTTGTGG	CATGGAGGAAGGAAGAGGAG
KRT18	ATATCACACGACTGCAGCTG	CTGGCAATCTGGGCTTGTAG
TP63	GAGCCAGAAGCCAATCTACA	TATTGCATGTCCTGGCAAAC
KRT5	TGGAGATCGCCACTTACCG	CCAGAGGAAACACTGCTTGTG
KRT14	GGCCTGCTGAGATCAAAGACTAC	CACTGTGGCTGTGAGAATCTTGTT
VIM	AAGTTGAGATAGCAGTCTTC	AGGTAGTCTAGTGAAGCTGT
KRT1	GATGAAATCAACAAGCGGACAA	TGGTAGAGTGCTGTAAGGAAATCAATT
IVL	ACTTATTTCGGGTCCGCTAGGT	GAGACATGTAGAGGGACAGAGTCAAG
CCL2	GAAGAATCACCAGCAGCAAGTG	GATCTCCTTGGCCACAATGG
CCL20	TGGCCAATGAAGGCTGTGA	GATTTGCGCACACAGACAACTT
CA2	AACAATGGTCATGCTTTCAACG	TGTCCATCAAGTGAACCCCAG
IL4R	CTGCCTGTTGTGCTATGTC	TCTGATCCCACCATTCTTTCT
IL13RA1	TGGGTGACAGAGCAAGACTC	CAGAGGAAAATGCTGTCGAA

Supplementary Table 5a. Primary antibodies for immunostaining of monolayer cell cultures

Antibody	Clone	Product nr	Manufacturer	Dilution
Rabbit anti-P63	H-129	sc-8344	Santa Cruz	1:100
Mouse anti-KRT14	LL002	50-255-2220	Novocastra	1:100

Supplementary Table 5b. Primary antibodies for immunostaining of HEEs

Antibody	Clone	Product nr	Manufacturer	Dilution
Mouse anti-KRT10	DE-K10	MK10	Euro-diagnostica	1:100
Mouse anti-IVL	Mon 150	-	[79]	1:20
Mouse anti-FLG	FLG01	MA5-13440	ThermoFisher	1:100
Rabbit anti-Ki67	SP6	ab16667	Abcam	1:200
Rabbit anti-CLDN1	polyclonal	51-9000	Invitrogen	1:400
Mouse anti-CLDN4	3E2C1	32-9400	Invitrogen	1:400

Supplementary Table 6. KEGG pathway analysis of DEG between iKC (CnT-30 condition) and pKC.
(This table is available upon request via the Radboud Data Repository: ru.rumc.p4fikc_r0005499a_dsc_696)

Supplementary Table 7. Ct values of CCL20 qPCR in pKC and iKC. pKC data is from a previous study and every row presents one keratinocyte donor.

	CT hARP	CT CCL20	dCT (CCL20-hARP)
pKC	17,91	32,16	14,25
	18,66	31,04	12,38
	17,09	27,57	10,48
	19,81	32,96	13,15
	18,36	26,98	8,62
	18,2	30,03	11,83
			Mean: 11,79
iPSC2-iKC P0	16.98	24.44	7.46
	17.07	24.25	7.18
	16.52	25	8.48
iPSC3-iKC P0	16.48	28.95	12.47
	16.43	28.78	12.35
	16.55	29.25	12.7

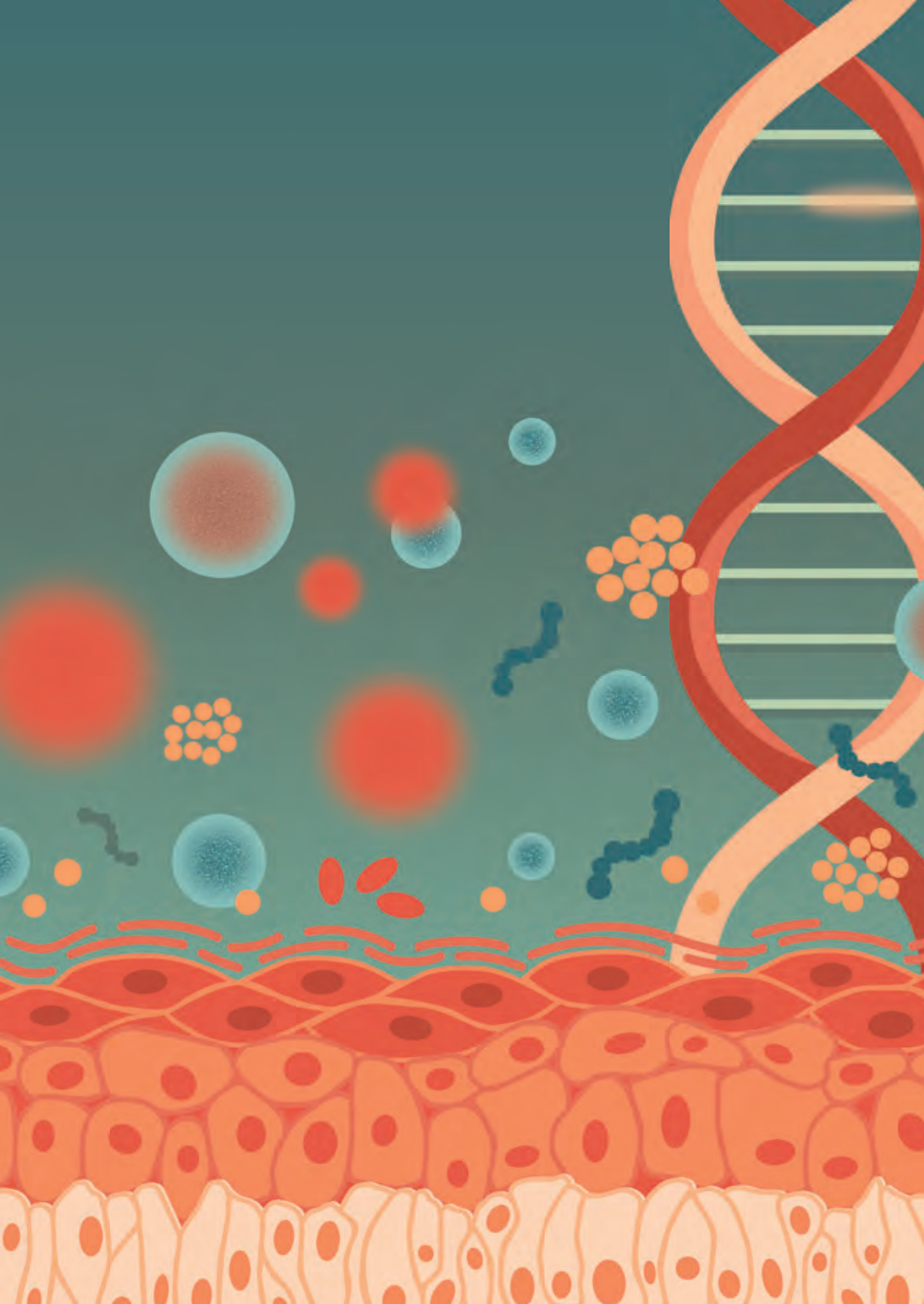

Chapter 9.

Summary, general discussion and future perspectives

General summary

As described in **chapter 1**, the epidermis provides an important barrier to the human body to retain water inside and harmful stimuli like pathogens outside. The keratinocyte's proliferation-differentiation balance and many structural proteins like filaggrin (FLG) play a key role in the epidermal barrier physiology. However, when epidermal homeostasis is disturbed, chronic inflammatory skin diseases such as atopic dermatitis (AD) can arise or worsen. The complex pathophysiology of AD, which is an interplay between genetic predisposition (e.g., *FLG* variants), the inflammatory milieu (e.g., T helper cell (Th)2, Th17 and Th22 cells and cytokines) and microbiome dysbiosis (e.g., *Staphylococcus* (*S.*) *aureus* colonization), varies between patients resulting in disease heterogeneity that impacts the efficacy of intervention strategies. Therefore, better understanding of underlying disease mechanisms is crucial for personalized and more effective treatment. Our perspective article (**Chapter 2**) stresses the important contribution of epidermal defects to AD and the need for understanding how keratinocytes contribute to inflammatory cell signaling in AD development. Moreover, the value of organotypic skin models and omics technologies are discussed to study the effects of genetic, immunologic, microbiome-mediated and environment-driven signaling events in keratinocytes. To generate these skin models, three main groups of epidermal cell types are available: primary keratinocytes, immortalized keratinocytes and stem-cell derived keratinocytes. Their advantages and disadvantages in dermatological research are discussed, next to the challenges we still face in modeling the multifactorial nature of AD. One of these challenges is the implementation of CRISPR/Cas9 genomic engineering in keratinocytes to study the effect of genetic predisposition on epidermal defects in AD. This is further entailed in **chapter 3** by a literature review on the tools used for CRISPR/Cas9-mediated editing of keratinocytes. We determined that variable editing efficiencies and low cell viability are major culprits for efficient genome editing of keratinocytes in experimental dermatology. To overcome these problems, we identified key success factors, including the use of immortalized keratinocytes with their extensive *in vitro* lifespan that facilitates the single-cell cloning procedure. In addition, electroporation of ribonucleoprotein (RNP) complexes is highly efficient for the transient expression of guide (g)RNA and Cas9 protein, while limiting the introduction of potential off-target effects. In the following empirical chapters of my thesis, the goal was to decipher disease mechanisms and key contributors to AD pathophysiology (**Chapter 4, 6, 7**), by development and usage of optimized and new AD models (**Chapter 4, 6, 7**), from various keratinocyte cell sources (**Chapter 6, 7, 8**), and a novel technology to quantitate epidermal barrier function (**Chapter 5**). Hereafter, I will provide more

extensive capsule summaries, discussion points and future perspectives per overall aim of my thesis.

Aim 1. To develop 3D human epidermal atopic dermatitis models and readouts to study disease pathophysiology

Summary

Our studies resulted in optimized or new human epidermal equivalent (HEE)-based models and relevant readout parameters for future research on AD disease mechanisms based on the following four innovations:

1. CRISPR/Cas9-based FLG knockout in immortalized keratinocytes mimics the effect of *FLG* loss-of-function variants (**Chapter 4**);
2. Electrical impedance spectroscopy (EIS) applied to HEEs generates a spectrum of impedances across many frequencies that correlates with epidermal differentiation (EIS^{diff}) and *stratum corneum* thickness (EIS^{sc}) (**Chapter 5**);
3. Exposure of HEEs to combinations of Th2 cytokines with interleukin (IL)-17A or IL-22 creates a disease-associated inflammatory milieu with varying degrees of epidermal barrier defects (**Chapter 6**);
4. Transcriptomic technologies (like RNA-seq used in this thesis) are powerful to compare *in vitro* models to *in vivo* skin, illustrating what we can and cannot model yet and fuel human model optimization strategies;
5. Topical application of microbiota on HEEs, exemplified by *S. aureus* colonization or infection, demonstrates effects of AD-associated microbiome dysbiosis and (long-term) epidermis-microbe interactions in health and disease (**Chapter 7**);
6. Bacterial strains isolated from an AD patient induced a stronger host defense response and infected basolateral culture medium quicker as compared to a laboratory strain. Thereby, AD patient-derived strains may be better suited to model skin infections in AD.

Discussion and future perspectives

Towards more personalized or AD endotype-specific in vitro models

Our developed models and readout methodologies are key in unraveling the effects of protein loss (FLG), presence of particular inflammatory cytokines (IL-4, IL-13, IL-17A, IL-22) and microbial colonization (*S. aureus*) on epidermal development. In the near future, these innovations can also provide a solid basis to develop disease phase (acute vs. chronic) or endotype-specific (e.g., ethnicity,

age) AD models. For instance, clinical studies have demonstrated which immune cells and mediators are more highly present in the skin of AD patients with specific endotypes as compared to healthy control skin, and which epidermal changes can be observed in these endotypes [1]. Using this knowledge, cytokines associated to the endotype of interest can be tested in HEEs while screening for the desired epidermal changes. As a result, the most optimal cocktail can be applied and the HEE serves as a drug screening platform for this specific endotype, albeit still not fully covering the (patient- or endotype-specific) complexity that contributes to the pathophysiology *in vivo*. Depending on the experimental question, extension of the models presented in this thesis will be required. To improve the resemblance of the genetic, inflammatory and microbial influences on the epidermis in AD, I propose the following model optimizations:

- With respect to genetic predisposition of AD by *FLG* variants, we used non-homologous end joining in **chapter 4** to disrupt the *FLG* gene, leading to an early stop codon in the third (and last) exon of the *FLG* gene and thus truncated protein. This facilitated identification of direct effects of FLG loss. However, patient variants are located in different regions of the *FLG* gene and may not result in a stop codon but a frameshift [2], which determines the functionality of the protein domains resulting in different effects sizes [3]. To reproduce patient variants, homology-directed repair could be used to provide donor DNA, as explained in **chapter 3**. However, this can be difficult if the patient variant is not close to a protospacer adjacent motif (PAM site, next to where Cas9 cuts) and therefore large DNA templates need to be incorporated. Emerging techniques like base-editing and prime-editing allow for precise base changes or small insertions/deletions respectively, of which prime-editing introduces the least off-target effects [4, 5]. These techniques could therefore be utilized to recreate one of the most common loss-of-function variants in AD patients in the Western population called p.R501X (c.1501C>T) [2]. Alternatively, primary keratinocytes [6] or induced pluripotent stem cell (iPSC)-derived keratinocytes [7] from AD patients with known *FLG* variants could be used, depending on the experimental questions or models. With the prerequisite that iPSC-derived keratinocytes will form skin models with a proper barrier function, these cells offer the possibility to generate full thickness skin equivalents with the same genetic background, by differentiation of patient-derived iPSC into multiple skin cell types, and subsequent genetic variant correction to correlate the genetic variant to functional epidermal defects. The practical difficulties of this approach are discussed below under "AIM 2".

- Our cytokine-driven AD models from **chapter 6** are relatively simple models that allow for unraveling direct effects of inflammatory cytokines on epidermal keratinocytes. However, to better resemble the disease complexity, inflammatory feedback loops between cell types are needed, which requires multicellular *in vitro* models. For example, atopic itch is a common and detrimental symptom of AD, which is caused by an interplay between keratinocytes, immune cells and neurons [8, 9]. Current keratinocyte-neuron interaction models are based on skin equivalents with neuronal cell line-derived neurons [10] or iPSC-derived organoids with neurons [11, 12]. Additional inclusion of immune cells would enable their interaction with the keratinocytes [13, 14] and allow validation of targeted drugs. Our recent review highlights immunocompetent AD models that incorporate T cells [15], but also group 2 innate lymphoid cells, Langerhans cells, dendritic cells, B cells and mast cells, along with their inflammatory mediators are associated with the disease [16]. Therefore, other immunocompetent models should be used as a basis for further research [17-20], although increasingly complex skin models also come with practical challenges. The major hurdle comes from the specific cell culture requirements per cell type that calls for optimized culture media formulations. By identifying the crucial components in the keratinocyte and immune cell media, and developing a single formulation, the longevity of multiple cell types in one model could be extended. Furthermore, multicellular models may benefit from a dynamic flow of cell culture media (e.g., microfluidic platforms) instead of the generally used static transwell plates, or the construction of tissue by bioprinting to control the spatial organization of cell types [15]. These advanced skin models have been discussed by European experts that join forces in the pan-European NETSKINMODELS consortium [15]. Such experts groups are key to form consensus opinions on the best suited models and technologies for applications in dermatological research.
- For future host-microbiome interaction studies, our bacterial inoculation method for microbial exposure of HEEs (**chapter 7**) can be used to colonize multiple (patient-derived) commensal and pathogenic bacteria, fungi [21-23], or full microbiomes. It should be considered that the epidermal model we used mimics colonization of microbiota at the surface of the *stratum corneum* under aerobic conditions. This favors aerobe bacterial species like *Staphylococcus* that increase in relative abundance over time as compared *Cutibacterium* species that only survive but do not expand [24]. Therefore, to better preserve microbial diversity, more complex models that include anaerobic and sebum-rich niches could facilitate the colonization of diverse microbial populations [25]. These anaerobic and sebum-rich niches in native skin are the sebaceous glands and hair follicles, for which skin models are scarce but in recent development [12, 26, 27].

In my thesis, we mainly focused on the host responses to *S. aureus*. However, to fully understand host-microbe interactions or to identify microbial targets for growth inhibition of pathogenic microbiota, human and microbial responses should be distinguished. Metatranscriptomics allows for mapping of the reads to the human genome assembly and retaining the other reads for microbial analyses [28], thereby allocating functional responses to either host or microbes. A quicker and cheaper alternative to analyze expression of pre-defined marker genes would be to separate human and microbial mRNA before qPCR analysis. For both techniques, the required mRNA input as well as the corresponding surface size of the 3D culture should be determined to ensure sufficient RNA yields for gene expression analysis.

- Ultimately, a "combined AD model" featuring a predisposing genetic *FLG* variant, a pathogenic inflammatory milieu, and microbiome dysbiosis including *S. aureus* overgrowth, would enable the investigation of interactions between all underlying disease factors, which is further discussed below under "AIM 3".

Application of molecular and functional readout analyses to in vitro AD models

Besides conventional morphology (H&E), gene (RT-qPCR) and protein (immunostaining) analyses used in this thesis for model characterization and validation, we focused on the development of quantitative barrier function technologies and applied comprehensive transcriptomic analyses to investigate model characteristics and disease mechanisms. The following considerations should be taken into account for data interpretation and their future use:

- The EIS technology and smart-lid application developed by Locsense for our HEE culture platform provides a relatively quick, medium throughput and standardized readout for epidermal barrier function with its fixed electrode setup and semiautomated handling (**Chapter 5**). In addition, it proved noninvasive, allowing for consecutive measurements, and reducing experimental scales. However, we experienced that, similar to what we observed in **chapter 7**, topical application of PBS on HEEs (necessary for conductance) can induce *stratum corneum* swelling after repetitive measurement and longer time of liquid immersion of the models during the measurement. Since the EIS machine currently measures HEEs successively, adapting the software to facilitate simultaneous measurement of HEEs will reduce exposure time to PBS and improve study outcomes. For future application of the EIS technique to decipher the pathophysiology of inflammatory skin diseases, we need to better understand what the EIS spectrum that we proposed to correlate with *stratum corneum* characteristics actually correlates to. We found a correlation between EIS^{sc} and *stratum corneum* thickness, but we could not determine

whether this simply means the number of cornified layers or the additional barrier properties of these extra layers. To investigate so, mass spectrometry and electron microscopy are recommended to evaluate *stratum corneum* structure and content like lipids [29, 30], keratin filaments [31] and proteins [32] that form the stratum corneum barrier [33]. Comparison of IL-4 + IL-13 (reduced EIS^{sc}) with IL-17A + IL-22 (increased EIS^{sc})-stimulated HEEs would aid these correlation experiments.

- For extensive molecular characterization of our AD models, bulk RNA-seq and spatial single-cell transcriptomics pipelines were employed and developed respectively (**Chapter 6**). Whereas bulk RNA-seq is an objective readout that does not require pre-determined target choices, spatial transcriptomics provided candidate gene expression information at the single-cell level. Hence, both showed to be complementary with the latter being extremely labor intense and requiring expert handling expertise for the sample preparation, analysis and data procurement. Furthermore, establishment of scRNA-seq of epidermal equivalents (including optimal dissociation protocols) would greatly accelerate model characterization, allowing whole transcriptome analysis and in silico spatial mapping of gene expression profiles. While these single-cell technologies are now widely used for healthy and AD skin biopsies [34-36], they are not commonly used for *in vitro* skin, with some exceptions [37-39]. Potentially, this scarcity relates to dissociation issues and difficulties obtaining large numbers of live cells from all *in vitro* epidermal cell layers. For instance, the granular epidermal layer appears underrepresented in scRNA-seq data, likely due to extensive crosslinking and advanced terminal differentiation process of cells, which leads to rapid cell death and loss of mRNA molecules [40, 41]. Nuclear RNA-seq could pose a solution to this problem by recovering more (subsets of) cell types and reducing dissociation bias [40], which may apply to granular keratinocytes that are tightly connected as compared to (supra)basal keratinocytes. Alternatively, spatial transcriptomics, as used in **chapter 6**, does not require cell dissociation and preserves the tissue's spatial context, but it does require prior selection of genes to be analyzed.

Comparison of in vitro epidermal models to in vivo skin for model optimization

The two optimized AD cytokine cocktails (Th2 + IL-17A versus Th2 + IL-22) induced similar but also distinct AD features in our epidermal model. The choice of which cytokine cocktail to perform follow-up experiments with was therefore based on overall similarity to *in vivo* AD skin. As representative *in vivo* data, we used I) a pseudobulk of keratinocyte transcriptomes acquired from scRNA-seq of skin biopsies, and II) full thickness skin transcriptomes obtained from microarray and bulk RNA-seq of skin biopsies. The retrieval of the first dataset was most optimal, since it allowed to compare our keratinocyte-only model to only keratinocytes

of the skin, however only four AD patients were included in this study [34]. The second method offered a less fair comparison between cell types present *in vitro* and *in vivo*, but with the strength of a greater sample size (188 AD patients). The use of publicly available data is a quick, cost-effective and sustainable way in scientific research, but one has to compromise as existing studies and their chosen methods may not fully align with own studies and experimental samples. In addition, to understand the implications of the *in vitro-in vivo* comparison, it is important to know characteristics of the patient cohort. In our case, the cytokine cocktail contained Th2 and Th17/22 cytokines in absence of Th1 cytokines, which represents the situation of acute AD [1], while the four patients of Rojahn et al. (2020) probably presented chronic AD as demonstrated by the differential expression of interferon responsive genes. Logically, this resulted in a lack of (Th1-driven) IFN signaling *in vitro* when transcriptomically comparing to *in vivo* data, thereby lowering the overlap in differentially expressed genes. Next to these biology-founded differences, we also encountered a better comparison of *in vitro* models based on the keratinocyte source used to generated them. We found a greater overlap of differentially expressed genes in N/TERT-2G AD models with AD patients, as compared to primary keratinocyte AD models. This, however, may not be biologically relevant but merely a technical issue resulting from the heterogeneity in responses of primary keratinocytes from different donors, while N/TERT-2G-derived HEEs showed less variation in transcriptional response, which increased statistical power and increased the number of significant differentially expressed genes that corresponded to the *in vivo* transcriptome.

Aim 2. To investigate which keratinocyte cell sources are valuable to unravel the different underlying genetic, inflammatory and microbiome mechanisms of AD

Summary

Considering primary keratinocytes as the gold standard for *in vitro* epidermal research, we characterized two alternative cell sources and compared them to primary cells (Table 1). Our research highlights that:

1. Immortal N/TERT-2G keratinocytes exhibit a similar response to the Th2 + IL-22 cytokine cocktail, with the exception of milder hyperproliferation and barrier impairment (**Chapter 6**). They also show comparable *S. aureus* colonization rates and antimicrobial peptide production upon infection *in vitro* (**Chapter 7**);
2. iPSC-derived or induced keratinocytes (iKC) seem suitable to model cytokine-driven epidermal differentiation defects, while their expression of cytokines and chemokines is less induced by the Th2 + IL-22 cocktail (**Chapter 8**);
3. scRNA-sequencing is highly valuable for determination of the cell maturation status and heterogeneity of iKC and reveals different cell populations in the iKC culture that are characterized by expression of specific cell surface markers.

Table 1. The AD hallmarks that can be modeled per keratinocyte cell type according to this thesis and literature. + Can be modeled; +/- Can be partially modeled; - Cannot be modeled

AD hallmark	**Cell type**	**Primary keratinocytes**	**N/TERT-2G immortalized keratinocytes**	**iPSC-derived keratinocytes**
Cytokine-driven	*Hyperproliferation*	+	+/-	Not investigated yet
	Epidermal differentiation defects	+	+	+ (only investigated in 2D monolayers)
	Impaired barrier	+	+/-	Not investigated yet
	Inflammatory gene expression	+	+	-
Genetics-driven	*Epidermal differentiation defects and impaired barrier*	Table 1 from Chapter 2, and [6]	+	Not investigated yet, but cells are available [7]
Pathogen-driven	*Antimicrobial peptide production*	+	+	Not investigated yet
	Epidermal infections	+	+	Not investigated yet

Discussion and future perspectives

The utility of alternative keratinocytes greatly depends on their similarity to the gold standard primary keratinocytes and requires in-depth characterization, which we started in **chapter 6 and 7**. To further benchmark N/TERT-2G immortal cells to primary keratinocytes, increasing the cytokine concentrations or testing hydrocortisone-free medium to assess whether hyperproliferation and barrier impairment become more prominent while maintaining cell viability would be useful. However, one must consider that N/TERT-2G cells are derived from one specific donor and, alike primary keratinocytes, inter-donor variability determines the cellular responses. Hence, the N/TERT cells may simply respond differently to cytokines than the primary keratinocytes tested here. This may be results from their origin, being foreskin-derived and known for differential responses as compared to primary keratinocytes [42]. Therefore, experimental studies using N/TERT-2G keratinocytes would benefit from validation with an extended panel of primary keratinocyte donors.

For the application of iPSC-derived keratinocytes, which are currently the least well characterized keratinocyte cell type for AD studies, the culture heterogeneity still seems a challenge (see scRNA-seq in **chapter 8**). This might be the reason that iKC are not yet capable to form an epidermal barrier similar to pKC when used to generate HEEs. The iKC population most similar to pKC demonstrated expression of integrin (ITG)A6+ on their cell surface, which allows for positive cell sorting. However, the scRNA-seq analysis should first be repeated with iKC at higher passage numbers, to determine whether passaging further induced maturation of a subpopulation or enriched keratinocyte-like cells and how this affects their cell surface marker expression profile. Hereafter, to demonstrate if iKC are suitable to model and decipher AD (alike studies with primary keratinocytes and N/TERT keratinocytes proposed under "AIM 1 and 3"), comparison of the response of unsorted iKC, sorted iKC and pKC to AD cytokines and bacteria is needed. Future extension of our preliminary scRNA-seq analyses to include the expression analysis of pattern recognition and cytokine receptors for the three identified iKC clusters would suggest the potential benefit of cell sorting. The next step would be to analyze the iKC response to heat-killed *S. aureus* or its supernatant in comparison to the response of pKC in 2D monolayers [43, 44]. Additionally, if the epidermal barrier of iKC-HEEs can be improved, even microbial colonization can be performed on 3D models. Currently, the only skin microbiota models using iPSC are skin organoids, which are cut open to flip the epidermis outward for bacterial colonization at the air-liquid interface [45]. However, barrier protein expression and function, as well as long-term bacterial colonization without infections, were neither investigated nor presented in this study.

Aim 3. To dissect how genetic predisposition, inflammatory cytokines and microbiome dysbiosis drive epidermal defects and how these can be restored upon treatment

Summary

We demonstrated the effects of three AD predisposing factors on epidermal functioning and its restoration through therapeutics (illustrated in Figure 1), emphasizing the potential of AD-HEEs to unravel disease pathophysiology and facilitate drug screening:

1. FLG knockout keratinocytes are not only deficient in FLG but also present a (partial) loss of other epidermal differentiation proteins and a compromised epidermal barrier in HEEs, which is restored by the re-expression of FLG (**Chapter 4**);
2. Epidermal models generated from keratinocytes with a knockout of differentiation or barrier proteins, or stimulated with inflammatory cytokines, exhibit lower EIS values and, therefore, compromised barrier function, linking these specific AD-related proteins and cytokines to barrier defects (**Chapter 5**);
3. The presence of IL-22 in the Th2 cytokine milieu drives key morphological and transcriptomic AD hallmarks, resulting in major skin barrier defects (**Chapter 6**);
4. The combination of epidermal differentiation-promoting (AHR ligand tapinarof) and inflammation-inhibiting (JAK1/3 inhibitor tofacitinib) drugs more effectively restores epidermal defects driven by multiple cytokines compared to single therapeutics;
5. A clinical *S. aureus* isolate from an AD patient induced a strong host defense response and cell culture infections, indicating that this strain was able to cause barrier defects. The antimicrobial peptides (AMP) produced in the epidermis could not prevent subsequent infections (**Chapter 7**);
6. Topical application of antibiotic fusidic acid inhibited growth, infection, and epidermal damage caused by the *S. aureus* strain of the AD patient.

Discussion and future perspectives

Successful AD model optimization, as proposed under "AIM 1", would require characterization of these models against the current ones (e.g., HEEs with patient *FLG* variants versus our FLG knockout), yielding information on the contribution of specific variants to epidermal barrier defects, or even the potential benefit of gene correction. In addition, to decipher the role of *S. aureus* in AD development and skin infections, multiple clinical *S. aureus* isolates from patients with clinically defined varying degrees of disease (e.g., SCORAD or EASI assessment-based) should

be screened in epidermal models for their infection potential and secretome, in order to pinpoint causal virulence factors and potential intervention strategies.

Knowledge on endotype-specific disease mechanisms from AD-HEE models could hint toward which patient groups would benefit from specific therapeutic strategies e.g., targeting particular cytokines (IL-4, IL-13, IL-22), receptors (IL-4R, AHR), or microbiota (antibiotics), and make the drug choices in clinics more efficient. While many different interaction studies can be performed *in vitro* to understand the underlying genetic, inflammatory and microbial imbalances in AD, the following poorly understood disease mechanisms can particularly be studied in our HEEs. Filaggrin breakdown products like trans-urocanic acid (UCA) and 2-pyrrolidone-5-carboxylic acid (PCA) influence the skin pH and *S. aureus* growth [46]. As natural moisturizing factors (NMFs) also contribute to the skin hydration status, and microbiota vary between body sites with different hydration status and pH [47], an interaction between FLG and microbial growth is suggested [48]. To investigate if *FLG* variants related to AD thereby also influence *S. aureus* growth and/or epidermal infections as seen in AD, host-microbe interaction studies between FLG wildtype and FLG null keratinocytes and various clinical isolates of *S. aureus* would be useful in HEE models. This complexified AD model would also accelerate drug screening or predict the effectiveness of gene therapies [49] or microbiome transplantation [50]. Currently, FDA-approved JAK inhibitors (e.g., abrocitinib, upadacitinib, baricitinib, tofacitinib), of which tofacitinib showed to be effective to prevent epidermal defects upon cytokines in this thesis, come with side-effects like infections [51]. Combination of immunocompetent skin models with our microbial colonization technique on epidermal equivalents will allow to test drug combinations that minimize this infection risk.

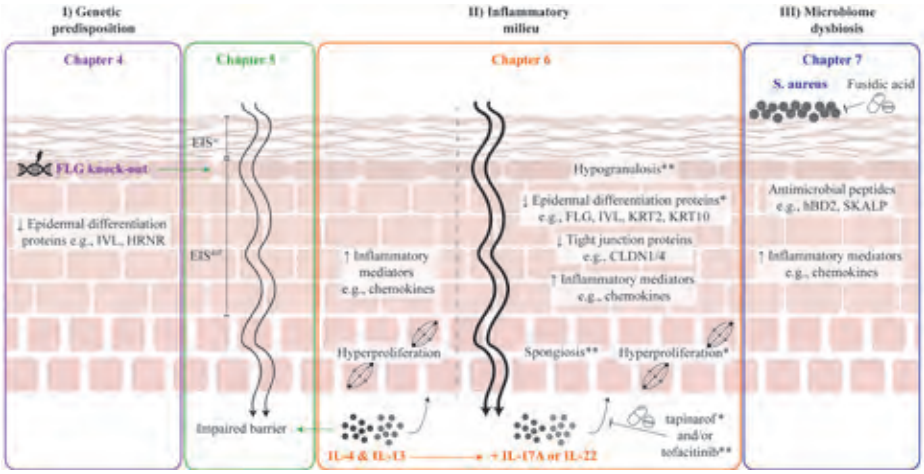

Figure 1. Summary of epidermal defects driven by genetic loss of FLG, AD-associated inflammatory cytokines, and *S. aureus* colonization as investigated through human epidermal equivalents in this thesis. The culture manipulation is visualized in bold and color, and effects thereof in black. The tested therapeutics are presented by blunt arrows (⊥). * shows the defects that are rescued by tapinarof, and ** by tofacitinib. Of note, the defects can be present in more epidermal layers than the text is annotated in.

Final consideration

"Altogether, I envision that comparing *in vitro* disease models to well-characterized *in vivo* patient skin tissue samples, using omics approaches, will drive the development of disease (endotype-specific) models. These models will not only reduce the need for experimental animals in unraveling disease mechanisms, but also facilitate drug screening, making decisions on therapeutic strategies more patient-centered and thereby, hopefully, more efficient."

References

1. Czarnowicki, T., et al., Atopic dermatitis endotypes and implications for targeted therapeutics. J Allergy Clin Immunol, 2019. **143**(1): p. 1-11.
2. Virolainen, S.J., et al., Filaggrin loss-of-function variants are associated with atopic dermatitis phenotypes in a diverse, early-life prospective cohort. JCI Insight, 2024. **9**(9).
3. Sandilands, A., et al., Filaggrin in the frontline: role in skin barrier function and disease. J Cell Sci, 2009. **122**(Pt 9): p. 1285-94.
4. Doman, J.L., et al., Designing and executing prime editing experiments in mammalian cells. Nat Protoc, 2022. **17**(11): p. 2431-2468.
5. Chen, P.J. and D.R. Liu, Prime editing for precise and highly versatile genome manipulation. Nat Rev Genet, 2023. **24**(3): p. 161-177.
6. Niehues, H., et al., Epidermal equivalents of filaggrin null keratinocytes do not show impaired skin barrier function. J Allergy Clin Immunol, 2017. **139**(6): p. 1979-1981.e13.
7. Devito, L., et al., Induced pluripotent stem cell line from an atopic dermatitis patient heterozygous for c.2282del4 mutation in filaggrin: KCLi001-A. Stem Cell Res, 2018. **31**: p. 122-126.
8. Wilson, S.R., et al., The epithelial cell-derived atopic dermatitis cytokine TSLP activates neurons to induce itch. Cell, 2013. **155**(2): p. 285-95.
9. Biazus Soares, G., T. Hashimoto, and G. Yosipovitch, Atopic Dermatitis Itch: Scratching for an Explanation. J Invest Dermatol, 2024. **144**(5): p. 978-988.
10. Freer, M., et al., Development of a mammalian neurosensory full-thickness skin equivalent and its application to screen sensitizing stimuli. Bioeng Transl Med, 2023. **8**(3): p. e10484.
11. Lee, J., et al., Generation and characterization of hair-bearing skin organoids from human pluripotent stem cells. Nat Protoc, 2022. **17**(5): p. 1266-1305.
12. Lee, J., et al., Hair-bearing human skin generated entirely from pluripotent stem cells. Nature, 2020. **582**(7812): p. 399-404.
13. Wallmeyer, L., et al., TSLP is a direct trigger for T cell migration in filaggrin-deficient skin equivalents. Sci Rep, 2017. **7**(1): p. 774.
14. Engelhart, K., et al., In vitro reproduction of clinical hallmarks of eczematous dermatitis in organotypic skin models. Arch Dermatol Res, 2005. **297**(1): p. 1-9.
15. Quílez, C., et al., Targeting the Complexity of In Vitro Skin Models: A Review of Cutting-Edge Developments. J Invest Dermatol, 2024. **144**(12): p. 2650-2670.
16. Brunner, P.M., E. Guttman-Yassky, and D.Y. Leung, The immunology of atopic dermatitis and its reversibility with broad-spectrum and targeted therapies. J Allergy Clin Immunol, 2017. **139**(4s): p. S65-s76.
17. Hölken, J.M., et al., A human 3D immune competent full-thickness skin model mimicking dermal dendritic cell activation. Front Immunol, 2023. **14**: p. 1276151.
18. Di Blasio, S., et al., The tumour microenvironment shapes dendritic cell plasticity in a human organotypic melanoma culture. Nat Commun, 2020. **11**(1): p. 2749.
19. Mulder, P.P.G., et al., Monocytes and T cells incorporated in full skin equivalents to study innate or adaptive immune reactions after burn injury. Front Immunol, 2023. **14**: p. 1264716.
20. Ouwehand, K., et al., Comparison of a novel CXCL12/CCL5 dependent migration assay with CXCL8 secretion and CD86 expression for distinguishing sensitizers from non-sensitizers using MUTZ-3 Langerhans cells. Toxicol In Vitro, 2010. **24**(2): p. 578-85.

21. Johansson, C., et al., Atopy patch test reactions to Malassezia allergens differentiate subgroups of atopic dermatitis patients. Br J Dermatol, 2003. **148**(3): p. 479-88.
22. Darabi, K., et al., The role of Malassezia in atopic dermatitis affecting the head and neck of adults. J Am Acad Dermatol, 2009. **60**(1): p. 125-36.
23. Choi, Y., et al., Comparative Analysis of Cutaneous Fungi in Atopic Dermatitis Patients and Healthy Individuals. Ann Dermatol, 2022. **34**(2): p. 118-124.
24. Larson, P.J., et al., Challenges in Developing a Human Model System for Skin Microbiome Research. J Invest Dermatol, 2021. **141**(1): p. 228-231.e4.
25. Szabó, K., et al., Factors shaping the composition of the cutaneous microbiota. Br J Dermatol, 2017. **176**(2): p. 344-351.
26. Su, Y., et al., Pre-aggregation of scalp progenitor dermal and epidermal stem cells activates the WNT pathway and promotes hair follicle formation in in vitro and in vivo systems. Stem Cell Res Ther, 2019. **10**(1): p. 403.
27. Vahav, I., et al., Reconstructed human skin shows epidermal invagination towards integrated neopapillae indicating early hair follicle formation in vitro. J Tissue Eng Regen Med, 2020. **14**(6): p. 761-773.
28. Malone, M., et al., Host-microbe metatranscriptome reveals differences between acute and chronic infections in diabetes-related foot ulcers. Apmis, 2022. **130**(12): p. 751-762.
29. Masukawa, Y., et al., Comprehensive quantification of ceramide species in human stratum corneum. J Lipid Res, 2009. **50**(8): p. 1708-19.
30. van Smeden, J., et al., LC/MS analysis of stratum corneum lipids: ceramide profiling and discovery. J Lipid Res, 2011. **52**(6): p. 1211-1221.
31. Norlén, L. and A. Al-Amoudi, Stratum corneum keratin structure, function, and formation: the cubic rod-packing and membrane templating model. J Invest Dermatol, 2004. **123**(4): p. 715-32.
32. Voegeli, R., et al., Efficient and simple quantification of stratum corneum proteins on tape strippings by infrared densitometry. Skin Res Technol, 2007. **13**(3): p. 242-51.
33. Matsui, T. and M. Amagai, Dissecting the formation, structure and barrier function of the stratum corneum. Int Immunol, 2015. **27**(6): p. 269-80.
34. Rojahn, T.B., et al., Single-cell transcriptomics combined with interstitial fluid proteomics defines cell type-specific immune regulation in atopic dermatitis. J Allergy Clin Immunol, 2020. **146**(5): p. 1056-1069.
35. He, H., et al., Single-cell transcriptome analysis of human skin identifies novel fibroblast subpopulation and enrichment of immune subsets in atopic dermatitis. J Allergy Clin Immunol, 2020. **145**(6): p. 1615-1628.
36. Mitamura, Y., et al., Spatial transcriptomics combined with single-cell RNA-sequencing unravels the complex inflammatory cell network in atopic dermatitis. Allergy, 2023. **78**(8): p. 2215-2231.
37. Stabell, A.R., et al., Single-cell transcriptomics of human-skin-equivalent organoids. Cell Rep, 2023. **42**(5): p. 112511.
38. Le Maître, M., et al., Characteristics and impact of infiltration of B-cells from systemic sclerosis patients in a 3D healthy skin model. Front Immunol, 2024. **15**: p. 1373464.
39. Reuter, C., et al., Vector-borne Trypanosoma brucei parasites develop in artificial human skin and persist as skin tissue forms. Nat Commun, 2023. **14**(1): p. 7660.

40. Wu, H., et al., Advantages of Single-Nucleus over Single-Cell RNA Sequencing of Adult Kidney: Rare Cell Types and Novel Cell States Revealed in Fibrosis. J Am Soc Nephrol, 2019. **30**(1): p. 23-32.
41. Cheng, J.B., et al., Transcriptional Programming of Normal and Inflamed Human Epidermis at Single-Cell Resolution. Cell Rep, 2018. **25**(4): p. 871-883.
42. Tjabringa, G., et al., Development and validation of human psoriatic skin equivalents. Am J Pathol, 2008. **173**(3): p. 815-23.
43. van der Krieken, D.A., et al., Gram-positive anaerobic cocci guard skin homeostasis by regulating host-defense mechanisms. iScience, 2023. **26**(4): p. 106483.
44. Ngo, Q.V., et al., Inflammatory Response Against Staphylococcus aureus via Intracellular Sensing of Nucleic Acids in Keratinocytes. Front Immunol, 2022. **13**: p. 828626.
45. Jung, S.Y., et al., Wnt-activating human skin organoid model of atopic dermatitis induced by Staphylococcus aureus and its protective effects by Cutibacterium acnes. iScience, 2022. **25**(10): p. 105150.
46. Miajlovic, H., et al., Effect of filaggrin breakdown products on growth of and protein expression by Staphylococcus aureus. J Allergy Clin Immunol, 2010. **126**(6): p. 1184-90.e3.
47. Smythe, P. and H.N. Wilkinson, The Skin Microbiome: Current Landscape and Future Opportunities. Int J Mol Sci, 2023. **24**(4).
48. Zeeuwen, P.L., et al., Gram-positive anaerobe cocci are underrepresented in the microbiome of filaggrin-deficient human skin. J Allergy Clin Immunol, 2017. **139**(4): p. 1368-1371.
49. Gorell, E., et al., Gene therapy for skin diseases. Cold Spring Harb Perspect Med, 2014. **4**(4): p. a015149.
50. Callewaert, C., et al., Skin microbiome transplantation and manipulation: Current state of the art. Comput Struct Biotechnol J, 2021. **19**: p. 624-631.
51. Adas, M.A., et al., The infection risks of JAK inhibition. Expert Rev Clin Immunol, 2022. **18**(3): p. 253-261.

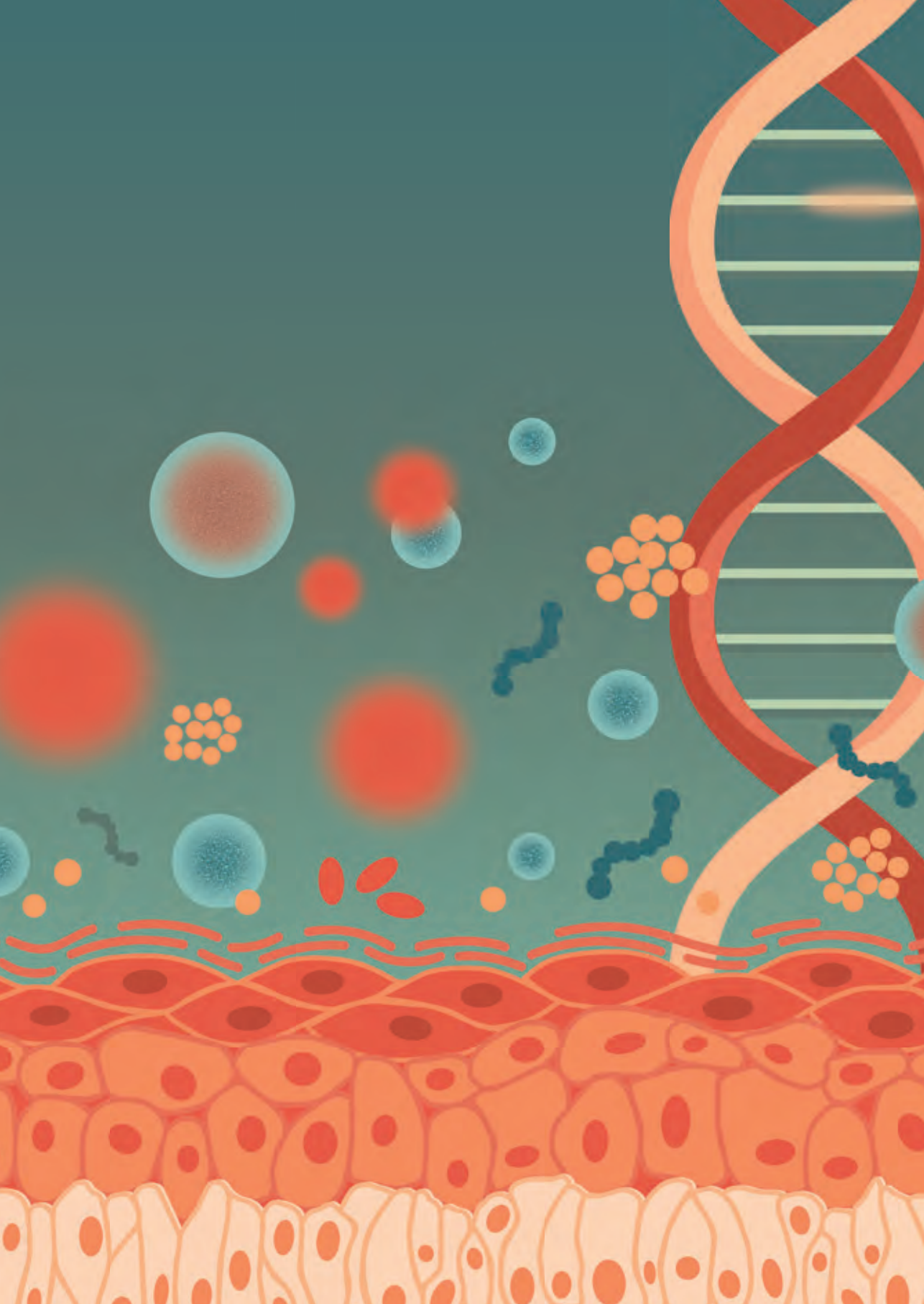

Chapter 10.

Nederlandse samenvatting

(Dutch summary)

In dit proefschrift heb ik laten zien hoe 3D huidmodellen geoptimaliseerd en gebruikt kunnen worden om de ziektemechanismen van atopisch eczeem, ook wel atopische dermatitis (AD) genoemd, beter te leren begrijpen. Dit is belangrijk om huidige behandelingen te verbeteren en nieuwe behandelingen te ontwikkelen, omdat er patiënten zijn die onvoldoende reageren of een terugval krijgen tijdens gebruik van hun medicatie.

In **hoofdstuk 1** beschrijf ik de opbouw en functie van de huid, met name van de buitenste laag, de opperhuid of epidermis. Een belangrijke functie van de epidermis is het vormen van een barrière die uitdroging voorkomt en ziekteverwekkers buitenhoudt. Zowel genetische aanleg, de aanwezigheid van overactieve cutane ontstekingscellen en hun cytokines (signaalmoleculen), als een veranderde samenstelling van het huid microbioom kunnen bijdragen aan een verstoring van de balans tussen proliferatie (celdeling) en differentiatie (cel specialisatie) van epidermale cellen, de keratinocyten. Dit alles kan leiden tot de ontwikkeling van AD. Mutaties in het filaggrine gen, wat codeert voor een belangrijk structureel eiwit van de epidermis, vormen de belangrijkste genetische aanleg voor AD. Veelvoorkomende ontstekingscellen in de huid van AD patiënten zijn de T helper cellen (Th)2, 17 en 22, die cytokines zoals interleukine (IL)-4, IL-13 en IL-22 uitscheiden. Daarnaast is aangetoond dat de microbiële samenstelling op de huid van AD patiënten minder divers is dan dat van gezonde vrijwilligers. In het microbioom is onder andere meer *Staphylococcus (S.) aureus* aanwezig. Dit noemen we dysbiose van het microbioom. De precieze gevolgen van deze drie bovengenoemde factoren op het functioneren van de epidermis zijn lastig te bestuderen in het menselijk lichaam (*in vivo*). De aanwezigheid van andere cellen dan keratinocyten vertoebeld het beeld. Daarnaast is het onethisch om deze ziekteprocessen aan te wakkeren in gezonde personen, en zijn proefdieren in veel opzichten te verschillend van mensen. Humane 3D huidmodellen (epidermale equivalenten) zijn daarom een waardevol alternatief. Voor het genereren van humane epidermale equivalenten kunnen verschillende cellen gebruikt worden, namelijk primaire keratinocyten van gezonde vrijwilligers, onsterfelijk gemaakte keratinocyten, of keratinocyten die zijn gedifferentieerd vanuit stamcellen. Elk van deze keratinocyten heeft zijn voor- en nadelen in het onderzoek naar AD, en daarom bepaalt de onderzoeksvraag welke het meest geschikt is. In **hoofdstuk 1 en 2** beschrijven we hoe de drie bovengenoemde ziekte aandrijvers (genetische aanleg, overactieve ontstekingscellen en microbioom dysbiose) gemodelleerd kunnen worden in 3D huidmodellen.

In **hoofdstuk 3** geven we een overzicht van methodes voor het genetisch modificeren van keratinocyten met de CRISPR/Cas9 techniek, en wat er nodig is voor de succesvolle toepassing van deze techniek. Deze kennis hebben we gebruikt in **hoofdstuk 4** om het filaggrine gen zodanig aan te passen waardoor keratinocyten een verkort en niet functioneel eiwit maken, zoals ook in AD het geval kan zijn. Het bijkomende effect was dat ook andere epidermale differentiatie-eiwitten verminderd tot expressie kwamen en dat de epidermale barrièrefunctie verslechterd was. Vervolgens hebben we in **hoofdstuk 5** deze barrièremeting, genaamd elektrische impedantiespectroscopie (EIS), verder gevalideerd voor het analyseren van 3D epidermale equivalenten. De EIS waardes konden we correleren aan de aanwezigheid van epidermale differentiatie-eiwitten en *stratum corneum* (hoornlaag) dikte.

Aan de hand van deze EIS techniek, evenals morfologie-, eiwit- en genanalyses, hebben we diverse combinaties van inflammatoire cytokines gekoppeld aan verschillende epidermale AD-kenmerken in **hoofdstuk 6**. Hierdoor hebben we ontdekt dat de aanwezigheid van IL-17A of IL-22 in een Th2 cytokine milieu (IL-4 en IL-13) leidt tot ernstigere epidermale defecten en grotere overeenkomsten met *in vivo* AD patiënten dan Th2 cytokines alleen. Deze combinatie van cytokines is dus een verbetering ten opzichte van het voorheen vaak gebruikte AD model met alleen Th2 cytokines. Deze defecten van ons epidermale AD model werden grotendeels hersteld door behandeling met een combinatie van AD medicijnen: aryl hydrocarbon receptor (AHR) stimulerende tapinarof en Janus Kinase (JAK) remmende tofacitinib.

Naast het modeleren van de inflammatoire oorzaak van AD, hebben we een manier gevonden om bacteriën aan te brengen op epidermale modellen om langdurige huid-microbioom interacties en dysbiose van het microbioom te onderzoeken (**Hoofdstuk 7**). We vonden dat een *S. aureus* laboratoriumstam een minder sterke afweerrespons veroorzaakt dan een klinische stam die geïsoleerd is van een AD patiënt. Ook veroorzaakten klinische stammen vaker infecties dan de laboratorium stam. Voor het modeleren van AD en microbioom onderzoek is het dus belangrijk om (klinische) stammen van AD patiënten te gebruiken. Ook konden we in dit huid-microbioom model gerichte behandelingen testen, waarbij topicale toepassing van fusidinezuur de bacteriële infecties en epidermale schade voorkwam.

Na het bestuderen van deze drie belangrijke factoren die bijdragen aan de pathofysiologie van AD, hebben we ook onderzoek gedaan naar alternatieve cellen om epidermale AD modellen mee te maken. Geïnduceerde pluripotente

stamcellen (iPSC) kunnen gemaakt worden van AD patiënten cellen, waardoor ze de genetische informatie bevatten die bijdraagt aan de ziekte ontwikkeling. Vervolgens kunnen deze iPSC, in theorie, gedifferentieerd worden naar verschillende huidcellen, waaronder keratinocyten. Echter, om ze voor AD onderzoek te gebruiken, moet de differentiatie van iPSC naar keratinocyt leiden tot een homogene populatie van geïnduceerde keratinocyten die vergelijkbaar functioneren als primaire keratinocyten (de gouden standaard in dermatologisch onderzoek). In **hoofdstuk 8** hebben we een geoptimaliseerd protocol beschreven om vanuit iPSC zoveel mogelijk keratinocyt-achtige cellen te verkrijgen. Daarnaast stellen we een methode voor om de gewenste cellen te selecteren op basis van membraaneiwit expressie, met behulp van MACS of FACS, om de heterogeniteit verder te reduceren. Om epidermale differentiatie na te bootsen en het nut van geïnduceerde keratinocyten in AD onderzoek te bestuderen, hebben we differentiatie stimulatoren calcium en serum gebruikt met of zonder AD-gerelateerde cytokines IL-4, IL-13 en IL-22. De geïnduceerde keratinocyten waren in staat om epidermale differentiatiemarkers tot expressie te brengen, wat werd tegengehouden door AD cytokines. Hierdoor lijken ze geschikt om epidermale differentiatie-defecten te bestuderen. Epidermale equivalenten gemaakt van geïnduceerde keratinocyten toonden stratificatie kenmerken en de vorming van een *stratum corneum*, hetgeen hun toepassing in de ontwikkeling van 3D huidmodellen benadrukt.

Algemene conclusies uit deze thesis zijn:

1. Geoptimaliseerde epidermale modellen en nieuwe uitleesmethodes zijn ontwikkeld en kunnen gebruikt worden om AD te bestuderen;
2. De waarde van alternatieve onuitputtelijke keratinocytbronnen voor AD onderzoek, waaronder onsterfelijk gemaakte keratinocyten en keratinocyten afgeleid van stamcellen, is aangetoond;
3. Meer inzichten zijn verkregen over de bijdrage van genetische aanleg, inflammatoire cytokines en dysbiose van het microbioom aan epidermale defecten in AD;
4. Het beïnvloeden van verschillende signaaltransductieroutes door een combinatie van medicijnen kan de effectiviteit van de interventie vergroten bij specifieke AD patiënten met een complexe inflammatoire component.

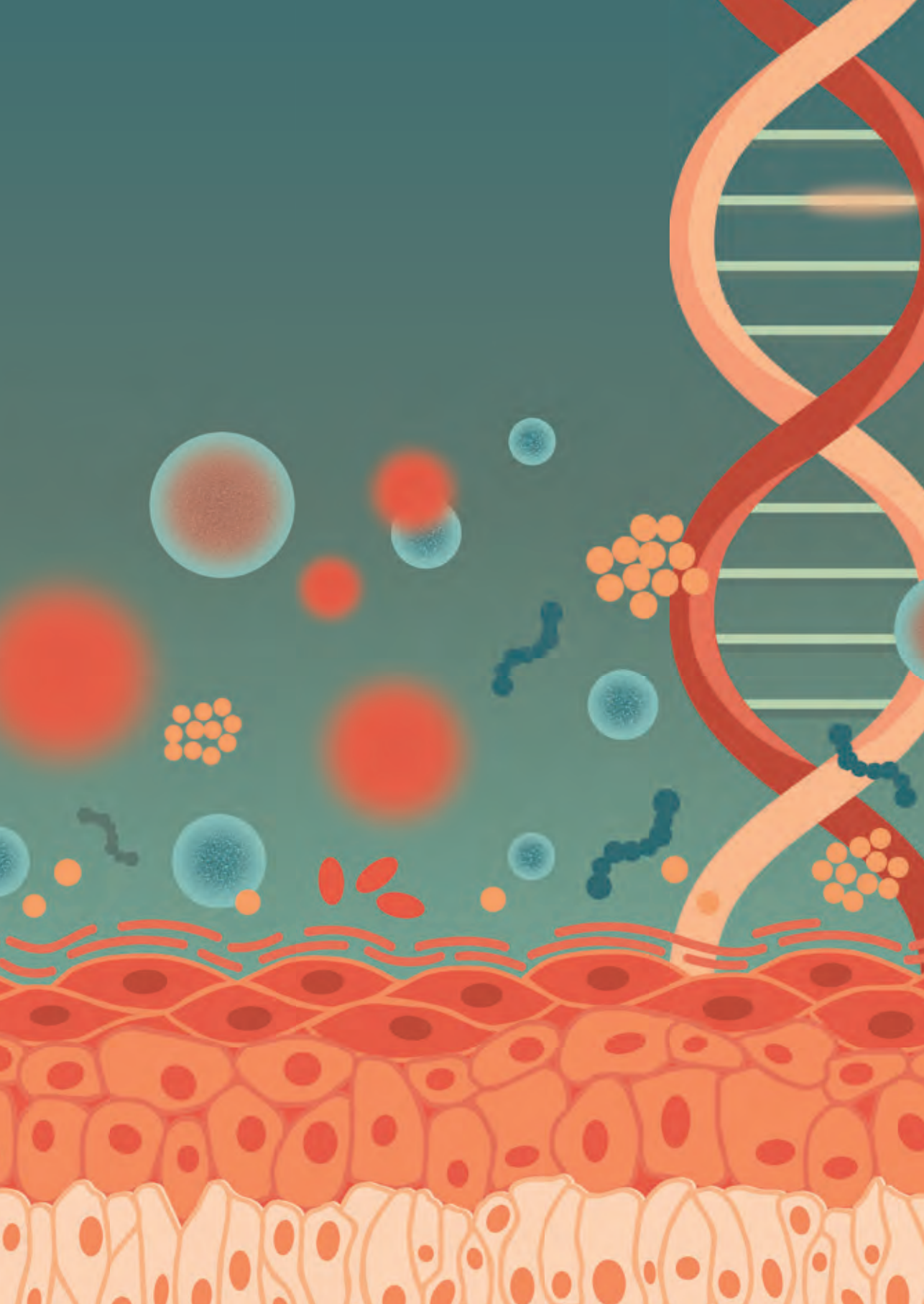

Chapter 11.

Appendices

List of publications

Publications related to this thesis:

1. Luca D. Meesters, Janou A.Y. Roubroeks, Aranka Gerritsen, Niels Velthuijs, Jaimy A. Klijnhout, Camille Laberthonnière, Ivonne M. van Vlijmen-Willems, Matthias Hübenthal, Diana Rodijk-Olthuis, Rens H.W. Peters, Gijs Rikken, Silke Szymczak, Nanna Fyhrquist, Harri Alenius, Stephan Weidinger, Jos P.H. Smits, Musa Mhlanga, Huiqing Zhou, Hanna Niehues, Ellen H. van den Bogaard. Dissecting key contributions of Th2 and Th17 cytokines to atopic dermatitis pathophysiology. *J Allergy Clin Immunol*. 2025 May 21:S0091-6749(25)00570-6. Online ahead of print.
2. Cristina Quílez, Luís B. Bebiano, Eleri Jones, Uroš Maver, Luca D. Meesters, Piotr Parzymies, Emma Petiot, Gijs Rikken, Ignacio Risueño, Hamza Zaidi, Tanja Zidarič, Sander Bekeschus, Ellen H. van den Bogaard, Matthew Caley, Helen Colley, Nuria Gago López, Sophia Letsiou, Christophe Marquette, Tina Maver, Rúben F. Pereira, Desmond J. Tobin, Diego Velasco. Targeting the Complexity of In Vitro Skin Models: A Review of Cutting-Edge Developments. *J Invest Dermatol*. 2024 Dec;144(12):2650-2670.
3. Noa J.M. van den Brink, Felicitas Pardow, Luca D. Meesters, Ivonne van Vlijmen-Willems, Diana Rodijk-Olthuis, Hanna Niehues, Patrick A.M. Jansen, Susan H. Roelofs, Matthew G. Brewer, Ellen H. van den Bogaard, Jos P.H. Smits. Electrical Impedance Spectroscopy Quantifies Skin Barrier Function in Organotypic In Vitro Epidermis Models. *J Invest Dermatol*. 2024 Nov;144(11):2488-2500.e4.
4. Gijs Rikken, Luca D. Meesters, Patrick A.M. Jansen, Diana Rodijk-Olthuis, Ivonne M.J.J. van Vlijmen-Willems, Hanna Niehues, Jos P.H. Smits, Peter Oláh, Bernhard Homey, Joost Schalkwijk, Patrick L.J.M. Zeeuwen, Ellen H. van den Bogaard. Novel methodologies for host-microbe interactions and microbiome-targeted therapeutics in 3D organotypic skin models. *Microbiome*. 2023 Oct 17;11(1):227.
5. Jos P.H. Smits, Noa J.M. van den Brink, Luca D. Meesters, Hadia Hamdaoui, Hanna Niehues, Patrick A.M. Jansen, Ivonne M.J.J. van Vlijmen-Willems, Diana Rodijk-Olthuis, Céline Evrard, Yves Poumay, Michel van Geel, Wiljan J.A.J. Hendriks, Joost Schalkwijk, Patrick L.J.M. Zeeuwen, Ellen H. van den Bogaard. Investigations into the FLG Null Phenotype: Showcasing the Methodology for CRISPR/Cas9 Editing of Human Keratinocytes. *J Invest Dermatol*. 2023 Aug;143(8):1520-1528.e5.
6. Luca D. Meesters, Hanna Niehues, Luke Johnston, Jos P.H. Smits, Patrick L.J.M. Zeeuwen, Sara J. Brown, Ellen H. van den Bogaard. Keratinocyte signaling in

atopic dermatitis: Investigations in organotypic skin models toward clinical application. *J Allergy Clin Immunol*. 2023 May;151(5):1231-1235.

7. Jos P.H. Smits, Luca D. Meesters, Berber G.W. Maste, Huiqing Zhou, Patrick L.J.M. Zeeuwen, Ellen H. van den Bogaard. CRISPR-Cas9-based genomic engineering in keratinocytes: from technology to application. *JID Innov*. 2021 Dec 1;2(2):100082.

Publications not related to this thesis:

8. Leander van Eekelen, Joey Spronck, Monika Looijen-Salamon, Shoko Vos, Enrico Munari, Ilaria Girolami, Albino Eccher, Balazs Acs, Ceren Boyaci, Gabriel Silva de Souza, Muradije Demirel-Andishmand, Luca D. Meesters, Daan Zegers, Lieke van der Woude, Willemijn Theelen, Michel van den Heuvel, Katrien Grünberg, Bram van Ginneken, Jeroen van der Laak, Francesco Ciompi. Comparing deep learning and pathologist quantification of cell-level PD-L1 expression in non-small cell lung cancer whole-slide images. *Sci Rep*. 2024 Mar 26;14(1):7136.
9. Danique A. van der Krieken, Gijs Rikken, Thomas H.A. Ederveen, Patrick A.M. Jansen, Diana Rodijk-Olthuis, Luca D. Meesters, Ivonne M.J.J. van Vlijmen-Willems, Bram van Cranenbroek, Renate G. van der Molen, Joost Schalkwijk, Ellen H. van den Bogaard, Patrick L.J.M. Zeeuwen. Gram-positive anaerobic cocci guard skin homeostasis by regulating host-defense mechanisms. *iScience*. 2023 Mar 23;26(4):106483.
10. Elke M. Muntjewerff, Luca D. Meesters, Geert van den Bogaart, Natalia H. Revelo. Reverse Signaling by MHC-I Molecules in Imnune and Non-Immune Cell Types. *Front Immunol*. 2020 Dec 15:11:605958.
11. Elke M. Muntjewerff, Luca D. Meesters, Geert van den Bogaart. Antigen Cross-Presentation by Macrophages. *Front Immunol*. 2020 Jul 8:11:1276.

+

List of (most common) abbreviations

2D	2-dimensional
3D	3-dimensional
AD	Atopic dermatitis
AHR	Aryl hydrocarbon receptor
ALI	Air liquid interface
AMP	Antimicrobial peptide
AUC	Area under the curve
BMP-4	Bone morphogenetic protein 4
Ca2+	Calcium
CA2	Carbonic anhydrase 2
CCL	C-C motif chemokine ligand
CLDN	Claudin
CRISPR/Cas9	Clustered Regularly Interspaced Short Palindromic Repeats/ CRISPR-associated protein 9
CXCL	C-X-C motif chemokine ligand
DEFB4	Defensin beta 4
DEG	Differentially expressed gene
EIS	Electrical impedance spectroscopy
FBS	Fetal bovine serum
FLG	Filaggrin
GO	Gene ontology
gRNA	Guide RNA
hBD2	Human beta defensin 2
HDR	Homology-directed repair
HEE	Human epidermal equivalent
HRNR	Hornerin
HSE	Human skin equivalent
(h)TERT	(Human) telomerase
IFN	Interferon
iKC	Induced keratinocyte
IL	Interleukin
iPSC	Induced pluripotent stem cell
IRF	Interferon regulatory factor
ITG(A)	Integrin (alpha)
IVL	Involucrin
JAK	Janus kinase

Ki67	(Antigen) kiel 67
KRT	Keratin
LOR	Loricrin
NELL2	Neural EGFL like 2
NHEJ	Non-homologous end joining
NHEK	Normal human epidermal keratinocyte
NMF	Natural moisturizing factor
PAM	Protospacer adjacent motif
P63	(Tumor) protein 63
pKC	Primary keratinocyte
PCA	Principal component analysis
PRR	Pattern recognition receptor
RA	Retinoic acid
RNP	Ribonucleoprotein
ROCK	Rho-associated protein kinase
S. aureus	*Staphylococcus aureus*
SB, SS, SG, SC	*Stratum basale, spinosum, granulosum, corneum*
Sc	Single-cell
Seq	Sequencing
SKALP	Skin–derived antileukoprotease
STAT	Signal transducer and activator of transcription
TEER	Transepithelial electrical resistance
TEWL	Transepidermal water loss
TFAP	Transcription factor AP
Th	T helper cell
TNF	Tumor necrosis factor
UMAP	Uniform manifold approximation and projection
ZNF	Zinc finger

Research data management

This research was supported by HealthHolland grant PAST4FUTURE (LSHM20043-HSGF) to Prof. dr. Ellen van den Bogaard and dr. Huiqing (Jo) Zhou. Isolation of primary cells from healthy volunteers was performed anonymously, by receiving the tissue without personal details and providing codes, and according to the principles of the Declaration of Helsinki. All data was stored on personal onedrive accounts from Radboudumc and the local Dermatology server of Radboudumc, which is supported by the Information and Communications Technology (ICT) department of Radboudumc and backed up regularly, or the local RIMLS-FNWI server of Radboud University. As second laboratory data and research protocol storage, the electronic labjournal Labguru, that is accessible to all researchers of the experimental Dermatology group, was used. Paper labjournals are stored in cabinets at the department of Dermatology, Radboudumc. All published data is available through open access on the journals website, and other datasets can be requested via the last author. In addition, data and metadata are stored in the Radboud Data Repository (ru.rumc.p4fcyto_r0005499a_dsc_385 and ru.rumc.p4fikc_r0005499a_dsc_696) and available upon request. Raw *in vitro* RNA-sequencing data from **Chapter 6** is published in the GEO database under GSE282371 in fastq and count table format including the metadata. For this chapter, *in vivo* RNA-sequencing data was re-used from Rojahn et al. (2020)* or the BIOMAP project (as described in chapter 6, datasets are available through ArrayExpress E-MTAB-8149 and GEO GSE130588 and GSE193309). Raw RNA-sequencing data from **Chapter 8** is available under GSE287810 for bulk RNA-seq and GSE285034 for scRNA-seq in the same format. Records will be made publicly available upon publication.

* Rojahn, T. B., Vorstandlechner, V., Krausgruber, T., Bauer, W. M., Alkon, N., Bangert, C., Thaler, F. M., Sadeghyar, F., Fortelny, N., Gernedl, V., Rindler, K., Elbe-Bürger, A., Bock, C., Mildner, M., & Brunner, P. M. (2020). Single-cell transcriptomics combined with interstitial fluid proteomics defines cell type-specific immune regulation in atopic dermatitis. The Journal of allergy and clinical immunology, 146(5), 1056–1069. https://doi.org/10.1016/j.jaci.2020.03.041

PhD Portfolio

Department: **Dermatology, Radboud Research Institute for Medical Innovation**
PhD period: **01-01-2021 until 31-01-2025**
PhD Supervisor(s): **Prof. dr. E.H. van den Bogaard, and dr. H. Zhou**
PhD Co-supervisor(s): **Dr. H. Niehues**

Training activities	Hours
Courses	**117**
• RIMLS introduction "In the lead of my PhD" (2021)	15
• Radboudumc – Introduction day (2021)	6
• RU – Projectmanagement voor Promovendi (2021)	56
• Literature review for your PhD (2022)	4
• Radboudumc – Scientific integrity (2022)	20
• The next step in my career (2024)	16
Seminars	**245**
• Seminars and journal clubs Dermatology (2021-2024)	104
• Seminars Molecular Developmental Biology (2021-2024)	32
• Sustainable research symposium (2021)	6
• RRR Inflammation and chronic disease (2021)	1,5
• hiPSC-based disease modelling (2021)	6
• Epithelial research meeting (2022)	10
• Team science pilot (2022)	12
• Radboud Research Rounds (RRR) Inflammatory disorders (2022)	3
• Meet the scientist – René Bindels (2022)	1
• TwinPreBioEnz meeting Belgrade (2023)	16
• Seminar Sue Gibbs (2023)	1
• Meet the Expert – How to prepare for your PhD defense (2023)	1,5
• Radboudumc research strategy day panel discussion (2023)	4
• Research Integrity Rounds (RIR) The learning curve (2023)	2
• DSSCR stem cell meeting (2023)	8
• Human Measurement Models Pogram Day (2023)	8
• RIR Artificial Intelligence and Research Integrity (2024)	2
• Meet the expert – Adobe Illustrator for beginners (2024)	2
• Next Generation ImmunoDermatology (NGID) project meeting (2024)	8
• Meet the expert –Peer review and rebuttal (2024)	1
• Career event incl. communication & networking workshops (2024)	8
• Human Measurement Models Pogram Day (2024)	8

Conferences	**250**
• European Society for Dermatological Research (ESDR) and European Epidermal Barrier Research Network (E2BRN) attendee (2021)	24
• New frontiers symposium and PhD Retreat (2021)	18
• Nederlandse Vereniging van Experimentele Dermatologie (NVED) oral presentation (2022)	24
• PhD Retreat (2022)	16
• ESDR attendee and E2BRN oral presentation (2022)	32
• PhD Retreat (2023)	16
• International Societies for Investigative Dermatology (ISID) Tokyo poster presentation (2023)	32
• Nederlandse Vereniging voor Dermatologie en Venereologie (NVDV) wetenschappelijke vergadering (2023)	8
• NVED oral presentation (2023)	16
• E2BRN oral presentation (2023)	16
• NVED oral presentation (2024)	16
• PhD Retreat (2024)	16
• NVED oral presentation (2025)	16
Other	**184**
• PhD council member, vice-chair and chair (2021-2024)	108
• UMC council member (2021-2022)	60
• Green Lab Initiative and Dermatology Green Team member (2022)	16
Teaching activities	
Lecturing	**8**
• Development, teaching and grading of work groups "Inflammatory diseases" course Biomedical Sciences master (2023-2024)	8
Supervision of internships / other	**351**
• Supervision of 5 master internship students (2021-2024)	315
• Supervision of 1 master literature review student (2022)	8
• Supervision of 1 master research proposal student (2023)	8
• Supervision of a Meet The PhD program group (2023)	20
Total	**1155**

Curriculum Vitae

Luca Dulce Meesters was born on January 21st 1997 in 's-Hertogenbosch. After finishing her atheneum at high school Jeroen Bosch College in 2015, she started the Biomedical Sciences bachelor at Radboud University. Her bachelor's internship at the laboratory of pediatric infectious diseases in Radboudumc, under supervision of prof. dr. Marien de Jonge and dr. Jeroen Langereis, was about nontypeable Haemophilus influenzae proteins as potential vaccine targets for COPD patients. She was also active as student ambassador at high schools and open days of the Radboud University to inform high school students about the study Biomedical Sciences, the Radboud University and Nijmegen as a student city. In 2018 she received her bachelor's certificate and continued with the Biomedical Sciences master at Radboud University. During her first internship at the laboratory of Dermatology in Radboudumc, supervised by prof. dr. Ellen van den Bogaard and dr. Gijs Rikken, she validated a 3D skin microbiome model to study host-microbe interactions. She wrote two literature theses with prof. dr Geert van den Bogaart, dr. Elke Muntjewerff and dr. Natalia Revelo, from the tumor immunology laboratory of Radboudumc, about antigen cross-presentation by macrophages, and reverse signaling by MHC-I molecules. Simultaneously, she worked as a student assistant in the computational pathology group of Radboudumc to assess microscopical tissue slides which contributed to training of AI systems. Her Dermatology internship project, both literature theses, and the work for computational pathology got published (see list of publications) in the years to follow. For her final master internship she went to the VIB-UGent Center for Medical Biotechnology to perform her research about the function of OTULIN in the skin supervised by prof. dr. Geert van Loo and dr. Esther Hoste, which was discontinued due to the covid-19 pandemic. As a replacement, she wrote a research proposal about linear ubiquitination in the skin. In 2020, she received her master's certificate with honors (cum laude). From 2021 until 2025, she worked as a PhD candidate in the laboratory of Dermatology of Radboudumc (with prof. dr. Ellen van den Bogaard and dr. Hanna Niehues) and the department of Molecular Developmental Biology of Radboud University (with dr. Huiqing (Jo) Zhou). This thesis is the final product of her project, called The Platform for Alternative Skin Tests for sustainable Future science (PAST4FUTURE or P4F). P4F was part of the Human Measurement Models programme, and was executed in collaboration with

the following consortium partners: Prof. dr. Sue Gibbs (VUMC), dr. Abdelouahab El Ghalbzouri (LUMC), dr. Christian Freund (LUMC), dr. Bouke Boekema (ADBC), dr. Stefan Bärtschi (CELLnTEC) and dr. Koen Dechering (TROPIQ). As a PhD candidate, she supervised multiple students during their internships, literature theses and work groups. She presented her research at various conferences for which she was awarded with the “best oral presentation prize” two times (at NVED and E2BRN annual meetings). The years after, Luca was also invited to join the jury for the best oral presentation prize of NVED and to chair a session at the annual meeting of E2BRN. Next to her laboratory research, she was active in the UMC council, Green Lab Initiative, and PhD council. As a member, vice-chair and chair of the PhD council, she collaborated with the research institute and graduate school to improve PhD-related policies, organized events like the annual PhD Retreat and social activities, and set up a new council including its communication platforms when the RIMLS and RIHS institutes merged into RRIMI. Luca currently works as a project manager at the Medical Microbiology department of Radboudumc, where she is responsible for the management of the EU funded EDCTP project 'Seasonal Malaria Vaccination Delivery' (SMV Delivery). In addition, she provides support and advises in acquisition, management and reporting of a diverse portfolio of other MMB research projects.

Dankwoord (Acknowledgements)

Hora finita! Dat was 'm dan.

Ik ben ontzettend dankbaar dat ik mijn promotieonderzoek bij de afdeling Dermatologie van het Radboudumc heb mogen doen. Naast dat het me veel heeft bijgebracht over de dermatologie en (laboratorium)onderzoekstechnieken, heb ik ook heel wat over mezelf en samenwerkingen geleerd. Dit alles heb ik natuurlijk mede te danken aan de mensen om mij heen. Gezien ik niet kort van stof ben en niemand wil vergeten, kan je er alvast goed voor gaan zitten. En om de traditie onder de Derma brabo's in stand te houden:

"Da ge bedankt zijt da witte! Houdoe en bedankt!"

Beste promotieteam,
Wat een girl power hebben wij getoond! Jullie zijn alle drie genomineerd geweest voor de "supervisor of the year award", dus dat zegt al veel. Ik heb tijdens mijn tijd bij de PhD council mijn ervaring met jullie vaak gebruikt als goed voorbeeld van hoe PhD supervisie eruit hoort te zien! **Prof. dr. Ellen van den Bogaard**, beste Ellen,, sinds ik mijn stage bij jou in het lab heb gelopen vind ik je een inspirerend persoon. Jij lijkt altijd de juiste woorden te vinden, en zou nog iets nutteloos kunnen verkopen. Vooral tegen je creativiteit kijk ik echt op. Je weet verschillende onderzoeksvelden met elkaar te verbinden, en hebt een encyclopedie aan studies (incl. auteur en jaartal) in je hoofd zitten. Ik ben trots dat jij mij hebt gevraagd een PhD bij je te komen doen en jouw bevestiging motiveerde mij enorm. Ook was je een gezellige gesprekspartner en borrel/feestgenoot. Ik kijk uit naar alle studies die jij nog met de groep gaat uitvoeren en publiceren, en wil je bedanken voor de uitdaging die je me hebt geboden en alles wat je mij hebt geleerd!

Lieve **(dr.) Hanna**, wat heb jij een eindeloos geduld met mensen. Hoe vaak ik ook bij je binnen liep, je verwelkomde me altijd met een lach en luisterend oor. Jij wist me vaak te motiveren door middel van je aanmoedigende feedback, ook als er nog veel verbetering nodig was. Ook jouw work-life balance is iets waar ik bewondering voor heb. Naast het onderzoek, heb ik veel van jou geleerd op het gebied van educatie. Ik hoop dat jij het net zo leuk vond om mij als je eerste PhD te begeleiden als dat ik het vond om door jou begeleid te worden!

Dear **(dr.) Jo**, even though you didn't know me before I started my PhD, you believed in me to successfully do a PhD in your group. I really learned a lot from you

about stem cell cultures and transcriptomics interpretation. Your door was always open when I needed you, even for refreshing my cells in the weekend (!), which I did not take for granted. You could be very direct (like a real Dutchie), but also regularly gave me compliments and showed me your enthusiasm for research. Also your efforts to socially keep the group together, with trips to Keukenhof or dinners, were very much appreciated.

Lieve paranimfen!
Jos, waddup nerd/roomie/beste collega/beastie/frikandellenkoning! Wat ben ik blij dat ik jou al die jaren letterlijk en figuurlijk aan mijn zijde heb gehad. Je hebt, misschien zonder dat je het in de gaten hebt gehad, een soort mentorrol voor mij ingevuld, omdat ik met inhoudelijke en persoonlijke vragen bij je terecht kon. Het was super bijzonder om met jou naar een congres in Tokyo, Japan te zijn geweest, dat is een ervaring die we niet meer vergeten. Verder heb ik veelvoudig de oren van je kop gekletst in de trein naar Oss/Den Bosch en heb ik je ruim een jaar mijn kantoorgenoot mogen noemen. We maakten altijd grapjes over dat we elkaars lievelingscollega waren, maar daar zat voor mij ook zeker een kern van waarheid in. Daarnaast konden we de laatste tijd goed met elkaar praten over onze sportschool avonturen en zochten we elkaar op als we motivatie nodig hadden. Bedankt voor alle grapjes, wijsheid en ook zeker onzin (lees: tiktok filmpjes) die je met mij hebt gedeeld. Ik wens iedereen een vriend, partner, vader, collega of begeleider zoals jij (KLEF)!

Chère **Camille**, I am grateful that you joined the Zhou lab relatively short after I did. The weekend you arrived, we met at the market square in Nijmegen to have a coffee and I immediately knew I liked you. You're kind, open en very helpful whenever someone needs you. After we went to Amsterdam for the ESDR conference and the personal talks we had there (what happens in Amsterdam, stays in Amsterdam), it felt like we got to a level of trust and comfort, which translated for us in acting crazy around each other. You were always around to kick me off my chair, and we had many coffee breaks together. It was also very special to see you finding and marrying your life partner, and I am happy I get to share the latter with you too next year. I am going to miss our brunches and girls nights, but luckily I am about to visit you and Steven in France!

Lieve **Jaimy**, wat begon als een stagiaire-begeleider relatie veranderde al snel in een vriendschap en daarna ook collegiale band. Zoals ik tijdens jouw masterdiploma-uitreiking al zei, zag ik jou meteen als nette en gemotiveerde jongen, ook al ben ik van dat eerste wel terug gekomen. Het is eigenlijk altijd een feestje als jij in de buurt

bent. Met je krukken bij Radboud Rocks, vanuit de kroeg door om de vierdaagse lopers uit te zwaaien, en als laatst overblijven bij de borrels op congressen. Ook jou heb ik nog even kantoorgenoot mogen noemen, en toen kon ik enorm genieten van jouw directheid en nuchterheid (ja, soms was je wel nuchter). Van jou heb ik geleerd dat het leven een feestje is, en dat ik als ik ergens niks meer aan kon doen me ook geen zorgen hoefde te maken! Ook lieve **Nina** moet ik even meenemen in deze paragraaf, want wat heb ik vaak mogen crashen bij jullie na borrels en feestjes. Jullie zijn twee toppers en ik weet zeker dat jullie je proefschriften ook mooi gaan afronden. Bedankt voor onze bijzondere vriendschappen en alle herinneringen die nog gaan komen!

Lieve collega's van lab Dermatologie:
Diana en **Ivonne**, wat zijn jullie gezellig, behulpzaam en attent! Er was altijd ruimte voor een praatje, over de (klein)kinderen of hobby's, maar jullie hebben ook enorm veel werk verzet om mij te ondersteunen tijdens mijn PhD. Bedankt dat jullie me nooit zat werden (of het niet lieten blijken) als ik weer bij jullie stond met een vraag. Hoe extra gezellig jullie werden na de benodigde alcoholische versnaperingen, heb ik bij Diana mogen ervaren en helaas bij Ivonne alleen van horen zeggen. Ik hoop dat we op mijn promotiefeestje verandering gaan brengen in dat laatste! Ik wens jullie veel werkplezier en geluk in jullie privéleven, en wil jullie bedanken voor de significante bijdrage aan mijn scriptie.

Patrick J (PJ), er zijn een paar dingen die ik van jou ga onthouden: je kennis van moleculaire biologie, passie voor biertjes, foute muzieksmaak (lees: vieze Jack), en soms leuke maar ook soms irritante grapjes;). Een kantoor delen met jou betekende muziek-vrijdag, rondslingerende papieren (OVERAL) en stipt op tijd meegesleurd worden naar de koffiekamer voor pauze. Natuurlijk heb ik veel van je geleerd, over restrictie-enzymen en lentivirussen enzo, maar vooral ook over gezelligheid op de werkvloer, Oktoberfest nummers en biersoorten.

Patrick Z (PZ), ik moet toegeven dat ik best heb moeten wennen aan jouw directheid en standvastigheid, maar na een persoonlijkheidstest met het hele team bleken wij gewoon veel op elkaar te lijken. Van jou heb ik veel geleerd over kwalitatief goed onderzoek doen, en er was niemand die zoveel spelfouten uit een presentatie, manuscript of scriptie kon halen als jij. Hopelijk blijven we met elkaar proosten op Untappd, en kan ik nog een keer bij je terecht met vragen over de reizen die jij al hebt gemaakt en ik nog wil maken!

Noor, jou leerde ik kennen als student van Noa en gezien ik zelf pas net met mijn PhD was begonnen zaten wij bijna in dezelfde levensfase en zochten elkaar dus ook buiten werktijd op. Je bent een super creatief persoon, zowel in de keuken, waar wij regelmatig van konden meegenieten, als in het maken van presentaties of organiseren van activiteiten voor de groep. Bedankt voor de gezelligheid de afgelopen jaren, en veel plezier en succes met je verdere promotietraject!

Rens, wat vond ik het knap hoe snel jij je (als een van de enige die geen stage bij ons had gelopen) ingelezen had in ons vakgebied. Je stelde altijd goede vragen, en ik heb goed kunnen profiteren van jouw handigheid in programma's zoals Graphpad. Ondanks dat we maar een jaar tegelijk PhD waren in Ellen's groep, heb ik genoten van jouw aanwezigheid op het lab/kantoor en tijdens borrels daarbuiten. Je was een fijne en geïnteresseerde collega en gesprekspartner!

Aranka, wij begonnen de week altijd gezellig met het bespreken van alle dingen die we in onze eerste koophuizen hadden gedaan. Daarnaast konden we ook heel goed samenwerken, want waar ik georganiseerd was, was jij dat nog een tikkeltje meer! Ik wil je natuurlijk sowieso bedanken voor je bijdrage aan "het cytokine paper" waar jij in korte tijd veel werk voor hebt verzet. Ik ben benieuwd hoe je het gaat vinden bij Kinderlongziekten in Utrecht.

Lieve oud-collega's van lab Dermatologie:
Danique, ik wil je bedanken voor de fijne ontvangst in het kantoor van jou en PJ. Ondanks dat je voor mijn komst echt "one of the guys" was, konden wij lekker over vrouwendingen praten zoals de beste krullen-crèmes. Ook hadden we open gesprekken over de eigenschappen die we in elkaar bewonderden en bij onszelf wilden verbeteren. Hopelijk zie ik je bij mijn verdediging en kunnen we weer even bijkletsen!

Gijs, mijn avontuur bij Dermatologie ben ik begonnen als jouw stagiaire en ik kan me geen gezelligere begeleider bedenken! Naast het kletsen over onze plannen buiten werk, heb ik natuurlijk ook heel veel geleerd over huid-microbioom onderzoek en heeft dit me een makkelijke start gegeven toen ik terugkwam als PhD (met als bewijs hoofdstuk 7 van mijn scriptie). Ook jouw relaxte houding ("komt wel goed"), o.a. terwijl je een PhD aan het afronden was met drie kinderen thuis en al een nieuwe baan, was iets waar ik bewondering voor had. Terwijl ik dit schrijf zijn we een maand verwijderd van jouw verdediging en ik wens je veel succes daarmee en je verdere toekomst!

Noa, tijdens mijn stage bij dermatologie leerde ik jou kennen als rustig persoon, maar ik ben blij dat ik tijdens mijn PhD ook jouw gekke kant heb mogen leren kennen! Ik vond het jammer toen je wegging, omdat het erg stil werd zonder jouw gezang in het lab, maar gelukkig hebben we samen nog het oude lab kunnen uitluiden. Ik vind het fijn dat we op precies dezelfde dag de acceptatie mail van onze theses kregen, want we kunnen goed overleggen over het geregel en het mooi samen afsluiten. Ik ben blij dat je zo'n leuke en bij jou passende baan hebt gevonden en wens je veel plezier en succes voor de toekomst!

Felicitas, dat het niet makkelijk is om op twee afdelingen je PhD te doen dat hebben wij wel ervaren, maar gelukkig hadden we elkaar om hierover te praten. Ik hoop dat je ondanks dat kan terugkijken op een leerzaam traject met ook leuke uitjes zoals de retreat van Mol (Dev) Bio, de PhD retreat verkleed als superhelden en ook samen naar de vierdaagsefeesten gaan (en jij zelfs karaoke zingen op het podium van plein '44: daredevil!). Nog even doorzetten en ook jij kan je PhD afronden, dus als je ooit hulp nodig hebt weet je me te vinden. Terwijl ik dit schrijf werk je als project coördinator, en ik hoop dat je je daar of in een ander vakgebied helemaal thuis gaat voelen!

Piet, ondanks dat we niet heel lang hebben samengewerkt, herinner ik jouw grappige verhalen en eindeloze inzet voor de afdeling. Volgens mij hield je er niet echt van om in de spotlight te staan, maar gelukkig ben je daar wel een paar keer in geplaatst door jouw goede inzet. Nadat jij met welverdiend pensioen ging, merkten we hoe fijn het was geweest om iemand in het team te hebben die goed is met ICT zaken waaronder de microscoop, maar hopelijk ben je nu lekker aan het genieten van je tijd met de familie!

Dear Zhou group:
Dulce, when you and Camille joined Jo's group just after me, I gained two unofficial mentors. I learned from you how to balance my perfectionism and being in control with letting go sometimes. Your experience with iPSC and even differentiating them into keratinocytes was of great help to me. But, next to that, we also had a lot of fun during coffee breaks, brunches, housewarmings, train rides and group outings. I am curious to see what your future career brings, but I hope it will be great!

Jos, ook jij had al ervaring met iPSC naar keratinocyt differentiatie en gaf me daarin mee dat het niet makkelijk was en ik niet te lang in een richting moest blijven hangen, en dat heeft geholpen! Ik heb je leren kennen als een grappig en creatief persoon, en het was nooit saai als jij er was. Dit laatste gold trouwens ook voor

jouw congres presentaties en recente verdediging. Ik ben blij dat je een super leuke nieuwe baan hebt gevonden.

Julian, ook jou ken ik ondertussen een tijdje, want toen ik met mijn PhD startte liep jij stage in onze groep en niet veel later begon je ook met je PhD. Echt iedereen die jouw hulp nodig had die kreeg hem ook, en voordat je het wist had je heel wat projecten lopen. Jouw doorzettingsvermogen, op werk en met alle persoonlijke dingen die je te verduren kreeg, is bewonderingswaardig! Ik wens je veel succes en plezier met het afronden van je eigen proefschrift en het vinden van een leuke nieuwe baan.

Yavuz, I have to thank you for the many times you covered for me in the lab when I was ill or you were in TC in the weekends! I hope you don't forget to think about yourself sometimes too. We worked together a lot over the last two years, and your experience with cell culture provided me with different perspectives. I wish you the best for the future.

Lieve moleculaire (ontwikkelings-) en celbiologie collega's:
Dear collaborators of "the cytokine paper" **Niels**, **Janou**, **Marijke**, **Musa**, I would like to thank you for the laboratory work, computational analyses and/or reviewing of the manuscript. I really enjoyed working together and it majorly improved the research project and paper!

Lieve borrel en karaoke-genootjes **Aniek M**, **Aniek V**, **Margit**, **Thomas**, **Jonas**, **Ruben**, wat hebben jullie me goed geholpen mijn gedachtes te verzetten na werk! Ik heb genoten van de afdelingsborrels, en misschien nog wel meer van de karaoke avondjes erna, maar ook van super gezellige PhD retreat momenten of mijn housewarming met jullie. Ik wens jullie veel succes met jullie verdere promotietraject of voor sommigen het schrijfproces en hoop dat we binnenkort (misschien wel na mijn verdediging) nog een keer in Roxy's te vinden zijn. Ook nog een bedankje aan **Cyriel** voor het gezelliger maken van de soms langdurige TC sessies, en natuurlijk **Siebren** voor de mental support in de trein en op de fiets onderweg naar werk!

Beste support system, staf (secretariaat), waaronder **Diny**, **Marieke**, **Amy** (Dermatologie), **Marion**, **Anita**, **Maaike** (RIMLS-FNWI). Jullie hebben alles een stukje makkelijker en leuker gemaakt op beiden afdelingen. Van administratieve taken tot de organisatie van leuke uitjes voor de afdeling, wat iedereen bij elkaar bracht en hield.

Beste klinische staf waaronder **prof. dr. Elke de Jong**, **dr. Juul van den Reek**, ik wil jullie super bedanken voor jullie feedback op mijn onderzoek en presentaties, en voor het klinische perspectief wat jullie mij hebben meegegeven. Hierdoor bleef ik in mijn achterhoofd houden waar we het uiteindelijk ook al het fundamentele onderzoek voor doen: de patiënten!

Lieve arts-onderzoekers **Sarah**, **Nikki**, **Malak**, **Charlotte**, **Liana**, **Linda** en **Josje**, wat zijn jullie een heerlijke groep meiden! **Sarah**, wij zijn tegelijk gestart en konden daardoor samen onze zenuwen overwinnen bij NVED praatjes, maar ook goed kletsen en tips uitwisselen tijdens verschillende fases van ons onderzoek. Ik vond het hartstikke gezellig toen ook **de rest** van de arts-onderzoekers werd aangenomen en ondanks dat we niet meer in hetzelfde gebouw zaten, hebben we elkaar regelmatig opgezocht voor leuke uitjes. Ik wens jullie allemaal ook veel succes met het afronden van jullie onderzoeken en proefschriften!

Lieve studenten **Priscilla**, **Roos**, **Jaimy** (alweer), **Bram** en **Wietske**. Wat hebben jullie allemaal hard meegewerkt aan het onderzoek en daarbij mijn leven een stukje makkelijker gemaakt. Ook was het gezellig om met leeftijdsgenoten te kletsen tijdens de saaie wachtstappen in het lab, of om feestjes mee te pakken buiten werktijd! Ik wens jullie veel succes in jullie carrière maar gezien de banen die jullie allemaal nu al hebben, gaat dat helemaal goedkomen.

Beste collega's van **plastische chirurgie**, zonder jullie was dit hele feestje sowieso niet doorgegaan, want alle huid en daarmee de huidcellen die we gebruikt hebben voor ons onderzoek komen bij jullie afdeling vandaan, dus dank daarvoor!

Dear team PAST4FUTURE, **Abdoel**, **Sue**, **Bouke**, **Stefan**, **Christian** and **Koen**. Thanks for your warm welcome four years ago and amazing feedback during the years. It's an honor to have worked with many important researchers in the field and I've learned a lot from all of you! I hope to see some of our P4F work being built on by your research groups and companies, among others by **Taco**, **Alesha** and **Marcel** to whom I transferred the stem-cell derived keratinocytes and I shortly got to collaborate with. Finally, thanks to the funders of the P4F project, HealthHolland, Samenwerkende Gezondheidsfondsen, Proefdiervrij, among whom **Carine** van Schie, who joined our user committee meetings and provided us with good feedback.

Dear external collaborators **Sara**, **Luke**, who co-wrote chapter 2 of this thesis, and BIOMAP consortium, specifically **Matthias** who co-wrote chapter 6 and performed

many computational analyses for this manuscript, I would like to thank you for your scientific contributions and the pleasant collaboration.

Dear board and scientific committees of **NVED** and **ESDR/E2BRN**, I would like to thank you for the multiple opportunities to present my work at your annual conferences, for the presentation prizes I received, and for the invitation to join the jury and chair a session. I learned a lot from all of these experiences and it made my PhD more memorable!

Beste **prof. dr. Alessandra Cambi, dr. Marieke Bolling, prof. dr. Nael Nadif Kasri**, ik wil jullie bedanken voor het lezen en positief beoordelen van mijn scriptie! Ik ben benieuwd naar jullie vragen (en die van de andere opponenten **dr. Esther Hoste, dr. Klaas Mulder en prof. dr. Elke de Jong**) en onze discussies tijdens mijn verdediging, maar dat ze interessant worden daar ga ik wel vanuit.

Lieve **Esmeralda**, toen ik onverwachts een nieuwe mentor moest zoeken dacht ik meteen aan jou! Ik kende je als docent van mijn master, maar jouw enthousiasme en leuke persoonlijkheid waren blijven hangen. Dankjewel voor de tips die je me hebt gegeven, die onder anderen mijn schrijfproces en loopbaan planning makkelijker en beter hebben gemaakt!

Lief mede-PhD council bestuur **Judith**, **Amina**, en **Lieke** en de rest van de council leden waaronder **Iris**, **Emma** en **Noor**, ik ben trots op hoe wij ons met zijn allen hebben ingezet voor alle Radboudumc PhD's! Hopelijk hebben we toch kleine veranderingen in gang gezet, die het promoveren voor generaties na ons makkelijker of leuker gaan maken. Daarnaast wil ik jullie bedanken voor de nodige afleiding en momenten om bij elkaar te ventileren, van borrels tot treinritjes met Iris. Vooral de (dansjes tijdens) PhD retreats met jullie ga ik niet vergeten!

Beste onderzoeksinstituut management team **Clasien**, **Judith**, **René** (RIMLS), **Marieke**, **Kathleen** en **Guillen** (RRIMI): Van jullie heb ik veel geleerd over het reilen en zeilen in het Radboudumc, van beleid maken tot evenementen organiseren. Ook wil ik jullie bedanken voor het bieden van een luisterend oor en oprecht open staan voor feedback op het Graduate School beleid. En om met een kritische noot te eindigen: elke stap die jullie hebben gezet voor de RUMC PhD's was een belangrijke, maar we zijn er nog niet!

Beste **Annemieke**, **Matthew**, **Annelie** en **Frank**, ik wil jullie bedanken voor jullie vertrouwen om mij als project manager Medische Microbiologie in het

Radboudumc aan te nemen. Tijdens het eerste sollicitatiegesprek voelde ik al dat het zou gaan klikken tussen ons, en het blijkt inderdaad dat wij (en **Markus**) goed kunnen samenwerken en het gezellig met elkaar hebben in de pauzes!

Lieve bachelor vrienden, waaronder **Willem** (en **Garrett**), **Anne**, **Nina**, **Emre**, en master vriendinnen **Veerle**, **Mara** en **Diante**. Waar sommigen van jullie ook met hun promotie-traject bezig zijn en we hier heerlijk over konden klagen en steun vonden bij elkaar, waren anderen er vooral voor gezelligheid buiten werktijd, maar allemaal was dit enorm belangrijk voor een goede werk-privé balans. Ik ben blij dat ik zulke slimme en leuke vrienden om me heen heb verzamelt, en kijk uit naar de komende PhD verdedigingen en andere mijlpalen die ik met jullie ga meemaken!

Beste vriendinnetjes uit Den Bosch, ook wel Luca's liefjes genoemd: Waar moet ik beginnen… Bij jullie heb ik eigenlijk maar een half woord nodig en jullie weten wat ik bedoel, maar daar is een dankwoord niet voor! Liefste **Mare**, ik heb jou niet voor niets als getuige gevraagd voor mijn bruiloft. Je bent niet alleen mijn nichtje, maar ook een van mijn beste vriendinnen. Naast je mentale steun tijdens mijn PhD tijd, was je er ook fysiek toen je in het weekend mee mijn celkweken ging verversen! De afgelopen jaren waren niet makkelijk op persoonlijk vlak, maar elke tegenslag trotseren we samen. Je bent een doorzetter en daarin ook een voorbeeld voor mij.

Liefste **Evie**, ook al 15 jaar aan mijn zijde, samen gelachen en samen gehuild, en ondertussen bijna als familie voor mij. Denkend aan hoe trots jij tegenover mij gaat zitten tijdens mijn verdediging krijg ik een glimlach op mijn gezicht. Ik hoop niet dat mijn paranimfen contact met jou hebben gezocht de afgelopen tijd, want als er iemand verschrikkelijke foto's heeft van mij van vroeger ben jij het wel… Bedankt voor je onvoorwaardelijke steun!

Liefste **Francien**, met jou kan ik uren praten (en feesten!). Als ik ooit direct hulp nodig heb, dan kan ik jou het beste van de drie bereiken;). Je was erbij op hoogtepunten, maar staat ook altijd klaar met goed advies. Ook jij hebt trots naast mij gestaan in het laboratorium voordat we naar de vierdaagsefeesten gingen. Ik wens iedereen een vriendin zoals jij, en mag zelf van geluk spreken dat ik er een heb!

Lieve **Maarten**, ook jij verdient een bedankje als een van mijn oudste vrienden (en onze ceremoniemeester volgend jaar). Jij bent een voorbeeld in je goede levensstijl, maar ook je doorzettingsvermogen met je dubbele studie. Jouw motivatie werkt aanstekelijk, maar met ons eetclubje (met **Jamie**) en gym-afspraken hebben we ook nodig kunnen klagen en van ons af kunnen zetten. Bedankt voor je steun van A tot Z.

Lieve schoonfamilie, **Nick**, **Marietje** en **Glenn**, bedankt voor jullie interesse in mijn onderzoek en de vooruitgang in betere en mindere tijden, maar ook zeker voor de afleiding zodat ik kon opladen voordat er een nieuwe werkweek begon! Volgend jaar worden jullie officieel mijn schoonfamilie, en dat is super bijzonder. Op nog veel succesvolle en leuke momenten samen!

Lieve familie,
Lieve **Jona**, wat ben je een heerlijk jong. Ik hoop dat je je onzekerheid wat vaker los kan laten, want die is nergens voor nodig. Je hebt een natuurlijk instinct om mensen te helpen, wat je enorm siert. Jij bent tot veel in staat, maar alles begint nu langzaam op zijn plek te vallen. Volgend jaar sta je als getuige op mijn bruiloft en ik kan me geen bijzonderder moment voorstellen om te laten zien hoeveel ik van je hou.

Lieve ome **Bert** (†), ik had niets liever gewild dan dat jij er vandaag bij was geweest, maar helaas is dat anders gelopen. Jij bent een enorm voorbeeld voor mij geweest. Er was volgens mij niemand waar jij niet mee overweg kon (of je kon het heel goed verbergen), je was een echt mensen mens en zag de goede kanten van anderen. Ook was je creatief, handig en had een enorme algemene kennis. Ik hoop, en weet, dat je trots op me bent en meekijkt vanaf boven. Je zit voor altijd in mijn hart. Gelukkig heb jij veel doorgegeven aan mijn lieve neef en nichten. In **Charlotte** en **Mare** zie ik jouw gekkigheid en humor terug, en in **Sebastiaan** jouw zachte en technische kant. De aanwezigheid vandaag van de andere helft van onze eetclub, jouw zus en mijn peettante, is ook heel belangrijk voor mij.

Lieve tante **Liek**, dat ik eerder een boek heb geschreven dan jij dat had ik niet verwacht, want wat maak jij veel boek-waardige dingen mee in je leven. Mare en ik konden altijd uren luisteren naar jouw verhalen en reisavonturen. Die laatste passie hebben we denk ik van je over genomen. Het feit dat je alleen knuffels wil van Mare en mij, zegt genoeg over onze band. Ik weet dat je altijd voor me klaar staat, en dat zal ik ook altijd voor jou doen!

Verder naar papa's kant van de familie, lieve ome **Roel**. Ik weet niet wat het is met die ooms van mij, maar ik heb het wel getroffen. Ook jij bent een super lief en inspirerend persoon. Dat je met pensioen ging heeft jou niet tegengehouden je verder te ontwikkelen en inlezen in onder andere economische zaken, dus het is mooi om te zien hoe jij en Brandon elkaar daarin vinden. Gelukkig voor mij ben je ook geïnteresseerd in medische ontwikkelingen. Door jou had ik extra het gevoel dat ik belangrijk werk deed en daar ben ik je dankbaar voor.

(Ons) pap en mam:
Lieve **papa**, ik wil jou eerst bedanken dat je je bèta-genen of passie voor bètawetenschappen aan me hebt doorgegeven, want anders stond ik niet waar ik nu sta. We hebben al heel mijn leven een bijzondere band. Als ik even mijn motivatie kwijt ben, hoef ik maar aan jouw trotse gezicht te denken en weet ik weer waar ik het voor doe. Bedankt voor de kleine en grote momenten die we hebben gedeeld. Het is gek maar ook heel fijn dat ik langzaamaan ook dingen voor jullie terug kan doen, want dat verdienen jullie nadat jullie jaren alles voor ons hebben gegeven!

Lieve **mama**, bedankt voor je onvoorwaardelijke steun. Als ik goed of slecht nieuws krijg, ben jij de eerste (of sóms tweede, na Brandon) die ik bel. Zoals velen kunnen beamen lijk ik niet alleen qua uiterlijk maar ook qua innerlijk enorm op jou, dus ik denk dat ik een deel van mijn succes daarmee ook aan jou te danken heb. Daarnaast heb je me ook leuke afleiding gegeven, waaronder tijdens onze paar-jaarlijkse stedentripjes. Met jou aan mijn zijde voel ik me sterker en trotser!

Allerliefste vriend en verloofde (!) **Brandon**, al 12 jaar sta jij aan mijn zijde, waarbij je me hebt zien veranderen van middelbare scholier tot doctor. Jouw heerlijke relativerende vermogen heeft mij vaak geholpen de afgelopen jaren. Je geeft mij de stabiele basis die ik af en toe hard nodig heb gehad. Het was niet altijd leuk als ik 's avonds moest werken of in het weekend weer op het lab stond, maar dat accepteerde jij omdat je wist dat het belangrijk was voor mij. Als mensen mij georganiseerd vinden dan kennen ze jou nog niet, want met de aankoop van ons huis, het plannen van vakanties en nu ook de organisatie van onze bruiloft worden er uitgebreide Excel sheets gemaakt in ons huishouden. Ik ben trots op wie jij bent, de goede baan die je hebt, en de fijne mensen die je om ons heen hebt verzameld. Ik heb veel zin in onze toekomst, want zoals je al zei tijdens je aanzoek: na al die jaren hebben we het nog steeds enorm leuk samen!

Bedankt allemaal, en proost op fijne samenwerkingen en mooie connecties!

Luca Dulce Meesters

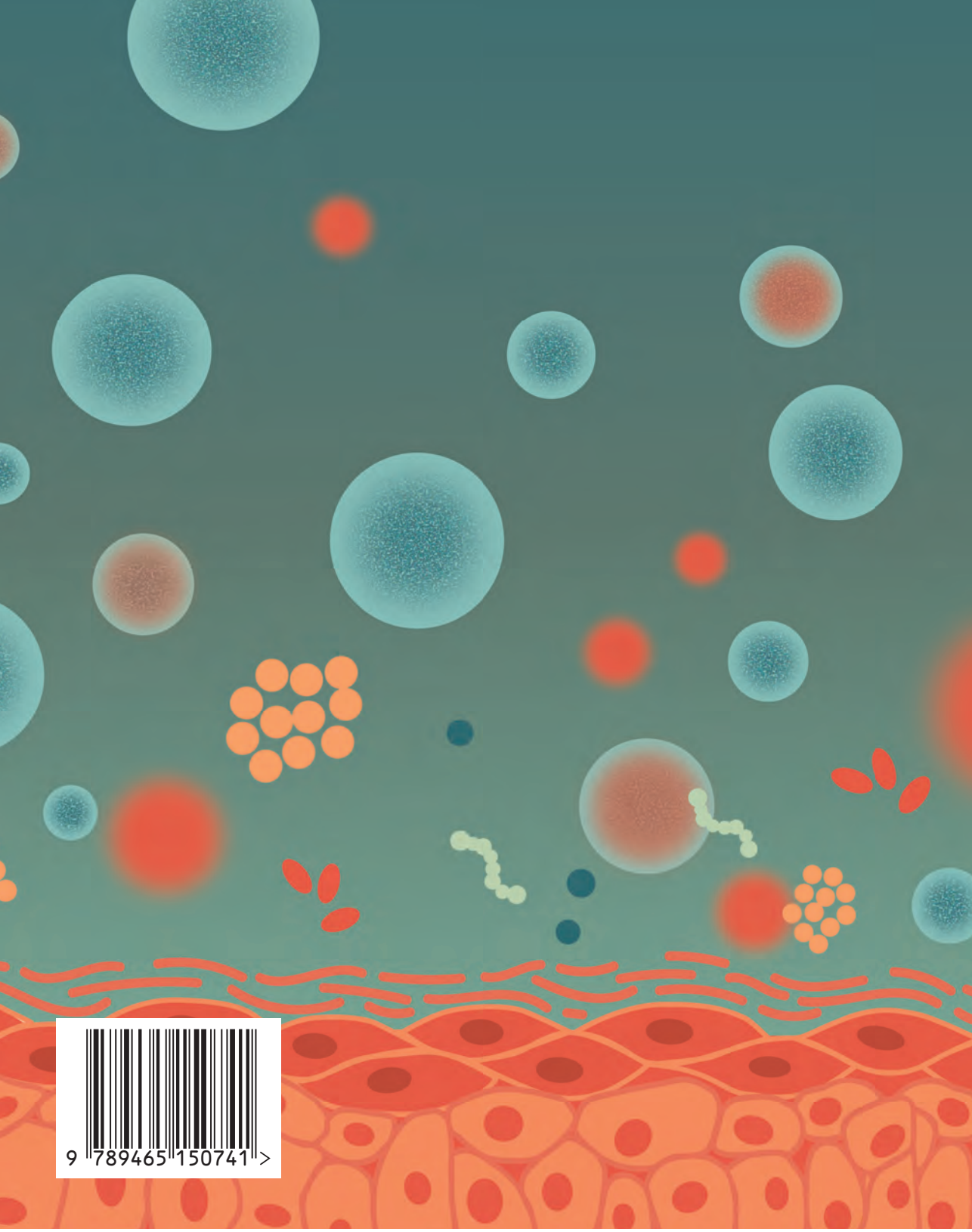

9 789465 150741 >

Radboudumc
university medical center

IN DEI NOMINE FELICITER

Radboud University